Investigation of Parameters Effecting Concrete Core Performance for Quality Control and Assurance

by

Marc Johnson

A thesis
presented to the University of Waterloo
in fulfillment of the
thesis requirement for the degree of
Master of Applied Science
in
Civil Engineering

Waterloo, Ontario, Canada, 2019

AUTHOR'S DECLARATION

I hereby declare that I am the sole author of this thesis. This is a true copy of the thesis, including any required final revisions, as accepted by my examiners.

I understand that my thesis may be made electronically available to the public.

Abstract

The ever-evolving concrete construction industry has required stronger concrete, faster turnarounds, and better durability. To achieve this, the concrete mixtures have changed drastically, including a large amount of cementitious materials, lower amount of water relative to the amount of cementitious materials, supplementary cementitious materials, and chemical admixtures. Each of these changes alters the properties and the behaviour of both fresh and hardened concrete. The standards and codes relating to the quality control and assurance of concrete structures were based on research conducted decades ago, which utilized on concrete mixtures which contained none of these changes and would not meet the expectations of modern concrete construction. The parameters of core testing, time, location, and direction of core extraction, the condition of the core between extraction and testing, the diameter, and the length-to-diameter (*l/d*) ratio of the core, all have effects on the results of the compressive strength test. Due to the property changes caused by the modern concrete mixtures, the effect that these parameters had on the result of the compressive strength test may or may not be true nowadays.

At the request of the Ministry of Transportation of Ontario, an experimental project was conducted to determine the effects that various parameters have on the day 28 compressive strength of concrete samples, and which combination of these parameters would be optimal for quality assurance testing purposes. In total, 8 sets of concrete structures were created and tested, totaling 884 concrete samples, of which 713 underwent compression testing. These sets of concrete samples included beams, wall sections to represent girder webs, large box structures, manhole risers, and standard concrete cylinders which were constructed in the University of Waterloo laboratory and in pre-cast manufacturer facilities. Other tests were conducted, including the bulk resistivity, rapid chloride permeability, and air void systems. These tests are not discussed in this thesis but were discussed elsewhere [1]. The purpose of this project was to determine how different core parameters affected the compressive strength results, and how modern concrete mixtures adhere to the current practices outlined in standards and codes. These parameters are the time of coring (day 3, 7, 14, and 28), location of the core along the length and height of a structure, direction of core extraction (perpendicular or parallel to the direction of casting), the condition of the core between extraction and testing (sealed in plastic or soaked in a saturated calcium hydroxide solution), the diameter of the core (75 mm or 100 mm), and the core *l/d* ratio (2 or 1.5). A statistical analysis was carried out at a 95% confidence level to determine these effects.

Each sample set varied a parameter to isolate its effect on the compressive strength. Once isolated, the effect of the parameters was determined through statistical comparisons. The time of coring was found to

have no significant effect on the day 28 compressive strength, regardless of how the core was conditioned between the coring and testing day. The height and length along a structure was also found to be insignificant, provided the concrete mixture included supplementary cementitious materials (SCMs) which reduce the bleed water. A similar conclusion was found for the direction of coring: provided the concrete mixture includes SCMs which reduce bleed water, there was no significant difference between the two directions of coring: perpendicular and parallel to the casting direction. However, the condition in which the core is stored between coring and testing was found to be significant. The cores which were soaked had a 2.3% lower compressive strength than cores sealed in plastic, as recommended by ASTM C42 [2]. The soaked cores were also half as variable with a coefficient of variation (CoV) of 4.73% compared to 9.31% for the sealed cores. The strength correction factor (SCF) in ACI 214 [3] of 0.917 for equating a sealed core compressive strength to a soaked core was found to be inadequate for the data presented, which found 0.977 to be adequate. Similar for the diameter of the samples: 75 mm diameter samples were found to have a 1.5% higher and 25% more variable compressive strength than 100 mm diameter samples. The SCF found in ACI 214 [3] was found to be adequate for the data presented. Lastly, the *l/d* ratio models presented in CSA A23.1 [4], ASTM C42/C39 [2, 5], and ACI 214 [3] were found to not adequately represent the data in this project. Instead, a modified version of the ACI 214 model was suggested; however, this model was sensitive to the input data. Another suggestion is to calculate a SCF for each unique concrete mixture and structure type by averaging the compressive strengths of samples with the standard *l/d* ratio of 2 to the compressive strengths of samples with a non-standard *l/d* ratio (i.e. $F_{l/d} = f_{c,l/d=2}/f_{c,l/d\neq 2}$). This second method provided SCFs on par with the modified ACI 214 model, while compensating for sensitivity in the concrete mixtures and construction techniques.

Once all the effects of the parameters discussed above are combined, the variability of 100 mm diameter samples with an *l/d* ratio of 1.5 was found to be less than the variability of 75 mm diameter samples with an *l/d* ratio of 2. To ensure equivalent variability in sets of samples, additional cores should be extracted, depending on the CoV of the sample data and the non-standard parameters. For example, with a CoV of 6.1%, four saturated cores with a 100 mm diameter and an *l/d* ratio of 1.5 or five saturated cores with a 75 mm diameter and an *l/d* ratio of 2 would be required to be equivalent to three standard cores. To ensure the same probability of passing quality assurance testing, where the average compressive strength of three cores must be at least $0.85f_c'$ with no single value below $0.75f_c'$ [3, 4], the limits may be changed to accommodate the increased variability associated with non-standard parameters on the core. For instance, with a CoV of 6.1%, five 75 mm diameter cores with an *l/d* ratio of 2 having no single value below $0.66f_c'$ would be equivalent to the current three 100 mm diameter cores with an *l/d* ratio of 2 having no single value below $0.75f_c'$.

All of findings above lead to the conclusions that concrete samples from modern concrete mixtures, which include high cementitious contents, low water to cementitious materials ratio, SCMs, and chemical admixtures, are not represented adequately by the current codes and standards.

Acknowledgements

I would like to profoundly thank Dr. Carolyn Hansson and Dr. Rania Al-Hammoud for their assistance throughout my graduate studies. Their guidance educated me in ways the classroom never could. I would like to express my gratitude to Adam Felinczak, the second graduate student on this project, and to my research group, Colin Van Niejenhuis, Peter Loudfoot, Leah Kristufek, and Ibrahim Ogunsanya, for their support and assistance throughout my graduate career. I would like to thank the University of Waterloo laboratory technicians, Douglas Hirst, Richard Morrison, and Peter Volcic, for their expertise and assistance with the planning and execution of the experimental portion of this research. I would also like to thank the many other graduate students who assisted with this project: Dylan Dowling, James St. Onge, Nicholas Charron, Kyle Balkos, Graeme Milligan, and Tim Tedford, without whom the experimental coring and testing would not have been possible.

I would like to thank the Ministry of Transportation of Ontario and its representatives for assistance with sample testing, collaboration with pre-cast manufacturers, feedback on project progress and direction, and funding. I would also like to thank the local ready-mix concrete producers and pre-cast manufacturers for providing the materials and construction of structures which allowed this research to be conducted on various concrete mixtures and construction environments.

Finally, I would like to thank my family and friends who supported me throughout my graduate studies.

Table of Contents

List of Figures

List of Tables

Chapter 1
Introduction

1.1 Background

Concrete has been used in construction for thousands of years, dating back to ancient Egyptian and Roman eras [6]. These early civilizations understood the simple properties of concrete: a quick hardening mixture that is strong in compression, but weak in tension. The Egyptians used mud and straw at the beginning, moving to lime and gypsum for use in pyramid construction [6]. The Romans built mainly with stone and mortar construction, with the mortar hardening through exposure to the carbon dioxide in the air, and not through chemical hydration as with concrete nowadays. For more important structures, naturally reactive volcanic sand was used. When this sand was paired with lime, which is crushed and burned limestone, and water, it hydrated and hardened. This was one of the first mass produced cementitious materials and was used to build countless wonders of the Roman Empire, including the Pantheon, the largest unreinforced concrete dome ever constructed [6]. The Romans utilized admixtures in this early concrete mixture, such as animal fat, milk, and blood [6]. However, the art of concrete manufacturing was lost when the Roman Empire fell, and progress was not made until 1793 when a method for producing lime through limestone containing clay was discovered. Portland cement was invented in 1824 when the proportions of finely ground clay and gypsum burned in a kiln and ground into a powder were refined. This cement was named “Portland” because, when hardened, it resembled the stone in Portland, England. Over time, this process was further refined, including the introduction of gypsum in the grinding process, controlling the rate of setting which allows more time for placement, the invention of rotary kilns by Thomas Edison in 1909, and air entrainment agents in 1930, which allows for greater resistance to freezing [6].

As time passed, more and more additives were created for the use with concrete mixtures, including supplementary cementitious materials (SCMs), superplasticizers, and retarders. SCMs were often unused byproducts of other industries such as coal combustion, iron and steel production, and ferro-silicon alloy production. When SCMs were first introduced into concrete mixtures, they were a cheap alternative to replace a portion of the cement required, as previously, the owners were discarding these SCMs. Some of these SCMs even enhanced the properties of the concrete mixture and the hardened concrete, and over time, SCMs were sought after for these benefits. With the decreasing coal combustion, recycling and importation instead of production of other materials, SCMs increased in price and became less common.

However, in recent years, due to the environmental impact of cement production, regulatory agencies have started to dictate a minimum amount of SCMs in concrete mixtures to reduce the environmental impact of concrete construction.

Many of the standards and codes relating to concrete testing were established in the period when SCMs were not common in the average concrete mixtures [2–4, 7]. However, over the past two decades, since the research conducted underlying these standards and codes was completed, the concrete construction industry has evolved, requiring stronger concrete, faster turnarounds, and better durability. The concrete mixtures have changed greatly to compensate, increasing the amount of cementitious materials in the mixture, introducing chemical admixtures to allow for ease of construction, and incorporating varying types and amounts of SCMs to achieve the performance required. All these changes alter the behaviour of both fresh and hardened concrete. Thus, some of the standards and codes established on the old concrete may not be accurate for modern concrete.

1.2 Research Significance

The Ontario standards currently allows for coring of a 100 mm diameter sample with length-to-diameter (*l/d*) ratio of 2 to be conducted between 7 and 10 days after casting and testing of these cores on day 28. The specified diameter, *l/d* ratio, allowed coring time, and how the core is stored between coring and testing have been defined through research conducted decades ago. In the ever-evolving industry of concrete construction, the effect of these parameters on the compressive strength of a concrete sample may have also changed. Understanding how these parameters effect modern concrete samples can allow for better use of extracted cores. However, if these parameters could be changed while still presenting the same results, the concrete industry could become more efficient and accurate, by potentially using smaller, less invasive cores for evaluation of the concrete structure.

1.3 Research Objectives

The main objective of this thesis is to determine those parameters that effect the results of a compressive strength test on core samples extracted from modern concrete mixtures. These include:

- Conditioning procedure: Comparison of the currently practiced conditioning states of concrete samples to determine which one leads to a more reproducible better result: soaked in a solution of saturated calcium hydroxide or dry sealed in plastic,
- Location and direction of coring: Determination of whether the location from which the core is extracted, with respect to the length and height along the sample, and direction of extraction,

perpendicular or parallel to the direction of concrete casting, effects the compressive strength of the core,

- Core dimensions: Verification of the current *l/d* ratio strength correction factors utilized in current codes with modern concrete mixtures,
- Diameter effects: Determination of the differences between 100 mm and 75 mm diameter cores with respect to the effects on the compressive strength test result.

All of the above objectives will lead to the conclusion of the optimal coring parameters for a 150 mm thick girder web, mainly: 100 mm diameter at 150 mm length (*l/d* ratio = 1.5) or 75 mm diameter at 150 mm length (*l/d* ratio = 2).

Chapter 2
Literature Review

This chapter discusses the literature on the topics related to this thesis. These topics include how modern concrete mixtures change the properties of concrete, factors which affect the compressive strength of concrete samples, and factors which affect the length-to-diameter ratio strength correction factor. While the effects of the constituents of the concrete mixture are not directly investigated in this thesis, some results obtained may be related to these different constituents; and therefore, a brief understanding of how these various constituents change the concrete properties is given.

2.1 Concrete Mixtures

The standards and code related to compressive strength testing and coring are mainly based on research conducted decades ago [2–4]. The concrete mixtures utilized have changed drastically since that research has been conducted. Nowadays, supplementary cementitious materials (SCMs), chemical admixtures, and different cements are commonplace in modern concrete mixtures. These constituents of the concrete mixtures are ever changing and can change the properties of the hardened concrete, which may affect the relationships found in the research that are used as a basis for the codes and standards. The SCMs included in modern concrete mixes include blast furnace slag, fly ash and silica fume, while admixtures, such as superplasticizers and retarders are also used frequently. In precast applications, high early (HE) strength cement is used for a faster turnaround in production. The following sections will discuss in detail how each of these affect the performance of concrete in terms of compression strength and durability, as well as other miscellaneous properties.

2.1.1 Supplementary Cementitious Materials (SCMs)

SCMs are added to the concrete mixture to reduce the amount of Portland cement used, for both environmental and financial reasons, and to improve the properties of the concrete in both the hardened and wet phases. Blast furnace slag is typically added to reduce the heat of hydration and improve workability [8–10]. Fly ash is added to allow for long-term strength development [11, 12]. Silica fume is added to increase the density of the microstructure, due to the extremely fine particles, which results in more durable and stronger concrete [13–16]. The next sections will discuss in more detail about these SCMs.

2.1.1.1 Ground Granulated Blast Furnace Slag

Ground granulated blast furnace slag (BFS) is an SCM which is a byproduct in the production of iron. The production of BFS can be controlled to ensure a low variability in the material and chemical properties. The BFS particles are small and smooth compared to cement [17], which increases workability of fresh concrete, but also increases the cohesiveness [9]. With a high fineness, BFS can also reduce bleeding [18]. The hydration reaction of BFS requires a high pH to initiate, which results from cement hydration [10]. Due to this requirement, the reaction is delayed, and a concrete containing BFS retards the hydration reaction at normal temperature by about 30-60 minutes [9]. Due to this delayed and continuous reaction, BFS provides a reduced heat of hydration, and a long-term strength gain [10], as shown in Figure 2.1.

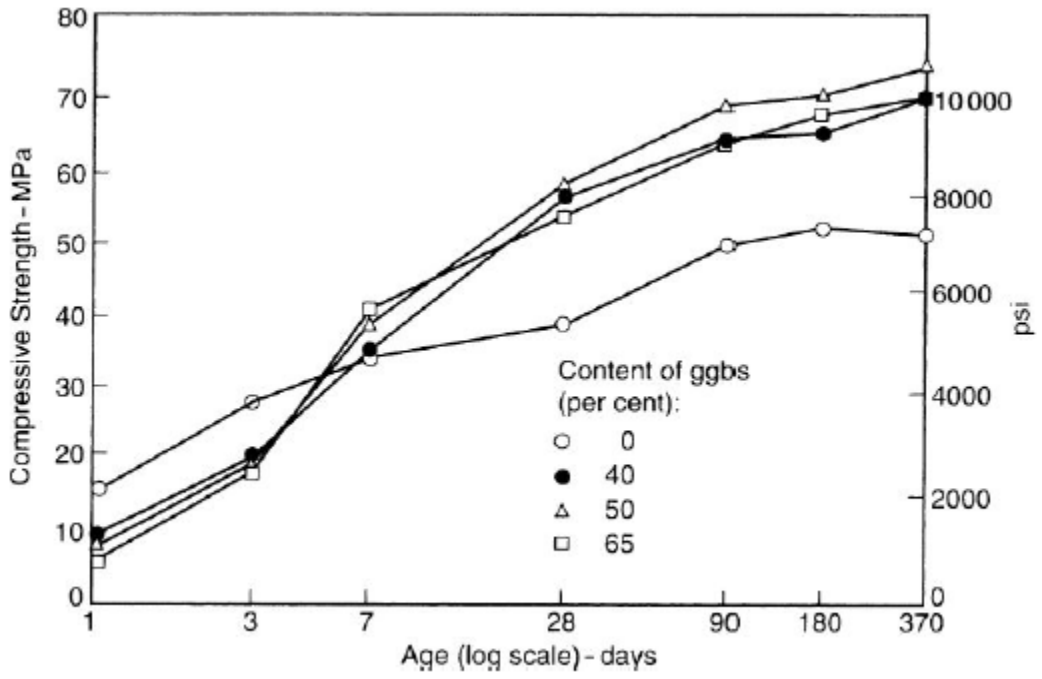

Figure 2.1: Compressive Strength of Concrete Cubes Containing Varying Amounts of BFS by Mass of Total Cementitious, Moist Cured at Room Temperature [10, 18]. Reprinted with Permission from Pearson Education Limited [18]

The use of steam curing on BFS concrete mixtures is beneficial as the reactivity of BFS increases at higher temperatures [14, 19]. Conversely, very low temperatures hinder the reaction, resulting in poor strength development below 10°C [20, 21]. From a durability standpoint, the denser microstructure and the increase in C-S-H, which is the main product of hydration, precipitated in the pore water, caused by the inclusion of BFS, decreases the permeability of the concrete [21, 22]. This decreased permeability

also decreases chloride diffusion [14, 21, 22]. However, the decreased permeability of BFS concrete mixture does not increase the concrete's resistance to freeze-thaw damage [8, 9, 18].

2.1.1.2 Fly Ash

Fly ash is a SCM which is obtained as a byproduct from coal power generation process [18]. There are three classifications for fly ash under ASTM C618 - Coal Fly Ash and Raw or Calcined Natural Pozzolan for Use in Concrete: Class N, Class F, and Class C [23]. The physical properties, including fineness, strength, water requirement, etc., are the same for each classification, with the chemical compositions differing [23]. Class F and Class N have similar chemical compositions as they are both acting as pozzolans, whereas Class C fly ash has both pozzolanic and cementitious properties and, thus, different chemical properties [23].

Fly ash requires a high alkalinity of the pore water to react, and when silica fume or blast furnace slag is also included in a concrete mixture, the alkalinity is reduced [24]. When included in a concrete mixture, fly ash typically reduces the water demand by 5-15% and increases workability [25, 26]. Fly ash also increases the long-term strength of concrete, compared to concrete mixtures containing cement only, by its pozzolanic nature and similar particle size to cement, with both fly ash and general use cement averaging at 10 μm in diameter [11, 12], allowing for good particle compaction [18]. From a durability standpoint, fly ash reduces the long-term permeability of the concrete, but can increase the rate of carbonation [27]. In fresh concrete, fly ash is more cohesive, has a reduced bleeding capacity, and has a slight retarding effect on the initial set time compared to a concrete mixture containing cement only [18]. The hydration process of fly ash is slow compared to Portland cement, and thus, and extended wet cure cycle is usually recommended [9]. This reaction rate increases as the temperature increases [9]. In large elements, the heat generated by the cement hydration accelerates the fly ash reaction and the properties of the concrete in the early days would differ from that of a smaller section, which results in standard cylinders not accurately representing the concrete element in the early days [18].

2.1.1.3 Silica Fume

Silica fume is a relatively new SCM, compared to BSF and fly ash. Silica fume is a byproduct of the manufacturing of silicon and ferrosilicon alloys and is pozzolanic in nature [18]. The production of silica fume is usually consistent in chemical and properties [18]. The particle size of silica fume is extremely small, with an average diameter of 0.15 μm [28], even when compared to other SCMs and cement and, thus, has high reactivity with the calcium hydroxide produced by the hydration of cement [18]. Silica fume has been found to significantly reduce bleeding, and increase the cohesion of the concrete mixture

[13, 29]. Due to the denser microstructure, silica fume decreases the permeability of the concrete, [29, 30], which results in an increase to the electrical resistance [31, 32], as well as a decreased chloride diffusion rate [14–16]. Due to its fineness, silica fume reacts quickly, and thus improves the early compressive strength of concrete containing silica fume [13]. This increased reactivity also increases the heat of hydration [13], and requires additional moist curing otherwise drying shrinkage is a possibility [18].

2.1.2 Chemical Admixtures

The use of chemical admixtures has been common in modern concrete. These admixtures can be natural or manufactured and can change the properties of both fresh and hardened concrete. Two common admixtures are superplasticizers, also known as high range water reducing agents, which are used to increase the workability of the fresh concrete without increasing the amount of water in the mixture, and set retarders, which delay the initial set of the fresh concrete to allow for more time during transport and placement. The next sections will discuss how these admixtures can affect the fresh and hardened concrete.

2.1.2.1 Superplasticizers

ASTM C494 - Standard Specification for Chemical Admixtures for Concrete discusses: retarding, water-reducing, and accelerating admixtures, and the combinations of these [33]. Superplasticizers are classified as water-reducing admixtures and are high range water-reducing agents. Modern superplasticizers are water-soluble organic polymers, typically lignosulphates or polycarboxylates, which are manufactured using a complex polymerization process. There are many parameters of the polymer which can be changed to affect how the superplasticizer effects the concrete performance, such as molecular mass, length of polymers, amount of cross-linking, and the molecular base [18]. The purpose of a superplasticizer is to increase the workability of fresh concrete and does so by inducing the cement particles with a negative charge, resulting in the cement particles repelling each other as well as water molecules [34]. With the use of a superplasticizer, a concrete mixture with a slump of 75 mm can become 200 mm when the superplasticizer is added [35]. A more typical use of superplasticizer is to produce a high strength concrete, by reducing the w/cm ratio, while keeping normal workability. No long-term effects of superplasticizers on the concrete compressive strength have been observed [18].

2.1.2.2 Retarders

Retarding admixtures slow the hydration reaction of concrete, to allow for more time to transport, and place the concrete. Retarding admixtures are popular in ready-mix concrete facilities to ensure that the concrete reaches the construction site in an acceptable condition, or in high-temperature scenarios, as increased ambient temperatures increases the reaction rate of concrete. The use of retarders in concrete mixtures tend to increase the plastic shrinkage, but drying shrinkage is not affected [18, 36]. This is due to the increased duration of the plastic stage of the concrete. Retarders have shown to have no effect on the compressive strength of the concrete [37].

2.1.3 High Early Strength Cement

High early (HE) strength cement is commonly used in precast concrete manufacturing to facilitate a fast turnaround on their products. High early strength cement usually has a higher C_3S content, and a more finely ground cement clinker than regular general use (GU) cement, both of which increase the reaction rate, and early strength gain. Due to the increased rate of hydration, the internal concrete temperature caused by hydration is also increased, compared to GU mixture, and as such, the temperature gradients of large elements can be difficult to control.

2.2 Factors Effecting Concrete Compressive Strength

Many studies have been conducted to determine the parameters that affect the compressive strength of concrete cores and cylinders. Some of the parameters investigated are discussed in this section.

2.2.1 Conditioning of Samples

The conditioning of the concrete cylinder or core refers to how the sample is stored after the core is extracted and before testing. This does not refer to the curing of a large concrete element. ASTM C42M [2] states that moisture conditioning involves wiping water from drilling of the core and allow the surface moisture to evaporate. After surface drying, but not later than 1 hour after drilling, the cores are to be sealed in individual containers or plastic bags until testing. A 2-hour window is permitted for wet sawing or end grinding, no later than 2 days after coring, after which the core must surface dry before being placed back in a sealed container. This process must be competed at least 5 days before testing to reduce any moisture gradients present in the sample [2]. This method of conditioning seals in the moisture with the sample until the testing day. If there is not enough water sealed inside, hydration cannot be fully completed. For concrete mixtures with w/cm ratios above 0.5, the amount of water present is adequate for hydration [38]. However, many modern concrete mixtures utilize w/cm ratios less than 0.5 and additional

water may be required for curing. The effects of inadequate curing are more pronounced on concrete mixtures which have a lower rate of strength development, such as those containing fly ash or BFS [39].

ACI 214.4R-10 [3] describes the effects of three conditioning methods on the results of the compressive strength test: air-dried, soaked, and standardized moisture conditioning. Air-dried samples, which are samples left out in open air at 16-21°C at an RH less than 60% for 7 days, have been found to have an on average 10-14% higher strength than the other conditioning types due to the drying shrinkage on the surface of the sample which induces a biaxial compression on the core of the sample, thus increasing the samples compressive strength [3]. Soaking the sample saturates the internal pores of the concrete which, when subject to an external load, is limited in migration due to the smallness of the capillary pore sizes. This would then cause pressure on the pore walls which would magnify any crack propagation and reduce the maximum external load the sample could carry [40]. Standardized treatment refers to the method specified above by ASTM C42M [2].

2.2.2 Location of Extracted Core

The location of the extracted core refers to where the core is drilled from a concrete element. This location is described by the height and length along the element as well as the depth within the element from which a core is extracted. The height of the specimen has been known for many years to affect the strength of the concrete, due to bleed water rising to the top of the specimen when the concrete is still fresh, resulting in a local area with a higher w/cm ratio and thus a lower strength [3, 41]. This effect can be seen in a height difference as little as 30-80 cm [41–43]. However, high-strength concrete may not follow this trend as the amount of bleed water diminishes with low w/cm ratios and this effect may not be present [44]. As discussed in Section 2.1, SCMs, such as silica fume [13, 18, 29], blast furnace slag [18], and fly ash [18], also reduce the amount of bleed water in the fresh concrete, and are common in high-strength and high-performance concrete. However, more research is needed in this area to determine if SCMs reduce the height effect.

The length along, and depth within, the specimen may affect the strength of the concrete in the earlier days as inner sections of the specimen would generate and retain heat better than outer sections [44]. This increased heat in the inner sections of the specimen would increase the reaction rate of the hydrating cement, allowing the inner sections to develop strength faster than the outer sections [18].

Other than the location within the geometry of the section, extracting a core from a flexural member under load cannot be relied upon due to microcracks and other large cracks that are present which reduce the compressive strength of the sample [45].

ACI 214.4 [3] and ASTM C42M [2] do not specify any modifications or guidelines on the location to extract cores for the use of compressive strength testing. However, ASTM C42M does contain a warning which states “concrete at the bottom tend[s] to be stronger than the concrete at the top” and to consider this in planning locations for obtaining cores [2].

2.2.3 Coring Direction of Sample

The coring direction refers to the direction from which the core is extracted relative to the direction of casting. If the core is extracted parallel to the direction of casting, the coring direction is said to be vertical, whereas perpendicular cores are said to be horizontal, since concrete is normally cast vertically, the vertical and horizontal nomenclature refers to the placement direction of the coring drill.

The effect of the direction from which the core is extracted from a concrete element on the strength of the extracted sample has been debated. The theory follows that as the concrete cures, excess bleed water settles under aggregates and creates a plane of weakness, as shown in Figure 2.2 below [41]. When cores are extracted horizontally, this plane of weakness aligns with the axis of force during the compressive test, and decreases the strength of the sample [41]. However, as discussed previously, modern concrete mixtures, incorporating SCMs and lower w/cm ratios, can reduce the amount of bleed water and may negate this effect. Multiple studies have found that cores drilled horizontally resulted in lower compressive strengths compared to cores drilled vertically [41, 46, 47], while others [48] found there was no significant difference.

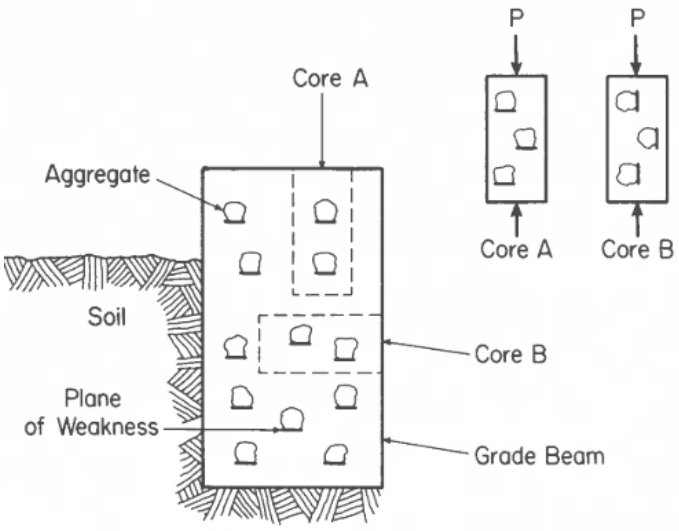

Figure 2.2: Plane of Weakness Caused by Bleed Water for Cores Extracted Horizontally and Vertically [41]. Reprinted with Permission from Elsevier [41]

2.2.4 Diameter of Sample

The diameter of a sample effects the compressive strength of the concrete by general size effects. There are two main theories on the size effects on the compressive strength of concrete samples: weakest link theory [49, 50] and summation of strength theory [49, 51]. The weakest link theory states that larger volume specimens are more likely to contain a defect, which lowers the overall strength of the specimen [49]. The summation of strength theory states that the strength of a specimen is the sum of the strengths of each individual part of specimen, which implies that the size of the specimen does not affect the strength [49, 51]. Bartlett and MacGregor [49] found that any observable size effects are too small and are overpowered by the variation in the strengths of the smaller diameter cores, as the smaller diameter cores were more variable [47, 52, 53]. Yip and Tam [43] suggested that five 50 mm cores had a similar variability in strengths as three 100 mm cores.

Smaller samples appear to be more susceptible to many factors including moisture, concrete mixture properties, coring damage, and testing procedures [54]. The relative strength loss due to soaking 50 mm diameter cores for 2 days before testing is more severe than soaking 100 mm diameter cores, due to the higher surface area to volume ratio of smaller diameter cores [55]. Another observed effect was that, as the core diameter decreases, larger aggregate sizes caused the strength of the core to decrease [52, 53]. When the concrete sample is a core, a smaller diameter core magnifies the effect of damage caused by coring by increasing the surface area to volume ratio of the core. This damage effect caused by coring will be discussed in detail in Chapter 2.3.5.

2.2.5 Reinforcement Present in Sample

ACI 214 [3] recommends trimming the core to remove the reinforcement as long as the required *l/d* ratio is maintained, while ASTM C42M [2] recommends not using cores with embedded reinforcement. However, if there is no possibility to extract a core that does not contain embedded reinforcement perpendicular to coring direction, then testing a sample is allowed under ASTM C42M, with discretion from the engineer, as a strength correction factor has not been accepted for cores with embedded reinforcement [2].

Some studies have been conducted on the effects of embedded reinforcement in concrete test specimens. Gaynor [56] found that the embedded reinforcement reduced the strength of cylinders by 4 to 9% for one bar of reinforcement. Loo et al. [57] conducted a study with 174 cylinders and 24 cores including steel reinforcement with diameters ranging from 6-20 mm, and concluded that the effect of steel reinforcement on the strength of the cylinders varied greatly with the *l/d* ratio of the cylinder. The

cylinder strengths decreased with the inclusion of steel reinforcement at *l/d* ratio of 2, and the effect of the embedded reinforcement decreases as the *l/d* ratio decreases to 1.0, at which point there are no significant effects on the cylinder strength [57]. Plowman et al. [58] found that the strength loss in the cylinders was maximized when the bar was located at the very center of the cylinder.

2.3 Length-to-Diameter (*l/d*) Ratio Strength Correction Factors (SCFs)

Standard practices of cylinder and core testing require the sample to have a length-to-diameter (*l/d*) ratio of 2 [2, 4, 59]. In some instances, achieving this *l/d* ratio is not possible and samples of lower *l/d* ratios are obtained, in most cases these samples are cores. Due to the method of testing, the platens at the top and bottom of the testing frame restrain lateral expansion and provide confinement of the sample [60, 61]. At an *l/d* ratio of 2, this effect is nearly negligible, while with a smaller *l/d* ratio, this effect is more prominent, and thus the strength of a shorter sample will be higher than those of standard length. As such, many studies have been conducted to investigate this effect and quantify the amount by which the strength is increased at lower *l/d* ratios. These studies ultimately found a strength correction factor (SCF) which is applied to samples with *l/d* ratios lower than 2 to normalize the strength of the sample to the standard size sample [7, 62–67].

2.3.1 *l/d* Ratio Strength Correction Factor (SCF) Models

Various studies have been conducted which generated a model to represent the SCF for different *l/d* ratios. One of the earliest studies to quantify the relationship between the strengths of different *l/d* ratios comes from the Concrete Society in 1976 [64] which proposed the following model:

$$F_{l/d} = \frac{2}{1.5 + d/l} \tag{2.1}$$

Chung, in 1979 [65], proposed the following model based on a semi-rational approach:

$$F_{l/d} = \frac{1}{1 + 0.8[1 - 0.5 * (l/d)]^2} \tag{2.2}$$

which included the Poisson's ratio of concrete near failure to obtain the 0.8. This model was valid for *l/d* ratios of 1 to 2. Chung later revised this model in 1989 [66] to include smaller cores with *l/d* from 0.4 to 2:

$$F_{l/d} = \frac{1}{1 + \frac{0.8}{l/d}[1 - 0.5 * (l/d)]^2} \tag{2.3}$$

Bartlett and Macgregor, in 1994 [7, 63], aggregated data from multiple sources with concrete containing ordinary Portland cement, ranging in compressive strength from 13.5 MPa to 95 MPa and created a model through non-linear weighted regression:

$$F_{l/d} = 1 - [0.117 - 4.3 * 10^{-4} * f_c]\left(2 - \frac{l}{d}\right)^2 \quad (2.4)$$

where f_c is the compressive strength of the unadjusted core with a *l/d* ratio not equal to 2, in MPa. In total, three models created with this form. Equation (2.4) above is for the case where the cores are soaked for 48 hours before testing in water. Other cases include standard treatment according to ASTM C42M [2], and dried for 7 days. These equations form the basis of the current standards and codes, including ASTM C42M [2], ACI 318 [68], and CSA A23.1 [4].

A more recent study conducted by Arioz et al. in 2006 [67] found a logarithmic model fit their data best:

$$F_{l/d} = 0.1385 \ln(l/d) + 0.9069 \quad (2.5)$$

With all the models discussed above, the following table shows the values of the *l/d* SCF for the various *l/d* ratios.

Table 2.1: Summary of *l/d* SCF from Various Models

Source	Equation Number	*l/d*=2.0	*l/d*=1.75	*l/d*=1.50	*l/d*=1.25	*l/d*=1.0
Concrete Society [64]	(2.1)	1.000	0.966	0.923	0.870	0.800
Chung 1979 [65]	(2.2)	1.000	0.988	0.952	0.899	0.833
Chung 1989 [66]	(2.3)	1.000	0.993	0.968	0.917	0.833
Bartlett and MacGregor Soaked [7, 63]	(2.4)	1.000*	0.993*	0.974*	0.941*	0.896*
Arioz et al. [67]	(2.5)	1.003	0.984	0.963	0.938	0.907
ASTM C42-18 [2]	N/A	1.000	0.980	0.960	0.930	0.870

* Calculated assuming f_c = 30 MPa

The SCF factors of Arioz et al. [67] and Bartlett and MacGregor [7, 63] are similar, and Arioz el al. state that the SCF found in their study was found to be very close to those proposed by Bartlett and MacGregor. In these two studies, the concrete mixture utilized are similar, with approximately 330 kg/m^3 of Portland cement used, and w/cm ratios of 0.55 and 0.60. Arioz et al. did not include superplasticizer or a water reducing admixture in their concrete mixtures, while 3 of 10 specimens utilized in Bartlett and MacGregor's study contained a superplasticizer. However, these concrete mixtures are not common in the

high-performance industry nowadays. For example, the concrete mixtures utilized by precast manufacturers for bridge girders contain upwards of 450 kg/m^3 of high-early strength cement and w/c ratios as low as 0.30. The vast difference in the concrete mixtures themselves, as well as the curing environment and other factors, could lead to difference results on the *l/d* SCFs. Since these studies have been conducted, the concrete industry has also moved towards including more supplementary cementitious materials (SCMs) to mitigate the environmental impacts of cement [69], which, as discussed in Chapter 2.1.1, can change the properties of the concrete significantly.

These models, particularly the model created by Bartlett and MacGregor [7, 63], considered the method of conditioning the sample, the location from which the sample was extracted, the compressive strength of the sample, diameter of the core, presence of reinforcement bars in the extracted core, and the damage caused by coring. Some of these factors were found not to be statistically relevant for the data set and were removed from consideration. However, they may have an effect in other data sets. The following section discusses in more detail how each of these parameters may affect the *l/d* ratio SCF. The final model created by Bartlett and MacGregor [7, 63], which was adopted by ACI 214.4R [3], is shown in Table 2.2.

2.3.2 Conditioning of Samples on *l/d* Ratio SCF

The effects of conditioning on the compressive strength of a sample are discussed above in Section 2.2.1. The effects that the conditioning type have on the *l/d* ratio have been included in the model created by Bartlett and MacGregor [7, 63]. The three conditioning states discussed previously, air-dried, soaked, and standardized moisture conditioning, are included in the model and adopted by ACI 214.4R-10 [3, 7, 63]. As discussed in Section 2.2.4, smaller samples appear to be more susceptible to the different conditioning types [54].

2.3.3 Location of Extracted Core on *l/d* Ratio SCF

The general effects that location has on the compressive strength of the core were discussed previously in Section 2.2.2. Bartlett and MacGregor, in their model for *l/d* ratio SCFs shown in Table 2.2, had considered these effects [63]. The *x* (length along specimen), *y* (height along specimen), and *z* (depth within specimen) coordinates for the location of each core were considered, and a modification factor based on these locations was applied to each core's compressive strength before a non-linear weighted regression was completed to develop the model above. Bartlett and MacGregor found the *y* coordinate, was significant in almost all of the elements investigated, while the *x*, and *z* coordinate respectively, were

Table 2.2: Magnitude and Accuracy of Strength Correction Factors for Converting Core Strengths Into Equivalent In-Place Strengths [3, 7, 63]. Authorized Reprint from ACI 214.4R-10 [3]

	Factor	Mean value	Coefficient of variation *V*, %
$F_{\ell/d}$: ℓ/d ratio[†]	Standard treatment[‡]:	$1 - \{0.130 - \alpha f_{core}\}\left(2 - \frac{\ell}{d}\right)^2$	$2.5\left(2 - \frac{\ell}{d}\right)^2$
	Soaked 48 hours in water:	$1 - \{0.117 - \alpha f_{core}\}\left(2 - \frac{\ell}{d}\right)^2$	$2.5\left(2 - \frac{\ell}{d}\right)^2$
	Dried[§]:	$1 - \{0.144 - \alpha f_{core}\}\left(2 - \frac{\ell}{d}\right)^2$	$2.5\left(2 - \frac{\ell}{d}\right)^2$
F_{dia}: core diameter	2 in. (50 mm)	1.06	11.8
	4 in. (100 mm)	1.00	0.0
	6 in. (150 mm)	0.98	1.8
F_{mc}: core moisture content	Standard treatment[‡]:	1.00	2.5
	Soaked 48 hours in water:	1.09	2.5
	Dried[§]:	0.96	2.5
F_d: damage due to drilling		1.06	2.5

[*]To obtain equivalent in-place concrete strength, multiply the measured core strength by appropriate factor(s) in accordance with Eq. (9-1).
[†]Constant α equals $3(10^{-6})$ 1/psi for f_{core} in psi, or $4.3(10^{-4})$ 1/MPa for f_{core} in MPa.
[‡]Standard treatment specified in ASTM C42/C42M.
[§]Dried in air at 60 to 70°F (16 to 21°C) and relative humidity less than 60% for 7 days.

only significantly in roughly half the elements [63]. ACI 214.10 [3], which adopted the model generated by Bartlett and MacGregor [63], does not include information about adjusting the strength of the extracted cores based on the location, only to extract cores from a random location to limit the location effects on the compressive strength.

2.3.4 Diameter of Sample on *l/d* Ratio SCF

In addition to the effects the diameter of the concrete sample has on the compressive strength, discussed previously in Chapter 2.2.4, the diameter of the sample also influences the *l/d* ratio SCF. Arioz et al. [52] and Bartlett and MacGregor [49] found that the *l/d* effect is greater for smaller diameter cores. At smaller diameter, effects such as aggregate size, coring damage, and conditioning type all influence the sample more than at larger diameters [54, 70]. Thus, Bartlett and MacGregor found the SCF of about 0.80 should be used for a 2 inch diameter core, instead of 0.88 for 4-inch diameter cores, at a *l/d* ratio of 1. Bartlett and MacGregor [7, 49] suggested a SCF for use with different diameter cores, shown above in Table 2.2, in conjunction with in the *l/d* ratio SCF.

2.3.5 Damage Caused by Coring on *l/d* Ratio SCF

The prevailing theory behind how coring effects the strength of a concrete core sample is that coring causes damage on the outer region of the core [71]. Coring can cause surface damage such as microcracking, which reduces the compressive strength on the outer region of the core [49, 72]. If the damaged region is assumed to have a constant thickness, regardless of diameter, the volume proportion of the damaged region will increase as the core diameter decreases, resulting in smaller diameter cores having a lower compressive strength [49, 72]. Arioz et al. [52] found that as the concrete strength increased, the effect of the damage caused by coring decreased. However, Malhotra [73] found the opposite, such that higher strength concretes had a lower core compressive strength, which was attributed to a higher resistance to drilling resulting in increased microcracks or other damage to the core. Overall, ACI 214 [3] includes a factor of 1.03 for damage caused by coring, as seen previously in Table 2.2, based on the research conducted by Bartlett and MacGregor [7, 63]. The compressive strengths seen in Bartlett and MacGregor varied from 20 MPa to 90 MPa [7, 63]; however, this factor does not include a provision about the compressive strength of the cores.

2.3.6 Reinforcement Present in Sample on *l/d* Ratio SCF

As discussed in Chapter 2.2.5, reinforcement present in the concrete sample lowers the compressive strength. This effect varies depending on the *l/d* ratio of sample [57], with the effect decreasing as the *l/d* ratio decreased. The location of the reinforcement within the sample also effects the amount the compressive strength is decreased, with the largest decrease occurring when the reinforcement is in the center of the sample [57]. There are no studies on how reinforcement within a sample directly effects the *l/d* ratio SCF.

2.3.7 Coring Direction on *l/d* Ratio SCF

No studies investigating the effect coring direction has directly to the *l/d* ratio SCF were found; however, as discussed above in Chapter 2.2.3, there are studies which show that cores drilled horizontally resulted in lower compressive strengths compared to cores drilled vertically [41, 46, 47], while others [48] found there was no significant difference. As stated previously, this decrease in strength may have been caused by bleed water, and many modern concrete mixtures have reduced amounts of bleed, and thus, this decrease may not be seen.

2.4 Summary of Literature Review

In summary, the parameters which effect the compressive strength of concrete samples have been studied thoroughly in the past. However, modern concrete mixes, which include SCMs and low w/cm ratios can have high strengths and can change the material properties of wet and hardened concrete. Changing the material properties of the concrete can change the relationships which were discussed in the previous sections. There is a lack of research on how these modern concrete mixtures affect the relationships of these various parameters. This thesis will discuss some of the parameters, namely the *l/d* ratio, diameter of sample, and conditioning of samples, and how modern concrete mixtures affect each of these parameters.

Chapter 3
Experimental Program

The following sections discuss the tests conducted on the samples and the structures investigated.

3.1 Tests Conducted

The tests conducted on cores and cylinders from the structures described in Section 3.2 during this project include: (i) compressive strength test, (ii) air void system, (iii) rapid chloride permeability test, and (iv) electrical resistivity measurement.

3.1.1 Compressive Strength Testing

All samples, cores and cylinders, were tested in compression following CSA A23.2-9C – Compressive Strength of Cylindrical Concrete Specimens [4]. The samples were tested in a hydraulic compression testing machine, as shown below in Figure 3.1, using the loading rates specified in CSA A23.2-9C: 0.15 MPa/s to 0.35 MPa/s. The samples were end-ground (Figure 3.2) to provide flat, parallel surfaces, the diameter was measured with a digital caliper twice at mid-height, and the length was measured twice end-to-end. Peak loads of each sample were recorded, as well as the failure type. Descriptions of the cores and cylinders were also recorded before testing, noting any voids, large pores, or locations of poor consolidation, and photographs were taken before and after testing. These precautions were taken in the event an unexpected result occurs, in order to determine the cause of the abnormality. Compressive strength testing was completed at the University of Waterloo (UW) laboratory.

Figure 3.1: Compressive Strength Testing Machine

Figure 3.2: End-Grinding of Cores

3.1.2 Air Void Systems

The air void parameters (size and spacing of the voids) of the hardened concrete were determined by an MTO testing laboratory following the procedure outlined in LS-432 [74] and ASTM C457 [75]. This test was conducted by the MTO. Figure 3.3 below shows a sample after the test had been completed, and the sample returned to the UW lab. The results of this test are not included in this thesis, but are included elsewhere [1].

Figure 3.3: Air Void System Sample After Analysis

3.1.3 Rapid Chloride Permeability

The concrete's ability to resist chloride ion penetration was determined using the rapid chloride permeability (RCP) test outlined in LS-433 [76] and ASTM 1202 [77]. The test was conducted between day 28 and day 32 after casting.

The procedure of this test involved cutting two 50 mm thick samples from the core or cylinder. These test samples were then air dried for 1 hour, the outer edge sealed, then the samples were placed in a vacuum desiccator for 3 hours. De-aerated water was then used to saturate the sample while still under vacuum for an additional hour. The vacuum was then turned off and the sample soaked for 18 ± 2 hours. After these preparations were complete, the test samples were placed into the testing cell, shown in Figure 3.4. A NaCl solution was placed on one side of the sample, and a NaOH solution was placed on the other side. A 60 V potential difference was applied between the solutions, i.e. across the sample and the resulting current through the sample was monitored every 30 minutes, for 6 hours. If the temperature of the test sample exceeded 90°C, the test was terminated. The charge passed was calculated by using numerical integration, specifically trapezoidal rule, on the current-time data. The results of this test are not included in this thesis, but are included elsewhere [1].

Figure 3.4: RCP Test Apparatus

3.1.4 Electrical Resistivity Measurements

An alternative to the RCP testing procedure is a bulk electrical resistivity measurement of the concrete. There currently is no standard test procedure to follow. The sample was measured as stated above for

compressive strength testing and was then submerged in water for five minutes before testing. The test apparatus, shown in Figure 3.5, consists of electrodes placed on either end of the sample, with a saturated sponge placed between the contacts and the concrete sample. The contacts measure the electrical resistance between the electrodes using a two-point uniaxial method (bulk resistivity).

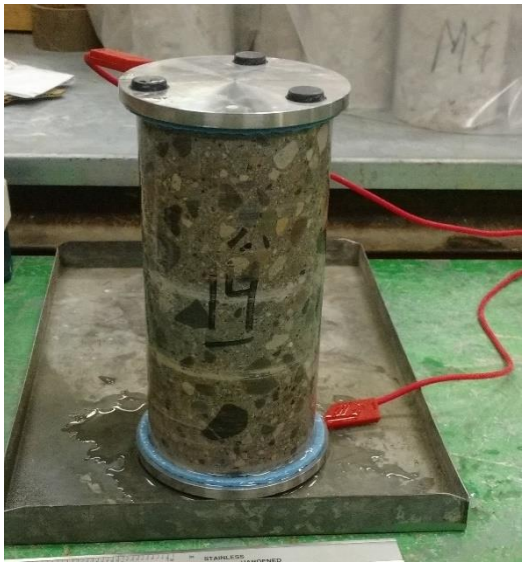

Figure 3.5: Electrical Bulk Resistivity Measurement

The resistivity, ρ, is calculated using a relationship between the measured resistance, R, and a geometry factor, k, which depends on the area, A, and length, L, of the sample being tested.

$$\rho = R \times k$$
$$k = \frac{A}{L} \tag{3.1}$$

The conductivity of the sample, which is the inverse of the resistivity measurement, has been found to have a linear relationship with charge measured in the RCP test, as shown in Equation (3.2) [78]:

$$Q = I * t = \frac{V}{R} * t = \frac{V}{\frac{L}{A}\rho} * t = \left(\frac{V * A * t}{L}\right) * \frac{1}{\rho} \tag{3.2}$$

where Q is the charge passed, I is the current passed, t is the time of the RCP test (6 hours), V is the voltage applied during the RCP test (60 V), L is the length of the RCP test sample (50 mm), A is the exposed area of the RCP test sample (100 mm diameter), and ρ is the electrical resistivity determined from this test.. As all the values in this equation except for ρ and Q are constant, the result of the RCP test, charge passed Q, and the electrical conductivity $1/\rho$ are linearly related [78]. The results of this test and the comparison to the RCP test are not included in this thesis, but are included elsewhere [1].

3.2 Structures Tested

The structural details, coring procedure and layout, concrete mixture, and curing regime are described below for each of the eight structures tested.

3.2.1 Beams B1 and B2

3.2.1.1 Structural Details

The first two sets of structures cast, cored, and tested were beams with a rectangular cross-section of 600 mm x 650 mm and a length of 2100 mm. Figure 3.6 shows the reinforcement details and dimensions of the beams. In total eight beams were cast: four from each set. The purpose of these beams was to simulate a large pier cap or abutment. Minimal steel reinforcement was placed to facilitate lifting and maneuvering the beams. A thermocouple was placed in the center of one beam from each set, to monitor the temperature throughout the testing period. The formwork was constructed of wood, and the same formwork was used for both sets of beams (Figure 3.7).

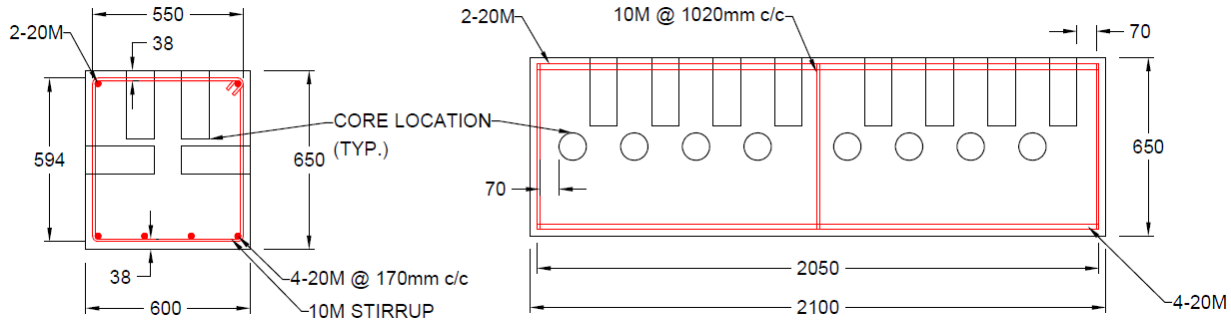

Figure 3.6: Structural Details for B1 and B2

3.2.1.2 Coring Procedure and Layout

Cores were drilled using a water-cooled diamond-tipped drill to a depth of 250 mm and broken out using a hammer and chisel. The samples were cut to a length of 200 mm to obtain a 2:1 length-to-diameter (*l*/*d*) ratio. Cores were extracted vertically from the top surface of the beam, and horizontally at mid-height of the beam, as shown in the cross section in Figure 3.6 above. In total, 4 beams were created for each cast and up to 32 cores were extracted from each beam, 16 vertically and 16 horizontally (Figure 3.8). The beams themselves were rotated instead of the coring drill for ease of coring.

Cores were extracted on days 3, 7, 14, and 28, and tested on days 3, 7, 28, and 56. On days 3 and 7, half the cored samples were tested after coring, and the other half were conditioned for testing on day 28.

Figure 3.7: Picture of Fresh Concrete in Wooden Formwork for Beams B1

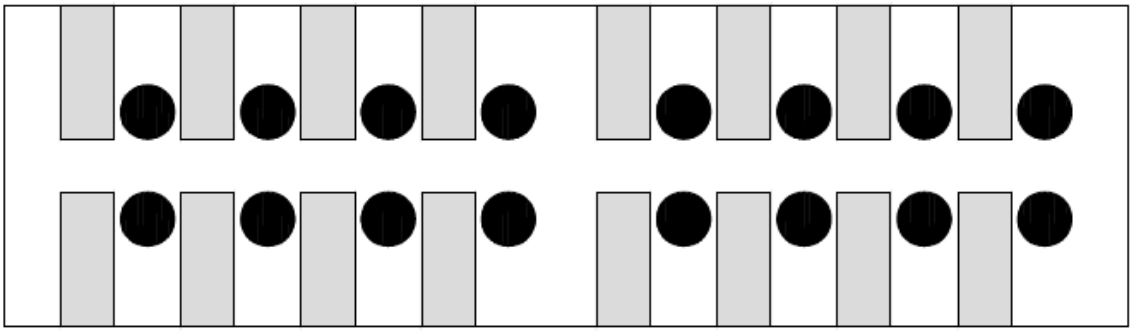

Figure 3.8: Top View Coring Outline for Beams B1 and B2

Conditioning consisted of either immersing the core in a calcium hydroxide solution or sealing the core in plastic in a dry state. On day 14, cores were extracted and conditioned until they were tested on day 28. Three of the cores extracted at day 28 were tested on the same day of coring, while the remaining cores drilled on day 28 were conditioned for testing on day 56. A summary of the core samples can be found in Table 3.1.

3.2.1.3 Core Sample Naming

The extracted cores were given an identification label depending on many parameters. The parameters which were recorded include: day cored, day tested, orientation of core (vertical or horizontal), side of beam extracted from (left or right with respect to the end of beam), and location along length of beam. The results of these cores are discussed in terms of an average of multiple cores and the exact location

Table 3.1: Core Sample Summary for Beams B1 and B2

Coring Date	Location	Test	Test Date	Conditioning	Quantity
Day 3/7/28[1]	Horizontal	Compression	Day Cored	N/A	3
Day 3/7/28[1]	Vertical	Compression	Day Cored	N/A	3
Day 3/7[2]	Horizontal	Compression	Day 28	Dry	3
Day 3/7[2]	Vertical	Compression	Day 28	Dry	3
Day 3/7[2]	Horizontal	Compression	Day 28	Saturated	3
Day 3/7[2]	Vertical	Compression	Day 28	Saturated	3
Day 3/7[2]	Vertical	RCP	Day 28	Dry	1
Day 3/7[2]	Vertical	RCP	Day 28	Saturated	1
Day 3/7[2]	Horizontal	RCP	Day 28	Dry	1
Day 3/7[2]	Horizontal	RCP	Day 28	Saturated	1
Day 3/7[2]	Vertical	Air Void	Day 28	Saturated	1
Day 3/7[2]	Horizontal	Air Void	Day 28	Saturated	1
Day 14	Horizontal	Compression	Day 28	Dry	3
Day 14	Vertical	Compression	Day 28	Dry	3
Day 14	Horizontal	Compression	Day 28	Saturated	3
Day 14	Vertical	Compression	Day 28	Saturated	3
Day 14	Vertical	RCP	Day 28	Dry	1
Day 14	Vertical	RCP	Day 28	Saturated	1
Day 14	Horizontal	RCP	Day 28	Dry	1
Day 14	Horizontal	RCP	Day 28	Saturated	1
Day 14	Vertical	Air Void	Day 28	Saturated	1
Day 14	Horizontal	Air Void	Day 28	Saturated	1
Day 28	Horizontal	Compression	Day 56	Dry	3
Day 28	Vertical	Compression	Day 56	Dry	3
Day 28	Horizontal	Compression	Day 56	Saturated	3
Day 28	Vertical	Compression	Day 56	Saturated	3

[1]These cores were extracted on days 3, 7, and 28, and all were tested on same day they were cored
[2]These cores were extracted on days 3 and 7, and all were tested on day 28

information is not included in the label (i.e. the side of beam and location along length of beam). Samples tested on the same day as they were cored were given the conditioning state of "Dry". Below are some examples of core and cylinder labeling:

Table 3.2: Core Sample Labelling Examples for Sets of Cores for Beams B1 and B2

Structure	Conditioning	Orientation	Day Cored	Day Tested	Label
B1	Saturated	Vertical	3	28	B1-S-V-3-28
B2	Dry	Horizontal	3	3	B2-D-H-3-3

Table 3.3: Cylinder Sample Labelling Examples for Beams B1 and B2

Structure	Conditioning	Day Tested	Label
B1	Saturated	28	B1-S-28
B2	Dry	3	B2-D-3

In some cases, parameters will be ignored. In those cases, the label will simply omit that parameter. For example, if a set of saturated cores from B1, cored on day 3 is discussed, regardless of the orientation of coring, the label would be "B1-S-3-28".

3.2.1.4 Concrete Mixture

The concrete mixture used for the B1 set of beams is a standard 30 MPa mixture used on MTO projects. The mixture contains general-use (GU) cement blended with blast furnace slag (BFS), and a 19 mm maximum aggregate size. The total cementitious content was 354 kg/m^3, with 9% being BFS. The water to cementitious materials ratio (w/cm) was 0.41. The slump at the time of casting was 90 mm, and the plastic air content was 4.8%. The detailed concrete mixture design can be found in Appendix A - Concrete Mixtures.

The concrete mixture used for the B2 set of beams is a High-Performance Concrete (HPC) that is a standard 50 MPa mixture used on MTO projects. The mixture contains general-use cement blended with silica fume (GUb-SF), and a 19 mm maximum aggregate size. The detailed mixture specifications were not provided by the concrete supplier, but the water to w/cm ratio was 0.35, the slump at the time of casting was 200 mm, and the plastic air content 6.0%.

3.2.1.5 Curing Regime

The curing regime for both structures was the same. The beams were covered in saturated burlap and plastic for 3 days after casting. On day 3, the beams were stripped from their formwork and cored to extract the day 3 samples. Afterwards, expansion plugs were placed into the core holes to limit moisture lost after the core was removed from the beam, as shown below in Figure 3.9. The beams were held in the UW laboratory at room temperature, without any cover, between coring days.

Figure 3.9: Photo of Expansion Plug Used to Seal Core Holes After Core was Removed

Cylinders were left to cure beside the beams until day 3, when they were removed from their moulds and placed in their respective conditioning state: moist cured in a moisture room or saturated in calcium hydroxide.

3.2.2 Girder Web G1

3.2.2.1 Structural Details

The third structure cast, cored, and tested in the UW lab was a wall with thickness 180 mm, width of 1715 mm, and height of 1615 mm (Figure 3.10). In total four walls were cast. One wall had thermocouples placed to monitor the temperature throughout the testing period, as shown in Figure 3.10. The purpose of this wall was to represent a precast girder web. The sections were reinforced with 10M bars in a grid with adequate spacing to extract cores, while simulating the dense reinforcement present in a precast girder web. Lifting anchors were placed in the top and on the face (not shown in Figure 3.10). Similar to the beams B1 and B2, these wall sections were cast in wooden formwork.

3.2.2.2 Coring Procedure and Layout

Cores were drilled through the wall, at a length of 180 mm, in two diameters: 100 mm and 75 mm. To facilitate coring, the walls were placed flat onto plywood and cores were drilled through the wall. The plywood assisted in preventing pop out of the cores. The cores were then cut to a length of 150 mm. This

length allowed the 75 mm diameter cores to have a *l/d* ratio of 2, while the 100 mm cores had a *l/d* ratio of 1.5. In total, 4 walls were cast; each coring day utilized one wall, to eliminate variable moisture lost

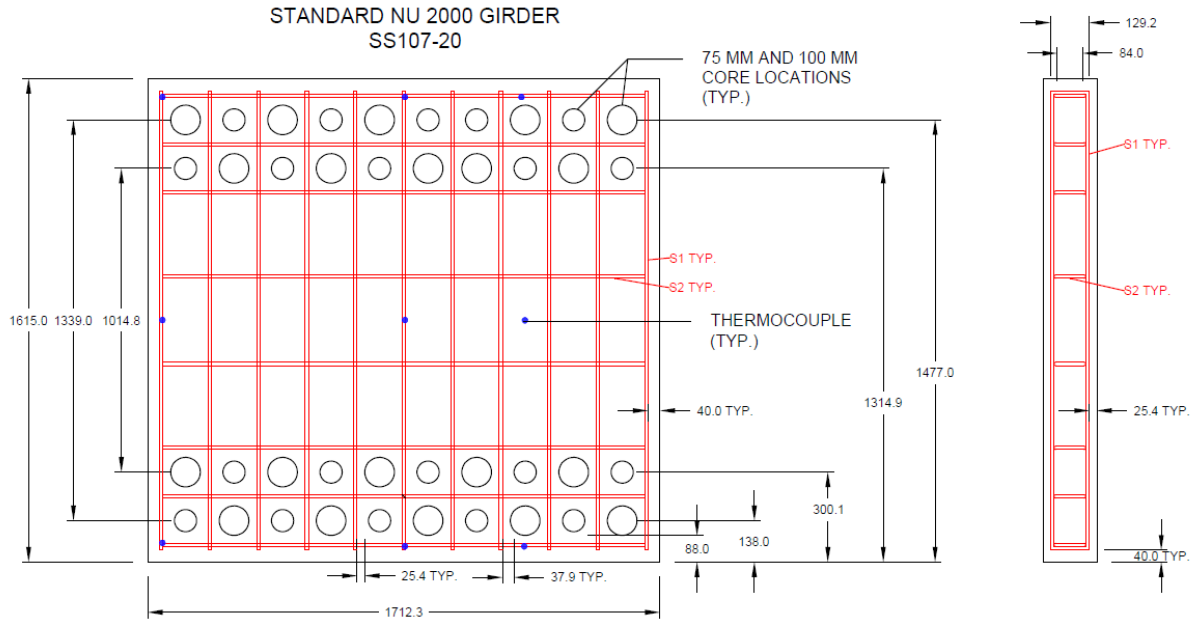

Figure 3.10: Structural Details for G1

and conditions between coring days. Coring was conducted on days 3, 7, and 28. The fourth wall was used as a control and contained thermocouples to measure the temperature of the concrete throughout the process.

The approximate coring layout is shown in Figure 3.10. In total, each wall provided 40 cores: 20 with a 75 mm diameter and 20 with a 100 mm diameter, half of which were from the top section of the girder web, and half from the bottom. The different core diameters were staggered in the coring layout to ensure that any effects caused by the location along the length and height of the wall would not be concentrated on one set of samples. The exact location of each core can be found in Appendix D - Raw Data.

Testing was conducted on days 3, 7, 28, and 56. Cores extracted on days 3 and 7 were tested on the day of coring and on day 28. On day 28, conditioned cores from days 3 and 7 were tested, and cores were extracted for testing at days 28 and 56. Cores that were tested on days other than their respective coring date were conditioned in a calcium hydroxide solution. Cores with 100 mm diameter were extracted from the top and bottom of the girder web section on days 3 and 7 for RCP testing, as well as on day 3 for air

void testing. The diamond tipped water-cooled coring drill was attached to the wall using cast-in-place anchors (not shown in Figure 3.10).

3.2.2.3 Core Sample Naming

The core labelling for the G1 structures is similar to that of beams B1 and B2. However, the location (top or bottom), and diameter of core (75 mm or 100 mm) was included in the label. Samples tested on the same day as they were cored were given the conditioning state of "Dry". In this test, there was only one conditioning type: Saturated. Examples are as follows:

Table 3.4: Core Sample Labelling Examples for Sets of Cores for Girder Web G1

Structure	Conditioning	Location	Core Diameter	*l/d* Ratio	Day Cored	Day Tested	Label
G1	Saturated	Top	75 mm	2	3	28	G1-S-T75-2-3-28
G1	Dry	Bottom	100 mm	1.5	3	3	G1-D-B100-1.5-3-3

Table 3.5: Cylinder Sample Labelling Examples for Girder Web G1

Structure	Conditioning	Day Tested	Label
G1	Saturated	28	G1-S-28
G1	Dry	3	G1-D-3

3.2.2.4 Concrete Mixture

The concrete mixture used for the G1 wall sections was modified from the G2 girder web, which was constructed at a precast manufacturer and is discussed below. The mixture contained 80% GU cement and 20% BFS for a total cementitious content of 600 kg/m^3, a w/cm ratio of 0.27, and had a maximum aggregate size of 14 mm. At the time of casting, the slump was 210 mm and the air content was 4.2%. The detailed concrete mixture can be found in Appendix A - Concrete Mixtures.

3.2.2.5 Curing Regime

The curing process for these wall sections was the same as the beams B1 and B2: the samples were covered in soaked burlap and plastic for 3 days, the formwork was stripped on day 3, and the structures were held in the UW lab at room temperature until their respective coring day. The cylinders were held with the structures until day 3 when they were demoulded and placed in a calcium hydroxide solution until testing.

3.2.3 Manhole Risers MH

3.2.3.1 Structural Details

The first structures cast, cored, and tested from a precast manufacturer were manhole risers, which are boxes with varying dimensions, but all with a wall thickness of 250 mm. The sections were reinforced with 10M bars in a grid on both the inner and outer face. The reinforcement was placed with a 25 mm cover, which allowed it to be cut out if present in the core. Lifting anchors were placed in the sides of the structures. Metal formwork was used for these structures. In total, seven structures were cored, all with different dimensions. An example of a 3000 mm x 2400 mm section, which correlates to the approximate interior dimensions, is shown in Figure 3.11. The dimensions of each structure cored is discussed in the next section.

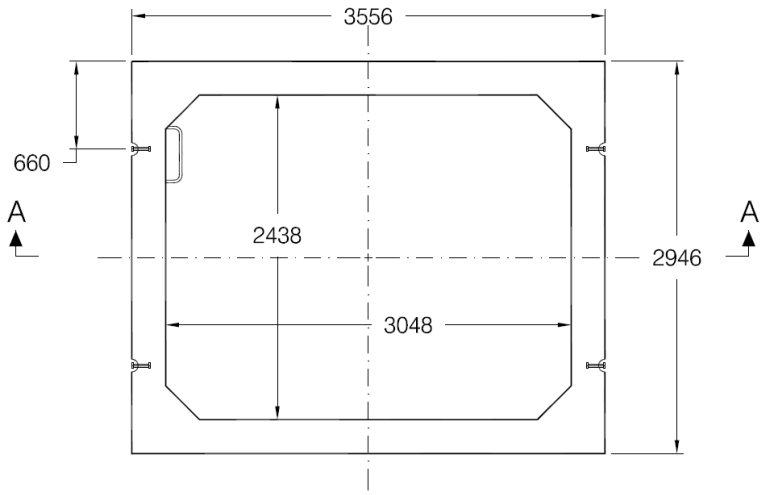

Figure 3.11: Example of a Manhole Riser (MH) Section with Dimensions of 3000 mm x 2400 mm

3.2.3.2 Coring Procedure and Layout

In total, seven sets of cores were extracted from seven separate manhole riser structures. Cores were drilled through the wall of the riser, at a length of 250 mm, at a diameter of 94 mm. The cores were then cut to a length to ensure a length-to-diameter ratio of 2. Coring was conducted on various days, determined by the precast manufacturer. The location from which the core was extracted was not recorded. All sets of cores had three replicates, except the MH1 set, which had ten replicates. Three standard cylinders corresponded to each set of cores, except for the MH1 set, which had six. Table 3.6 below outlines the structures from which the samples were cored and important dates, including the date of casting, date of coring, date received by the UW laboratory, and the date tested.

Table 3.6: Structure from Which Samples were Cored and Dates

Sample Set	Structure Dimensions (mm)	Date Cast	Date Cored	Date Received	Date Tested
MH1	2400 x 1800	Oct 13, 2017	Oct 27, 2017 (Day 14)	Nov 2, 2017 (Day 20)	Nov 10, 2017 (Day 28)
MH2	2400 x 1800	Oct 30, 2017	Nov 3, 2017 (Day 4)	Nov 7, 2017 (Day 8)	Nov 27, 2017 (Day 28)
MH3	3000 x 2400	Oct 31, 2017	Nov 3, 2017 (Day 3)	Nov 7, 2017 (Day 7)	Nov 28, 2017 (Day 28)
MH4	2400 x 1800	Nov 9, 2017	Nov 30, 2017 (Day 21)	Dec 6, 2017 (Day 27)	Dec 7, 2017 (Day 28)
MH5	3000 x 2400	Nov 10, 2017	Nov 30, 2017 (Day 20)	Dec 6, 2017 (Day 26)	Dec 8, 2017 (Day 28)
MH6	3000 x 1800	Nov 24, 2017	Nov 30, 2017 (Day 6)	Dec 6, 2017 (Day 12)	Dec 22, 2017 (Day 28)
MH7	3000 x 1800	Nov 27, 2017	Nov 30, 2017 (Day 3)	Dec 6, 2017 (Day 9)	Dec 22, 2017 (Day 25)

All the sample sets were tested on their respective day 28, except for sample set MH7. The day 28 testing day for MH7 corresponded with Christmas Day and the UW lab is closed over the winter holidays. As such, the MH7 sample set was tested on its day 25.

3.2.3.3 Core Sample Naming

The core labelling for the MH structures is similar to that of the previous structures. In this test, there was only one conditioning type: Dry. Examples are as follows:

Table 3.7: Core Sample Labelling Examples for Sets of Cores for Manhole Risers MH

Structure	Conditioning	Day Cored	Day Tested	Label
MH1	Dry	14	28	MH1-D-14-28
MH5	Dry	20	28	MH5-D-20-28

Table 3.8: Cylinder Sample Labelling Examples for Manhole Risers MH

Structure	Conditioning	Day Tested	Label
MH1	Dry	28	MH1-D-28
MH5	Dry	28	MH5-D-28

3.2.3.4 Concrete Mixture

The concrete mixture used for the MH structures was a dry cast mix with a very low w/cm ratio. The mixtures used for each of the structures was based on the same mix design, but material amounts slightly varied between casts. The mixtures contained 66% GU cement and 33% BFS for a total cementitious content of 325-345 kg/m^3, a w/cm ratio of 0.20-0.24, and had a maximum aggregate size of 13 mm. The detailed concrete mixtures can be found in Appendix A - Concrete Mixtures. Note that the mix volume for each mix was 1.35 m^3, and the design strength, f_c', is 40 MPa.

3.2.3.5 Curing Regime

All structures underwent the same curing regime. Following the cast, the manhole risers were steam cured for 6 hours and then placed in outdoor storage. Cylinders were held with the risers during curing and were demoulded after steam curing and placed outside alongside the riser. Both cylinders and cores were left outdoors until they were collected and brought to the UW lab and stored at room temperature and humidity until testing.

The only sample sets to differ from this schedule were samples MH4-MH7. These sample sets were all cored on November 30th and were brought inside for storage on December 4th until they were collected on December 6th. The reminder of the regime was kept the same.

3.2.4 Girder Web G2

3.2.4.1 Structural Details

The second structure cast, cored, and tested in a precast manufacturer's facility was a wall with a thickness of 160 mm, width of 2400 mm, and height of 1300 mm (Figure 3.12). The wall was to represent a precast girder web. Coring was completed by supporting the walls flat on wooden blocks and cores were drilled through the wall. The wall contained minimum reinforcement using 15M bars at 300 mm on center to create a grid. Thermocouples were placed, as shown in Figure 3.12, to monitor the temperature throughout the testing period. Lifting anchors were fitted at the top of the section and in the front face. The formwork used to construct this section was steel (Figure 3.13).

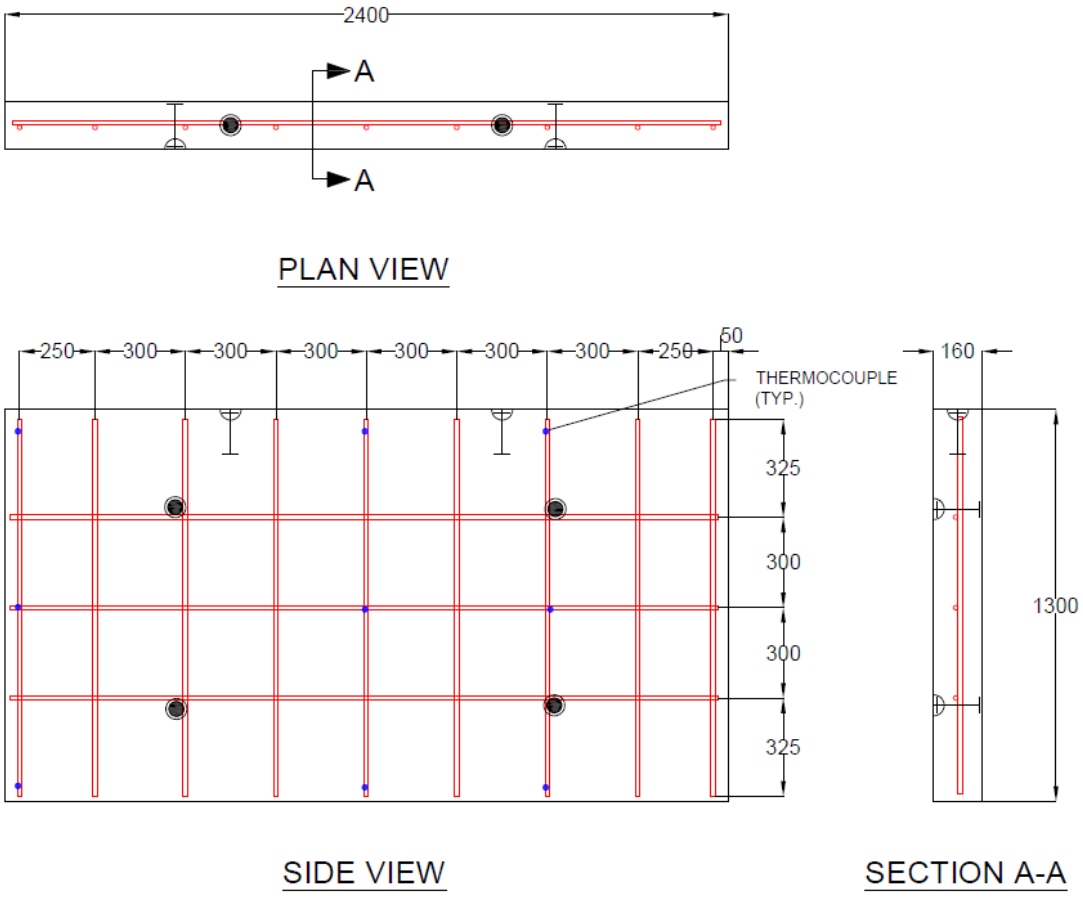

Figure 3.12: Girder Web G2 Dimensions

3.2.4.2 Coring Procedure and Layout

Coring of the sample was conducted on days 3 and 28. On day 3, 22 cores were drilled and on day 28, 9 cores were drilled. Table 3.9 summarizes the number of cores taken each day and the purpose of each core. Please note, cores for compression testing were 75 mm in diameter to allow for an *l/d* ratio of 2, while those used for air void analysis and RCP testing were 100 mm in diameter.

See Figure 3.14 for the approximate location from which the cores were drilled. The exact location of each core can be seen in Appendix D - Raw Data. In addition to the core samples, 12 cylinders were cast for compression testing on days 1, 3, 7, and 28.

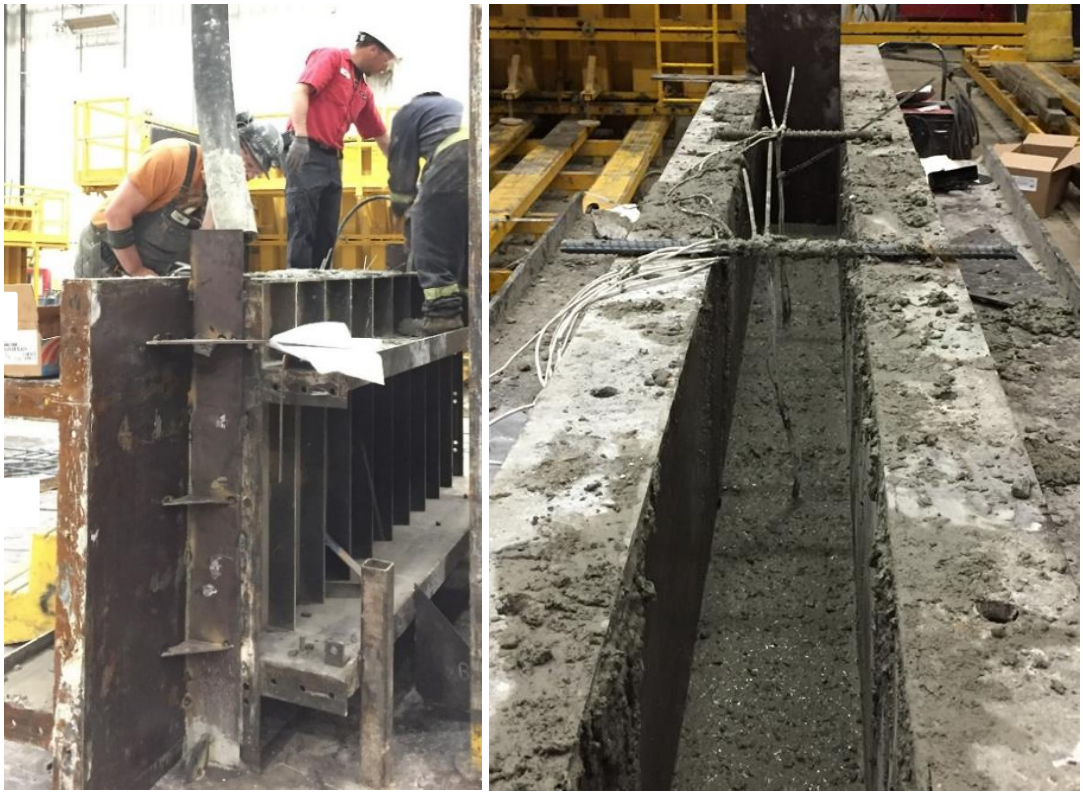

Figure 3.13: G2 Formwork and Fresh Concrete in Form

Table 3.9: Core Sample Summary for Girder Web G2

Coring Date	Location	Test	Test Date	Quantity
Day 3	Top	Compression	Day 3	3
Day 3	Top	Compression	Day 28	3
Day 3	Top	Air Void	Other	1
Day 3	Top	RCP	Day 28	1
Day 3	Middle	Compression	Day 3	3
Day 3	Middle	Compression	Day 28	3
Day 3	Bottom	Compression	Day 3	3
Day 3	Bottom	Compression	Day 28	3
Day 3	Bottom	Air Void	Other	1
Day 3	Bottom	RCP	Day 28	1
Day 28	Top	Compression	Day 28	3
Day 28	Middle	Compression	Day 28	3
Day 28	Bottom	Compression	Day 28	3

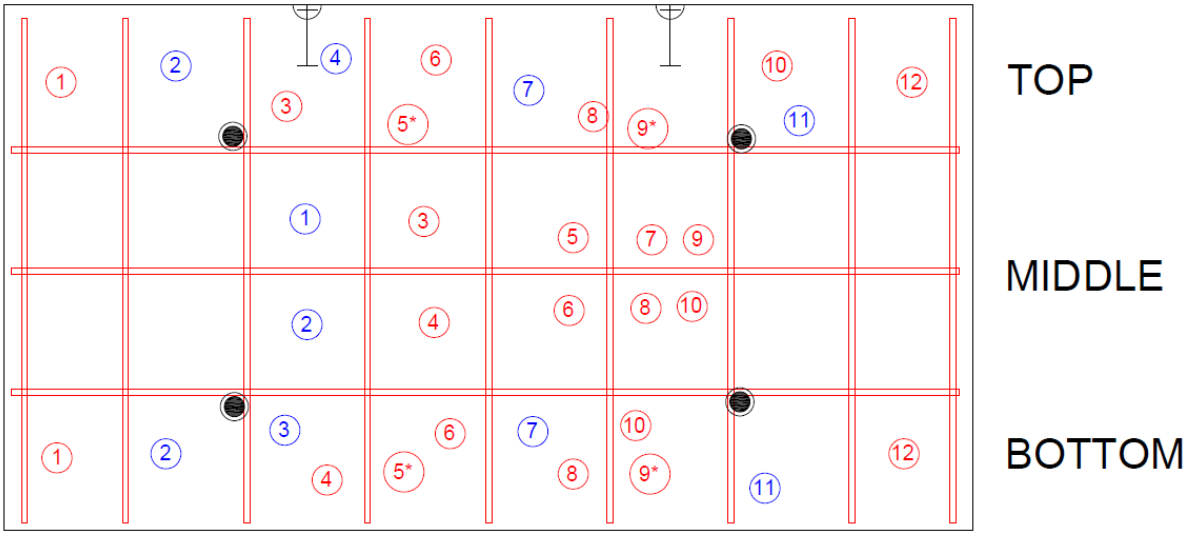

Figure 3.14: Coring Location Layout

Cores numbered 5 and 9, from both the top and bottom, were drilled with a 100 mm diameter coring barrel. The red cores were drilled on day 3 and the blue cores were drilled on day 28. Only 3 of the 4 blue cores from each of the top, middle, and bottom levels were required on day 28 and the additional core was meant as an extra in the event of issues during coring. Since there were no issues encountered, the additional cores were not taken.

The wall section was placed flat, supported by wooden blocks, and cored vertically, through the width of the wall section using a diamond tipped, water-cooled, vacuum seal coring drill. The wall section was elevated approximately 16" off the ground during day 3 coring and most cores fell from the wall section onto the granulated ground below. On day 28 coring, the wall section was elevated approximately 8" above the ground and once again, the cores fell onto the ground before collection. There were no apparent signs of damage on the cores, internally or externally, caused by this fall. Core holes were not plugged or grouted following day 3 coring and were left exposed to the elements. This exposure to a winter environment included variable temperatures, above and below 0°C, and variable moisture, which could have affected the test results of the core samples taken on day 28 near the previously cored locations. The temperature experienced by the structure is discussed in Section 4.3.9 Core Results: Temperature Effects.

3.2.4.3 Core Sample Naming

The core labelling for the Girder Web G2 is similar to that of the Girder Web G1. The notable differences include the lack of a diameter parameter, as all cores tested in compression had the same diameter, and the extra location parameter: middle of web. Samples tested on the same day as they were

cored were given the conditioning state of "Dry". In this test, there was only one conditioning type: saturated. Examples are as follows:

Table 3.10: Core Sample Labelling Examples for Sets of Cores for Girder Web G2

Structure	Conditioning	Location	Day Cored	Day Tested	Label
G2	Saturated	Top	3	28	G2-S-75-3-28
G2	Dry	Bottom	3	3	G2-D-B-3-3

Table 3.11: Cylinder Sample Labelling Examples for Girder Web G2

Structure	Conditioning	Day Tested	Label
G2	Saturated	28	G2-S-28
G2	Dry	3	G2-D-3

3.2.4.4 Concrete Mixture

The concrete mixture used for the G2 girders was based on a typically used prestressed, precast girder mixture design. The mixture contained a total of 627 kg of cementitious materials, with 75% being Type 30 cement (HE), and 25% BFS, with a 13 mm maximum aggregate size. The w/cm ratio was 0.32, and at the time of casting, the concrete had a slump of 225 mm and a plastic air content of 6.2%.

3.2.4.5 Curing Regime

The exposed top surface of the wall was covered with presoaked burlap and two layers of polymeric tarpaulin following the cast. The wall was demoulded after approximately 18 hours and placed in a steam curing kiln 2 hours after demoulding. The wall was removed 72 hours after the concrete was cast from the kiln for coring of day 3 samples and returned to the kiln until day 7. After the wall had completed 7 days of curing, it was removed from the kiln and placed outside until day 28 coring. This structure was cast in winter, and thus the outdoor temperature was below 0°C at times.

Cylinders were held with the structure during the curing process until day 3, at which point the cylinders were brought to the UW lab, demoulded, and placed in a calcium hydroxide solution until testing day.

3.2.5 Girder Section G3

3.2.5.1 Structural Details

The girder section had a 3000 mm length of a standard NU 2000 section, as shown in Figure 3.15. The section contained only two vertical rebar stirrups, offset slightly from either ends of the section, which extended out of the formwork for the purpose of lifting and moving the section. This structure was cast, and cored in a manufacturer's facility, and testing was completed by both the manufacturer on site, and at an MTO approved testing facility. Steel formwork was used for the construction of this section.

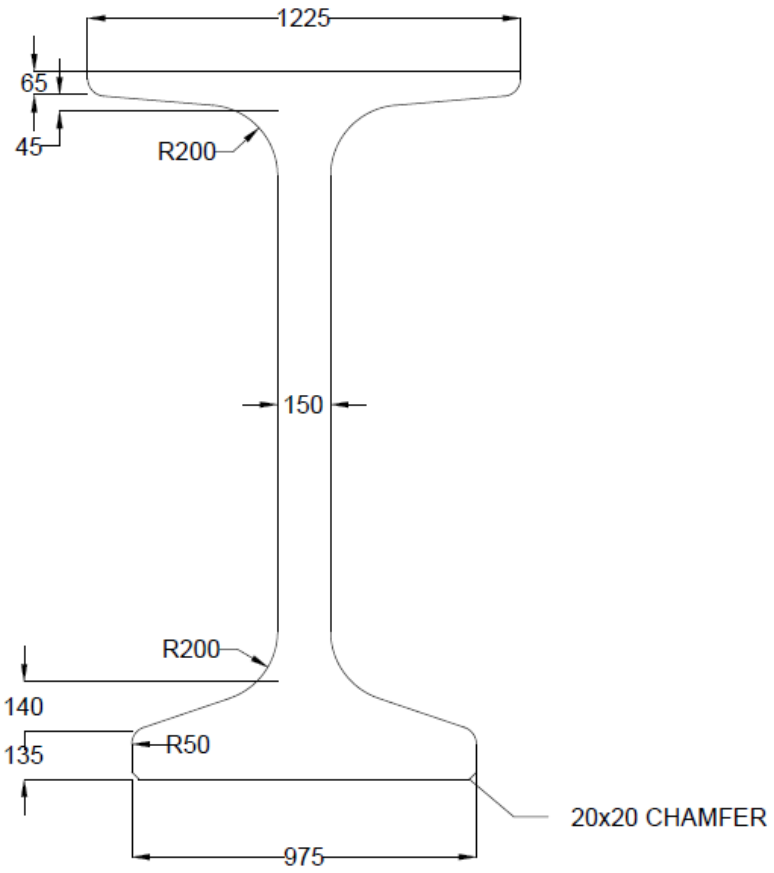

Figure 3.15: Standard NU 2000 Girder Section Used for Girder Section G3

3.2.5.2 Coring Procedure and Layout

Cores were drilled with a diameter of 94 mm and a varying length depending on the location of the core. Cores were extracted horizontally from the top, middle, and bottom of the web, and vertically through the bottom flange and into the center of the top flange (Figure 3.16). The lengths of the cores were 160 mm

through the web, 200 mm through the bottom flange, and varied between 150 mm and 180 mm through the top flange. Therefore, *l/d* ratios varied from 1.5 to 2.3. Coring was conducted with post-installed anchors to attach a water-cooled diamond tipped coring drill.

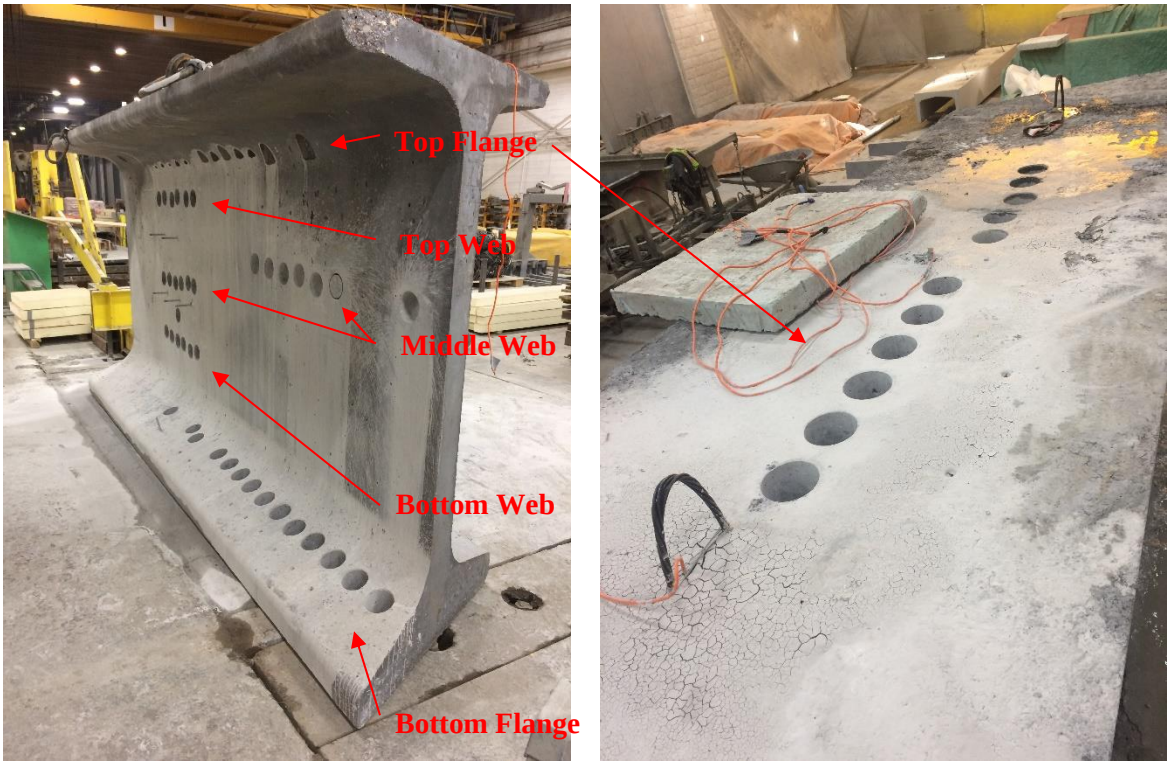

Figure 3.16: Left: Photo of Core Locations of G3. Right: Photo of Top of Section Showing Top Flange Cores

On day 3, the middle of the web, bottom flange, and top flange were cored. The cores extracted from the middle height of the web were tested on days 3 and 28 while the cores extracted from the top and bottom flange were tested on days 3, 7, and 28. On day 28, the top, middle, and bottom of the web, bottom flange, and top flange were all cored and tested on the same day. Cores tested on days other than the day of coring were moist cured which entailed conditioning the sample in a moisture room. A summary of core samples extracted is given in Table 3.12. The core holes were not sealed between coring days. The approximate height from the bottom of the section of the cores extracted from the bottom, middle, and top of the web is 600 mm, 1100 mm, and 1600 mm respectively. Cylinders were tested on days 1, 3, 7, 28, and 56.

Table 3.12: Core Sample Summary for Girder Section G3

Coring Date	Location	Test	Test Date	Quantity
Day 3	Top Flange	Compression	Day 3	3
Day 3	Middle Web	Compression	Day 3	3
Day 3	Bottom Flange	Compression	Day 3	3
Day 3	Top Flange	Compression	Day 7	3
Day 3	Bottom Flange	Compression	Day 7	3
Day 3	Top Flange	Compression	Day 28	3
Day 3	Top Flange	Air Void	Other	1
Day 3	Top Flange	RCP	Day 28	1
Day 3	Middle Web	Compression	Day 28	3
Day 3	Bottom Flange	Compression	Day 28	3
Day 3	Bottom Flange	Air Void	Other	1
Day 3	Bottom Flange	RCP	Day 28	1
Day 28	Top Flange	Compression	Day 28	3
Day 28	Top Web	Compression	Day 28	6
Day 28	Middle Web	Compression	Day 28	6
Day 28	Bottom Web	Compression	Day 28	6
Day 28	Bottom Flange	Compression	Day 28	3

3.2.5.3 Core Sample Naming

The core labelling for the Girder Section G3 is similar to that of the Girder Webs G1 and G2. The notable differences include a lack of differing diameters, as all cores tested in compression had the same diameter, the extra location parameters: middle of web, top flange, and bottom flange, and the moist conditioning type in place of the saturated conditioning type. Samples tested on the same day as they were cored were given the conditioning state of "Dry". In this test, there was only one conditioning type: Moist. Examples are as follows:

Table 3.13: Core Sample Labelling Examples for Sets of Cores for Girder Section G3

Structure	Conditioning	Location	Day Cored	Day Tested	Label
G3	Dry	Top Web	28	28	G3-D-T-28-28
G2	Moist	Bottom Flange	3	28	G3-M-BF-3-28

Table 3.14: Cylinder Sample Labelling Examples for Girder Section G3

Structure	Conditioning	Day Tested	Label
G3	Moist	28	G3-M-28
G3	Dry	3	G3-D-3

3.2.5.4 Concrete Mixture

The concrete mixture used for this girder section is a standard 55 MPa prestressed, precast girder mixture used in MTO projects. The mixture contains GUb-SF, and 20% fly ash for a total cementitious content of 475 kg/m^3, and utilized a maximum aggregate size of 14 mm. The w/cm ratio was 0.29, the slump was 220 mm, and the air content of the fresh concrete was 6.0%. The detailed concrete mixture design can be found in Appendix A - Concrete Mixtures.

3.2.5.5 Curing Regime

The section was steam cured, which entails placing a tarp over the section and injecting steam into this environment. The steam curing lasted until the internal temperature of the concrete reached the required, proprietary temperature limit. This is typically 6 to 8 hours of injecting steam. The section was then cured with soaked burlap and plastic until day 3. After coring on day 3, the section was kept inside the precast manufacturers plant until day 28, near room temperature.

The cylinders were placed under the tarp with the structure until the structure was demoulded and then the cylinders were placed into a water tank. Cores tested on the same day as coring were tested by the precast manufacturer, while the cores tested on days after coring were transported to an MTO facility for testing. These cores were transported in buckets, wrapped in soaked burlap and bubble wrap for protection. Once received, the cores were placed in a moisture room until testing.

3.2.6 Valve Chamber VC

3.2.6.1 Structural Details

The last structure cast, cored, and tested was a large box structure in a precast manufacturer's facility with wall thickness of 254 mm, exterior dimensions of 2946 mm by 1880 mm and a height of 2267 mm (Figure 3.17). This box was designed as a valve chamber and was cast for the purpose of extracting a large number of cores from a structure. The section was minimally reinforced with 15M bars on a grid. The spacing of the vertical bars was 500 mm on walls A and C, and 250 mm on walls B and D, and the

spacing of the horizontal bars was 350 mm on all walls. Lifting anchors were placed on walls B and D. Steel formwork was used for this structure. Thermocouples were placed, as shown in Figure 3.17, to monitor the temperature throughout the testing period.

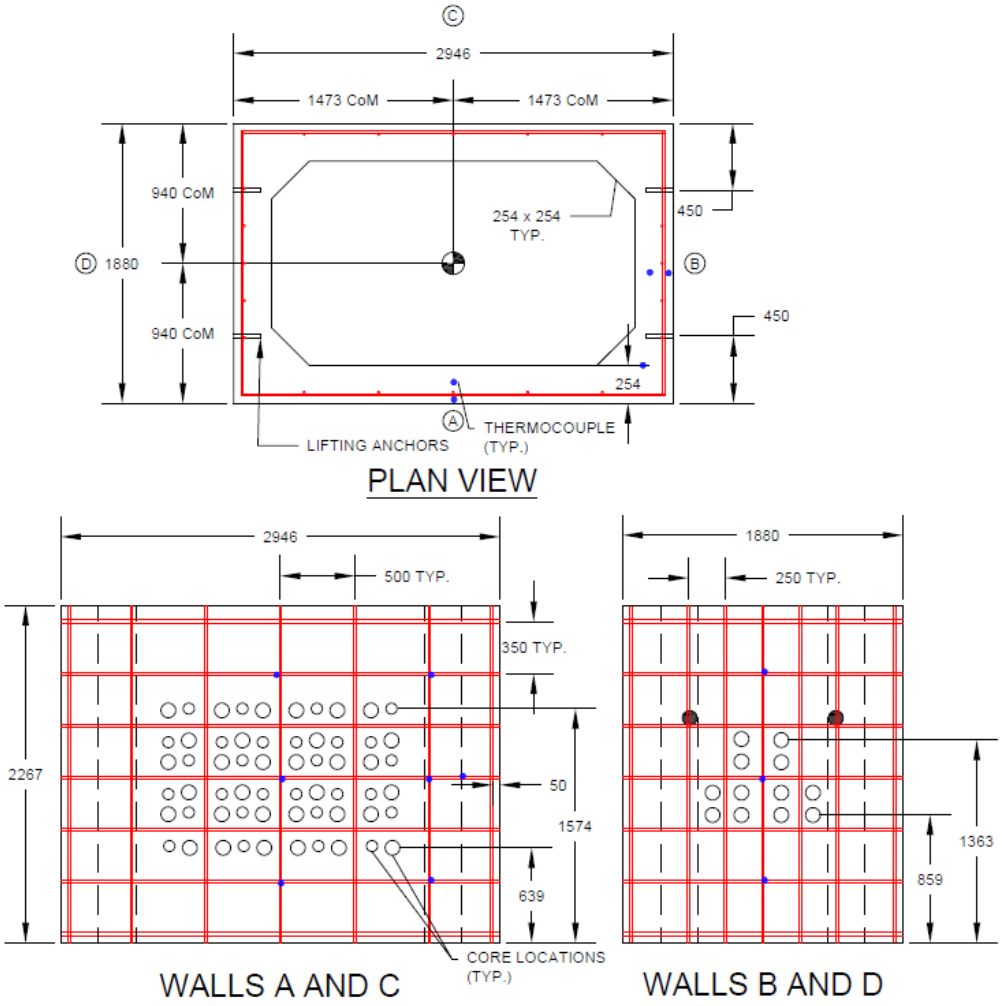

Figure 3.17: Valve Chamber (VC) Shape, Dimensions, Reinforcement Layout, and Approximate Coring Layout

3.2.6.2 Coring Procedure and Layout

Coring of the sample was conducted on days 3, 7, 14, and 28. Figure 3.17 above shows the approximate coring layout, while the exact location of each core can be found in Appendix D - Raw Data. Table 3.15 summarizes the number of cores taken each day and the purpose of each core. Please note, cores from walls A and C were 75 mm and 100 mm in diameter, while cores from walls B and D were 94 mm in diameter. The 120 cores extracted from walls A and C on day 14 were tested for an investigation into the *l/d* ratio and diameter effects.

Table 3.15: VC Core Sample Summary

Coring Date	Wall	Test	Test Date	Quantity
Day 3	B	Compression	Day 3	3
Day 3	B	Compression	Day 28	3
Day 3	B	RCP	Other	1
Day 7	D	Compression	Day 7	3
Day 7	D	Compression	Day 28	3
Day 7	D	RCP	Other	1
Day 7	D	AVS	Other	1
Day 14	A	Compression	Day 28	60
Day 14	C	Compression	Day 28	60
Day 14	B	Compression	Day 28	3
Day 14	B	RCP	Other	1
Day 28	D	Compression	Day 28	3

In addition to the core samples, 18 cylinders were cast for compression testing on days 3, 7, 14, 21 and 28, and RCP testing. A rebar locator was used to find the approximate location of the steel reinforcement to limit the possibility of coring through the steel reinforcement. The coring was completed using a water-cooled diamond tipped coring drill. Post-installed anchors were used to fasten the coring drill to the valve chamber. Core holes were plugged, with the same plugs as used with Beams B1 and B2 and shown in Figure 3.9, to limit the impact of the holes on the curing of the valve chamber as the same wall was cored on multiple days. Cores tested on days other than the day they were cored were conditioned in a solution of saturated calcium hydroxide.

3.2.6.3 Core Sample Naming

The core labelling for VC is similar to that of the previous structures. Samples tested on the same day as they were cored were given the conditioning state of “Dry”. In this test, there was only one conditioning type: Saturated. Examples are as follows:

Table 3.16: Core Sample Labelling Examples for Sets of Cores for VC

Structure	Conditioning	Day Cored	Day Tested	Label
VC	Dry	28	28	VC-D-28-28
VC	Saturated	3	28	VC-S-3-28

Table 3.17: Cylinder Sample Labelling Examples for VC

Structure	Conditioning	Day Tested	Label
VC	Saturated	28	VC-S-28
VC	Dry	3	VC-D-3

3.2.6.4 Concrete Mixture

The concrete mixture used for this structure was a self-consolidating concrete (SSC), which is not typically used on MTO projects. The mixture had a total cementitious content of 480 kg, with 75% HE cement and 25% BFS, and a w/cm ratio of 0.36. The concrete had an air content of 7.9% at casting, a slump flow of 580 mm, and utilized a maximum aggregate size of 19 mm. The detailed concrete mixture can be found in Appendix A - Concrete Mixtures.

3.2.6.5 Curing Regime

The exposed top surface of the box was covered with an insulated tarpaulin following the cast. The valve chamber was demoulded after approximately 18 hours and held indoors for the next 24 hours, after which it was placed outdoors for the remainder of the test. The cylinders were kept with the structure until it was placed outdoors, at which point the cylinders were kept indoors. The cylinders were brought to the UW lab on day 3 after coring, demoulded, and placed in a calcium hydroxide solution. This test was conducted during the winter, thus temperatures below 0°C were experienced.

3.2.7 Cylinder Cast CC

3.2.7.1 Structural Details

An additional large-scale cylinder cast was conducted in collaboration with the same precast manufacturer as the VC structure, at a later time. The purpose of this test was to isolate the effect of damage caused by coring through direct comparison with the VC structure by keeping all parameters as close as possible, with the only difference being that these are cylinders, instead of cores. Plastic moulds

with lids were used. A photograph of the cylinder moulds before concrete casting is shown in Figure 3.18. Thermocouples were placed in a 100 mm x 200 mm, a 100 mm x 150 mm, and a 75 mm x 150 mm cylinder, as well as one thermocouple for the ambient temperature.

Figure 3.18: Photo of Cylinder Moulds Used for Cylinder Cast (CC) Before Concrete was Placed

3.2.7.2 Test Matrix

In total, there were four sets of dimensions used, similar to the VC set: 100 mm by 200 mm, 100 mm by 150 mm, 75 mm by 150 mm, and 75 mm by 112.5 mm. These dimensions give the *l/d* ratios of 2 and 1.5 for each diameter, matching those of the VC set. The number of cylinders cast in each dimension set varied between 30 and 35 for testing on day 28. Standard cylinders were also cast for testing on days 3, 7, 14, 21, and 28.

3.2.7.3 Cylinder Sample Naming

The cylinder labelling for CC is similar to that of the previous structures. In this test, there was only one conditioning type: Saturated. Examples are as follows:

Table 3.18: Cylinder Sample Labelling Examples for Sets of Cylinders for CC

Structure	Conditioning	Diameter	*l/d* Ratio	Day Tested	Label
CC	S	100	2	28	CC-S-100-2-28
CC	S	75	1.5	28	CC-S-75-1.5-28

Table 3.19: Standard Cylinder Sample Labelling Example for CC

Structure	Conditioning	Day Tested	Label
CC	Saturated	14	CC-S-14

3.2.7.4 Concrete Mixture

The concrete mixture used for this structure was a self-consolidating concrete (SSC), which is not typically used on MTO projects. The design mixture was identical to the concrete mixture used on VC. The mixture contained a total cementitious content of 480 kg, with 75% HE cement and 25% BFS, for a w/cm ratio of 0.36. The concrete had an air content of 7.8% at casting, a slump flow of 655 mm, and utilized a maximum aggregate size of 19 mm. The detailed concrete mixture can be found in Appendix A - Concrete Mixtures.

3.2.7.5 Curing Regime

As with the other parameters, the curing regime was kept as close to the VC as possible. The cylinders were held indoors for 46 hours then brought to the UW laboratory where the lids were removed, and the cylinders were placed outdoors. The standard cylinders, for testing of days 3, 7, 14, 21, and 28, were placed indoors until day 3, at which point they were demoulded, end ground, and either tested or immersed in a solution of saturated calcium hydroxide. As with the VC structure, this test was conducted during the winter, thus outdoor temperatures below 0°C were experienced. The cylinders which were placed outdoors were brought indoors and demoulded on day 14 and immersed in a solution of saturated calcium hydroxide. These cylinders were end ground between day 15 and 21, which was similar to the VC cores. The cylinders were only removed from the solution of calcium hydroxide for no more than one hour for end grinding.

Chapter 4
Experimental Results

This chapter presents the experimental results relating to the compressive strength, air void analysis, and density of the cores and cylinders from each structure tested, as well as the temperature monitoring of the structure. It also includes a preliminary analysis and discussion of the data relating to each structure. Chapter 5 will include the analysis and discussion of all the data together. The raw data can be found in Appendix D - Raw Data.

4.1 Preliminary Analysis Methodology

The analysis and preliminary discussion of the data in this chapter is limited to inferences made using statistical methods within the datasets. Two two-tailed statistical methods are utilized and are used as a preliminary analysis to determine if different parameters, such as the location from which a core is extracted, are affecting the properties of the concrete. These are the F-test of equality of variances, and a two-sample T-test of equality of means [79]. The F-test is first conducted to determine if the two sample sets (for example, vertically and horizontally extracted cores) share an equal variance. If these two sample sets do not share an equal variance, the parameter may be introducing error into the compressive strength test result which is increasing the variance of one of the sample sets. The following equations show how this is determined:

Null Hypothesis	$H_o: \sigma_1^2 = \sigma_2^2$	
Test Statistic	$F_o = S_1^2/S_2^2$	(4.1)
Test Criterion	Reject Null: $F_o > F_{\alpha/2,n_1-1,n_2-1}$ *or* $F_o < F_{1-\alpha/2,n_1-1,n_2-1}$	

The null hypothesis, H_o, is that the two sample sets originate from the same population, which has a variance, σ_i^2. The test statistic, F_o, is calculated using the samples' variances, S_i^2, and if the test statistic is outside the bounds of the test criterion, determined by the F distribution utilizing the degrees of freedom of each sample set, $n_i - 1$, and the significance level, α, then the null hypothesis is rejected, and the sample sets do not originate from the same population, which has a variance of σ_i^2.

The second statistical method is a two-sample T-test to determine if the means of two sample sets are different. If the means of two sample sets are different, the parameter investigated is increasing or decreasing the result of the compressive strength test. This statistical test depends on whether the sample sets' variances are equal or unequal, which was determined previously using the F-test, and is shown

below in Equation (4.2). In this case, the null hypothesis is that the two sample sets have the same mean, μ_i. Calculating the test statistic, t_o, and comparing the result to the test criteria, with degrees of freedom ν, the null hypothesis is either rejected, and the sample sets have different means, or accepted, and the sample sets have the same mean. The significance level of 5% has been chosen for these tests, which means that there is a 5% chance that a type 1 error has been made, i.e. the rejection of the null hypothesis when it should not have been rejected. This is also known as a 95% confidence level.

	Unequal Variances	**Equal Variances**
Null Hypothesis	$H_o: \mu_1 = \mu_2$	$H_o: \mu_1 = \mu_2$
Test Statistic	$t_o = \dfrac{\mu_1 - \mu_2}{S_p\sqrt{\dfrac{1}{n_1} + \dfrac{1}{n_2}}}$ $S_p = \dfrac{(n_1 - 1)S_1^2 + (n_2 - 1)S_2^2}{n_1 + n_2 - 2}$ $\nu = n_1 + n_2 - 2$	$t_o = \dfrac{\mu_1 - \mu_2}{\sqrt{\dfrac{S_1^2}{n_1} + \dfrac{S_2^2}{n_2}}}$ $\nu = \dfrac{\left(\dfrac{S_1^2}{n_1} + \dfrac{S_2^2}{n_2}\right)^2}{\dfrac{(S_1^2/n_1)^2}{n_1 - 1} + \dfrac{(S_2^2/n_2)^2}{n_2 - 1}}$
Test Criterion	Reject Null: $\lvert t_o \rvert > t_{\alpha/2,\nu}$	Reject Null: $\lvert t_o \rvert > t_{\alpha/2,\nu}$

(4.2)

A test to determine if the sample set included an outlier was also completed, following the procedure of ASTM E178 [80]. This test, shown below in Equation (4.3), was conducted on the low and high values, x_1 and x_n (e.g. high and low compressive strength results), in each data set to check for both low and high outliers.

Null Hypothesis	$H_o: x_1 \; or \; x_n \; is \; not \; an \; outlier$
Test Statistic	$T_1 = \dfrac{\bar{x} - x_1}{S}, \qquad T_n = \dfrac{x_n - \bar{x}}{S}$
Test Criterion	Reject Null: $T_1, T_n > \dfrac{t_{\alpha/2n,n-2}}{\sqrt{1 + \dfrac{n t_{\alpha/2n,n-2}^2 - 1}{(n-1)^2}}}$

(4.3)

The test statistic, T_1 or T_n, is calculated by determining the standardized distance from the mean, by calculating the distance between the value in question, x_1 or x_n, and the mean, $\bar{x}$, and dividing by the standard deviation of that sample set, S. This test statistic is then compared to the test criterion provided by ASTM E178 [80], which includes the value of the t-distribution given the significance value, α, and number of samples in the data set, n. If the test statistic is larger than the test criterion, that value is an

outlier, and removed from the data set. This process is completed until all outliers are removed. Outliers are denoted in Appendix D - Raw Data.

4.2 Temperature Monitoring

Temperature probes were placed in the concrete structures. For the Beam B1, a temperature probe was placed in one of the four beams cast, as well as one monitoring the ambient temperature. Figure 4.1 below shows the temperature profile over 28 days, with the days of coring, day 3, 7, 14, and 28, marked, while Figure 4.2 shows the first 7 days. On the coring days, there is a temperature dip due to the use of water to cool the coring drills. The maximum temperature reached during the hydration period was 40.8°C.

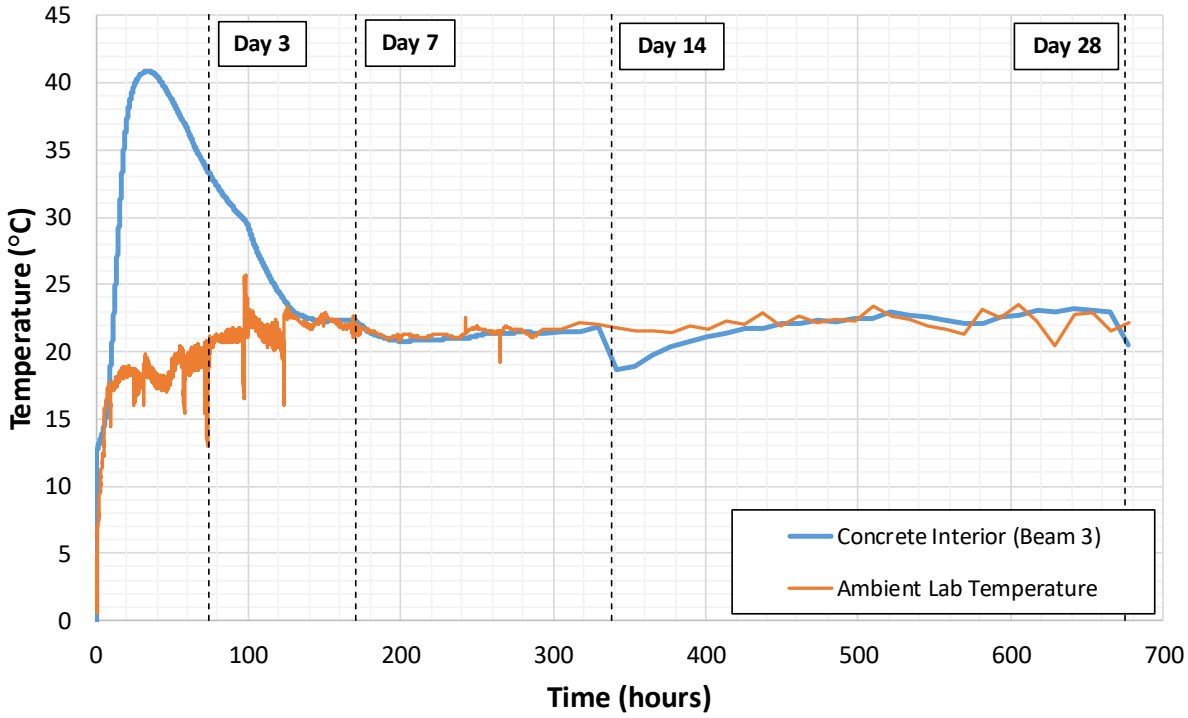

Figure 4.1: Temperature Monitoring of Beam B1 Over 28 Days

The temperature monitoring data for the other structures can be found in Appendix B.3 Temperature Monitoring. The temperature probe layout for each structure was discussed previously in their respective subsection in Section 3.2. Table 4.1 below summarizes the maximum temperatures for each structure in various locations.

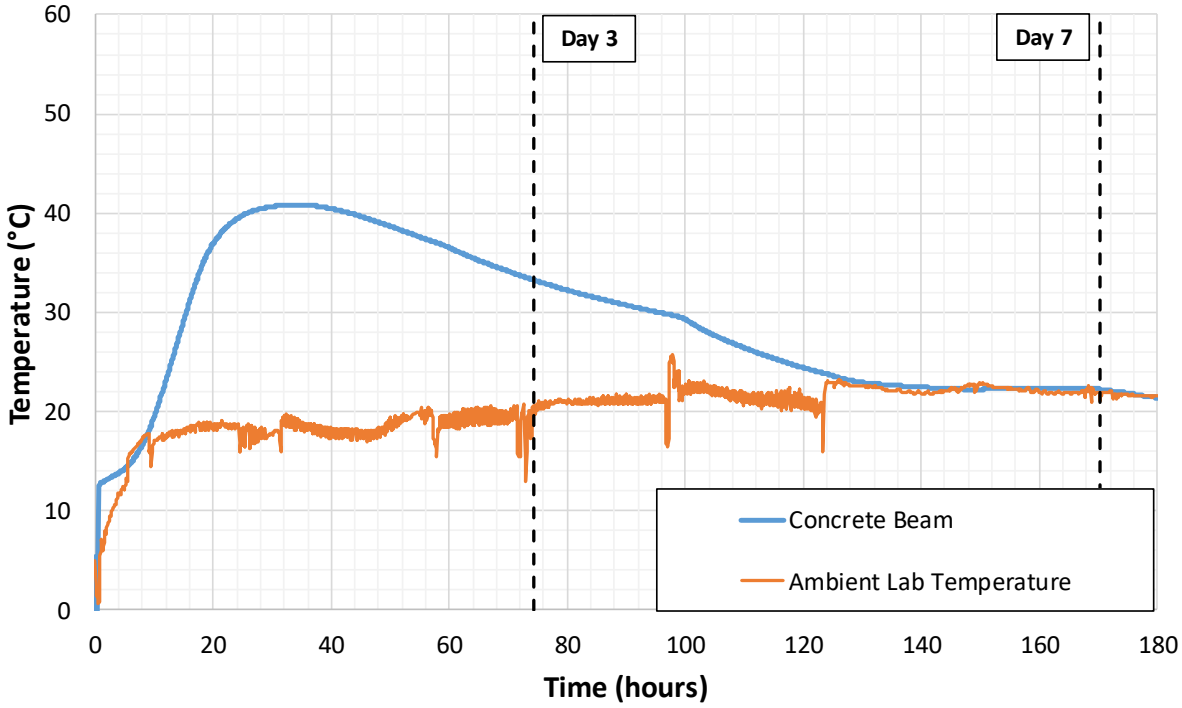

Figure 4.2: Temperature Monitoring of Beam B1 Over 7 Days

Table 4.1: Summary of Maximum Temperatures for Various Locations of Each Structure

Structure and Location	Maximum Temperature (°C)
B1	40.8
B2	55.7
B2 Cylinder	24.2
G1 Middle-Middle	57.0
G1 Cylinder	30.8
G2 Middle-Middle	49.3
G3 Middle Web	61.5
G3 Top Flange Surface	71.0
VC Middle-Middle Big Wall	46.9
VC Corner	51.2
CC 100 mm l/d = 2	24.0
CC 75 mm l/d = 2	21.6

4.3 Compression Strength Results

This section presents the results of the compressive strength tests of all the structures tested: B1, B2, G1, G2, G3, MH, VC, and CC. Both cylinder and core results are shown. The effect of coring date, direction of coring, location, conditioning, diameter, length-to-diameter (*l*/d) ratio, temperature experienced, and density on the compressive strength of the core are briefly analyzed and discussed. Error bars in figures represent one standard deviation from the average value.

4.3.1 Cylinder Results

The compressive strengths of the cylinders for all structures are shown below in Figure 4.3. The three conditioning states, dry (D), moist (M), and saturated (S), refer to how the cylinder was stored before testing. For simplicity of plotting, the day 3 cylinder results are shown under each of the different conditioning states, as they were removed from their moulds on day 3 and had not been conditioned. The "moist" cylinders were placed in a moisture room, which maintains a relative humidity of 100%, the "saturated" cylinders were placed in a calcium hydroxide solution, and the "dry" cylinders were sealed in plastic until the testing day.

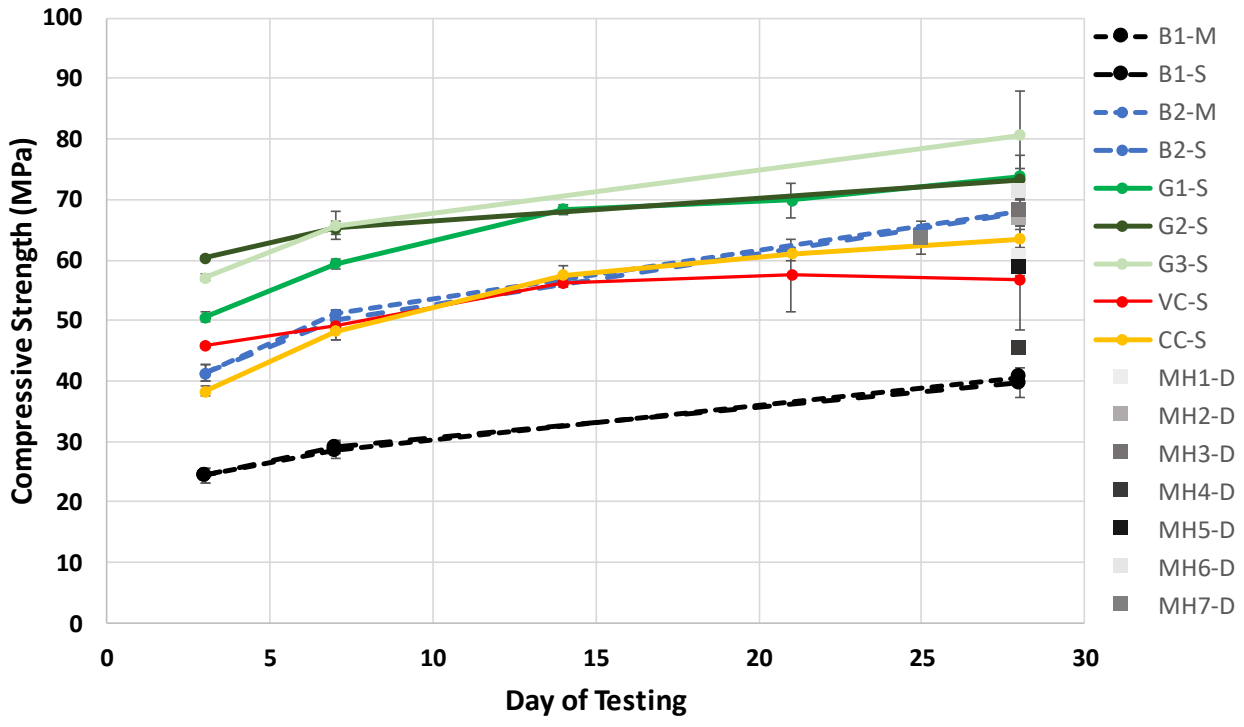

Figure 4.3: Compressive Strength of Cylinders from All Structures

Only the B1 and B2 structures had cylinders in multiple conditioning states: moist and saturated. As seen in the figure above, there was no difference in compressive strength results between the moist and saturated cylinders, which was corroborated by the F and T-test discussed previously at a 95% confidence level.

4.3.2 Core Results: Timing of Core Extraction

Beams B1 and B2 had cores extracted on days 3, 7, 14, and 28. Figure 4.4 below shows the compressive strength on Day 28 of cores which were extracted on the various coring days, in both the dry and saturated conditioning states, and vertical and horizontal coring direction. Cores extracted on days 3, 7, and 14 were conditioned either dry or saturated in calcium hydroxide until the day 28 testing. As the figure below shows, the compressive strengths of the dry cores on all days were not different than the day 28 dry core; however, the saturated cores were of lower compressive strength than the day 28 dry core. The F-test determined that all the variances are equal to the variance of the day 28 dry core, except the B1-D-V-3-28, and B1-S-V-3-28 core sets. The T-test showed that only the B1-S-H-14-28 core sets were different that their day 28 tested counterparts, at a 95% confidence level. This shows that, regardless of coring day, the strength of the sample when tested on day 28 is the same for this structure.

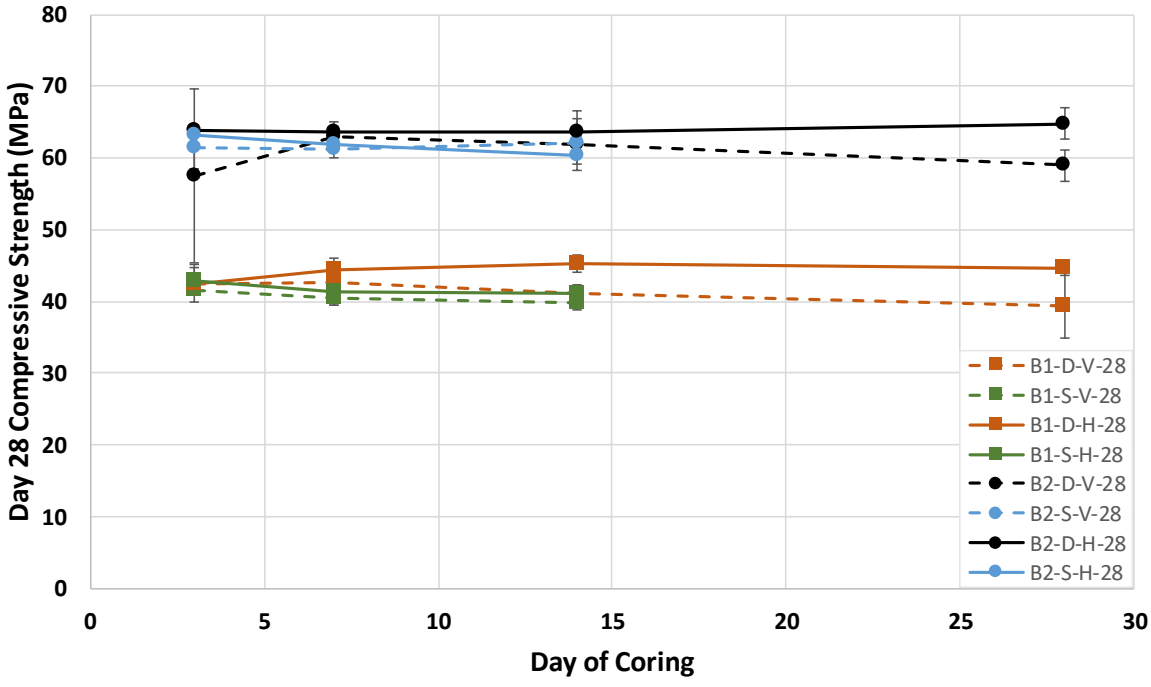

Figure 4.4: Day 28 Compressive Strength of Beams B1 and B2 Cores Extracted on Various Days, in Saturated and Dry Conditions, and Vertical and Horizontal Coring Directions

A similar process was conducted for structures G1, G2, G3, and VC, as cores from these structures were also extracted at various days. These figures can be found in Appendix B.1. A summary table showcasing which datasets had statistically different variances or means is shown below in Table 4.2. The P-value, which is the probability of the test statistic, F_o or t_o, occurring, are also shown in Table 4.2. If the P-value is smaller than the significance level, α, chosen, which is 0.05 for these tests, the null hypothesis is rejected, and the variances or means are different. All other comparisons were found to be statistically not different at a 95% confidence level. In total, 41 datasets were tested, of which 8 were statistically different.

Table 4.2: Summary Table of Statistically Unequal Variances or Different Means When Comparing Core Extraction Date

Datasets	Result of F-Test (Variances)	P-Value of F-Test	Result of T-Test (Means)	P-Value of T-Test
B1-D-V-3-28 B1-D-V-28-28	Unequal	0.0027	Not Different	0.7562
B1-S-V-3-28 B1-D-V-28-28	Unequal	0.0003	Not Different	0.8813
B1-S-H-14-28 B1-D-H-28-28	Equal	0.4320	Different	0.0163
G2-S-B-3-28 G2-D-B-28-28	Equal	0.4295	Different	0.0232
G2-S-M-3-28 G2-D-M-28-28	Unequal	0.0228	Not Different	0.957
G3-M-BF-3-28 G3-D-BF-28-28	Unequal	0.0132	Not Different	0.6372
VC-S-3-28 VC-D-28-28	Equal	0.2728	Different	0.0002
VC-S-7-28 VC-D-28-28	Equal	0.8036	Different	0.0126

The VC structure had three datasets for comparison, two of which were statistically different. The third dataset contained an outlier which decreased the dataset to two samples. This makes it difficult for the T-test to show that two datasets are different.

In total, there were four datasets in which there was a difference in compressive strength on day 28 between different coring days: B1-S-H-14 and B1-D-H-28, G2-S-B-3 and G2-D-B-28, VC-S-3 and VC-D-28, and VC-S-7-28 and VC-D-28. The differences seen in the VC dataset can be attributed to the curing conditions: samples cored at earlier times had a longer time to cure indoors in a saturated conditioning state compared to the structure, which was left outdoors in sub-zero temperatures. This will be discussed in Section 4.2.9 Core Results: Temperature Effects. The G2 dataset also experienced some temperature effects discussed in Section 4.2.9, as well as some consolidation issues leading to large voids present in the cores resulting in lower compressive strength results. In the remaining 35 comparisons, only one was found to be statistically different. Therefore, there does not appear to be a difference between the core extraction dates with respect to the compressive strength on day 28.

4.3.3 Core Results: Vertically vs. Horizontally Drilled

Beams B1 and B2 had cores which were extracted parallel to the direction of casting (Vertical), and perpendicular to the direction of casting (Horizonal). Previous research has shown that the direction of coring can impact the compressive strength of a core [41]. Figure 4.5 below shows the day 28 compressive strengths of cores that were extracted vertically and horizontally, in both the dry and saturated conditioning states. As shown in the previous section, there was only one case where the average compressive strength of cores tested on day 28 differed based on the core extraction date in the B1 and B2 datasets. As such, the values shown in Figure 4.5 are the average values over all the coring days for each conditioning state.

Figure 4.5 shows that the values, in some cases, do differ, and the difference is more noticeable in the dry conditioning state. By inspection, it appears that the horizontal cores have a relatively higher compressive strength compared to their vertical counterparts. However, statistically, only the B1-D data sets showed a difference in mean at a 95% confidence level. The horizontal cores in B1-D had a 6% high compressive strength than the vertical cores.

This observation is different than that found in the literature [41]. As discussed in Section 2.2.3 Coring Direction of Sample, the bleed water settles under the aggregates, and when the core is extracted horizontally, that bleed water forms a plane of weakness which is in line with the direction of testing, thus weakening the horizonal samples compared to the vertical samples. There are two possible explanations as to why this effect was not seen in these tests. The first is that the horizontal cores were lower in the beam than the vertical cores (Figure 3.6) and that caused a slight height effect, boosting the compressive strength of the horizontal cores. The other explanation is the concrete mixtures included SCMs which

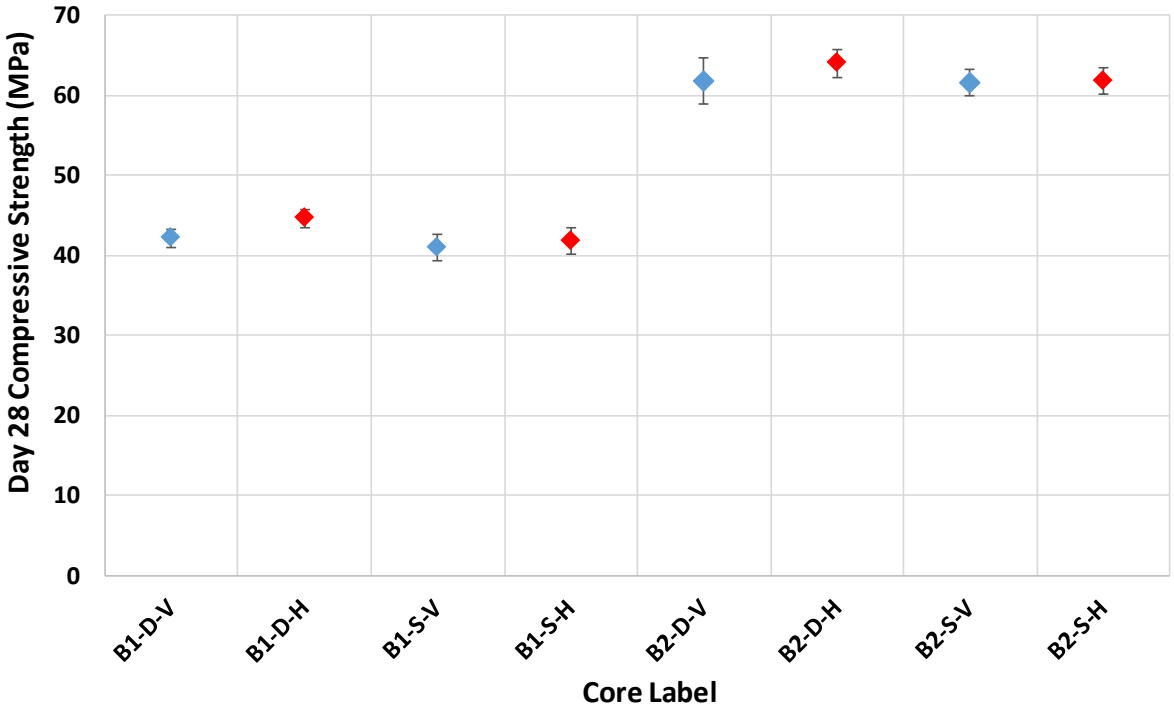

Figure 4.5: Day 28 Compressive Strength of Beams B1 and B2 Vertical (Red) and Horizontal (Blue) Cores, in both Dry and Saturated Conditioning States

reduced the amount of bleed water present. With the reduced amount of bleed water, this plane of weakness would not have formed.

For this comparison, there were four sets of horizontal/vertical cores, only one was statistically different, while the others showed no statistical difference. Therefore, in modern concrete mixtures, which include SCMs and low w/cm ratios, the effect bleed water has on the compressive strength may be reduced, and the effect of coring direction may no longer be apparent.

4.3.4 Core Results: Variation along Height of Structure

Structures G1, G2, and G3 were all sections of a girder. G1 and G2 were only the web component, while G3 was a full section of a girder. Cores were extracted from the top and bottom of G1, from the top, middle, and bottom of G2, and from the bottom flange, bottom of the web, middle of the web, top of the web, and top flange from G3. Figure 4.6 below shows the Day 28 compressive strength from these locations. The G1 dataset is split based on the diameter and *l/d* ratio, and the G2 and G3 datasets are split based on the day of coring and their respective conditioning types.

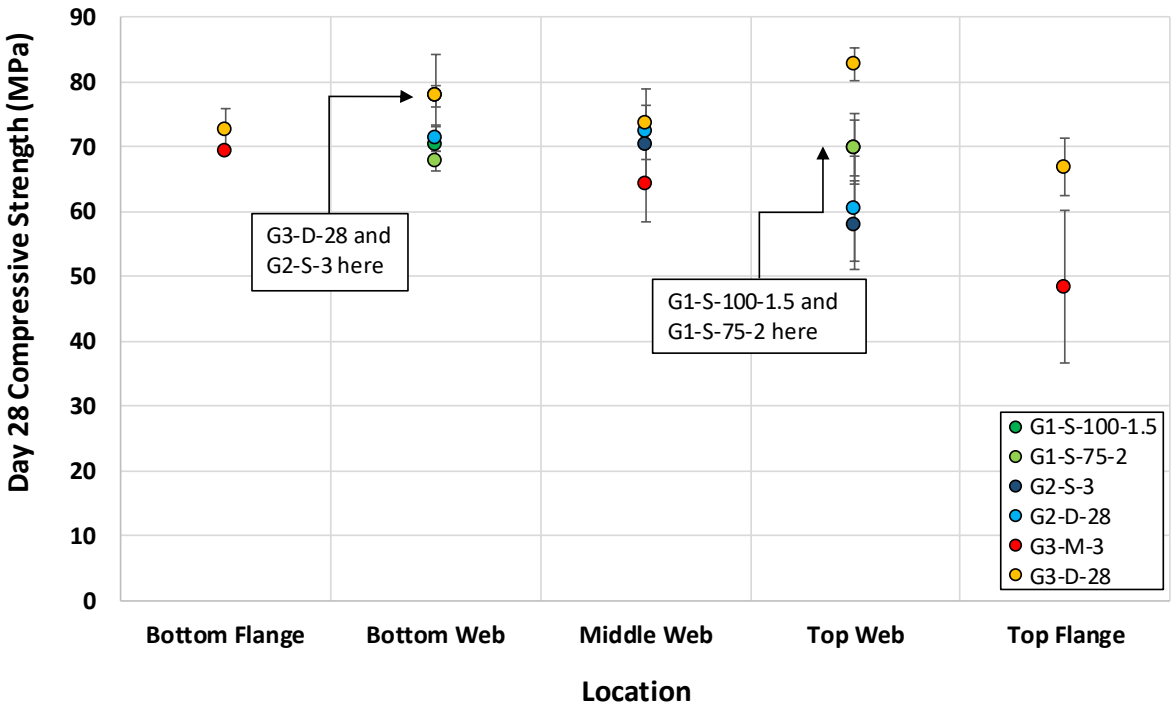

Figure 4.6: Day 28 Compressive Strength of G1, G2, and G3 Cores, Extracted from Various Heights, on Various Days

In the figure above, the G1 points are virtually identical, and show no difference with respect to the height. The G3-D-28 dataset appears to have no relation between the compressive strength and the height from which the core was extracted; however, G3-M-3 does show a slight relation where compressive strength decreases with height. Table 4.3 below summarizes the datasets which have statistical differences at a 95% confidence level. As can be seen in the table below, the G1 dataset has an unequal variance, while the means are not different. G2 has a difference in means only in the day 3 cores. However, the G3 cores exhibited large entrapped air voids which would have caused or, at least, contributed to the difference in variance. The G3 dataset had many different means, most of which deal with the Top Web location, as it appears to have a higher average strength compared to the other locations, even the Top Flange.

As discussed in Section 2.2.2 Location of Extracted Core, previous research has indicted that a core extracted from a higher location would have a lower strength than those cored from lower levels. This can be seen in Figure 4.6 for some cases (G2 and G3-M-3), but not for others (G1, G3-D-28).

Table 4.3: Summary of Height Effect Datasets with Differences

Datasets	Difference	P-Value
G1-S-T75-2 G1-S-B75-2	Unequal Variances	0.0165
G2-S-T-3 G2-D-B-3	Different Means	0.0287
G2-D-T-28 G2-D-M-28	Unequal Variances	0.0172
G3-M-BF-3 G3-M-M-3	Unequal Variances	0.0072
G3-M-BF-3 G3-M-TF-3	Unequal Variances	0.0035
G3-D-TF-28 G3-D-T-28	Different Means	0.0291
G3-D-TF-28 G3-D-B-28	Different Means	0.0308
G3-D-T-28 G3-D-M-28	Different Means	0.0073
G3-D-T-28 G3-D-BF-28	Different Means	0.0172

Another dataset, VC, had cores extracted at various heights, but without a definition of "Top" or "Bottom". However, the actual location of the center of each core was measured. This was also done for the G1, and G2 datasets. The G3 dataset had the heights of cores reasonably estimated, via photographs and engineering drawings. With the actual measurements, Figure 4.7 below shows the ratio of the Day 28 core compressive strength to the average of all the Day 28 core compressive strength results from that structures versus the actual height of the center of the core.

From Figure 4.7, the trend of decreasing strength in the G2 and G3 structure can be seen as the height increases, except for the "Top Web" (1600 mm) location of G3. However, this trend is not seen in the G1 and VC structures. The G2 dataset had some consolidation issues during construction which may explain the height effect being present in that dataset. VC was a self-consolidation concrete (SCC) mixture which is cohesive and very workable, and thus does not produce much bleed water, which is the leading theory

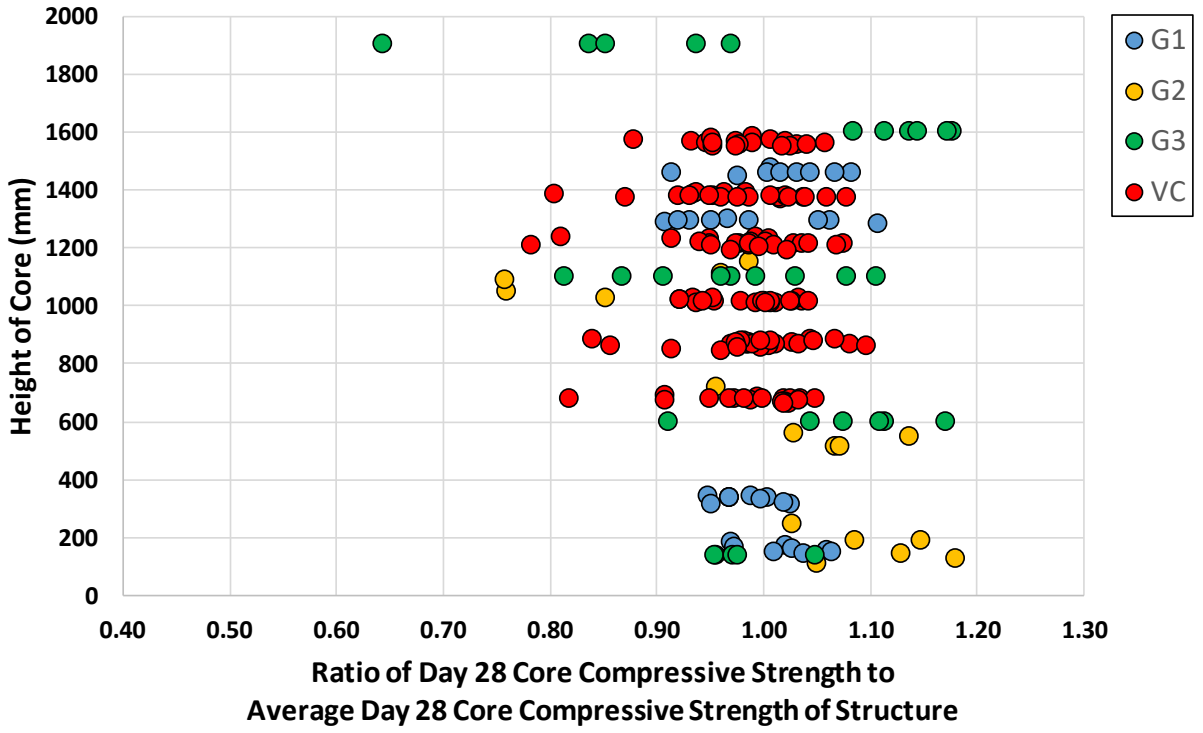

Figure 4.7: Ratio of Day 28 Compressive Strength to Average Day 28 Compressive Strength of G1, G2, G3, and VC Cores, Extracted from Various Heights

on why the height effects the compressive strength. Similarly, G1 was constructed in the UW laboratory, and was well consolidated. The G1 concrete mixture included 25% slag and a low w/cm ratio, which would reduce, if not completely remove, any bleed water, and thus, any height effect on the compressive strength. Lastly, the G3 structure was constructed by a precast manufacturer without the supervision of any UW students or technician. As such, no explanation can be given for the results seen. In conclusion, the effect of height on the compressive strength of a core, in reasonably constructed structures, is not as apparent as in the past due to the use of SCMs, low w/cm ratios, and superplasticizers in modern concrete mixtures.

4.3.5 Core Results: Variation along Length of Structure

Similar to the previous section, the center of core locations in the horizontal direction were measured in structures G1, G2, and VC. Figure 4.8 below shows the ratio of the Day 28 core compressive strength to the average of all the Day 28 core compressive strength results from that structures versus the horizonal distance between the center of the structure and the center of the core. Data for G3 were not included in the figure due to difficulties in accurately estimating the horizontal distances from photographs received.

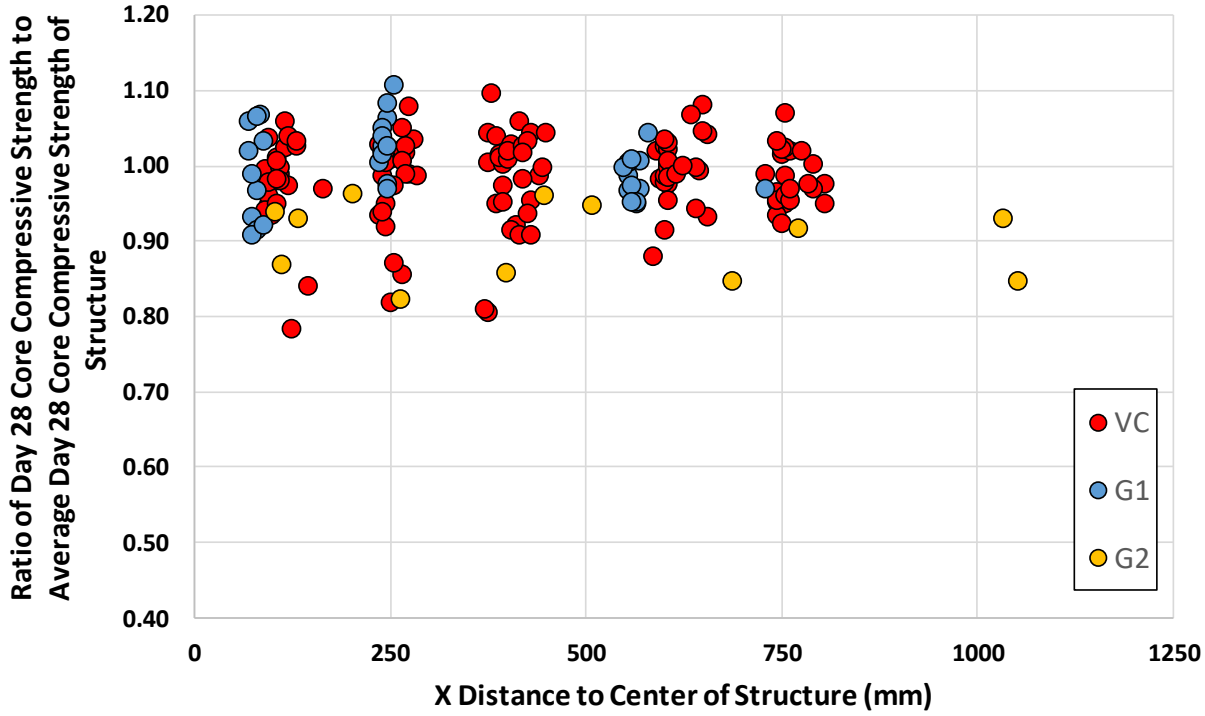

Figure 4.8: Ratio of Day 28 Compressive Strength to Average Day 28 Compressive Strength of G1, G2, and VC Cores, Extracted from Various Distances from Center

As seen in Figure 4.8, there does not appear to be a trend between the length along the structure and the compressive strength. This was corroborated by analysis of the data which gave a correlation coefficient of -0.0129, which shows no correlation.

4.3.6 Core Results: Dry vs. Saturated

When a core was extracted and was to be tested at a later date, that core was conditioned either in the Dry or Saturated conditioning types until testing. The Dry conditioning type was also used to describe cores that were extracted and tested on the same day; however, continuing inside the structure is not the same as being sealed in plastic. To adequately compare the effect of the Dry and Saturated conditioning types, only Dry samples which were sealed in plastic were considered. The only structures in which samples were dry sealed in plastic were those from the Beams B1 and B2. Figure 4.9 below shows the Dry and Saturated cores extracted on various days, all tested on day 28.

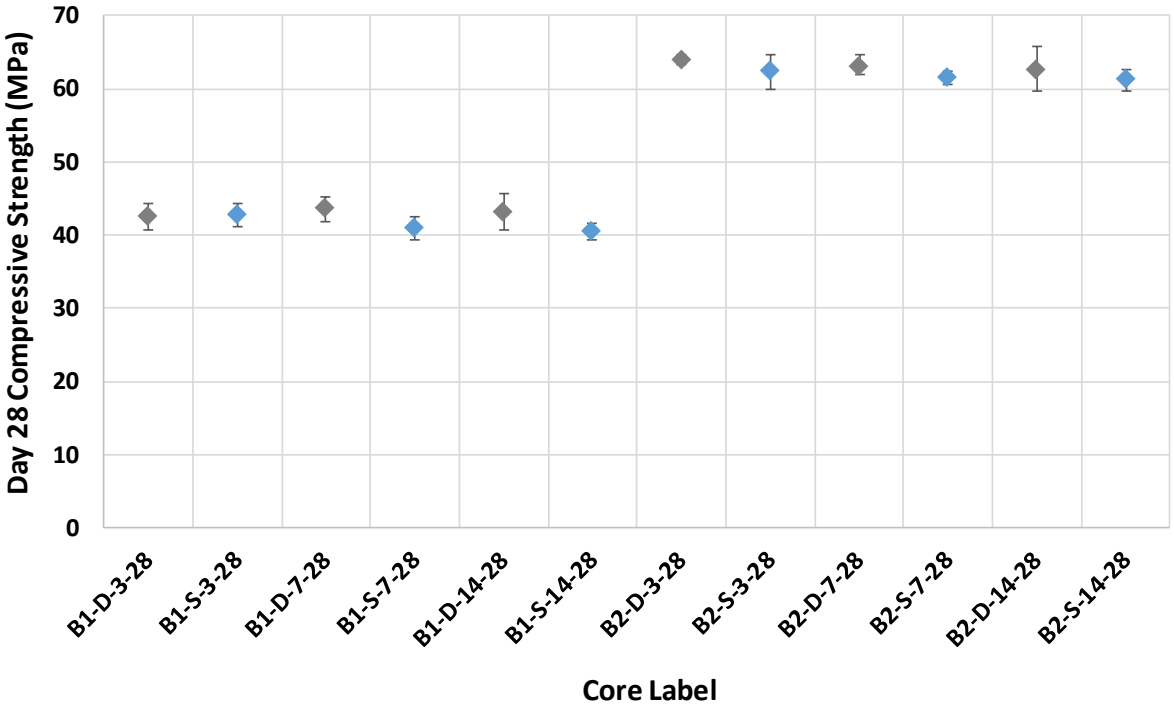

Figure 4.9: Day 28 Compressive Strength of Beams B1 and B2 Dry (Grey) and Saturated (Blue) Cores, Extracted on Various Days

The Saturated cores appear to have a lower compressive strength compared to their counterpart Dry cores. When comparing cores extracted on the same day, the Dry and Saturated cores were statistically different in two of the six comparisons: B1-7-28 and B2-7-28. The Saturated cores had a 6.4% and 2.8% lower compressive strength than their Dry counterparts, respectively. The B2-3-28 cores had unequal variances, but the same means, at a 95% confidence level. This effect will be discussed in more detail in Chapter 5.

4.3.7 Core Results: Diameter

Multiple structures tested utilized 75 mm diameter cores and cylinders: G1, G2, VC, and CC. G2 only used 75 mm diameter cores, and thus there is no 100 mm diameter cores to compare results. The G1 structure utilized both 100 mm and 75 mm diameter cores, but at different *l/d* ratios. Both diameter cores had a length of 150 mm which meant the 100 mm diameter samples had a *l/d* ratio of 1.5, while the 75 mm diameter cores had a *l/d* ratio of 2. VC, where cores were extracted, and CC, where cylinders were cast, had both the 100 mm and 75 mm diameters samples, at both *l/d* ratios of 1.5 and 2.

Figure 4.10 below shows the G1, VC, and CC samples at the 100 mm and 75 mm diameters, at their respective *l/d* ratios. The G2 data was excluded due to a lack of a counterpart. The G1 data is not a direct comparison of diameters as there is also a differing *l/d* ratio between the 75 mm and 100 mm diameter cores. The VC and CC are direct comparisons of the diameter as the *l/d* ratios are the same. The G1 data is the averaged compressive strength of all the cores tested on Day 28, regardless of core extraction date, and conditioning type, as the previous sections showed that neither effected the compressive strength. The G1 data is split between the top and bottom cores.

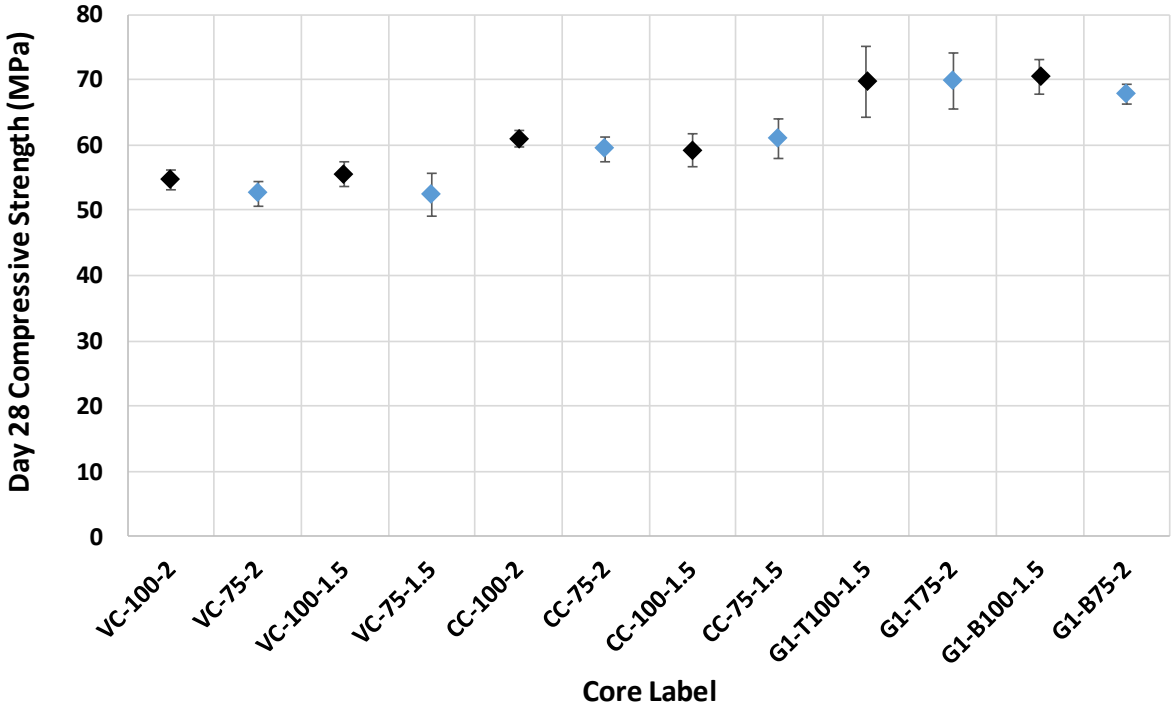

Figure 4.10: Day 28 Compressive Strength of G1, VC, and CC Samples, with 100 mm (Black) and 75 mm (Blue) Diameters, and 2.0 and 1.5 *l/d* Ratios. G1 Data Split Between Top and Bottom

From Figure 4.10 above, the 75 mm diameter samples exhibited a lower compressive strength in three of the four cases in the VC and CC datasets. The CC datasets have statistically different means, with equal variances. The VC samples with a *l/d* ratio of 2 have different means, while the *l/d* ratio of 1.5 has unequal variances. For the G1 datasets, no samples were found to be different. However, the compounding effect of diameter and *l/d* ratio may be contributing. The *l/d* ratio will be discussed in the next section, and both the diameter and *l/d* ratio effects will be discussed in more detail in Chapter 5.

4.3.8 Core Results: Length-to-Diameter Ratio

The same datasets that were used in Section 4.3.7 is used for the comparison of the *l/d* ratios: G1, VC, and CC. Figure 4.11 below shows the datasets, comparing the *l/d* ratios.

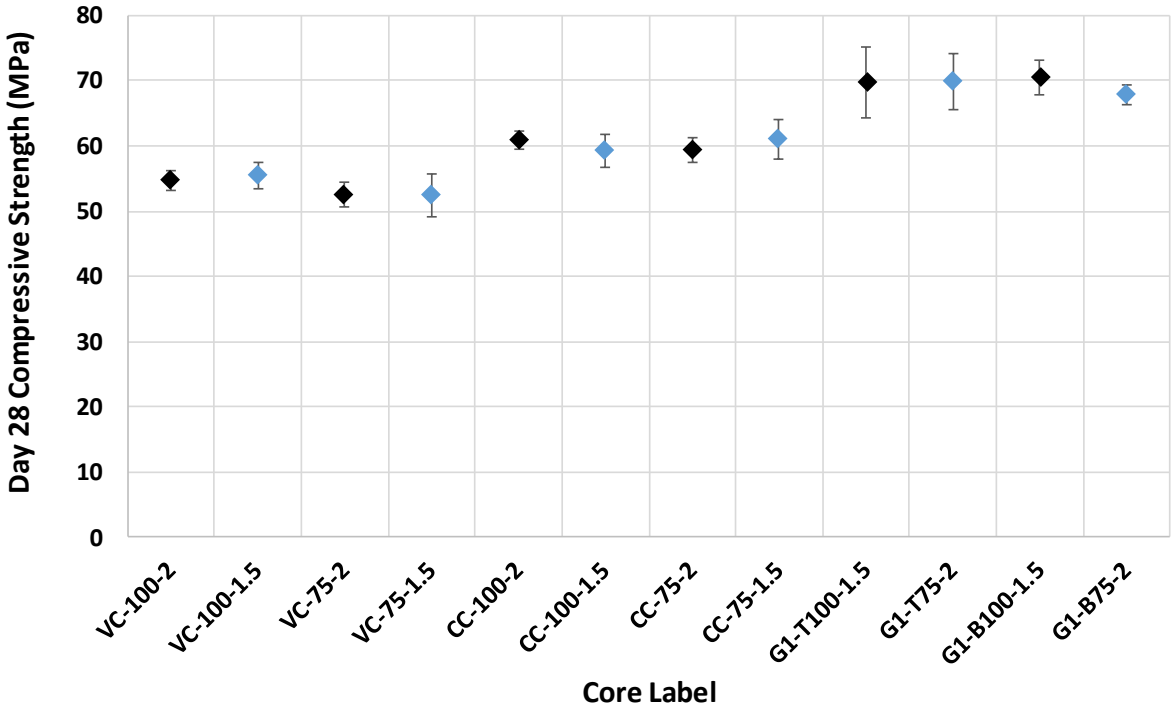

Figure 4.11: Day 28 Compressive Strength of G1, VC, and CC Samples, with *l*/d Ratios of 2 (Black) and 1.5 (Blue), with Diameter of 100 mm and 75 mm. G1 Data Split Between Top and Bottom

The compressive strengths of the cores with varying *l/d* ratios in the VC and CC datasets show similar means, but different variances. This observation was corroborated by the F-Test, which concludes that three of the four datasets in the VC and CC structures had unequal variances, with the VC-100 data sets having equal variances, at a 95% confidence level. The G1 dataset, similar to the previous section, is split between the top and bottom observations, and no differences were found in the means nor the variances. The *l/d* ratio effect is discussed in more detail in Chapter 5.

4.3.9 Core Results: Temperature Effects

Some of the structures tested experienced cold temperatures before Day 28: G2, MH, VC, and CC. ACI 318-14 [68], CSA A23.1-14 [4], and OPSS 909 [81], 1350 [69], and 904 [82] all restrict the temperature of concrete during curing to a minimum of 10°C. During curing is defined differently in each of these standards; however, the majority of the standards agree that once the concrete has reached 75% f_c', it may

experience lower temperatures. The temperature monitoring data of these structures can be found in Section 0. MH and VC had cores extracted at various times before Day 28, and conditioned until Day 28, G2 only had cores extracted on Day 3 and Day 28, and the cylinders from CC were conditioned from Day 14 until Day 28. Therefore, to investigate the effect of low temperature exposure on the concrete compressive strength, CC was not included in the dataset as there is only one timeframe in this dataset. Figure 4.12 below shows the Day 28 compressive strength of the cores compared to the length of conditioning, which is the period of time between when the cores were placed in their respective conditioning type and day 28 testing, which for most samples was the coring date. However, dataset MH was not placed into the dry conditioning state directly after coring.

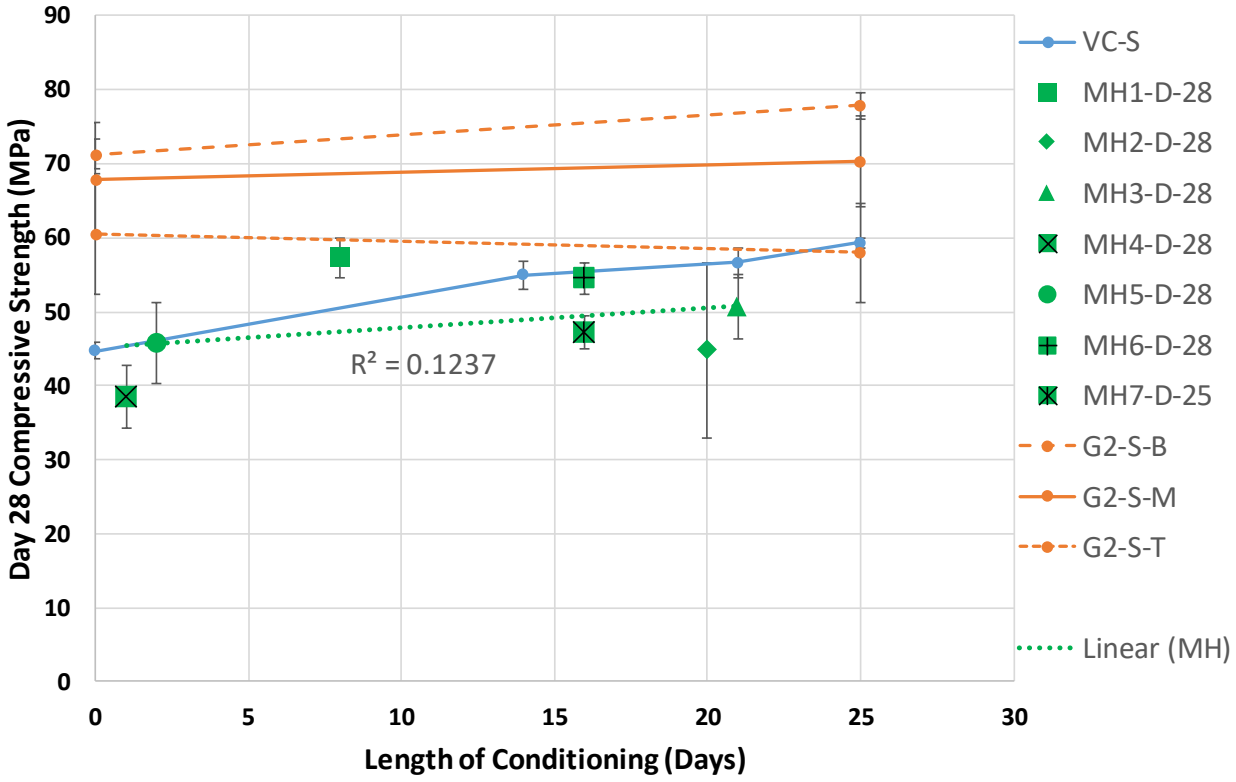

Figure 4.12: Day 28 Compressive Strength of VC, MH, and G2 Cores, with Varying Lengths of Conditioning. G2 Data Split Between Top, Middle, and Bottom

Please note that MH7 was not tested on Day 28, but Day 25. This is due to Day 28 being during the Christmas period when the UW laboratory was closed. Within the G2 structure, only G2-S-B shows a difference between the cores extracted and tested on Day 28, and the cores which were extracted on Day 3 and conditioned for 25 days until Day 28, at a 95% confidence level. The VC dataset does show significant difference between the various lengths of conditioning and the Day 28 result. Statistically, the

Day 3 and 7 extracted cores have different means than the Day 28 extracted cores; however, the Day 14 extracted cores are not different than the Day 28 cores – this is primarily due to an outlier in the Day 14 extracted cores which reduced the sample size to two. The MH dataset is harder to compare as each set of data was extracted from a different element, in different conditions, with no other cores for comparison from the same element. A small trend regarding an increase in the Day 28 compressive strength can be seen as the length of conditioning increases; however, the R^2 of 0.1393 shows that there is no statistical relation.

4.3.10 All Results: Density Effects

Before compression testing, each sample was weighed and measured. From this, an approximate density was calculated. The sample densities of B1 cores are plotted against the day 28 compressive strength in Figure 4.13 to determine if there is a relation between the two variables. A linear trendline was added, and the R^2 value of 0.0039 shows that there is no correlation between density and compressive strength in this dataset. Plots for the other structures can be found in Appendix B.2. Table 4.4 below summarizes the R^2 of all structures.

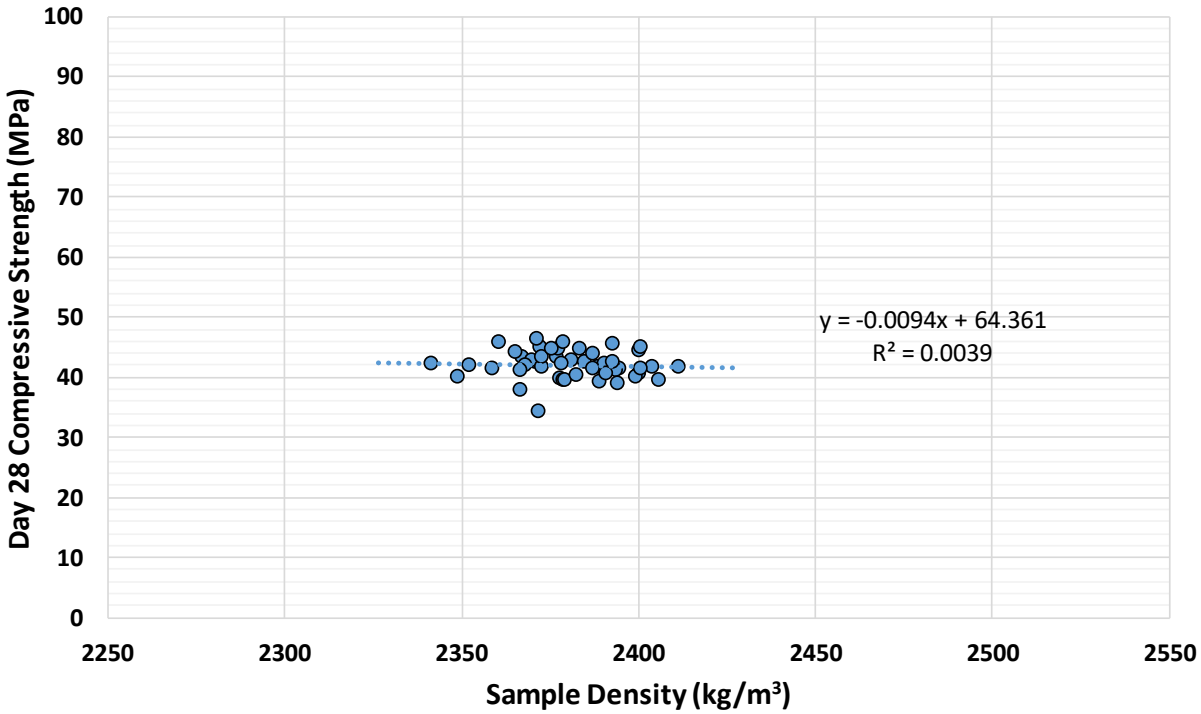

Figure 4.13: Day 28 Compressive Strength of Beam B1 Samples versus Sample Density (Others Found in Appendix B.2)

Table 4.4: Summary Table of R^2 of Day 28 Compressive Strength Versus Density for All Structures

Structure	R^2
B1	0.0039
B2	0.0801
G1	0.1215
G2	0.7187
G3	0.5334
MH	0.0015
VC	0.0719
CC	0.0384

Other than G2 and G3, the R^2 values show that the density and the compressive strength are not correlated. The G2 structure had some consolidation issues during construction, leading to large voids in the samples tested. These large voids are not common in concrete construction and contributed greatly in reducing the density and the compressive strength. The G3 structure was constructed by a precast manufacturer without the supervision of any UW students or technician. As such, no explanation can be given for the results seen. A correlation test was conducted on all the data and resulted in a correlation of 0.0064. While the G2 and G3 structures show good correlation between compressive strength and density, the overall dataset showed that there is no correlation.

4.4 Air Void Analysis

The air void system of a number of samples was analyzed by an MTO certified commercial laboratory (MTO) and by the University of Waterloo (UW). The testing method utilized differed between the testing locations. The naming convention for the sample label is “Structure-Location-Day Cored-Conditioning Type”. Table 4.5 below shows the results of those tests. These data may be used in later sections for discussion. OPSS 1350 [69] requires a minimum air content of 3.0%, and a maximum spacing factor of 0.230 mm, or 0.250 mm for high-performance concrete and silica fume mixtures. The values which exceed the limits of OPSS 1350 are highlighted in the table below.

Table 4.5: Air Void Analysis for Beam B1 Samples

Sample Label	Completed by:	Air Content (%)	Spacing factor (mm)	Paste Content (%)	Specific Surface (mm^{-1})
B1-D-H-3	UW	2.06	0.201	-	36.15
B1-S-H-3	UW	1.72	0.313	-	25.13
B1-D-V-7	UW	2.92	0.170	-	36.60
B1-S-V-7	UW	3.06	0.172	-	35.38
B1-S-H-28	MTO	4.8	0.163	33.04	32.89
B1-S-V-14	MTO	4.5	0.175	33.70	31.71
B2-S-H-28	MTO	6.3	0.162	32.30	28.92
B2-S-V-14	MTO	3.9	0.149	29.93	37.71
G1-S-T-3	MTO	4.2	0.319	41.11	19.65
G1-S-B-3	MTO	3.3	0.238	34.89	27.19
G2-S-T-3	MTO	6.9	0.171	35.00	27.22
G2-S-B-3	MTO	5.3	0.197	34.00	26.53
G3-M-TF-3	MTO	10.2	0.115	27.10	22.95
G3-M-BF-3	MTO	10.6	0.144	26.60	17.35
VC-S-7	MTO	8.7	0.196	33.10	19.39

Chapter 5
Statistical Analysis and Discussion

This chapter discusses in detail the relationships between the different parameters and the performance of the concrete by aggregating the datasets together and performing statistical analysis including regression, analysis of variance, and probability. The parameters investigated are the conditioning type, diameter of the sample, length-to-diameter (*l/d*) ratio, and damage caused by coring.

5.1 Regression Model

Based on the research conducted by MacGregor and Bartlett [7], ACI 214 [3] proposes a correction model, to relate the strength of a non-standard sample to the strength of a standard sample, which has the form:

$$f_{c,s} = F_{mc}F_{l/d}F_{dia}F_{dam}f_{c,ns} \tag{5.1}$$

where $f_{c,s}$ is the compressive strength of a standard sample, $f_{c,ns}$ is the compressive strength of a non-standard sample, and $F_{mc}, F_{l/d}, F_{dia}$, and F_{dam} are all strength correction factors (SCFs) which adjust the compressive strength result of a non-standard to be equivalent to the compressive strength result of a standard sample. A standard sample was defined, in this case, as a cylinder tested on day 28, with a diameter of 100 mm, an *l/d* ratio of 2, and underwent a saturated conditioning state. Each of the SCFs above adjusted the result of the compressive strength test when the parameter is non-standard. F_{mc} adjusted the result if the conditioning used on the sample between coring or demoulding and testing was not a saturated conditioning state, $F_{l/d}$ related the *l/d* ratios if the *l/d* ratio was not 2, F_{dia} related to the diameter of the sample if the diameter was not 100 mm, and F_{dam} related to the damage caused by coring. Each of the SCFs is discussed separately in Section 5.2.

5.1.1 Methodology

The statistical program, R [83], was utilized to run non-linear regression analysis to determine the effect that each parameter has on the compressive strength of a non-standard sample. The regression analysis was initially run once using the least squares method then, using the residuals from the initial model, a second model was calculated using the weightings of $1/residuals^2$. This second model was used for each discussion. Each factor will be discussed individually in the following sections. Some factors, especially $F_{l/d}$, have multiple methods of calculation by many researchers over the years. The

Prediction Sum of Squares (PRESS) was utilized to determine which model best represents the data collected [84]:

$$PRESS = \sum_{i=1}^{n} \left(Y_i - \hat{Y}_i\right)^2 \tag{5.2}$$

where Y_i is the unadjusted strength of the ith sample, and $\hat{Y}_i$ is the adjusted strength of the ith sample using a model developed without the ith sample in the data set. As such, n regressions with datasets of $n-1$ samples are required to calculate the PRESS. This criterion shows the error associated with predicting the SCF on a sample strength without using that data point in the regression.

5.1.2 Methodology of Variance

The variability of the SCFs was calculated using two methods. The first method is the theoretical variability derived from the equation of the SCF, F, using the first order approximation, and the error associated with the coefficients generated by regression, β_i, as follows:

$$V = \frac{\sqrt{Var[F]}}{E[F]} = \frac{\sqrt{\sum_{i=1}^{n} \frac{\partial F}{\partial \beta_i} Var[\beta_i]}}{F} \tag{5.3}$$

The variability calculated above, V, is the coefficient of variation, CoV, defined as the standard deviation, $\sqrt{Var[F]}$, divided by the expected value, $E[F]$. The data was assumed to follow a normal distribution and, thus, the SCF would also be normally distributed, allowing the expected value of the SCF, $E[F]$, to be the value of the SCF, F. The assumption of independence between the coefficients of regression, β_i, allows Equation (5.3) to be simplified as stated above, ignoring the correlation between coefficients.

The second method of determining the variability of the factors captures the variability of the input data as well. This method was outlined by Bartlett and MacGregor [71]. The correction factors all have the following form:

$$\bar{f}_{standard} = F_i \, f_{not\ standard} \tag{5.4}$$

where F_i is the SCF, $\bar{f}_{standard}$ is the average standard compressive strength, and $f_{not\ standard}$ is the individual compressive strength of a non-standard sample. The ratio of test to predicted strength is:

$$R_i = \frac{\bar{f}_{standard}}{F_i \, f_{not\ standard}} \tag{5.5}$$

Due to the error associated with $\bar{f}_{standard}$, $f_{not\ standard}$, and F_i, the first order approximation of variability of R_i includes the variability of each of these terms:

$$Var[R_i] = (E[R_i])^2 * \left(\frac{Var[\bar{f}_{standard}]}{(\bar{f}_{standard})^2} + \frac{Var[f_{not\ standard}]}{(\bar{f}_{not\ standard})^2} + \frac{Var[F_i]}{F_i^2} \right) \tag{5.6}$$

Since F_i is equating $f_{not\ standard}$ and $\bar{f}_{standard}$, $(E[R_i])^2$ would approximate to 1, allowing Equation (5.6) to be simplified to:

$$Var[R_i] = V_{f_{standard}}^2 + V_{f_{not\ standard}}^2 + V_{F_i}^2 \tag{5.7}$$

where $V_{f_{standard}}$ and $V_{f_{not\ standard}}$ are the known CoVs of the input and output data respectively, and V_{F_i} is the unknown CoV of the factor F_i. Since the value of V_{F_i} varies for each observation, a closed form solution cannot be used. However, in a weighted regression, the variance factor, which is equal to the square of the standard error, equals one if the weighting is appropriate [71, 85]. Thus, the CoV of the SCF can be determined with the following iterative process:

i. Guess a value of V_{F_i},
ii. Calculate Equation (5.7), the variance of the test to predicted ratio, for each observation,
iii. Calculate the weight of each test to predicted ratio as the inverse of the variance calculated in step (ii),
iv. Calculate the average and variance factor for the weighted test to predicted ratios. The estimated value of V_{F_i} from step (i) is correct if the variance factor equals 1. Repeat until the variance factor equals 1.

This second method captures the true variability of the factor, while the first method only captures the theoretical variability caused by the regression [71].

5.2 Strength Correction Factors

This section discusses the strength correction factors (SCFs), including the datasets utilized, models, results, variability, and comparison to existing SCFs.

5.2.1 Effect of Conditioning

As discussed in previous chapters, samples were conditioned from the day of extraction or demolding, until the day of testing. There were three types of conditioning conducted: dry, saturated, and moist. Dry samples were sealed in plastic after coring. Saturated samples were placed in a solution of saturated calcium hydroxide. Moist samples were placed in a 100% RH room. The moist conditioning state was only utilized on cylinders in the B1 and B2 structures, and a select number of cores from the G3 structure.

5.2.1.1 Data Analysis

The dataset utilized for determination of this SCF consisted of the B1 and B2 cores. The G3 dataset did include moist samples but did not have an adequate number of corresponding dry samples for comparison; whereas, the B1 and B2 samples had samples which were placed in dry and saturated conditions, with all other parameters the same. Therefore, the effect of conditioning can be isolated. The day 28 cored and tested samples were excluded from the analysis since those samples were not conditioned but left exposed to the laboratory conditions until cored, prepared, and tested, thus introducing large amounts of water to the sample prior to testing whereas the earlier cored dry samples had been sealed for at least 14 days before testing. Therefore, this dataset contains 72 cores, 36 of which were dry conditioned, and 36 were saturated. All samples were cored on days 3, 7, or 14, tested on day 28, had a *l/d* ratio of 2, and a diameter of 100 mm. The only difference between the samples was the conditioning state, and the direction of coring. However, in Chapter 4, the difference between the vertical and horizontal samples was found to not be significantly different. To determine the factor, F_{mc}, a direct comparison between the dry cores and the saturated cores was made. The saturated cores were set as the standard value, and the dry cores were multiplied by F_{mc}, given below:

$$F_{mc} = 1 + \beta_{dry} Z_{dry} \tag{5.8}$$

where β_{dry} is a coefficient determined by regression and Z_{dry} is an indicator variable which is 1 when the core is the dry conditioned, and 0 for the saturated condition. Therefore, in the standard case of saturated conditioning, the value of F_{mc} is 1. Using R [83], the value of β_{dry} was found. The variability associated with this factor can be calculated by Equation (5.9), using the first order approximation method. The second method, discussed in Section 5.1.2, was also used. A summary of the values is shown below in Table 5.1.

$$V_{mc} = \frac{\sqrt{Var[F_{mc}]}}{E[F_{mc}]} = \frac{\sqrt{Z_{dry}^2 Var[\beta_{dry}]}}{1 + \beta_{dry} Z_{dry}} \tag{5.9}$$

Table 5.1: Summary of F_{mc} Regression

Coefficient	Value	Standard Error	P-value	Value of F_{mc}	Theoretical V_{mc} (%)	True V_{mc} (%)
β_{dry}	-0.023	0.000068	<2.22E-16	0.977	0.007	12.325

From the table above, the value of β_{dry} is negative, indicating that the dry sample's compressive strength must be decreased in order to be equal to that of a saturated sample. The difference between the two methods of variance calculation can also be seen. The first method, the first-order approximation, is the theoretical V and the true variability is the second method discussed, which incorporates the variability of the input data. This CoV only applies if the factor applies, i.e. the sample is not saturated, otherwise V_{mc} would be zero. The CoV of the input data is 9.31% for the dry conditioned samples, and 4.73% for the saturated conditioned samples.

5.2.1.2 Discussion of Results

The SCF, F_{mc}, given in the above section indicates that saturating the sample reduces the compressive strength of the sample. This matches with previous research of Popovics [40] who found that saturating a concrete sample before testing reduced the compressive strength greatly compared to when the sample is dried before testing. Popovics' reasoning is that when the sample is saturated, the outer region of the concrete sample is trying to expand and does so faster than the interior, due to the limited permeability of the concrete sample restricting the amount of water ingress. This creates a lateral biaxial tension in the sample, and reduces the overall compressive strength of the sample [40].

ACI 214 [3] gives a SCF for saturated samples of 1.09 with the standard sample being the dried sample. Therefore, the inverse is the factor for dried samples when the standard is defined as the saturated sample, which is 0.917. For comparison, the SCF found above was 0.977. To determine if the new SCF is statistically different than the existing SCF, the confidence interval of the new SCF is found, and if the existing factor is included in the confidence interval, then they are not statistically different:

$$\begin{aligned} \hat{\beta}_{dry} - t_{n-m-1,\alpha/2}\widehat{SE} \leq \beta_{dry} \leq \hat{\beta}_{dry} + t_{n-m-1,\alpha/2}\widehat{SE} \\ -0.023 - t_{70,0.05/2} * 0.00897 \leq \beta_{dry} \leq -0.023 + t_{70,0.05/2} * 0.00897 \\ -0.023 - 1.994 * 0.00897 \leq \beta_{dry} \leq -0.023 + 1.994 * 0.00897 \\ -0.041 \leq \beta_{dry} \leq -0.005 \end{aligned} \quad (5.10)$$

where $\hat{\beta}_{dry}$ is the estimate of the value of β_{dry} given regression, which is -0.023, $t_{n-2,\alpha/2}$ is the value of a two-tailed T-distribution with degrees of freedom of $n - m - 1$, where n is the number of samples in the regression, and m is the number of coefficients regressed, and significance α, and $\widehat{SE}$ is the standard error associated with $\hat{\beta}_{dry}$. The value of -0.023, which is the β_{dry} of the existing model, is not included in the confidence interval of the new SCF. Thus, the new model and the existing model are statistically different at a 95% confidence level. Figure 5.1 below shows the predicted compressive strength of the dry samples and the residual between the predicted compressive strength and the standard, along with an unconservative 5% error line.

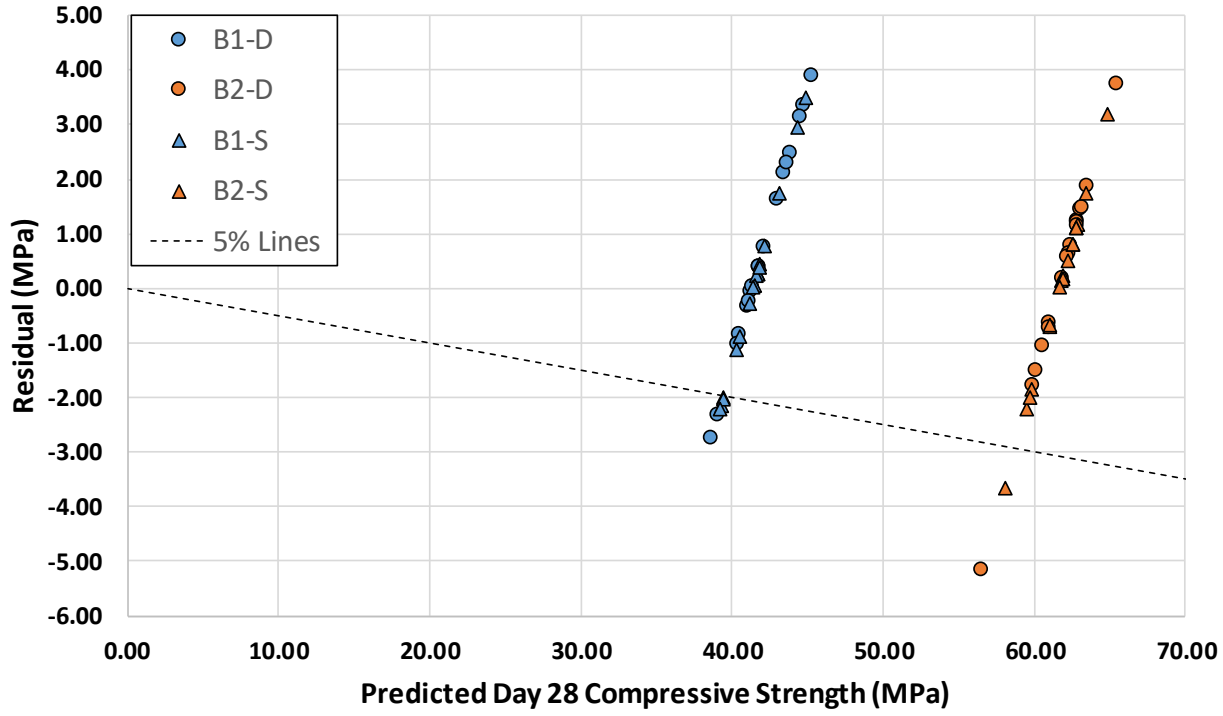

Figure 5.1: B1 and B2 Predicted Day 28 Compressive Strength versus the Residual between the Predicted Sample Day 28 Compressive Strength and the Standard Considering Conditioning

The graph above shows that 7 of the 18 dry B1 samples, 2 of the 17 dry B2 samples, 6 of the 18 saturated B1 samples, and 1 of the 18 saturated B2 samples were outside the ±5% error line. The data points follow a linear trend as Equation (5.8) is a linear equation with only one parameter: the conditioning state. The $\bar{f}_{standard}$ is also the same for all the cores in each set, which is the average compressive strength of the saturated cores.

5.2.2 Effect of Length-to-Diameter Ratio

Samples with a length-to-diameter (*l/d*) ratio of 1.5 and 2 were tested. CSA A23 [4], ASTM C42M [2], and ACI 214 [3] all include a SCF for when a specimen has a *l/d* ratio less than 2. This specimen can be either a drilled core or a cast cylinder. This section will discuss how the *l/d* ratio was analyzed, and present and discuss the results of the analysis.

5.2.2.1 Data Analysis

Models of various forms have been proposed and utilized in the past to calculate the *l/d* ratio strength correction factor, $F_{l/d}$ [3, 4, 62–67]. These models were used as proposed and some, which were an outcome of a regression analysis, underwent regression analysis again with the data collected to determine if the original model is adequate for the current samples. These models were incorporated into Equation (5.1) as the function which represents $F_{l/d}$. The PRESS statistic was utilized to determine which model best represented the dataset.

The dataset contains the results from the VC and CC structures, which contains 122 cores and 123 cylinders, respectively. These datasets were utilized since there was a direct comparison sample for each sample tested, since both sets included samples with diameters of 100 mm and 75 mm, and *l/d* ratios of 1.5 and 2 in both diameters. The only difference between the structure sets is that VC is only cores and CC is only cylinders. Other data which could have been included is G1 and G3. G1 has 75 mm diameter samples at a *l/d* ratio of 2, and 100 mm diameter samples at a *l/d* ratio of 1.5. G3 has mainly 100 mm diameter samples at a *l/d* ratio of 1.5, with a few at a *l/d* ratio of 2. The reason these data were not included was that there is no direct comparison between samples. G1 would have effect contribution from both diameter and *l/d* ratio factors simultaneously. The G3 dataset on the other hand has location and coring direction effects as well.

Table 5.2 below shows the models investigated, where models noted with R [83], signify the model was regressed with the data collected, otherwise the model was an existing model. Models noted with an asterisk (*) were not significant at a 5% confidence level. Average values of the predicted SCFs for *l/d* ratios of 2 and 1.5 are also shown. Lower values of PRESS signify a better fit of the model.

Table 5.2: Models Evaluated with *l/d* SCF and PRESS

#	$F_{l/d}$ Model	Source	$\bar{F}_{l/d=2}$	$\bar{F}_{l/d=1.5}$	PRESS	
1	$\frac{2}{1.5 + d/l}$	The Concrete Society (1976) [64]	0.995	0.921	3455	
2	$\frac{1}{1 + 0.8(1 - 0.5 * l/d)^2}$	Chung (1979) [65]	1.000	0.950	2079	
3	$\frac{1}{1 + 0.8 * \left(d/l\right)\left(1 - 0.5 * \left(l/d\right)\right)^2}$	Chung (1989) [66]	1.000	0.966	1635	
4	$1 * Z_{l/d=2} + 0.96 * Z_{l/d=1.5}$	CSA A23 [4]	1.000	0.960	1784	
5	$1 - \{0.117 - 4.3 * 10^{-4} * f_{core}\}\left(2 - l/d\right)^2$	ACI 214-14 [3]	1.000	0.976	1469	
6	$0.1385 \ln\left(l/d\right) + 0.9069$	Arioz et al. (2006) [67]	1.000	0.962	1731	
7	$\bar{f}_{l/d=2} \Big/ \bar{f}_{l/d=1.5}$	Meininger (1977) [62]	1.000	0.995	1121	
8	$1 - 627\left(2 - l/d\right)^{17.35}$	Bartlett and MacGregor (1994) [63]	1.000	0.993	1449	R*
9	$1 - 0.2437\left(2 - l/d\right) + 0.0660\left(4 - \left(l/d\right)^2\right)$	Bartlett and MacGregor (1994) [63]	1.000	0.993	1369	R
10	$1 - \{-0.4776 + 8.349 * 10^{-3} * f_{core}\}\left(2 - l/d\right)^{0.2607}$	ACI 214-14 [3]	0.998	0.999	987	R
11	$1 - \{-1.5039 + 2.633 * 10^{-2} * f_{core}\}\left(2 - l/d\right)^2$	ACI 214-14 [3]	1.000	0.998	1052	R
12	$0.02323 \ln(l/d) + 0.9840$	Arioz et al. (2006) [67]	1.000	0.962	1360	R

Notes: * - Not significant at a 95% confidence level
R – Values regressed using R

As shown in Table 5.2, $\bar{F}_{l/d=2}$ is approximately 1.0 for all the models, and the value of $\bar{F}_{l/d=1.5}$ varies from 0.921 to 0.999 depending on which model is chosen to represent $F_{l/d}$. The best models overall were the regressed ACI 214 models, with the lowest PRESS values of 987 and 1052. The only difference between these two models is that the exponent was regressed in one case and left as 2 in the other case.

Both versions outperformed all other models tested, with the regressed exponent model having the best PRESS. The Meininger [62] model, which averages the values of the samples with a *l/d* ratio of 2 to the samples with a *l/d* ratio of 1.5, was better than all the models other than the ACI 214 models.

The variability of the models representing $F_{l/d}$ can be found using the methodology found in Section 5.1.2. The first order approximation of variability equations of each model is shown in Appendix C.1. The CoV associated with the model representing $F_{l/d}$ is summarized below in Table 5.3. The CoV of the input data is 5.00% for *l/d* ratio of 2, and 6.79% for *l/d* ratio of 1.5.

Table 5.3: Summary of Variability of $F_{l/d}$ Models

#	$F_{l/d}$ Model	Theoretical $V_{l/d}$ (%) at *l/d*=1.5	True $V_{l/d}$ (%) at *l/d*=1.5
1	$\frac{2}{1.5 + d/l}$	1.508	6.785
2	$\frac{1}{1 + 0.8(1 - 0.5 * l/d)^2}$	0.256	6.850
3	$\frac{1}{1 + 0.8 * \left(d/l\right)\left(1 - 0.5 * \left(l/d\right)\right)^2}$	0.208	6.919
4	$1 * Z_{l/d=2} + 0.96 * Z_{l/d=1.5}$	0.036	6.883
5	$1 - \{0.117 - 4.3 * 10^{-4} * f_{core}\}\left(2 - l/d\right)^2$	0.559	6.968
6	$0.1385\ \ln\left(l/d\right) + 0.9069$	0.063	6.904
7	$\bar{f}_{l/d=2} \Big/ \bar{f}_{l/d=1.5}$	0.012	6.985
8	$1 - 627\left(2 - l/d\right)^{17.35}$	0.899	7.058
9	$1 - 0.2437\left(2 - l/d\right) + 0.0660\left(4 - \left(l/d\right)^2\right)$	4.642	7.051
10	$1 - \{-0.4776 + 8.349 * 10^{-3} * f_{core}\}\left(2 - l/d\right)^{0.2607}$	0.594	7.111
11	$1 - \{-1.5039 + 2.633 * 10^{-2} * f_{core}\}\left(2 - l/d\right)^2$	0.916	7.036
12	$0.02323\ \ln(l/d) + 0.9840$	0.098	7.062

5.2.2.2 Discussion of results

The best models in the previous section were the ACI 214 models, model #9 and #10, as well as the Meininger model, model #7, as they had the lowest PRESS values. In model #10, the ACI 214 model, the regressed exponent tended to approach zero, signifying the *l/d* ratio does not affect the *l/d* SCF, which is counterintuitive. Therefore, this model was disregarded. The next best model was the Meininger model, which averaged the values. However, this may not be viable, as a set of samples at *l/d* ratios of both 2 and 1.5 would be required. To determine if the newly regressed ACI 214 model is different than the existing model, the confidence intervals on the coefficients of regression was completed, following Equation (5.10) above. The results are shown below in Table 5.4, with the model form shown below:

$$1 - \{\beta_1 - \beta_2 * f_{core}\}\left(2 - {}^{l}/_{d}\right)^2 \tag{5.11}$$

Table 5.4: Results of Confidence Intervals on Coefficients of Regression of ACI 214 Model

Coefficient	Confidence Interval of Regressed	Existing Value
$\beta_1 = -1.5086$	$-1.5600 \leq \beta_1 \leq -1.4479$	0.1300
$\beta_2 = -2.644 * 10^{-2}$	$-2.744 * 10^{-2} \leq \beta_2 \leq -2.522 * 10^{-2}$	$4.300 * 10^{-4}$

As can be seen above, the existing values of the ACI 214 fall outside the confidence interval of the newly regressed model, showing that the models are statistically different. The confidence interval on the SCF itself, $F_{l/d}$, for an *l/d* ratio of 1.5 is: $0.978 \leq F_{l/d} \leq 0.984$, for $f_{core} = 60\ MPa$. Therefore, the SCF of 0.96 for an *l/d* ratio of 1.5 from ASTM C42/C39 [2, 5] and CSA A23.1 [4] is not valid for this model.

An interesting note from the models analyzed above is that averaging the strengths of cores with *l/d* ratio of 2 and of 1.5 produced results on par with the other models regressed, signified by the PRESS value, other than the ACI 214 model. If possible, testing on each concrete mixture and structure type could produce individualized factors for each situation that are more accurate than generalized SCFs. Figure 5.2 below shows the predicted compressive strengths using the ACI 214 model of the VC and CC versus the residual of the predicted sample and the standard, and an unconservative 5% error line, and Figure 5.3 shows this for Meininger's Model.

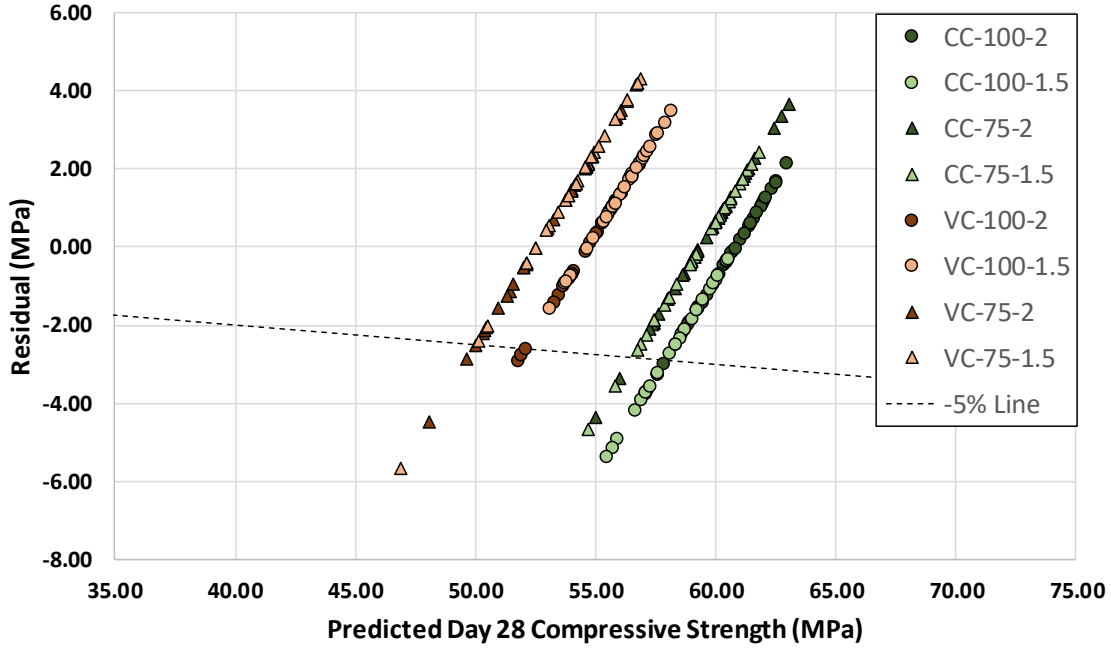

Figure 5.2: CC and VC Predicted Day 28 Compressive Strength using ACI 214's Model versus the Residual between the Predicted Sample Day 28 Compressive Strength and the Standard Considering *l/d* Ratio

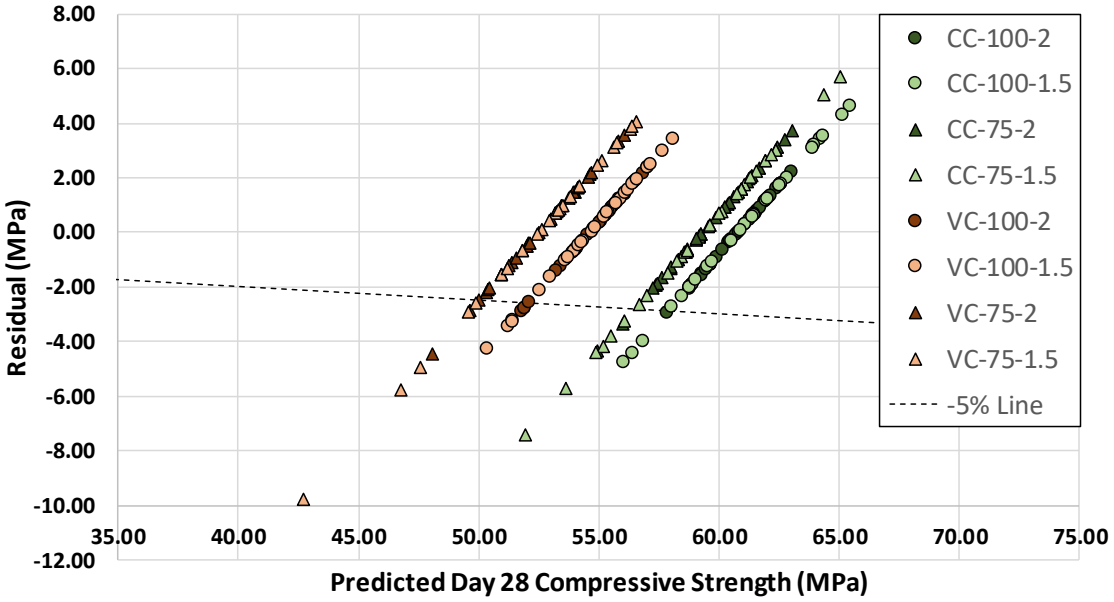

Figure 5.3: CC and VC Predicted Day 28 Compressive Strength using Meininger's Model versus the Residual between the Predicted Sample Day 28 Compressive Strength and the Standard Considering *l/d* Ratio

For the ACI 214 Model, in total, 23 of the 245 samples were more than 5% errors on the unconservative side. Of those 23, 13 were in the CC-100-1.5 dataset, 2 in CC-75-2, 2 in CC-75-1.5, 3 in VC-100-2, 2 in VC-75-2, and 1 in VC-75-1.5. As the datasets became more variable, i.e. smaller diameter or *l/d* ratio, the number of samples with larger errors increased. For the Meininger's Model, 25 of the 245 samples were more than 5% errors on the unconservative side. Of those 25, 3 were in the C-100-1.5 dataset, 2 in CC-75-2, 6 in CC-75-1.5, 3 in VC-100-2, 4 in VC-100-1.5, 2 in VC-75-2, and 5 in VC-75-1.5. Again, as the datasets became more variable, the number of samples with larger errors increased. Meininger's Model contains slightly more data points which are unconservative compared to ACI 214's Model.

5.2.3 Effect of Sample Diameter

Samples with diameters of 100 mm and 75 mm were tested. CSA A23[4] requires that the diameter of a sample is at least three times the maximum aggregate size, with a 100 mm minimum diameter recommended. ASTM C42M [2] requires the minimum diameter to be the larger of 94 mm or two times the maximum aggregate size. ACI 214 [3] allows the use of cores with diameters as small as 50 mm, but recommends the use of 100 mm diameter. Only ACI 214 [3] contains a factor to adjust the strength of various diameters to 100 mm samples. This section will discuss how the diameter effect was analyzed, and present and discuss the results of the analysis.

5.2.3.1 Data Analysis

The dataset used for this analysis consisted of the VC and CC samples, which contains 122 cores and 123 cylinders, respectively. These sample sets were utilized because the effect of the diameter can be isolated, as there were 100 mm and 75 mm diameter samples with the same *l/d* ratios. Both the *l/d* ratios of 2 and 1.5 were included in these datasets. Other datasets which had 75 mm diameter samples included: G1, and G2. G1 had both 75 mm and 100 mm cores extracted. However, both samples had a length of 150 mm which resulted in differing *l/d* ratios for each diameter. Therefore, including the G1 dataset would require accounting for the *l/d* ratio effects as well. G2 had only 75 mm diameter samples with no 100 mm diameter counterparts for comparison. For these reasons, only the VC and CC datasets were selected. The CC and VC datasets include 245 samples, with roughly 30 samples in each diameter and *l/d* ratio combination.

The diameter SCF has been modelled using two methods, shown in the equations below:

$$F_{dia} = 1 + Z_{dia}\beta_{\text{dia}} \tag{5.12}$$

$$F_{dia} = 1 + Z_{dia}(Z_{l/d=2}\beta_{l/d=2} + Z_{l/d=1.5}\beta_{l/d=1.5}) \tag{5.13}$$

where $\beta_{dia}, \beta_{l/d=2}, \beta_{l/d=1.5}$ are coefficients determined by regression, and $Z_{dia}, Z_{l/d=2}, Z_{l/d=1.5}$ are indicator variables: Z_{dia} is 0 for 100mm diameter samples and 1 for 75mm diameter samples, $Z_{l/d=2}$ is 1 for samples with an *l/d* ratio of 2, and 0 otherwise, and $Z_{l/d=1.5}$ is 1 for samples with an *l/d* ratio of 1.5, and 0 otherwise. Therefore, F_{dia} is 1 for 100mm diameter samples in both models and determined by regression for the 75mm diameter cores. In Equation (5.13), the factor will be dependent on the sample's *l/d* ratio, while Equation (5.12) is not. Using R, the values of β were found. The variability associated with this factor can be calculated by Equation (5.14), using the first order approximation method. The second method, discussed in Section 5.1.2, was also used. A summary of the values is shown below in Table 5.5.

$$V_{mc} = \frac{\sqrt{Var[F_{dia}]}}{E[F_{dia}]} = \frac{\sqrt{Z_{dia}^2 Var[\beta_{dia}]}}{1 + \beta_{dia}Z_{dia}}$$
$$and \ \frac{\sqrt{Z_{dia}^2(Z_{l/d=2}^2 Var[\beta_{l/d=2}] + Z_{l/d=1.5} Var[\beta_{l/d=1.5}]}}{1 + Z_{dia}(Z_{l/d=2}\beta_{l/d=2} + Z_{l/d=1.5}\beta_{l/d=1.5})} \tag{5.14}$$

Table 5.5: Summary of F_{dia} Regression

Coefficient	Value	Standard Error	P-value	Value of F_{dia}	PRESS	Theoretical V_{dia} (%)	True V_{dia} (%)
β_{dia}	0.015	0.0000535	<2.22E-16	1.015	1147	0.005	8.497
$\beta_{l/d=2}$	0.033	0.0001855	<2.22E-16	1.033	1024	0.018	8.025
$\beta_{l/d=1.5}$	-0.005	0.0009384	4.15E-6	0.995		0.094	

From the table above, the value of β can be positive or negative, depending on the model and the *l/d* ratio. The first model checked, increases the strength of 75 mm diameter samples by 1.5% in order to be equivalent to a 100 mm diameter sample. Once the factor is dependent on the *l/d* ratio, it increases to 1.033 for samples with an *l/d* ratio of 2 and decreases to 0.995 for samples with an *l/d* ratio of 1.5. This indicates that the 75 mm diameter samples with an *l/d* ratio of 1.5 have a higher compressive strength than the 100 mm diameter samples and needs to be reduced to become equivalent. This is the opposite as the first model and is due to the CC-sample set with an *l/d* ratio of 1.5, which had a higher compressive

strength in the smaller diameter, resulting in the negative value of $\beta_{l/d=1.5}$. The second model has a lower PRESS which indicates a better fit. The true variability also indicates that the second model is less variable. The CoV only applies if the factor applies, i.e. the sample is not 100 mm diameter, otherwise V_{dia} would be zero. The CoV of the input data for the first model is 6.10% for the 75 mm diameter samples, and 3.86% for the 100 mm diameter samples. The CoV of the data used for the second model is 4.88% for 75 mm diameter, and 3.86% for 100 mm diameter samples at an *l/d* ratio of 2, and 6.85% for 75 mm diameter, and 5.60 % for 100 mm diameter samples at an *l/d* ratio of 1.5.

5.2.3.2 Discussion of Results

Previous research has shown that smaller diameter samples are more susceptible to many factors [54], and especially more susceptible to the *l/d* ratio [49]. When the diameter model was separated to include the *l/d* parameter, the diameter effect was more pronounced. ACI 214 [3] includes a factor of 1.03 for equating 75 mm diameter samples to 100 mm diameter samples, which means that $\beta_{dia} = 0.03$. To determine if the newly regressed diameter factor models are different than the existing model, the confidence intervals on the coefficients of regression was completed, following Equation (5.10) above. The results are shown below in Table 5.6.

Table 5.6: Results of Confidence Intervals on Coefficients of Regression of Diameter Factor

Coefficient	Confidence Interval of Regressed	Existing Value
$\beta_{dia} = 0.0147$	$0.0145 \leq \beta_{dia} \leq 0.0148$	
$\beta_{l/d=2} = 0.0329$	$0.0325 \leq \beta_{l/d=2} \leq 0.0333$	0.03
$\beta_{l/d=1.5} = -0.0045$	$-0.0067 \leq \beta_{l/d=1.5} \leq -0.0024$	

As can be seen above, the existing values of the diameter factor fall outside the confidence interval of the newly regressed model; however, if the $\beta_{l/d=2}$ was rounded, the value would be 0.03, which matches the existing value. Therefore, for samples with an *l/d* ratio of 2, the existing factor may be adequate. The approximate CoV of the existing factor is 5.9%, which is lower than the 8.0% CoV found in the previous section. Therefore, the existing model is still adequate with the new model. Figure 5.4 and Figure 5.5 below show the predicted compressive strengths using both regressed models of the VC and CC versus the residual of the predicted sample and the standard, and an unconservative 5% error line.

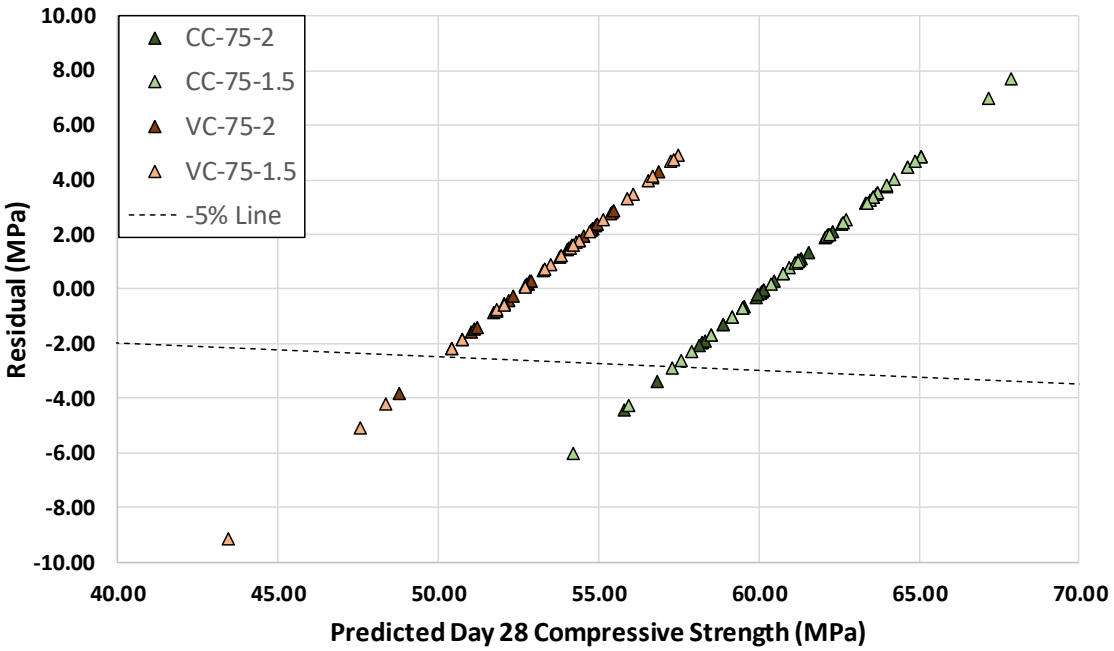

Figure 5.4: CC and VC Predicted Day 28 Compressive Strength Using Model 1 versus the Residual between the Predicted Sample Day 28 Compressive Strength and the Standard Considering Diameter

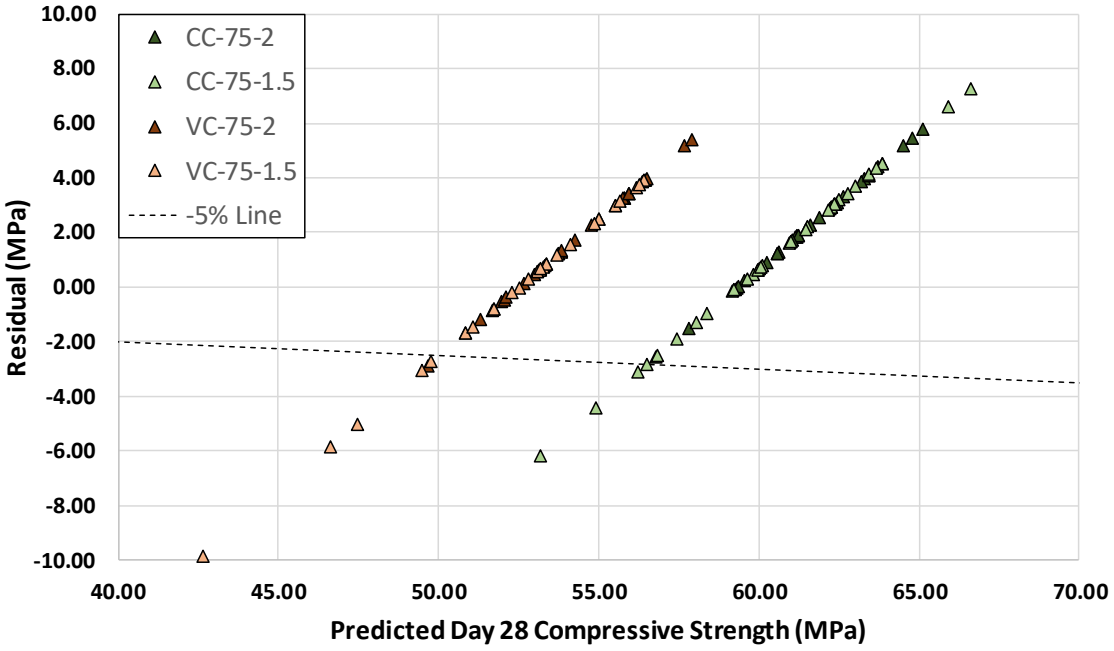

Figure 5.5: CC and VC Predicted Day 28 Compressive Strength using Model 2 versus the Residual between the Predicted Sample Day 28 Compressive Strength and the Standard Considering Diameter

In total, 8 of the 125 75 mm diameter samples were below the 5% error line in model 1, and 9 in model 2. Model 2 had a lower PRESS compared to model 1, with approximately the same number of samples which were unconservative.

5.2.4 Effect of Damage Caused by Coring

In all the structures tested, cylinders and cores were both tested. As discussed previously, coring causes damage to the outer region of the core, which reduces the compressive strength. ACI 214 [3] includes a factor of 1.06 to compensate for damage caused by coring. This section discusses the coring damage by investigating the data collected to create a SCF due to the damage caused by coring.

5.2.4.1 Data Analysis

Even though both cylinders and cores were tested in each dataset, only the samples from the CC and VC datasets are utilized in this analysis. The cores from the VC structure and the cylinders from the CC dataset were nearly identical in all aspects: concrete mixture, curing conditionings, number of samples tested, diameter, and *l/d* ratio. The other datasets, while there are cylinders which could be used as the standard to compare the cores to, do not have the amount of isolation which the CC and VC datasets allow. This dataset contains 116 cores and 129 cylinders. These sample sets are roughly split into four groups of diameter 75 mm and 100 mm, and *l/d* ratio 1.5 and 2. The cylinders were set as the standard value, and the cores were multiplied by F_{dam}, represented by three models given below:

$$F_{dam} = 1 + \beta_{dam1} Z_{core} \tag{5.15}$$

$$F_{dam} = 1 + (\beta_{100@2} Z_{100@2} + \beta_{100@1.5} Z_{100@1.5} + \beta_{75@2} Z_{75@2} + \beta_{75@1.5} Z_{75@1.5}) Z_{core} \tag{5.16}$$

$$F_{dam} = 1 + \left(1 - \frac{\beta_{dam2}}{D}\right)^{-1} Z_{core} \tag{5.17}$$

where β_i are coefficients determined by regression and Z_i are indicator variables which are 1 when the condition is met, and 0 otherwise. For example, $Z_{75@2}$ is 1 when the sample is 75 mm diameter and has an *l/d* ratio of 2, and 0 otherwise. Note that in the standard case of a cylinder, the value of F_{dam} is 1 in each model, due to Z_{core}. Using R, the values of β_i were found. The variability associated with these factors can be calculated by using the first order approximation method and is shown in Appendix C.2. The second method, discussed in Section 5.1.2, was also used. A summary of the values is shown in Table 5.7.

Table 5.7: Summary of F_{dam} Regression

Coefficient	Value	Standard Error	Diameter (mm)	*l/d* Ratio	Value of F_{dam}	PRESS	Theoretical V_{dam} (%)	True V_{dam} (%)
β_{dam1}	0.111	0.0008561	N/A	N/A	1.111	727	0.077	7.446
$\beta_{100@2}$	0.114	0.0010709	100	2	1.114	934	0.096	7.675
$\beta_{100@1.5}$	0.130	0.0018643	100	1.5	1.130		0.165	
$\beta_{75@2}$	0.064	0.0010737	75	2	1.064		0.101	
$\beta_{75@1.5}$	0.149	0.0008740	75	1.5	1.149		0.076	
β_{dam2}	8.8775	0.0180119	100	N/A	1.097	599	0.010	7.742
			75	N/A	1.134		0.014	

In all the models, other than $\beta_{75@2}$, results in factors nearly double the existing factor of 1.06. The difference between the theoretical and the true variability can also be seen. This CoV only applies if the factor applies, i.e. the sample is a core, otherwise V_{dam} would be zero. The CoV of the input data is 7.51 % for the cores, and 7.73 % for the cylinders.

5.2.4.2 Discussion of Results

Previous research concludes that smaller diameter samples were exposed to more damage caused by coring due to the increased surface area to volume ratio in smaller samples [48, 65]. However, that was not the case in the above analysis, as the $\beta_{75@2}$ was nearly half the value of $\beta_{100@2}$. To determine if the values are statistically different than each other, in the case of model 2, and from the existing value, a 95% confidence interval on the values was found following Equation (5.10). The results are shown in Table 5.8.

From Table 5.8, the existing factor of 1.06 is only close to the value of $\beta_{100@1.5}$,. Within each model, the factors are independent of each other as well, i.e. $\beta_{75@2}$ and $\beta_{75@1.5}$ are statistically different. With this data, the existing factor may not be adequate. The approximate CoV of the existing factor is 2.5%, which is lower than the 7.5-7.8% CoV found in the previous section. Figure 5.6 shows the predicted compressive strengths using only the last model of the VC and CC versus the residual of the predicted sample and the standard, and an unconservative 5% error line. In total, 12 of the 117 cores were below the 5% error line, with 9 of those in the VC-100-1.5 dataset.

Table 5.8: Results of Confidence Intervals on Coefficients of Regression of Damage Factor

Coefficient	Confidence Interval of Regressed Coefficient	Confidence Interval of Regressed F_{dam}	Existing Value of F_{dam}
β_{dam1}	$0.1095 \leq \beta_{dam1} \leq 0.1134$	$1.1095 \leq F_{dam} \leq 1.1134$	1.06
$\beta_{100@2}$	$0.1111 \leq \beta_{100@2} \leq 0.1159$	$1.1111 \leq F_{dam} \leq 1.1159$	
$\beta_{100@1.5}$	$0.0619 \leq \beta_{100@1.5} \leq 0.0668$	$1.0619 \leq F_{dam} \leq 1.0668$	
$\beta_{75@2}$	$0.1259 \leq \beta_{75@2} \leq 0.1344$	$1.1259 \leq F_{dam} \leq 1.1344$	
$\beta_{75@1.5}$	$0.1474 \leq \beta_{75@1.5} \leq 0.1514$	$1.1474 \leq F_{dam} \leq 1.1514$	
β_{dam2}	$8.8358 \leq \beta_{dam2} \leq 8.9176$	$1.0969 \leq F_{dam,100} \leq 1.0979$ $1.1335 \leq F_{dam,75} \leq 1.1349$	

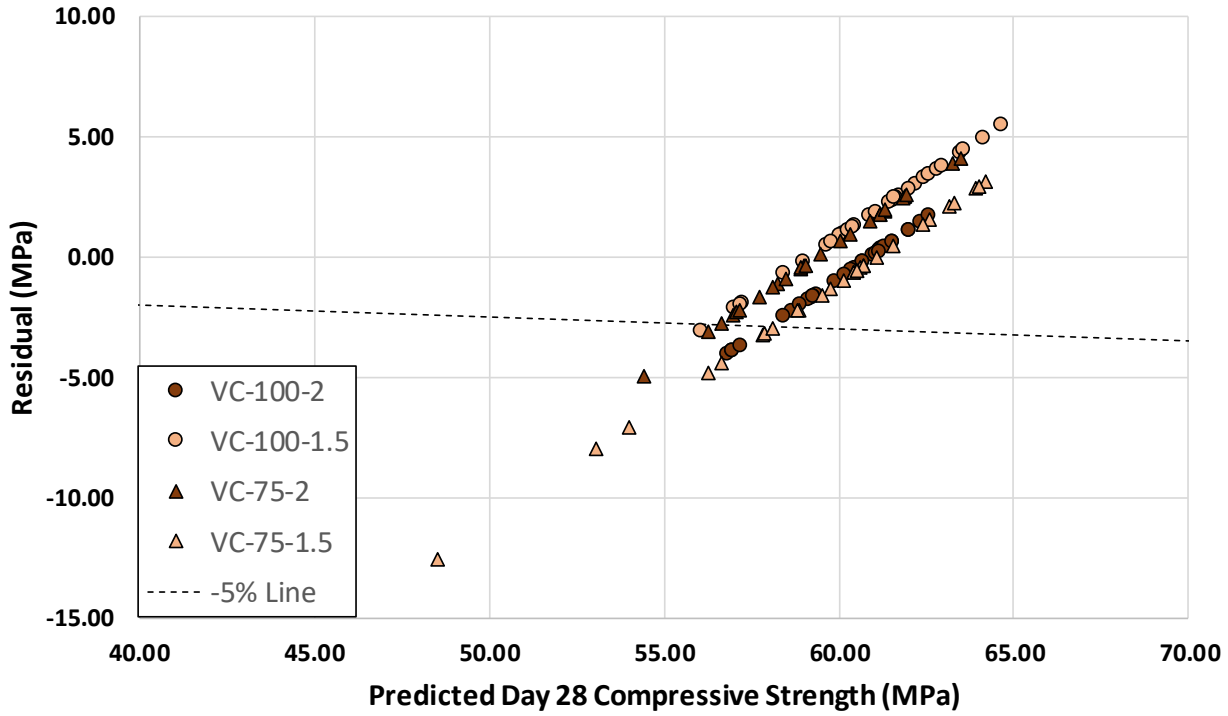

Figure 5.6: CC and VC Predicted Day 28 Compressive Strength Using Model 3 versus the Residual between the Predicted Sample Day 28 Compressive Strength and the Standard Considering Damage

5.2.5 Combination of All Strength Correction Factors

Now that all the factors have been found individually, they can all be applied to the whole dataset to determine wellness of fitness, which contains 443 samples. As some of the factors had multiple models

which were acceptable, all combinations of those models were checked to determine which resulted in the least squared errors. Figure 5.7 shows the predicted compressive strengths using only the best fit model of the all the datasets versus the residual of the predicted sample and the standard, and an unconservative 5% error line.

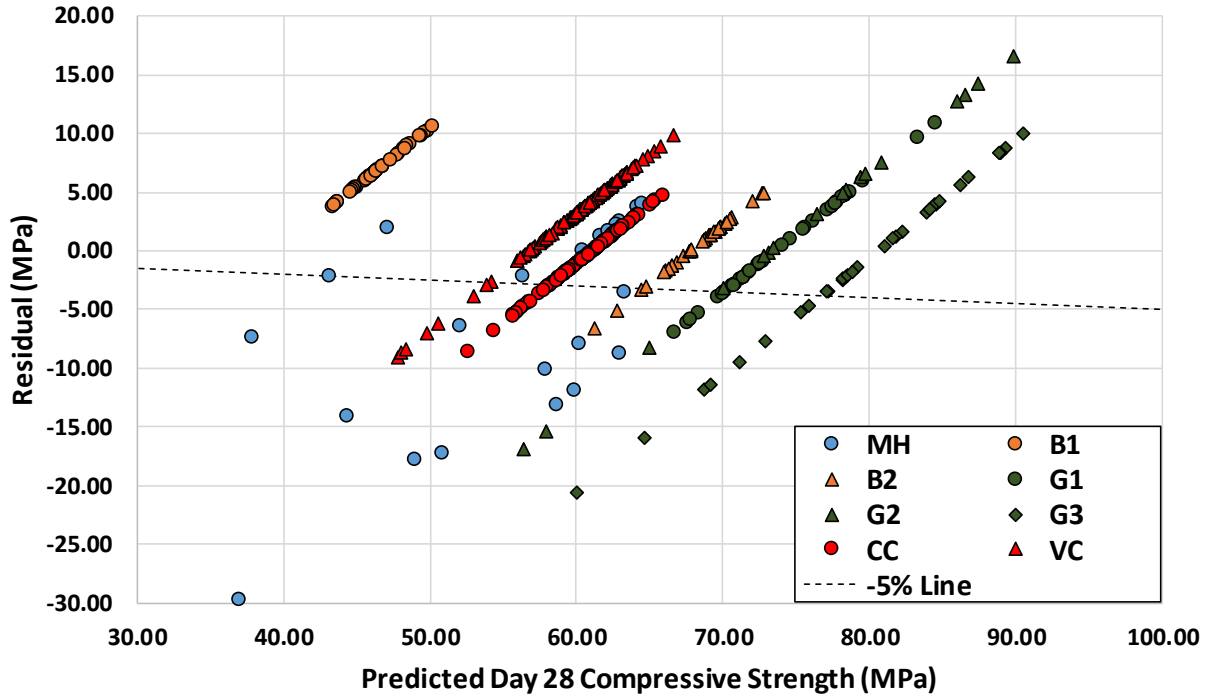

Figure 5.7: All Predicted Day 28 Compressive Strength, using All SCFs, versus the Residual between the Predicted Sample Day 28 Compressive Strength and the Standard

The model utilized in the above figure is shown below:

$$f_{c,s} = F_{mc}F_{l/d}F_{dia}F_{dam}f_{c,ns} \tag{5.18}$$

$$F_{mc} = 1 + \beta_{dry}Z_{dry} = 1 - 0.0234 * Z_{dry} \tag{5.19}$$

$$F_{l/d} = \bar{f}_{l/d=2} \Big/ \bar{f}_{l/d=sample\ l/d} \tag{5.20}$$

$$F_{dia} = 1 + Z_{dia}\beta_{\text{dia}} = 1 + 0.0147 * Z_{dia} \tag{5.21}$$

$$F_{dam} = 1 + \beta_{dam1}Z_{core} = 1 + 0.1111 * Z_{core} \tag{5.22}$$

where each model has been discussed in their own respective sections. In total, 55 of the 443 data points were below the 5% unconservative line. A more detailed breakdown of these unconservative values is shown in Table 5.9.

Table 5.9: Combined SCF Model Unconservative Values Summary

Dataset	Total Number of Samples	Unconservative Samples	
MH	22	12	55%
B1	39	0	0%
B2	41	2	5%
G1	36	6	17%
G2	17	3	18%
G3	31	8	26%
VC	129	7	5%
CC	128	17	13%
Total	443	55	12%

As can be seen in the above table, the MH and G3 datasets have a large portion of their samples as unconservative samples. Even considering these unconservative datasets, the overall unconservative samples is 12% of the total number of samples. With the MH and G3 datasets removed, the overall number drops to 40 unconservative samples of 404 total samples, consisting of 10%.

5.3 Equivalent Variability of Samples

Conventionally, cores for compressive strength testing are extracted in sets of three. These three cores are typically of standard parameters: 100 mm diameter, *l/d* ratio of 2, and conditioned using standard procedure. However, there are times when these parameters are not possible to achieve, for example in areas of heavily congested rebar. The SCFs discussed above equate the non-standard sample to a standard sample, with the variation associated with each factor. However, the number of cores generally remains at three when the variability of the cores increases, which is often inappropriate. One method to determine the required number of samples when the variability of the data changes is to maintain the confidence interval (CI) of the baseline data. For example, if three standard cores have an average compressive strength of $\mu \pm \varepsilon$, then this CI of $\pm\varepsilon$ should be maintained by increasing the number of samples in order to reach this CI.

Since the compressive strength of a concrete sample is a normally distributed random variable, the average of multiple samples is also a normally distributed random variable, with a mean $\bar{X}$ and variance s^2/n [86, p. 275]. The CI of the mean is:

$$\bar{X} - t_{\alpha/2,n-1} * \frac{s}{\sqrt{n}} \leq \mu \leq \bar{X} + t_{\alpha/2,n-1} * \frac{s}{\sqrt{n}} \quad (5.23)$$

where $t_{\alpha/2,n-1}$ is the value of the student's distribution at a significance level of $\alpha/2$ and degrees of freedom $n-1$, and μ is the population mean compressive strength. Equation (5.23) can be simplified by dividing by $\bar{X}$:

$$\frac{\mu}{\bar{X}} = 1 \pm t_{\alpha/2,n-1} * \frac{s/\bar{X}}{\sqrt{n}} \quad (5.24)$$

The term $s/\bar{X}$ is the CoV of the sample data. As the number of samples, n, increases, the CI shrinks through the $1/\sqrt{n}$ and the $t_{\alpha/2,n-1}$ terms. Using this equation, the required number of non-standard samples can be determined by finding the minimum number of samples to achieve an equal or lower CI to three standard samples. With an initial $CoV = 6.1\%$, the baseline CI, for the average compressive strength of three standard cores, can be calculated as $\mu \pm 15.15\%$. The $CoV = 6.1\%$ was chosen for this calculation as that is the average CoV of all the datasets tested, weighted towards the number of samples tested. Table 5.10 shows the number of non-standard samples required to have an equivalent CI as the three standard cores' CI for various levels of CoV.

Table 5.10: Equivalent Number of Non-Standard Samples to Standard Samples to Maintain the Confidence Interval on the Average Compressive Strength for Various CoVs

CoV	Saturated				Dry			
	100 mm Diameter		75 mm Diameter		100 mm Diameter		75 mm Diameter	
	l/d=2	*l/d*=1.5	*l/d*=2	*l/d*=1.5	*l/d*=2	*l/d*=1.5	*l/d*=2	*l/d*=1.5
5.0%	3	5	5	7	7	9	9	10
6.1%	3	4	5	6	6	7	7	8
10.0%	3	4	4	4	5	5	5	5
15.0%	3	4	4	4	4	4	4	4

As the CoV increases, the number of samples required to have an equivalent CI decrease. The reason for this is the baseline CI with an increased CoV is large, and thus, the number of samples required to have an equivalent CI is less than would be required for a smaller CI that would be present for the lower CoVs. For example, the CI of three standard cores at a CoV of 5% is $\pm$ 12.42%, whereas the CI at a CoV of 15% is $\pm$37.26%. As such, the number of samples required to maintain the CI of $\pm$12.42% is much higher than the number of samples required to maintain the CI of $\pm$37.26%. In practicality, extracting a large number of cores is not possible. Therefore, for lower CoV data, conditioning cores in a dry

condition would not be recommended due to the number of cores required to maintain the confidence interval of the standard core.

Current codes, such as CSA A23.1 [4] and ACI 214 [3], dictate three standard cores are to be tested when the cylinder tests do not meet the required f_c'. The average compressive strength of these cores is required to be at least $0.85f_c'$ with no samples below $0.75f_c'$ [3, 4]. This standard requirement can be utilized to find an equivalent requirement for a larger number of non-standard cores. Bartlett and Lawler [87] investigated this statistical relation and proposed to modify these requirements, but keep the probability of failure equal to that of the current standards' requirements. The following process explains how the requirements can be modified.

As stated before, the core compressive strength results can be assumed to be independent and normally distributed. Thus, the probability of a compressive strength lower than $0.75f_c'$ can be found using the cumulative distribution function, Φ, for the normal distribution:

$$\Phi(x) = \int_{-\infty}^{x} \frac{1}{\sqrt{2x}\sigma} e^{-\left(\frac{(x-\mu)^2}{2\sigma^2}\right)} dx \tag{5.25}$$

where x is the compressive strength in question, $0.75f_c'$ in this case, μ is the mean of the core samples' compressive strength, σ is the standard deviation of the core samples' compressive strength, all normalized to f_c'. The probability that a core has a compressive strength below $0.75f_c'$ is then $\Phi(x = 0.75f_c')$, which will be called $P_{<0.75f_c'}$. The probability that the sample compressive strength is greater than $0.75f_c'$ is then $(1 - P_{<0.75f_c'})$, and $\left(1 - P_{<0.75f_c'}\right)^n$ for n cores having a compressive strength greater than $0.75f_c'$. As can been seen, as the number of samples increases, the probability of all samples exceeding $0.75f_c'$ decreases.

Bartlett and Lawler [87] suggested a different requirement for sample sets of more than three cores to have the same probability of failure as a sample set of three cores. This method was to decrease the $0.75f_c'$ limit based on the number of samples to a new limit, kf_c', where k is determined for the probabilities of failure to be equal:

$$1 - \left(1 - P_{<kf_c'}\right)^n = 1 - \left(1 - \mathrm{P}_{<0.75f_c'}\right)^3 \tag{5.26}$$

This method can be calculated when needed to determine the new failure requirement, kf_c', for any number of samples. Equation (5.26) can be rearranged to find the probability of the equivalent failure limit, kf_c', occurring:

$$P_{<kf_c'} = 1 - \left(1 - \mathrm{P}_{<0.75f_c'}\right)^{3/n} \tag{5.27}$$

With this equivalent probability, the new minimum strength limit can be found using the inverse cumulative distribution function for the normal distribution, which is the inverse of Equation (5.25) where the probability is known, $P_{<kf_c'}$, and $x = k$ is unknown. For example, with $\mu/f_c' = 0.85$, which is the mean compressive strength of the samples normalized to f_c', and $V = 6.1\%$, the probability $\mathrm{P}_{<0.75f_c'}$ is 2.68%. From Table 5.10, five saturated 75 mm diameter cores with an *l/d* ratio of 2 are required to have the same confidence interval as three standard cores. The probability of failure, $\mathrm{P}_{<kf_c'}$, for those five cores is then 1.62%. Using the inverse normal distribution with $\mu/f_c' = 0.85$ and $V = 6.1\%$, $k = 0.663$; therefore, the new limit for this case would be $0.66f_c'$. For other non-standard configurations, the corresponding limit to the number of sample required, stated in Table 5.10, is shown in Table 5.11.

Table 5.11: Number of Samples and New Limit k, where kf_c' is the Minimum Strength Required for an Equivalent Confidence Interval on Average Compressive Strength and Failure Probability as Three Standard Cores, for Various μ/f_c' and V

$\frac{\mu}{f_c'}$	V (%)	Saturated				Dry			
		100 mm Diameter		75 mm Diameter		100 mm Diameter		75 mm Diameter	
		l/d=2	*l/d*=1.5	*l/d*=2	*l/d*=1.5	*l/d*=2	*l/d*=1.5	*l/d*=2	*l/d*=1.5
0.85	5.0	3-0.75	5-0.66	5-0.64	7-0.58	7-0.55	9-0.50	9-0.49	10-0.45
	6.1	3-0.75	4-0.69	5-0.66	6-0.62	6-0.59	7-0.55	7-0.54	8-0.50
	10.0	3-0.75	4-0.71	4-0.70	4-0.68	5-0.65	5-0.64	5-0.63	5-0.61
	15.0	3-0.75	4-0.71	4-0.71	4-0.70	4-0.69	4-0.68	4-0.68	4-0.67
0.90	5.0	3-0.75	5-0.63	5-0.60	7-0.52	7-0.47	9-0.41	9-0.39	10-0.34
	6.1	3-0.75	4-0.66	5-0.63	6-0.57	6-0.53	7-0.48	7-0.47	8-0.42
	10.0	3-0.75	4-0.70	4-0.69	4-0.66	5-0.63	5-0.60	5-0.59	5-0.57
	15.0	3-0.75	4-0.71	4-0.70	4-0.69	4-0.68	4-0.66	4-0.66	4-0.65

In Table 5.11, the damage factor is not considered as the cores are being equated to a standard 100 mm diameter, *l/d*=2, saturated core and not to a cylinder. The value of μ/f_c' does not change as the SCFs are designed to equate a non-standard sample's compressive strength to a standard sample's compressive strength, thus the μ/f_c' stays the same, at the expense of increased variability. The initial $V = 6.1\%$, but when parameters are changed to non-standard parameters, that CoV increases due to the addition of the SCFs. An interesting note is that the 100 mm diameter, *l/d*=1.5 samples have a lower variability than the 75 mm diameter, *l/d*=2 samples, indicated by the higher k factor of the 100 mm diameter, *l/d*=1.5

samples. The variabilities of these sample sets are 10.63% and 11.49% respectively. As the initial V increases, the k factor for non-standard equivalences increases, as the increased variability associated with the SCFs has less impact if the input data is more variable. Similarly, as the initial μ/f_c' increases, the k factor decreases as the probability $P_{<0.75f_c'}$ decreases for the standard sample. When this probability decreases, the increased variability for the non-standard samples results in lower k factors to match this lowered $P_{<0.75f_c'}$.

Table 5.10 and Table 5.11 above were developed using statistical methods to demonstrate that increased variability of samples has implications on the number of samples required for equivalence. In practicality, large number of cores cannot be feasibly extracted. The reduced limit k for CSA A23.1 [4] and ACI 214 [3] requirements are also derived from statistical methods, and intended to demonstrate that these code requirements become harsher with larger variation in data caused by non-standard parameters. However, it is not practical in some of the cases. For instance, reducing the limit k to 0.34 is not recommended, and the discretion of the overseeing engineer is required to determine what k limit is acceptable in practical use.

Chapter 6
Summary, Conclusions, and Future Work

This thesis discussed the extraction and testing of concrete core samples from various elements constructed in the University of Waterloo laboratory and pre-cast manufacturing facilities. In total, 8 sets of concrete samples were created and tested, totaling 884 concrete samples, of which 713 underwent compression testing. Other tests included the bulk resistivity, rapid chloride permeability (RCP), and air void systems. These tests were not discussed in this thesis but were discussed elsewhere [1]. The purpose of the compression tests was to determine how the parameters of the core compressive test affected the result of the test, and how appropriate the current practices outlined in standards and codes to modern concrete mixtures. These parameters are the time, location, and direction of core extraction, the conditioning of the core between extraction and testing, the diameter, and the length-to-diameter (*l/d*) ratio of the core. The following summary and conclusions of the data presented previously are statistically valid at a 95% confidence level.

6.1 Summary

- The timing of core extraction had no effect on the result of the day 28 compressive strength test.
- The direction of coring (i.e. perpendicular or parallel to the direction of concrete casting) had little to no effect on the compressive strength test due to the reduced bleed water in the concrete mixture caused by the inclusion of SCMs in the concrete mixture.
- The height along a structure from which a core is extracted had no effect on the compressive strength of the core given that the structure is reasonably well constructed and contains SCMs which reduce the amount of bleed water, such as the concrete mixtures utilized in the structures tested.
- The length along a structure from which a core is extracted had no effect on the compressive strength of the core.
- Cores immersed in saturated calcium hydroxide between extraction and testing had a lower compressive strength, by 2.3%, than cores sealed in plastic. Also, the cores sealed in plastic were twice as variable with a CoV of 9.31% compared to the immersed cores which had a CoV of 4.73%.

- The smaller diameter samples (75 mm) exhibited a higher compressive strength, by 1.5% on average, and 25% higher variability than samples with a diameter of 100 mm.
- The compressive strengths of concrete samples with an *l/d* ratio of 1.5 were found to be slightly lower (0.5%) and 40-45% more variable than those with an *l/d* ratio of 2.
- The longer the concrete experienced low temperatures before day 28, the lower its compressive strength.
- The slight variations in density of a concrete sample had no effect on the compressive strength, given that the structure was reasonably well constructed and of normal density.

6.2 Conclusions

- The conditioning state of immersing the concrete sample in a saturated calcium hydroxide solution produced compressive strength results with lower variability than sealing the samples in plastic. This soaked conditioning state reduced the compressive strength of the sample by approximately 2.3%, which is drastically less than the 8.3% suggested by ACI 214 [3]. This immersed method of conditioning is preferable over the sealed in plastic method which is recommended by ASTM C42 [2].
- The current models for calculating the *l/d* ratio strength correction factor (SCF) utilized by ACI 214 [3], ASTM C42 [2] and C39 [5], and CSA A23.1 [4] were found to be inadequate for the data presented. The model presented by Meininger [62], which consists of averaging the compressive strengths of samples with the standard *l/d* ratio of 2 to the compressive strengths of samples with a non-standard *l/d* ratio produced the best results (i.e. $F_{l/d} = f_{c,l/d=2}/f_{c,l/d\neq 2}$). Therefore, calculating a SCF for each type of concrete utilized would produce the most accurate results.
- The 75 mm diameter samples had a more variable and higher compressive strength compared to the 100 mm diameter samples. The SCF found in ACI 214 [3] for equating the compressive strength of a 75 mm sample and a 100 mm diameter sample was found to be adequate. The additional CoV suggested by ACI 214 [3] caused by the use of the factor was found to be high at 8.0% compared to the 5.9% found with the data presented. However, a higher CoV would allow for a more conservative estimate. Therefore, the existing model was found to be adequate.
- The compressive strength reduction caused by the damage of coring was found to be much greater than estimated in ACI 214 [3]. ACI 214 [3] suggests a SCF of 1.06 to compensate for the

damage caused by coring, while the data presented utilized a factor of 1.10 for cores with a diameter of 100 mm and 1.13 for cores with a diameter of 75 mm.

- With consideration of all the factors discussed above, cores with a diameter of 100 mm and *l/d* ratio of 1.5 have a lower variability than cores with a diameter of 75 mm and *l/d* ratio of 2. As stated above, cores immersed in a saturated calcium hydroxide solution are less variable than cores sealed in plastic.
- To ensure equivalent variability in sets of samples, additional cores should be extracted, depending on the CoV of the sample data, and the non-standard parameters. For example, with a CoV of 6.1%, four saturated cores with a 100 mm diameter and an *l/d* ratio of 1.5 or five saturated cores with a 75 mm diameter and an *l/d* ratio of 2 would be required to be equivalent to three standard cores.
- To ensure the same probability of passing quality assurance testing, where the average compressive strength of three cores must be at least $0.85f_c'$ with no single value below $0.75f_c'$, the limits may be changed to accommodate the increased variability associated with non-standard parameters on the core. For instance, with a CoV of 6.1%, five 75 mm diameter cores with an *l/d* ratio of 2 having no single value below $0.66f_c'$ would be equivalent to the current three 100 mm diameter cores with an *l/d* ratio of 2 having no single value below $0.75f_c'$.

6.3 Recommendations for Future Work

Recommendations for future work include expanding the tests and analysis completed in this thesis to more types of structures and concrete mixtures to generate more comprehensive models. Including data from previous research conducted on modern concrete mixtures to increase the sample size would be beneficial in generating these models. Lastly, a more thoroughly planned experimental design could yield more statistically valid results by increasing the number of samples tested and isolating the parameters of interest.

Letter of Copyright Permission

American Concrete Institute

Always advancing

Marc Johnson
University of Waterloo
200 University Avenue West
Waterloo, Ontario N2L 3G1
CANADA

February 20, 2019

Subject: Use of ACI Copyrighted Material

Your request to:

___X___ Use information/figures/tables indicated below. Please credit American Concrete Institute, author(s) and publication.

___X___ Reprint the information described in the quantity indicated. Please add a note to the reprint similar to: *Authorized reprint from (publication) (issue/volume/year as appropriate.)*

_____ Payment of Right-to-Reprint fee of ($0) is required.

Permission is granted to reference and reprint *Table 9.1* from *ACI 214.4R-10, 2010.*

Signed: Angela Matthews Date: 20 February 2019

Angela Matthews
Editor, Publishing Services
Angela.Matthews@Concrete.org

Gmail

Re: REPUBLICATION USE REQUEST FORM - Marc Johnson

PearsonedEMA, Permissions <permissions@pearson.com> Wed, Feb 20, 2019 at 3:06 AM
To: Marc Johnson <marc.johnson@uwaterloo.ca>

Good day Marc

I trust you are well.

Thank you for providing me with the relevant information.

I am pleased to be able to grant permission for your use of Figure 13.3 ***of Properties of Concrete by A.M. Neville, ISBN 9780273755807,*** in your MASc thesis, currently titled as ***: Investigation of Parameters Effecting Concrete Core Performance for Quality Control and Assurance*** at ***University of Waterloo.***

Permission is granted free of charge, subject to acknowledgement to author/title and ourselves as publishers.

Permission does not extend to material that has been acknowledged to another source.

Acknowledgement: Title, author, Pearson Education Limited and Copyright line as it appears in our publication (note where figure and diagrams are reproduced, this acknowledgement is to appear immediately below them.

This permission is for non-exclusive electronic rights in the English language for one use only.

Wishing you all the best with your thesis.

Kind Regards
Allison Bulpitt
Global Innovations & Services
Pearson UK

4th Floor, Auto Atlantic

Corner Hertzog Boulevard and Heerengracht

Cape Town, 8001

South Africa

E: permissions@pearson.com

Learn more at za.pearson.com

Pearson

[Quoted text hidden]

Gmail

Marc Johnson <marc.johnson333@gmail.com>

RE: Obtain permission request - Journal

Lingayath, Roopa (ELS-CHN) <r.lingayath@elsevier.com> Wed, Mar 27, 2019 at 1:27 AM
To: Marc Johnson <marc.johnson@uwaterloo.ca>

ELSEVIER

Dear Mr. Marc Johnson

We hereby grant you permission to reprint the material below at no charge **in your thesis** subject to the following conditions:

RE: Figure 2, An introduction to concrete core testing, B.A. Suprenaut, Civil Engineering for Practicing and Design Engineers, Volume 4, Issue 8

Proposed Use: To be used in thesis

1. If any part of the material to be used (for example, figures) has appeared in our publication with credit or acknowledgement to another source, permission must also be sought from that source. If such permission is not obtained then that material may not be included in your publication/copies.

2. Suitable acknowledgment to the source must be made, either as a footnote or in a reference list at the end of your publication, as follows:

"This article was published in Publication title, Vol number, Author(s), Title of article, Page Nos, Copyright Elsevier (or appropriate Society name) (Year)."

3. Your thesis may be submitted to your institution in either print or electronic form.

4. Reproduction of this material is confined to the purpose for which permission is hereby given

5. This permission is granted for non-exclusive world **English** rights only. For other languages please reapply separately for each one required. Permission excludes use in an electronic form other than submission. Should you have a specific electronic project in mind please reapply for permission.

6. This includes permission for the Library and Archives of Canada to supply single copies, on demand, of the complete thesis. Should your thesis be published commercially, please reapply for permission- Canada

Thanks & Regards,

Roopa Lingayath

Sr Copyrights Coordinator - Global Rights

Elsevier | Health Content Operations

(A division of Reed Elsevier India Pvt. Ltd.)

International Tech Park | Crest - 5th Floor | CSIR Road | Taramani | Chennai 600 113 | India

Tel: +91 44 3378 4167 | Fax: +91 44 4299 4568

E-mail: r.lingayath@elsevier.com | url: www.elsevier.com

From: marc.johnson@uwaterloo.ca <marc.johnson@uwaterloo.ca>
Sent: 15 February 2019 20:20
To: Rights and Permissions (ELS) <Permissions@elsevier.com>
Subject: Obtain permission request - Journal

*** External email: use caution ***

Title: Mr. Marc Johnson

Institute/company: University of Waterloo
Address: 200 University Avenue West
Post/Zip Code: N2L 3G1
City: Waterloo
State/Territory: Ontartio
Country: Canada
Telephone: 519-998-8945
Email: marc.johnson@uwaterloo.ca

Type of Publication: Journal

Journal Title: Civil Engineering for Practicing and Design Engineers
Journal ISSN: 0277-3775
Journal Volume: 4
Journal Issue: 8
Journal Year: 1985
Journal Pages: 607 to 615
Journal Author: B.A. Suprenaut
Journal Article title: AN INTRODUCTION TO CONCRETE CORE TESTING

I would like to use: Figure(s)
Quantity of material: 1
Excerpts:
Are you the author of the Elsevier material? No
If not, is the Elsevier author involved? No
If yes, please provide details of how the Elsevier author is involved:
In what format will you use the material? Print and Electronic
Will you be translating the material? No
If yes, specify language:
Information about proposed use: Reuse in a thesis/dissertation
Proposed use text: The thesis will be posted on an online institutional repository (UWSpace).
Additional Comments / Information: The desired figure I would like to use from the article is Figure 2: Planes of Weakness Due to Bleeding in a Grade Beam

References

[1] A. Felinczak, “Evaluation of Early In-Place Concrete Performance Based on Test Results of Cores and Cylinders,” University of Waterloo, 2018.

[2] ASTM Standard C42, “Standard Test Method for Obtaining and Testing Drilled Cores and Sawed Beams of Concrete,” *ASTM International*, vol. 23, no. 11, p. 7, 2018.

[3] ACI Committee 214, “ACI 214.R-10 Guide for Obtaining Cores and Interpreting Compressive Strength Results,” 2010.

[4] Canadian Standards Association, *A23.1-14 Concrete Materials and Methods of Concrete Construction / A23.2-14 Test Methods and Standard Practices for Concrete*. 2014.

[5] ASTM Standard C39, “Standard Test Method for Compressive Strength of Cylindrical Concrete Specimens,” *ASTM International*, pp. 1–7, 2016.

[6] O. Kirca, “Ancient binding materiaIs, mortars and concrete technoIogy: history and durability aspects,” *Structural Analysis of Historical Constructions*, pp. 87–94, 2005.

[7] F. M. Bartlett and J. G. MacGregor, “Equivalent Specified Concrete Strength from Core Test Data,” *Concrete International*, vol. 17, no. 3, pp. 52–58, 1995.

[8] V. S. Dubovoy, S. H. Gebler, P. Klieger, and D. A. Whiting, “Effects of Ground Granulated Blast-Furnace Slags on Some Properties of Pastes, Mortars, and Concretes,” *ASTM International*, vol. STP897, pp. 29–48, 1986.

[9] ACI Committee 226, “Ground Granulated Blast-Furnace Slag As a Cementitious Constituent in Concrete.,” *ACI Materials Journal*, vol. 84, no. 4, pp. 327–342, 1987.

[10] F. J. Hogan and J. W. Meusel, “Evaluation for Durability and Strength Development of a Ground Granulated Blast Furnace Slag,” *Cement, Concrete, and Aggregates*, vol. 3, no. 1, pp. 40–52, 1981.

[11] A. Fernández-Jiménez and A. Palomo, “Characterisation of Fly Ashes. Potential Reactivity as Alkaline Cements,” *Fuel*, vol. 82, no. 18, pp. 2259–2265, 2003.

[12] D. P. Bentz, E. J. Garboczi, C. J. Haecker, and O. M. Jensen, “Effects of cement particle size distribution on performance properties of Portland cement-based materials,” *Cement and Concrete Research*, vol. 29, no. 10, pp. 1663–1671, 1999.

[13] D. Roy, “The Effect of Blast Furnace Slag and Related Materials on the Hydration and Durability of Concrete,” *ACI Special Publication*, vol. 131, no. SP131, pp. 195–208, 1992.

[14] R. J. Detwiler, C. A. Fapohunda, and J. Natale, “Use of supplementary cementing materials to increase the resistance to chloride ion penetration of concretes cured at elevated temperatures,” *ACI Materials Journal*, vol. 91, no. 1, pp. 63–66, 1994.

[15] Rasheeduzzafar, S. S. Al-Saadoun, and A. S. Al-Gahtani, “Reinforcement corrosion-resisting characteristics of silica-fume blended-cement concrete,” *ACI Materials Journal*, vol. 89, no. 4, pp. 337–366, 1992.

[16] O. S. B. Al-Amoudi, Rasheeduzzafar, M. Maslehuddin, and S. N. Abduljauwad, “Performance of Plain and Blended Cements in High Chloride Environments,” *ACI Special Publication*, vol. 145, no. SP145, pp. 539–555, 1994.

[17] H. Wan, Z. Shui, and Z. Lin, “Analysis of geometric characteristics of GGBS particles and their influences on cement properties,” *Cement and Concrete Research*, vol. 34, no. 1, pp. 133–137, 2004.

[18] A. M. Neville, *Properties of Concrete*, 5th ed. Harlow: Pearson Education Limited, 2011.

[19] P. J. Robins, S. A. Austin, and A. Issaad, “Suitability of GGBFS as a cement replacement for concrete in hot arid climates,” *Materials and Structures*, vol. 25, no. 10, pp. 598–612, 1992.

[20] Concrete Library of JSCE No. 28, “Recommendation For Construction Of Concrete Containing Ground Granulated Blast-Furnace Slag As An Admixture,” *Concrete Library of JSCE*, 1996.

[21] J. Daube and R. Bakker, “Portland Blast-Furnace Slag Cement: A Review,” *ASTM International*, vol. STP897, pp. 5–14, 1986.

[22] V. Sivasundaram and V. M. Malhotra, “Properties of concrete incorporating low quantity of cement and high volumes of ground granulated slag,” *ACI Materials Journal*, vol. 89, no. 6, pp. 554–563, 1992.

[23] ASTM Standard C494, “Standard Specification for Coal Fly Ash and Raw or Calcined Natural Pozzolan for Use in Concrete,” *ASTM International*, 2017.

[24] A. L. A. Fraay, J. N. Bijen, and Y. M. de Haan, “The reaction of fly ash in concrete: a critical examination,” *Cement and Concrete Research*, vol. 19, no. 2, pp. 235–246, 1986.

[25] K. Horiguchi, T. Chosokabe, T. Ikabata, and Y. Suzuki, “The Rate of Carbonation in Concrete

Mode with Blended Cement," *Concrete Durability*, vol. 145, pp. 917–932, 1994.

[26] R. A. Helmuth, "Water-reducing properties of fly ash in cement pastes, mortars, and concretes: causes and test methods," *ACI Special PublicationACI*, vol. 91, pp. 723–740, 1986.

[27] M. D. A. Thomas, G. J. Osborne, J. D. Matthewsf, and J. B. Cripwell, "A comparison of the properties of OPC, PFA and ggbs concretes in reinforced concrete tank walls of slender section," *Magazine of Concrete Research*, vol. 42, no. 152, pp. 127–134, 1990.

[28] F. Sanchez and C. Ince, "Microstructure and macroscopic properties of hybrid carbon nanofiber/silica fume cement composites," *Composites Science and Technology*, vol. 69, no. 7–8, pp. 1310–1318, 2009.

[29] K. H. Khayat and P. C. Aitcin, "Silica fume in concrete - an overview, in Fly Ash, Silica Fume, Slag, and Natural Pozzolans in Concrete," *ACI Special Publication*, vol. 132, pp. 835–872, 1992.

[30] M. D. Cohen and a Bentur, "Durability of Portland Cement - Silica Fume Pastes in Magnesium Sulfate and Sodium Sulfate Solutions," *ACI materials journal*, vol. 85, no. 3, pp. 148–157, 1988.

[31] I. L. H. Hansson and C. M. Hansson, "Electrical resistivity measurements of portland cement based materials," *Cement and Concrete Research*, vol. 13, no. 5, pp. 675–683, 1983.

[32] W. E. Ellis, E. H. Riggs, and W. B. Butler, "Comparative results of utilization of fly ash, silica fume and GGBFS in reducing the chloride permeability of concrete," *ACI Special Publication*, vol. 126, no. SP126, pp. 443–458, 1991.

[33] ASTM Standard C494, "Standard Specification for Chemical Admixtures for Concrete," *ASTM International*, p. 10, 2017.

[34] M. Prior and A. Adams, "Introduction to Producers' Papers on Water-Reducing Admixtures and Set-Retarding Admixtures for Concrete," *STP266-EB Symposium on Effect of Water-Reducing Admixtures and Set-Retarding Admixtures on Properties of Concrete*, pp. 170–179, 1960.

[35] A. Meyer, "Experiences in the use of superplasticizers in Germany," *ACI Special Publication*, vol. 62, no. SP62, pp. 21–36, 1979.

[36] C. F. Scholer, "The influences of retarding admixtures on volume changes of concrete," 1975.

[37] A. Baskoca, M. H. Ozkul, and S. Artirma, "Effect of chemical admixtures on workability and strength properties of prolonged agitated concrete," *Cement and Concrete Research*, vol. 28, no. 5, pp. 737–747, 1998.

[38] B. Persson, “Moisture in concrete subjected to different kinds of curing,” *Materials and Structures*, vol. 30, no. 9, pp. 533–544, 1997.

[39] M. Ben-Bassat, P. J. Nixon, and J. Hardcastle, “The Effect of Differences in the Composition of Portland-Cement on the Properties of Hardened Concrete,” *Magazine of Concrete Research*, vol. 42, no. 151, pp. 59–66, 1990.

[40] S. Popovics, “Effect of curing method and final moisture condition on compressive strength of concrete,” *ACI Journal Proceedings*, vol. 83, no. 4, p. 83, 1986.

[41] B. Suprenant, “An Introduction to Concrete Core Testing,” *Civil Engineering for Practicing and Design Engineers*, vol. 4, no. 8, pp. 607–615, 1985.

[42] N. Petersons, “Should standard cube test specimens be replaced by test specimens taken from structures?,” *Mat??riaux et Constructions*, vol. 1, no. 5, pp. 425–435, 1968.

[43] W. K. Yip and C. T. Tam, “Concrete strength evaluation through the use of small diameter cores,” *Magazine of Concrete Research*, vol. 40, no. 143, pp. 99–105, 1988.

[44] R. Yuan, M. Ragab, R. Hill, and J. Cook, “Evaluation of Core Strength in High-strength concrete.” Concrete International, pp. 30–34, 1991.

[45] A. Szypula and J. Grossman, “Cylinder vs. Core Strength.” Concrete International, pp. 55–61, 1990.

[46] A. Takahata, T. Iwashimizu, and U. Ishibashi, “Construction of a High-Rise Reinforced Concrete Residence Using High-Strength Concrete,” *High-Strength Concrete*, no. SP-121, pp. 741–755, 1991.

[47] A. Ergün and G. Kürklü, “Assessing the relationship between the compressive strength of concrete cores and molded specimens,” *Gazi University Journal of Science*, vol. 25, no. 3, pp. 737–750, 2012.

[48] D. L. Bloem, “Concrete Strength Measurement - Cores versus Cylinders,” *Proceedings, American Society for Testing and Materials*, vol. 65, pp. 668–696, 1965.

[49] F. M. Bartlett and J. G. MacGregor, “Effect of Core Diameter on Concrete Core Strengths,” *ACI Materials Journal*, vol. 91, no. 5, pp. 460–469, 1994.

[50] W. Weibull, “A Statistical Theory of the Strength of Materials,” *Ingeniorsvetenskapsakademiens*, vol. 151, p. 45, 1939.

[51] J. Tucker, “Effect of Dimensions of Specimens upon the Precision of Strength Data,” *ASTM Proceeding 1945*, vol. 45, pp. 952–959, 1945.

[52] O. Arioz, K. Ramyar, M. Tuncan, A. Tuncan, and I. Cil, “Some factors influencing effect of core diameter on measured concrete compressive strength,” *ACI Materials Journal*, vol. 104, no. 3, pp. 291–296, 2007.

[53] M. Tuncan, O. Arioz, K. Ramyar, and B. Karasu, “Assessing concrete strength by means of small diameter cores,” *Construction and Building Materials*, vol. 22, no. 5, pp. 981–988, 2008.

[54] J. Bungey, “Determining concrete strength by using small-diameter cores,” *Magazine of Concrete Research*, vol. 31, no. 107, pp. 91–98, 1979.

[55] F. M. Bartlett and J. G. MacGregor, “Cores from high-performance concrete beams,” *ACI Materials Journal*, vol. 91, no. 6, pp. 567–576, 1994.

[56] R. Gaynor, “Effect of Horizontal Reinforcing Steel on the strength of Molded Cylinders,” *Journal of American Concrete Institute*, vol. 62, no. 7, pp. 837–840, 1965.

[57] Y. Loo, C. Tan, and C. Tam, “Effects of embedded reinforcement on the measured strength of concrete cylinders.,” *Magazine of Concrete Research*, vol. 41, no. 146, pp. 11–18, 1989.

[58] J. M. Plowman, W. F. Smith, and T. Sherriff, “Cores, Cubes and the Specified Strength of Concrete.,” *Structural Engineer*, vol. 52, no. 11, pp. 421–426, 1974.

[59] ACI Committee 318, *ACI 318-11 Building Code Requirements for Structural Concrete*. 2011.

[60] K. Newman and L. Lachance, “The Testing of Brittle Materials Under Uniform Uniaxial Compressive Stress,” *ASTM International*, vol. 64, pp. 1044–1067, 1964.

[61] N. S. Ottosen, “Evaluation of Concrete Cylinder Tests Using Finite Elements,” *Journal of Engineering Mechanics*, vol. 110, no. 3, pp. 465–481, 1984.

[62] R. C. Meininger, F. T. Wagner, and K. W. Hall, “Concrete Core Strength-The Effect of Length to Diameter Ratio,” *Journal of Testing and Evaluation*, vol. 5, no. 3, pp. 147–153, 1977.

[63] F. M. Bartlett and J. G. MacGregor, “Effect of Core Length-to-Diameter Ratio on Concrete Core Strengths,” *ACI Materials Journal*, vol. 91, no. 4, pp. 339–348, 1994.

[64] Concrete Society, “Concrete Core Testing for Strength,” *Technical Report No. 11*. The Concrete Society, London, 1976.

[65] H.-W. Chung, “Effect of Length/Diameter Ratio on Compressive Strength of Drilled Concrete

Core—A Semi-Rational Approach," *American Society for Testing and Materials*, vol. 1, no. 2, pp. 68–70, 1979.

[66] H.-W. Chung, "On Testing of Very Short Concrete Specimens," *Cement. Concrete. And Aggregates*, vol. 11, no. 1, pp. 40–44, 1989.

[67] O. Arioz, K. Ramyar, M. Tuncan, and A. Tuncan, "Effect of Length-to-Diameter Ratio of Core Sample on Concrete Core Strength — Another Look," *Journal of Testing and Evaluation*, vol. 36, no. 1, pp. 2–5, 2006.

[68] ACI Committee 318, "Building Code Requirements for Structural Concrete (ACI 318-14)," *ACI Structural Journal*, p. 524, 2014.

[69] OPSS 1350, "Material Specification for Concrete - Materials and Production," pp. 1–33, 2016.

[70] Ö. Ariöz, M. Tuncan, K. Ramyar, and A. Tuncan, "A comparative study on the interpretation of concrete core strength results," *Magazine of Concrete Research*, vol. 58, no. 2, pp. 117–122, 2006.

[71] F. M. Bartlett and J. G. MacGregor, "Assessment of Concrete Strength in Existing Structures," *NRC Canada*. pp. 1029–1037, 1994.

[72] M. McIntyre and A. Scanlon, "Interpretation and application of core test data in strength evaluation of existing concrete bridge structures," *Canadian Journal of Civil Engineering*, vol. 17, no. 3, pp. 471–480, 1990.

[73] V. M. Malhotra, "Contract Strength Requirements-Cores Versus In Situ Evaluation," *ACI Journal Proceedings*, vol. 74, no. 4, pp. 163–172, 1977.

[74] LS-432, "Method of Test for Microscopical Determination of Air Void System Parameters in Hardened Concrete," no. 28. Ministry of Transportation of Ontario.

[75] ASTM Standard C457, "Standard Test Method for Microscopical Determination of Parameters of the Air-Void System in Hardened Concrete 1," *ASTM International*, vol. 05, pp. 1–15, 2013.

[76] LS-433, "Method of Test for Electrical Indication of Concrete ' s Ability to Resist Chloride Ion Penetration," no. 26. Ministry of Transportation of Ontario.

[77] ASTM Standard C1202, "Standard Test Method for Electrical Indication of Concrete's Ability to Resist Chloride Ion Penetration," *ASTM International*, no. C, pp. 1–8, 2012.

[78] H. Layssi, P. Ghods, A. R. Alizadeh, and M. Salehi, "Electrical Resistivity of Concrete," *Concrete International*, no. May, pp. 41–46, 2015.

[79] D. C. Montgomery, *Design and Analysis of Experiments*, 8th ed. John Wiley & Sons Inc., 2013.

[80] ASTM Standard E178, "Standard Practice for Dealing With Outlying Observations," *ASTM International*, vol. 14, no. August, pp. 1–17, 2016.

[81] OPSS 909, "Construction Specification for Prestressed Concrete - Precast Girder," pp. 1–32, 2016.

[82] Ontartio Provinical Standard Specification, "OPSS 904 - Construction Specification for Concrete Structures," pp. 1–26, 2014.

[83] R Core Team, "R: A Language and Environment for Statistical Computing." R Foundation for Statistical Computing, Vienna, Austria, 2018.

[84] D. M. Allen, "The Relationship between Variable Selection and Data Augmentation and a Method for Prediction," *Technometrics*, vol. 16, no. 1, pp. 125–127, 1974.

[85] A. W. Peterson and A. E. Peterson, "Moblie Boundary Flow: An Assessment of Velocity and Sediment Discharge Relationships," *Canadian Journal of Civil Engineering*, vol. 15, no. 4, pp. 539–546, 1988.

[86] R. Walpole, R. Myers, S. Myers, and K. Ye, *Probability and Statistics for Engineers and Scientists*, 8th ed. Upper Saddle River, NJ: Pearson Education Limited, 2007.

[87] F. M. Bartlett and J. S. Lawler, "Strength Compliance Evaluation with More than Three Core Specimens," *Concrete International*, vol. 33, no. 12, pp. 0–3, 2011.

[88] Government of Canada, "Historical Data - Climate - Environment and Climate Change Canada," 2018. [Online]. Available: http://climate.weather.gc.ca/historical_data/search_historic_data_e.html.

Appendix A - Concrete Mixtures

Table A.1: Detailed Concrete Mixture for Beam B1

Material	Quantity (per m^3 of concrete)
Type 10 Cement (GU)	262 kg
Slag	90 kg
Water	145 kg
w/cm ratio	0.41
Large Aggregate (19 mm)	1170 kg
Fine Aggregate	675 kg
Air Entraining Agent	45 mL
High Range Water Reducer	325 mL

Table A.2: Detailed Concrete Mixture for Girder Web G1

Material	Quantity (per m^3 of concrete)
Type 10 Cement (GU)	480 kg
Slag	120 kg
Water	163 kg
w/cm ratio	0.27
Large Aggregate (13 mm)	845 kg
Fine Aggregate	756 kg
Air Entraining Agent	600 mL
High Range Water Reducer	3000 mL

Table A.3: Detailed Concrete Mixture for Manhole Risers MH

Material	Quantity (per m^3 of concrete)						
	MH1	**MH2**	**MH3**	**MH4**	**MH5**	**MH6**	**MH7**
Type 10 Cement (GU)	304 kg	285 kg	292 kg	291 kg	290 kg	299 kg	284 kg
Slag	161 kg	157 kg	152 kg	157 kg	154 kg	157 kg	153 kg
Water	106 L	95 L	98 L	109 L	98 L	92 L	89 L
w/cm	0.23	0.22	0.22	0.24	0.22	0.20	0.21
Large Aggregate (13 mm)	1160 kg	1171 kg	1170 kg	1179 kg	1178 kg	1155 kg	1151 kg
Fine Aggregate	1603 kg	1618 kg	1616 kg	1629 kg	1628 kg	1663 kg	1657 kg
High Range Water Reducer				1500 mL			
Mix Temp. (°C)	17.0	13.0	13.5	10.0	14.5	15.0	21.0

Table A.4: Detailed Concrete Mixture for Girder Web G2

Material	Quantity (per m^3 of concrete)
Type 30 Cement (HE)	470 kg
Slag	157 kg
Water	194 kg
w/cm ratio	0.32
Large Aggregate (13 mm)	919 kg
Fine Aggregate	606 kg
Air Entraining Agent	1500 mL
High Range Water Reducer	3700 mL

Table A.5: Detailed Concrete Mixture for Girder Section G3

Material	Quantity (per m^3 of concrete)
Type 10 Cement (GU)	350 kg
Silica Fume	34 kg
Fly Ash	91 kg
Water	110 kg
w/cm ratio	0.29
Large Aggregate (14 mm)	918 kg
Fine Aggregate	795 kg
Air Entraining Agent	100 mL
High Range Water Reducer	4150 mL

Table A.6: Detailed Concrete Mixture for VC and CC

Material	Quantity (per m^3 of concrete)
Type 30 Cement (HE)	360 kg
Slag	120 kg
Water	170 kg
w/cm ratio	0.36
Large Aggregate (19 mm)	787 kg
Fine Aggregate	866 kg
Air Entraining Agent	930 mL
High Range Water Reducer	3120 mL

Appendix B - Additional Compressive Strength Results

B.1 Core Results: Timing of Core Extraction

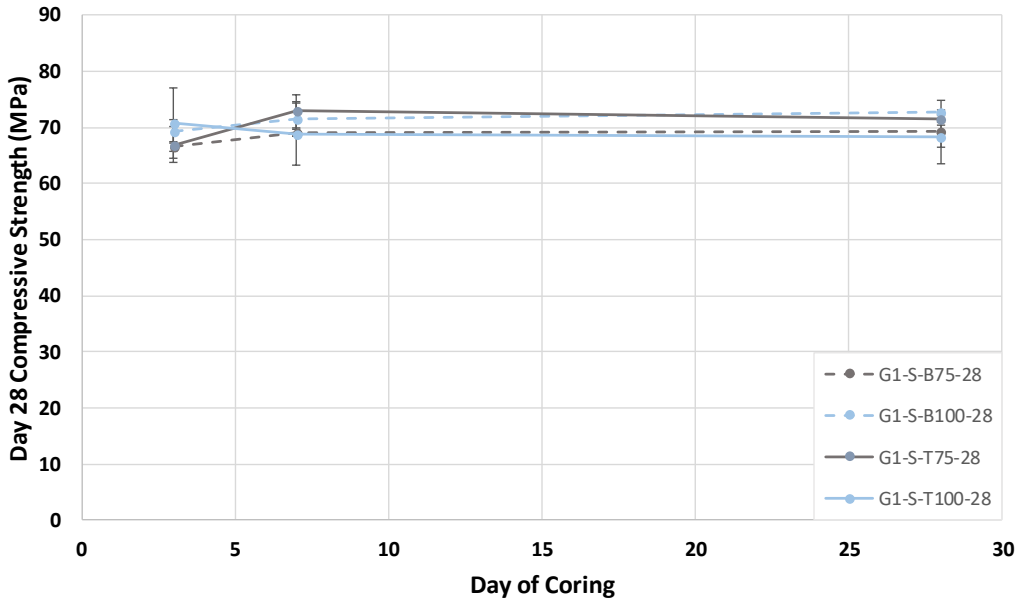

Figure B.1: Compressive Strength of Girder G1 Cores Extracted on Various Days, Tested on Day 28 from both Top and Bottom Locations, and in 100 mm and 75 mm Diameter. Day 28 Extracted Cores were in the Dry Condition, While Others were Saturated

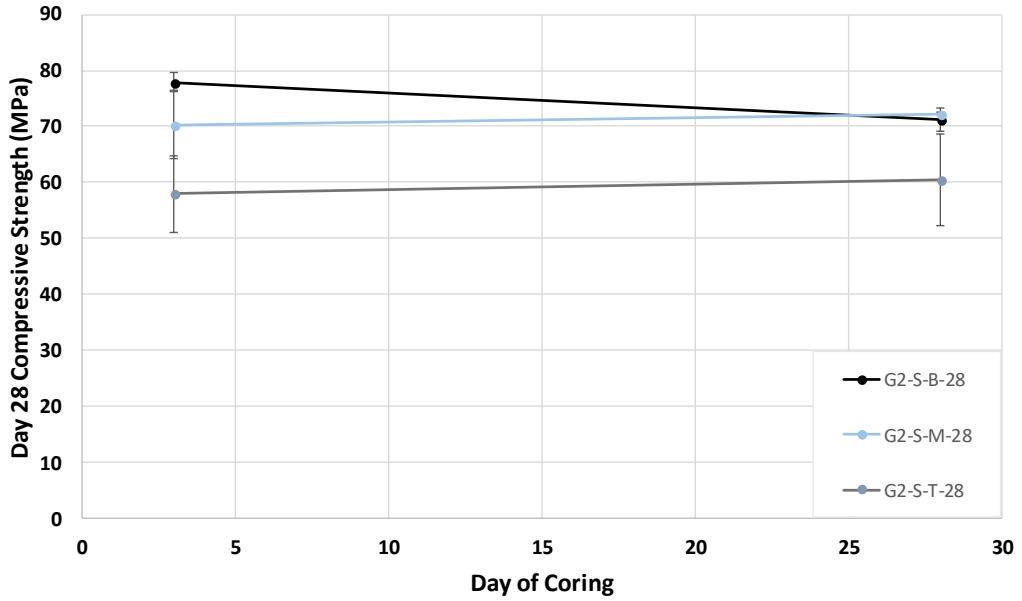

Figure B.2: Compressive Strength of Girder G2 Cores Extracted on Various Days, Tested on Day 28 from Top, Middle, and Bottom Locations. Day 28 Extracted Cores were in the Dry Condition, Day 3 were Saturated

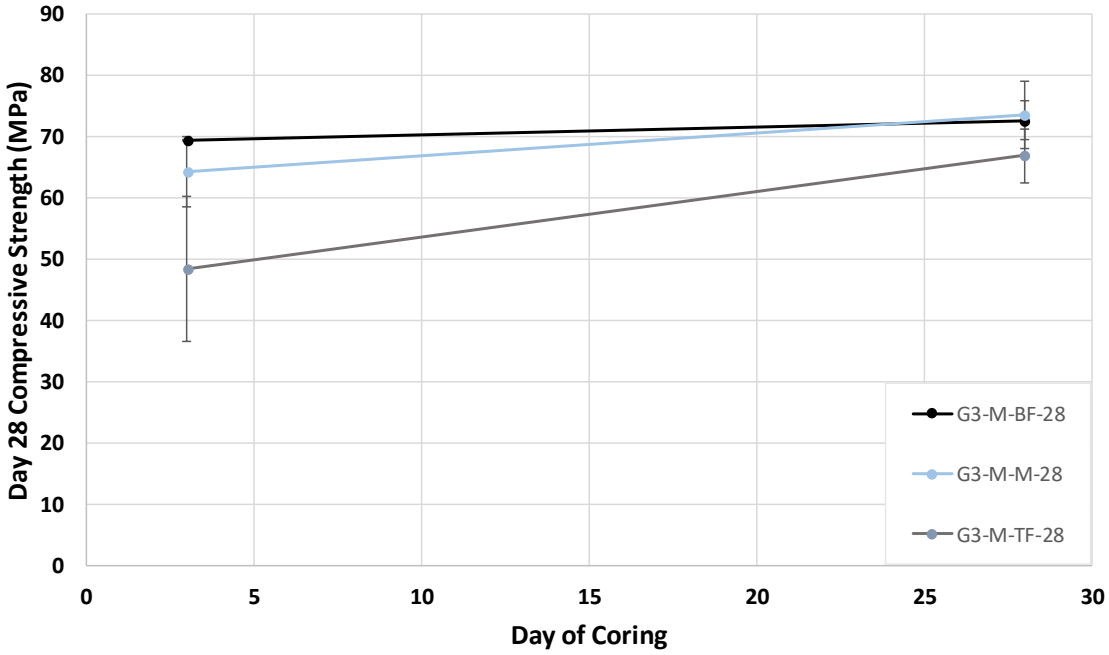

Figure B.3: Compressive Strength of Girder G3 Cores Extracted on Various Days, Tested on Day 28 from Top Flange, Middle Web, and Bottom Flange Locations. Day 28 Extracted Cores were in the Dry Condition, Day 3 were Moist

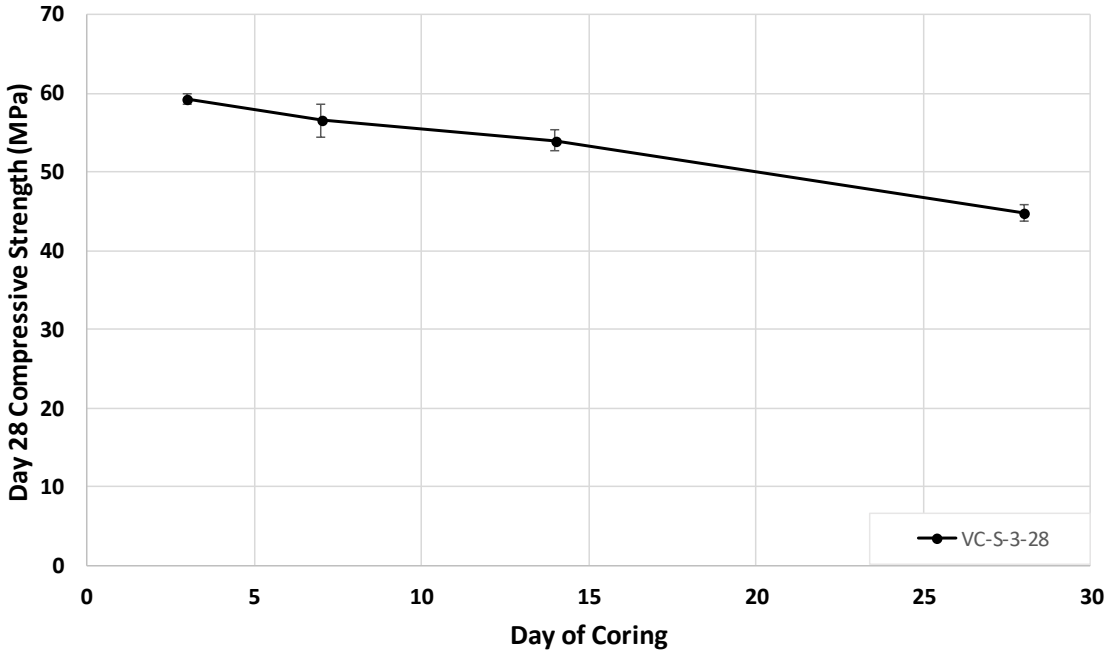

Figure B.4: Compressive Strength of Valve Chamber VC Cores Extracted on Various Days, Tested on Day 28 from. Day 28 Extracted Cores were in the Dry Condition, While Others were Saturated

B.2 All Results: Density

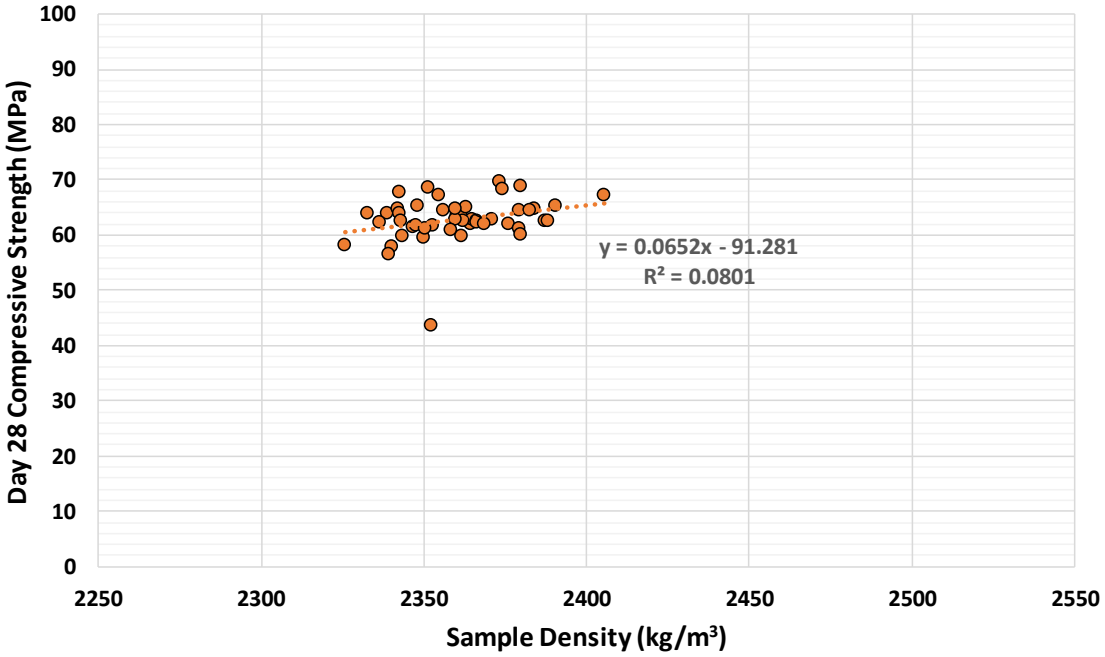

Figure B.5: Day 28 Compressive Strength of Beam B2 Samples versus Sample Density

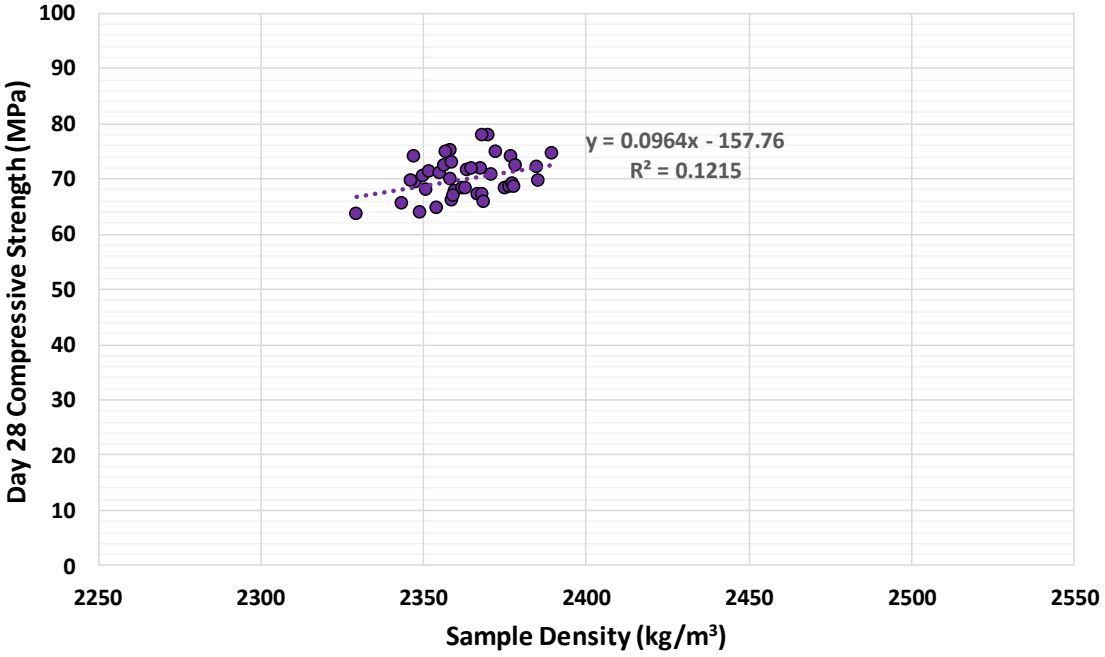

Figure B.6: Day 28 Compressive Strength of Girder G1 Samples versus Sample Density

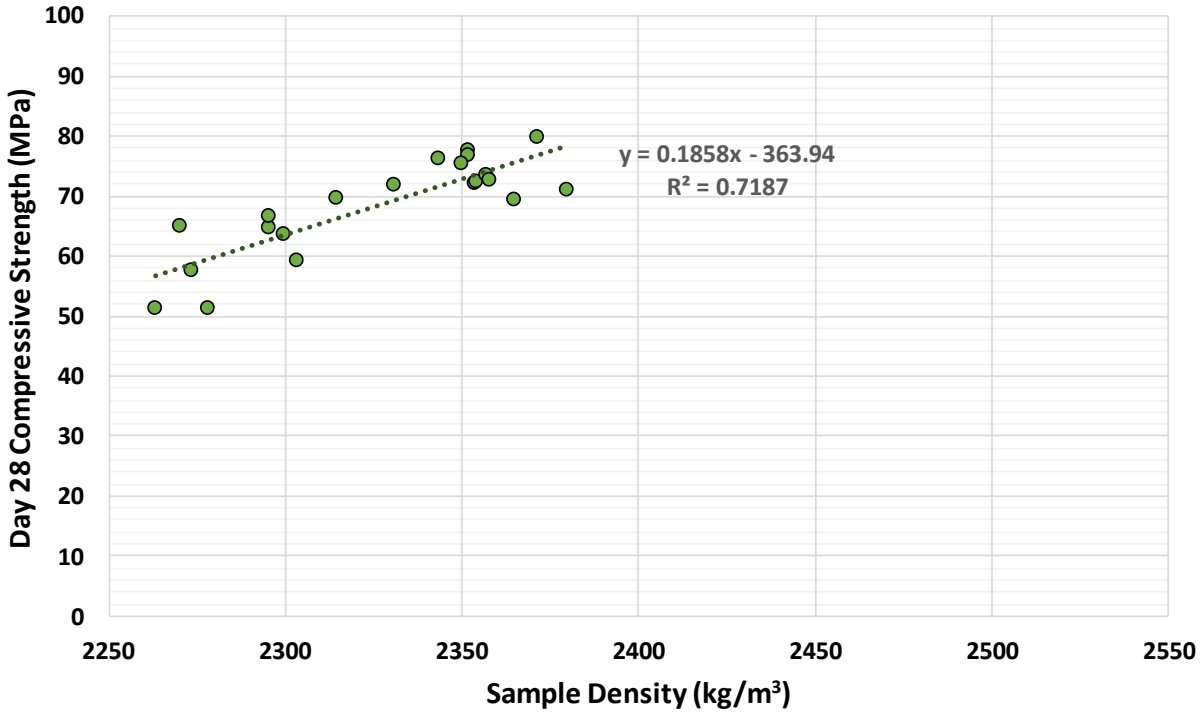

Figure B.7: Day 28 Compressive Strength of Girder G2 Samples versus Sample Density

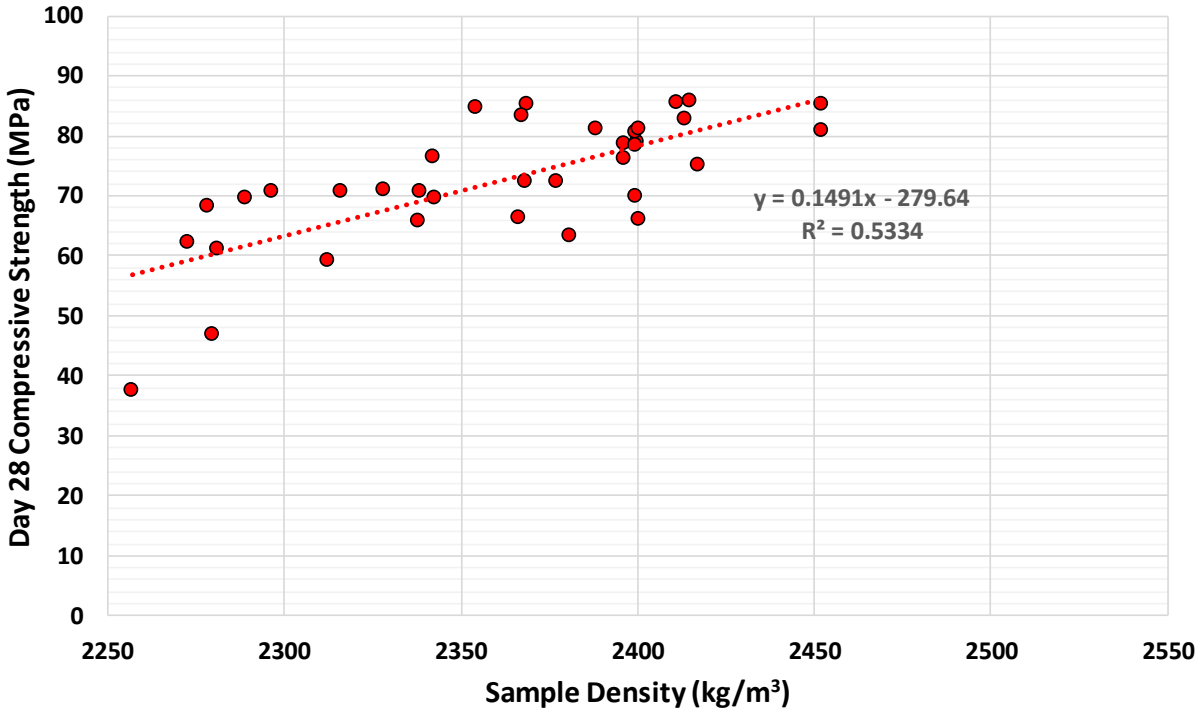

Figure B.8: Day 28 Compressive Strength of Girder G3 Samples versus Sample Density

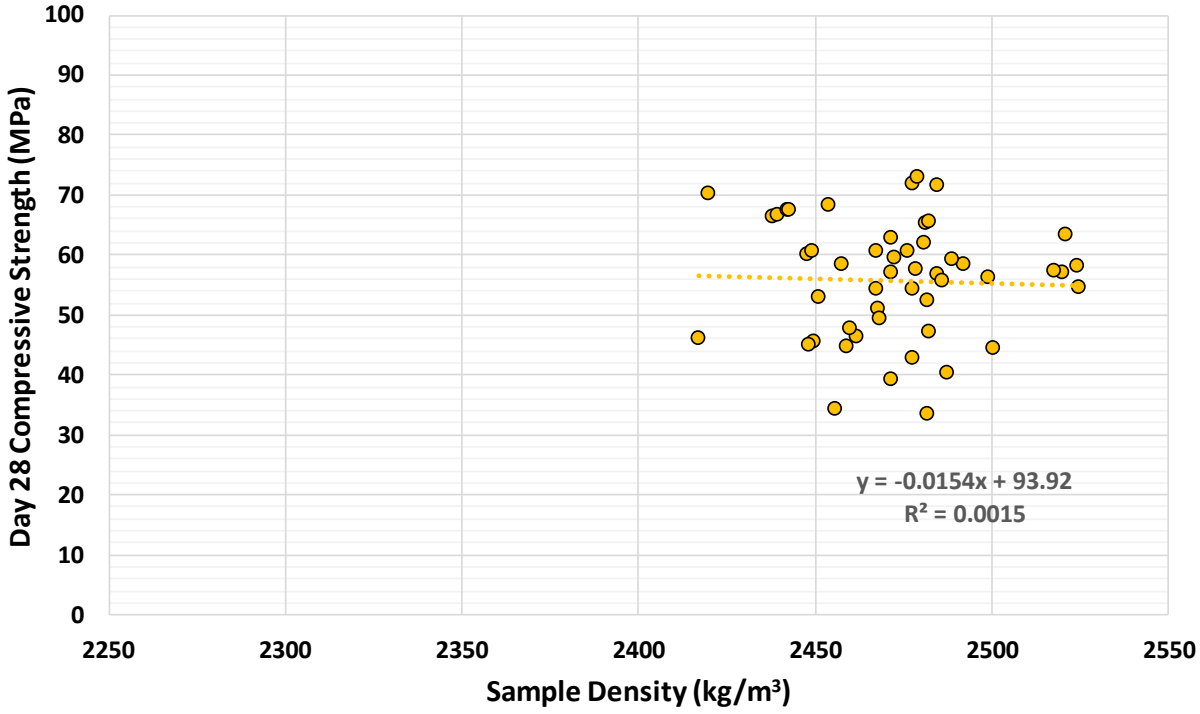

Figure B.9: Day 28 Compressive Strength of MH Samples versus Sample Density

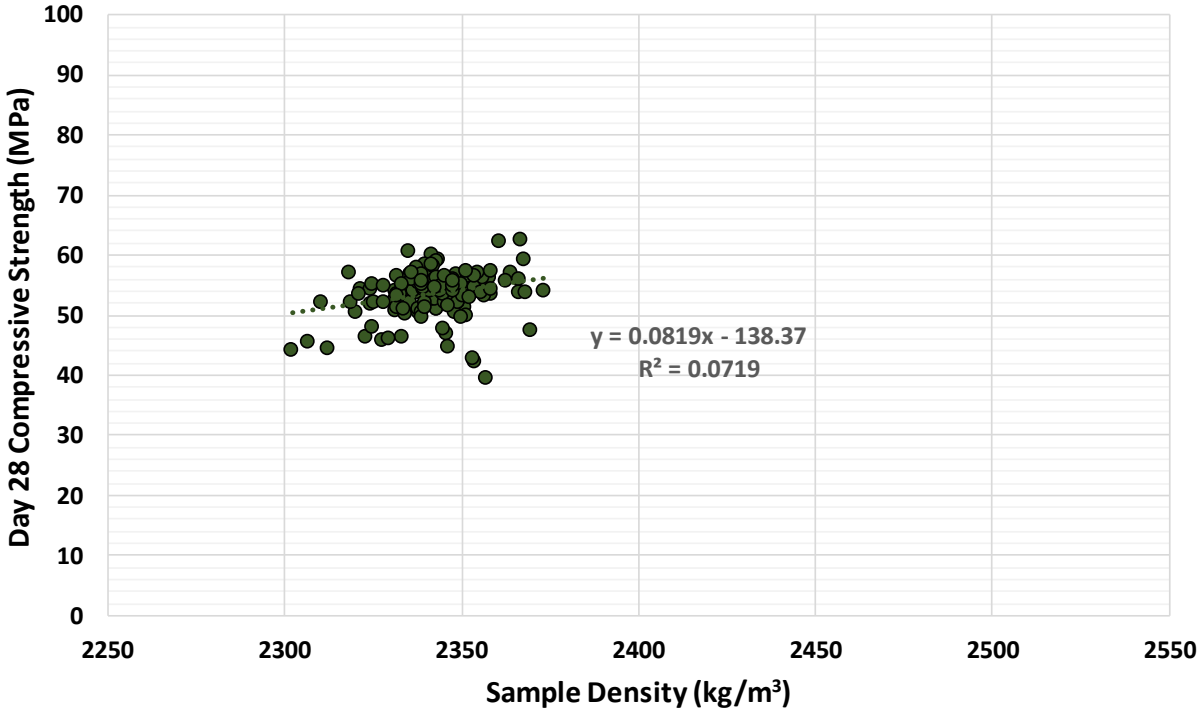

Figure B.10: Day 28 Compressive Strength of VC Samples versus Sample Density

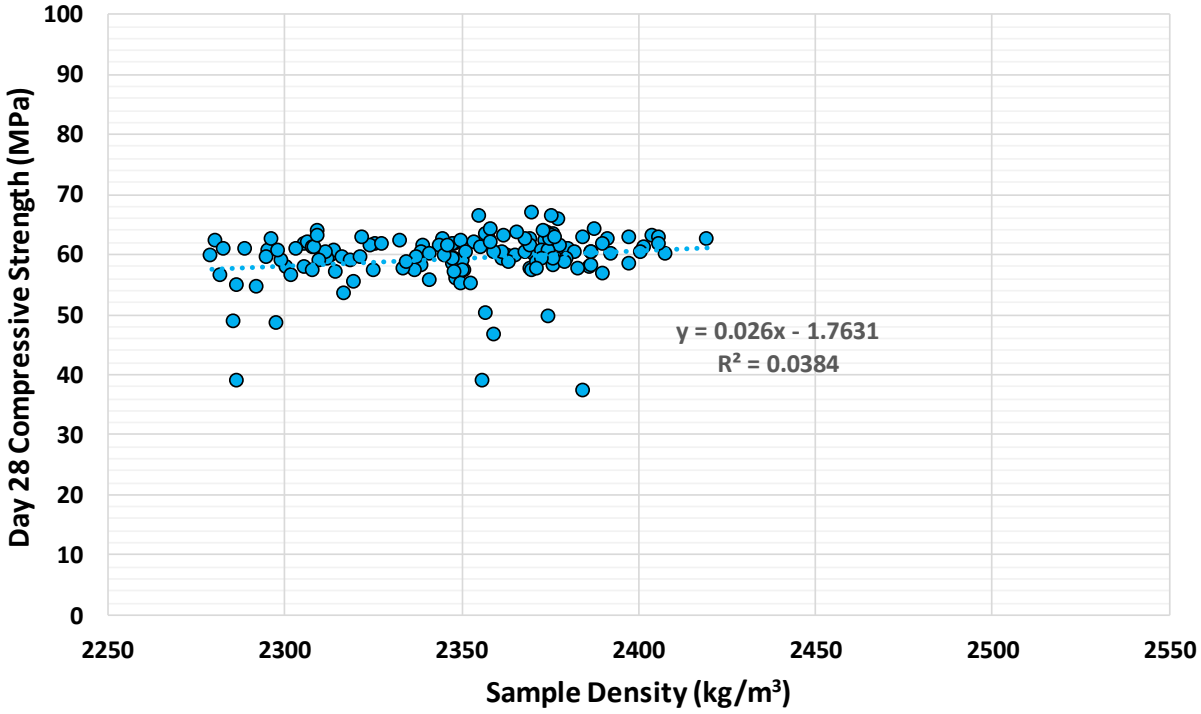

Figure B.11: Day 28 Compressive Strength of CC Samples versus Sample Density

B.3 Temperature Monitoring

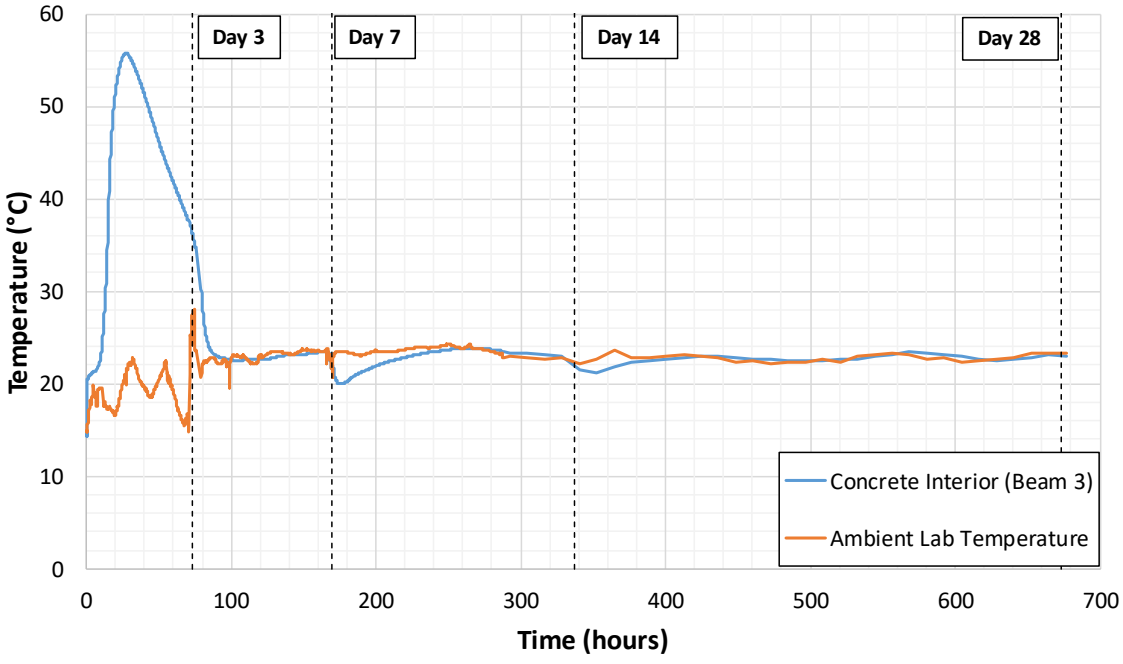

Figure B.12: Temperature Monitoring of Beam B2 over 28 Days

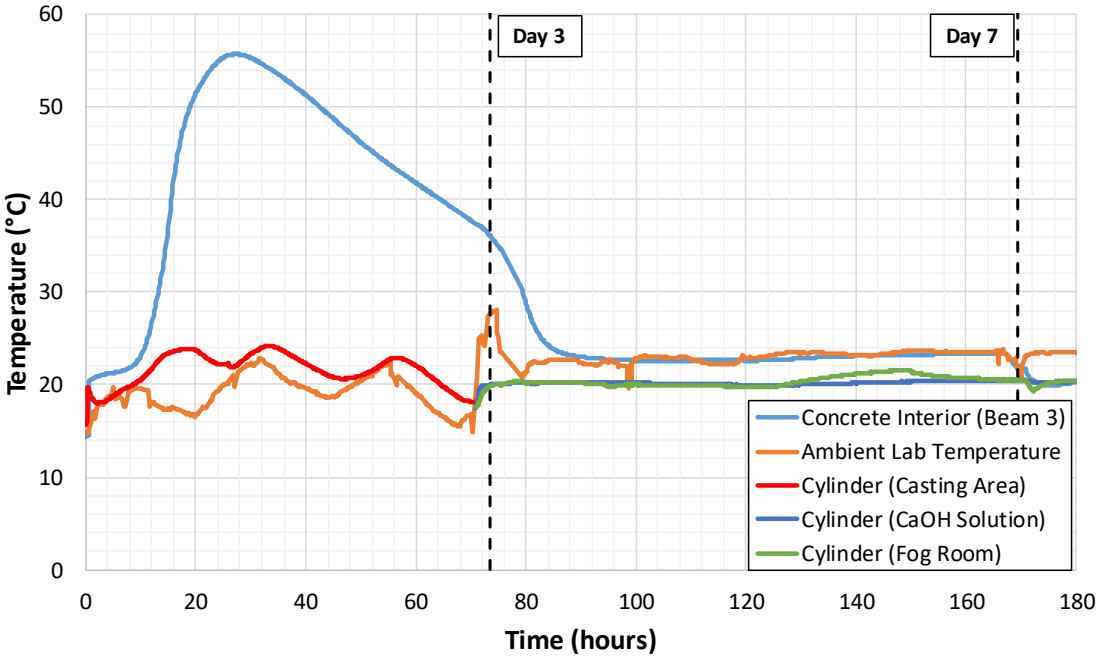

Figure B.13: Temperature Monitoring of Beam B2 over 7 Days, Including Cylinders

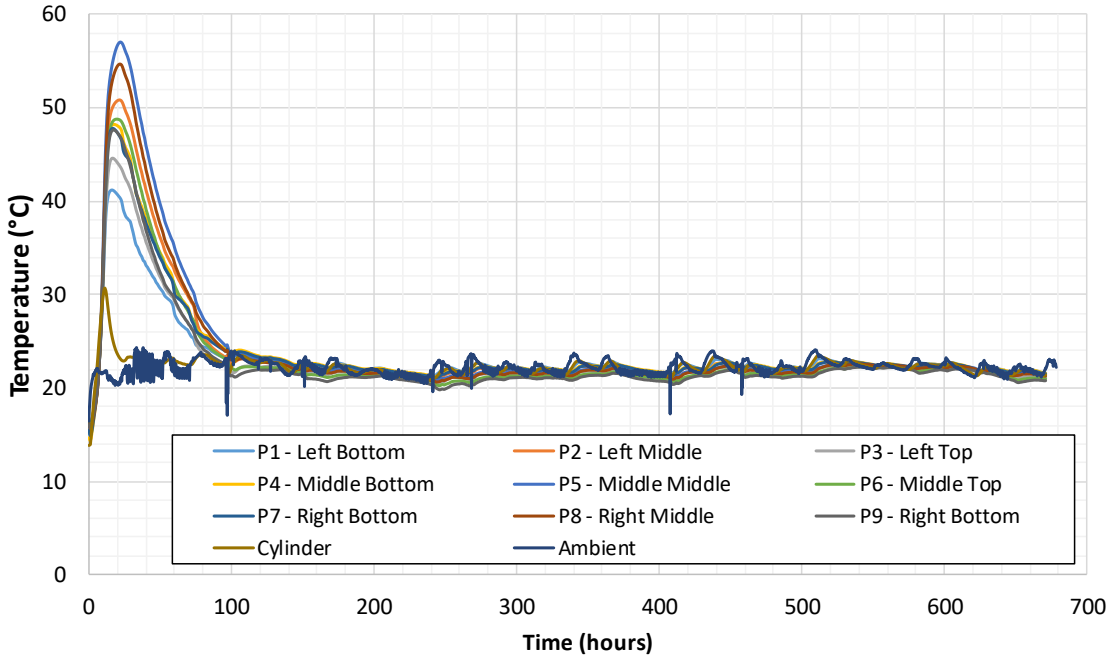

Figure B.14: Temperature Monitoring of Girder G1 at Multiple Locations over 28 Days

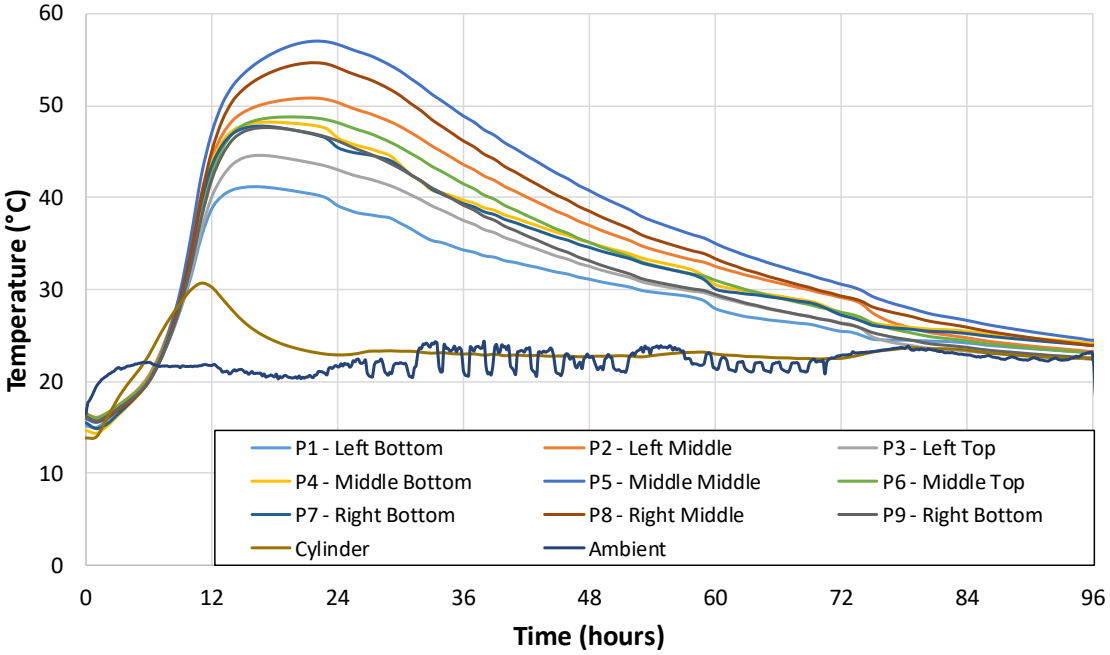

Figure B.15: Temperature Monitoring of Girder G1 at Multiple Locations over 3 Days

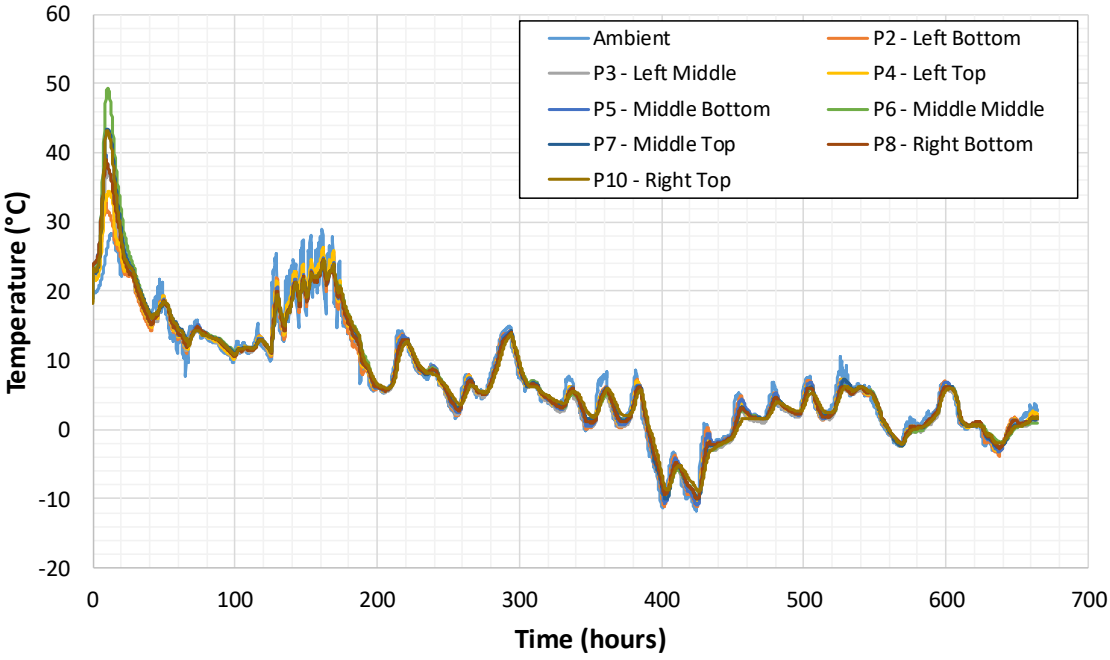

Figure B.16: Temperature Monitoring of Girder G2 at Multiple Locations over 28 Days

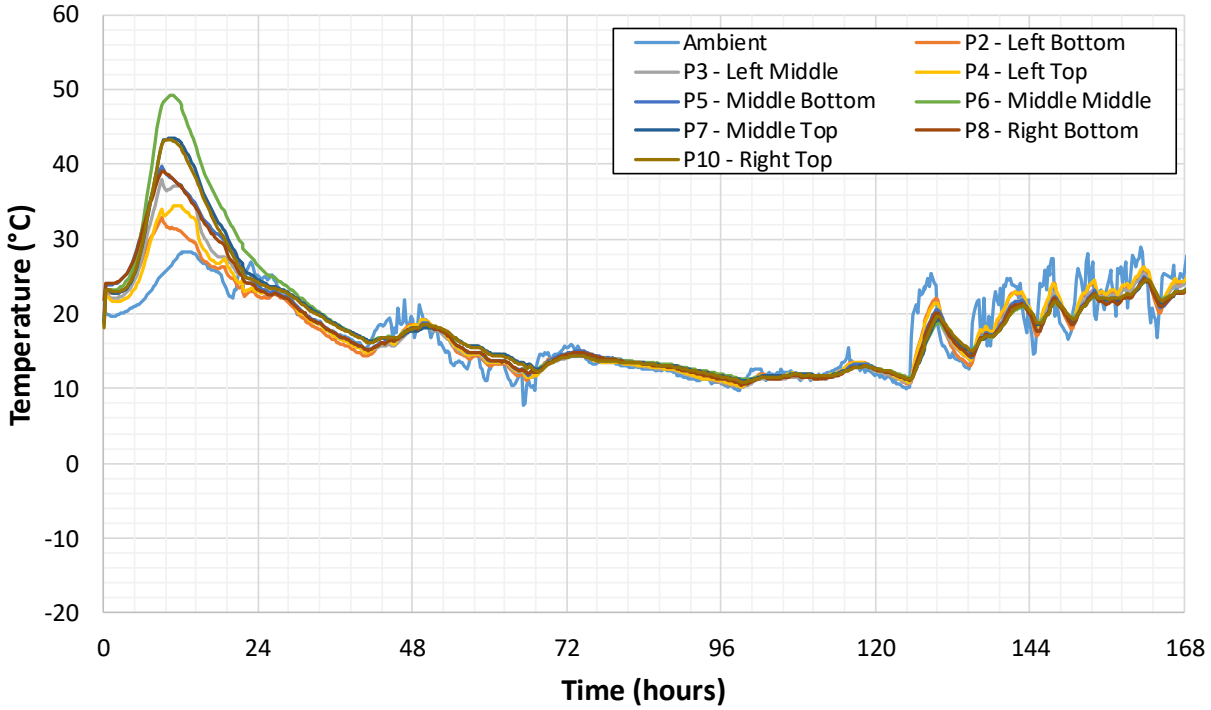

Figure B.17: Temperature Monitoring of Girder G2 at Multiple Locations over 7 Days

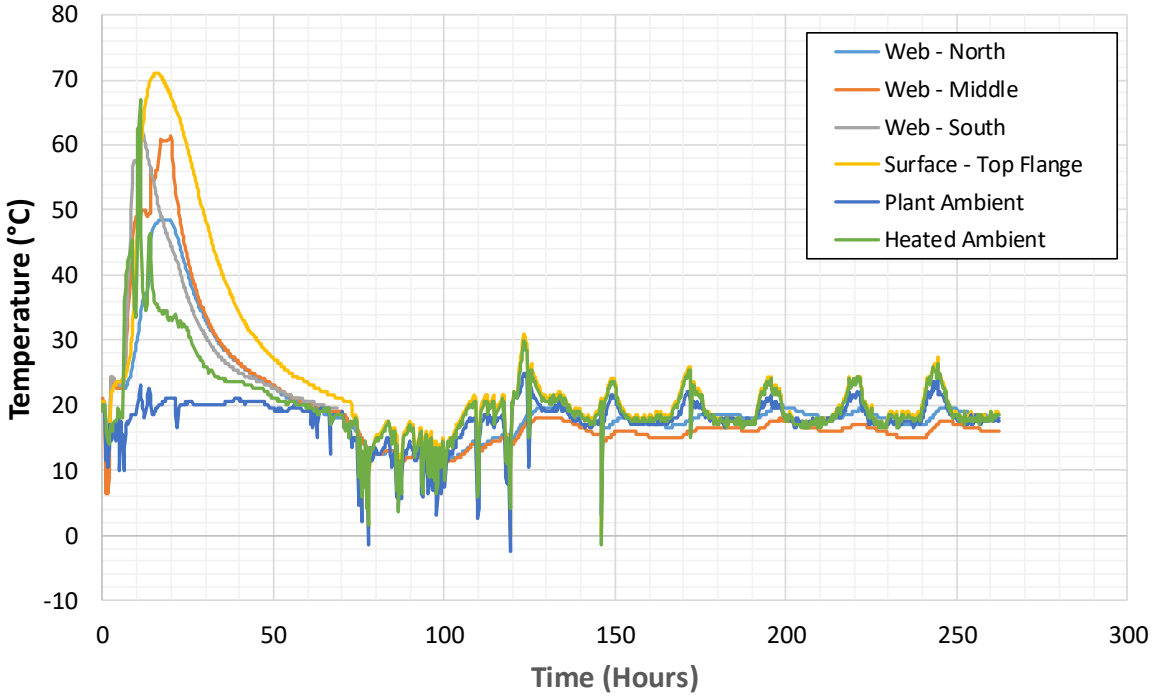

Figure B.18: Temperature Monitoring of Girder G3 at Multiple Locations over 11 Days

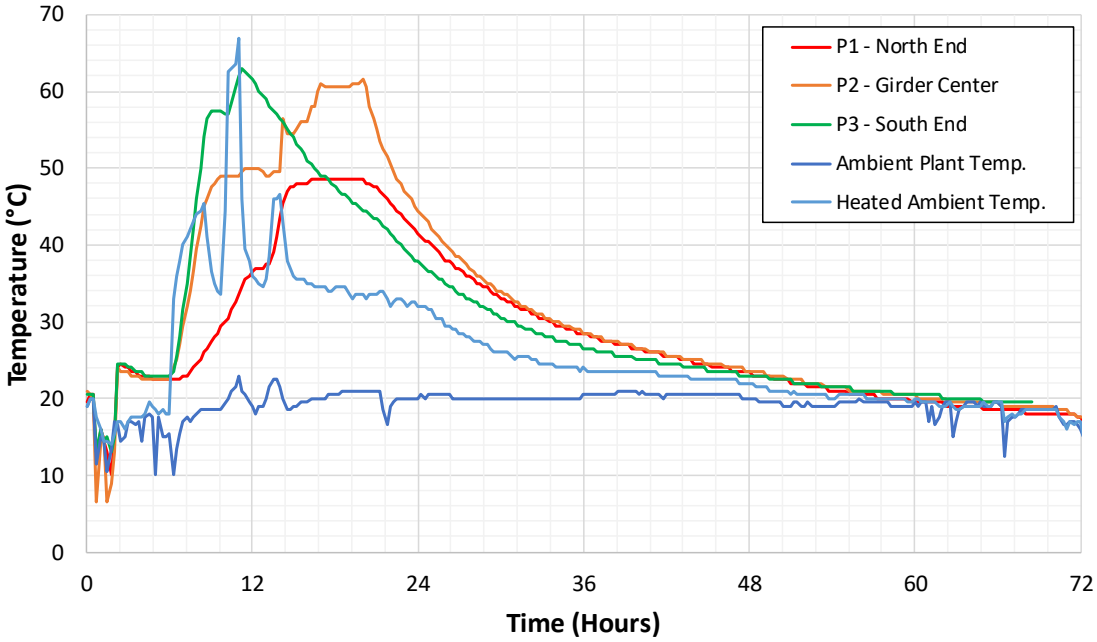

Figure B.19: Temperature Monitoring of Girder G3 at Multiple Locations over 3 Days

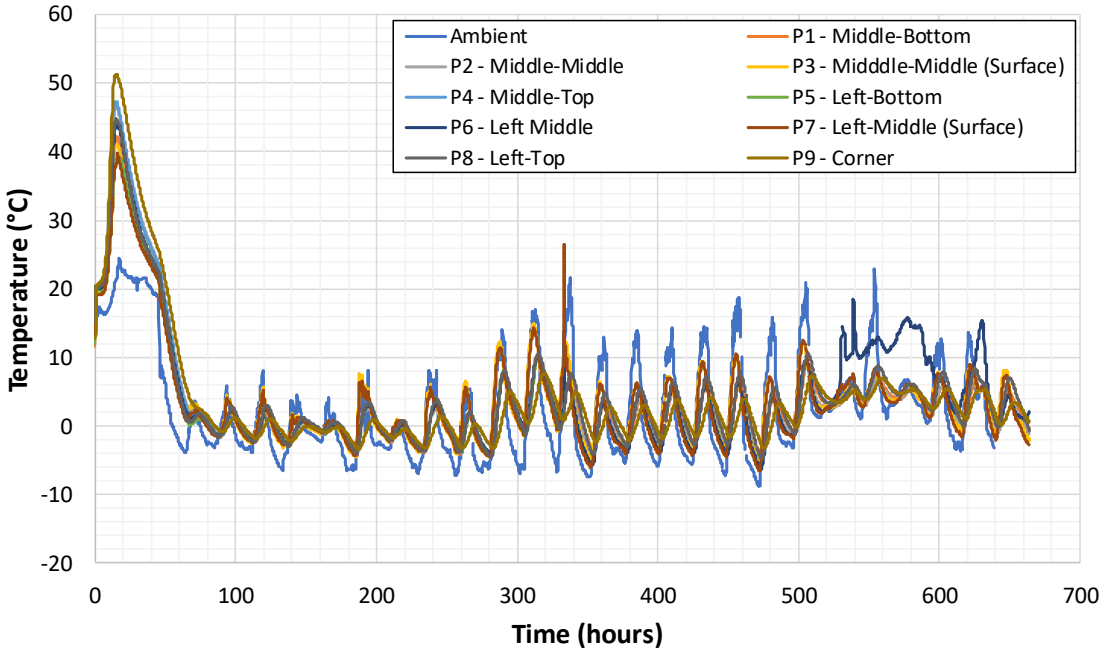

Figure B.20: Temperature Monitoring of VC on Big Wall at Multiple Locations over 28 Days

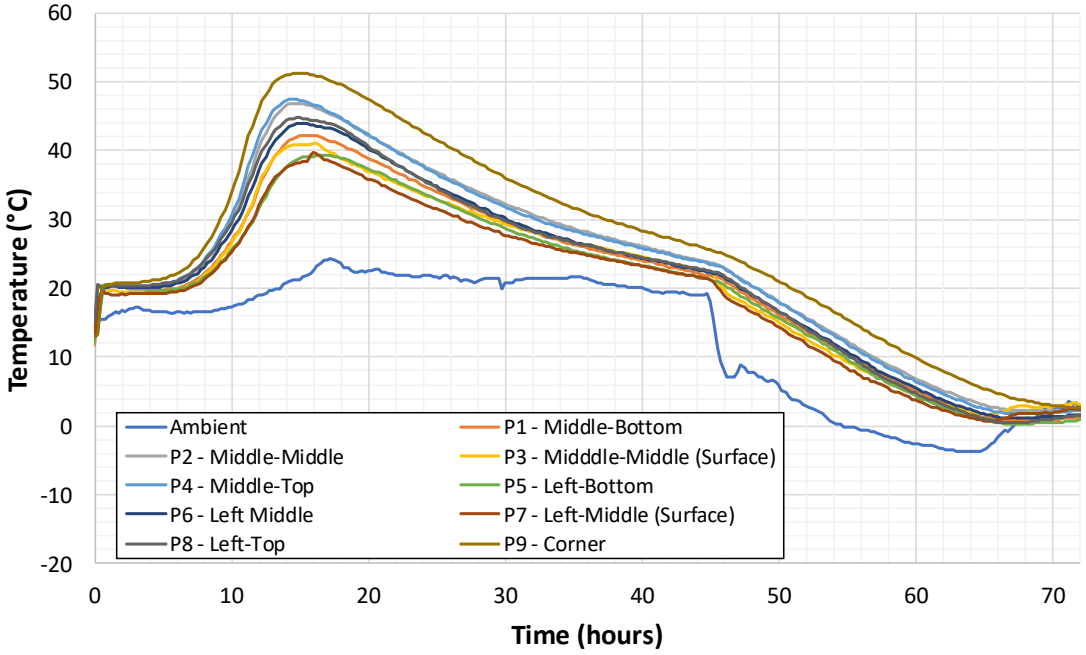

Figure B.21: Temperature Monitoring of VC on Big Wall at Multiple Locations over 3 Days

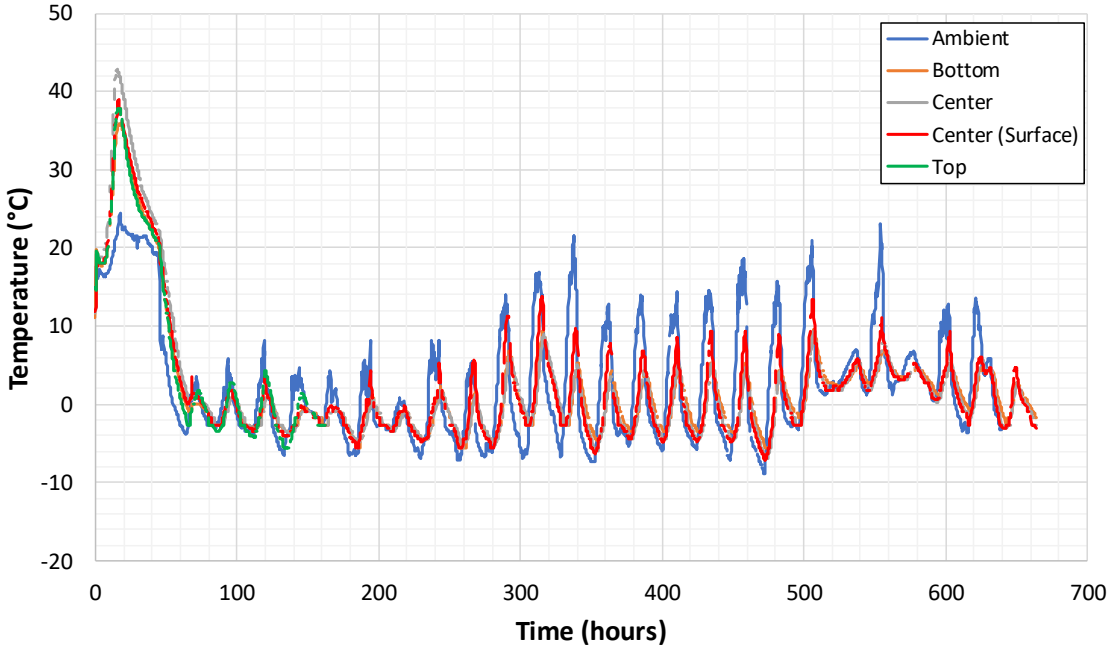

Figure B.22: Temperature Monitoring of VC on Small Wall at Multiple Locations over 28 Days

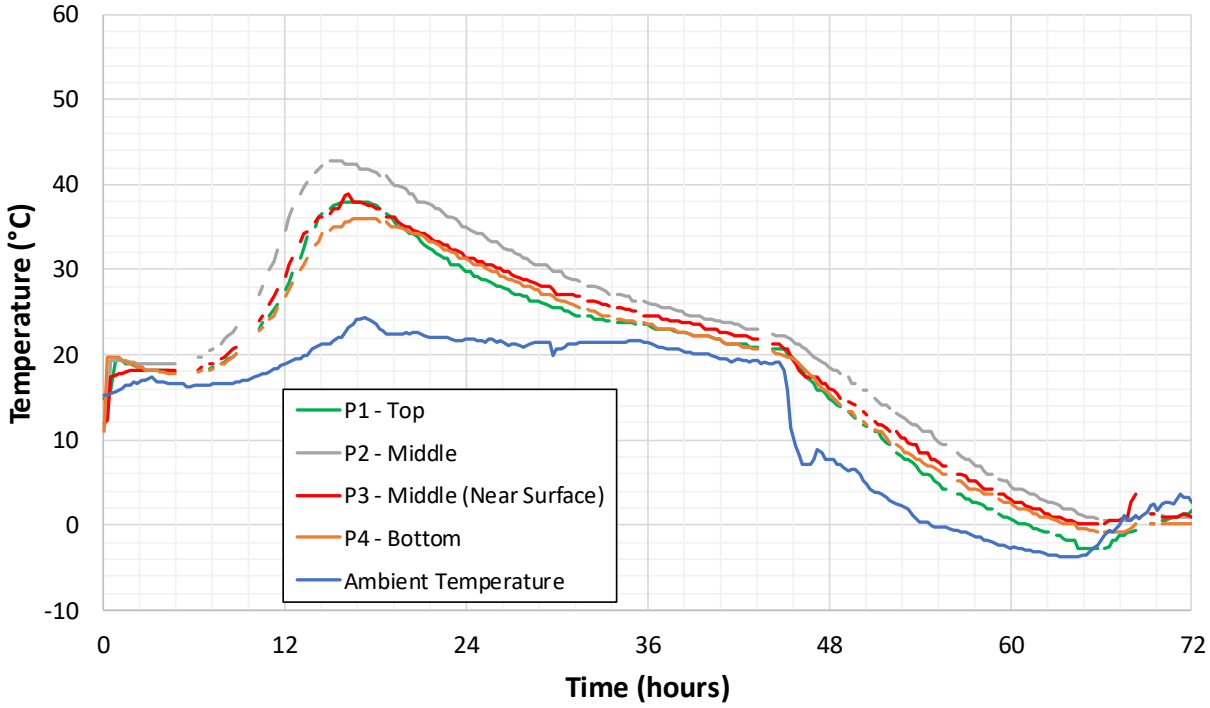

Figure B.23: Temperature Monitoring of VC on Small Wall at Multiple Locations over 3 Days

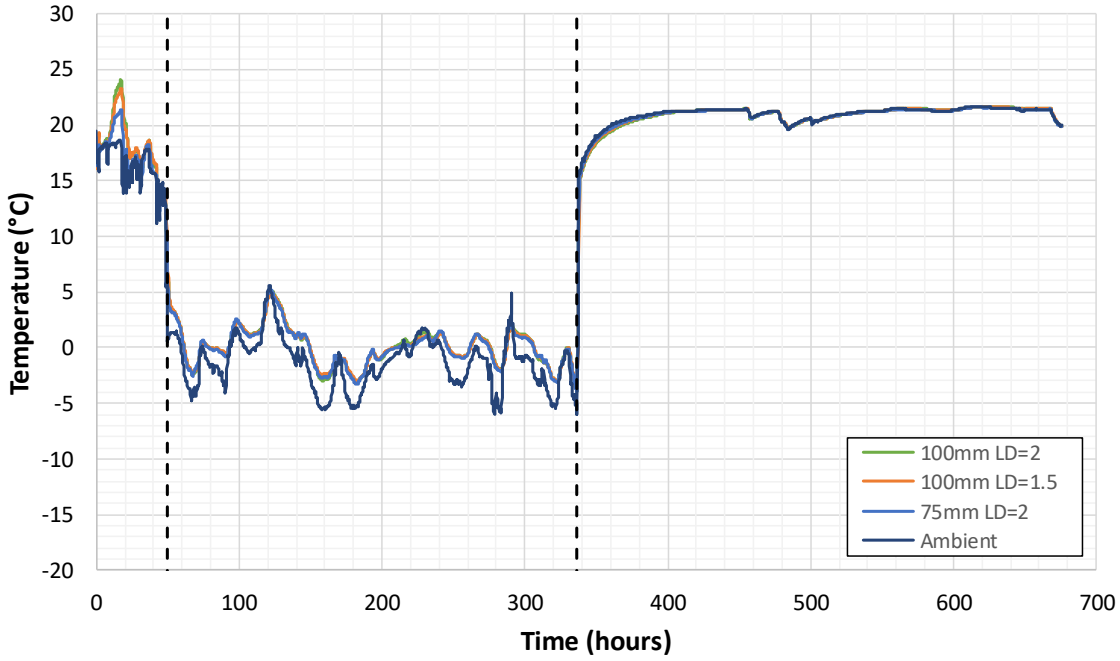

Figure B.24: Temperature Monitoring of Multiple CC Cylinders over 28 Days

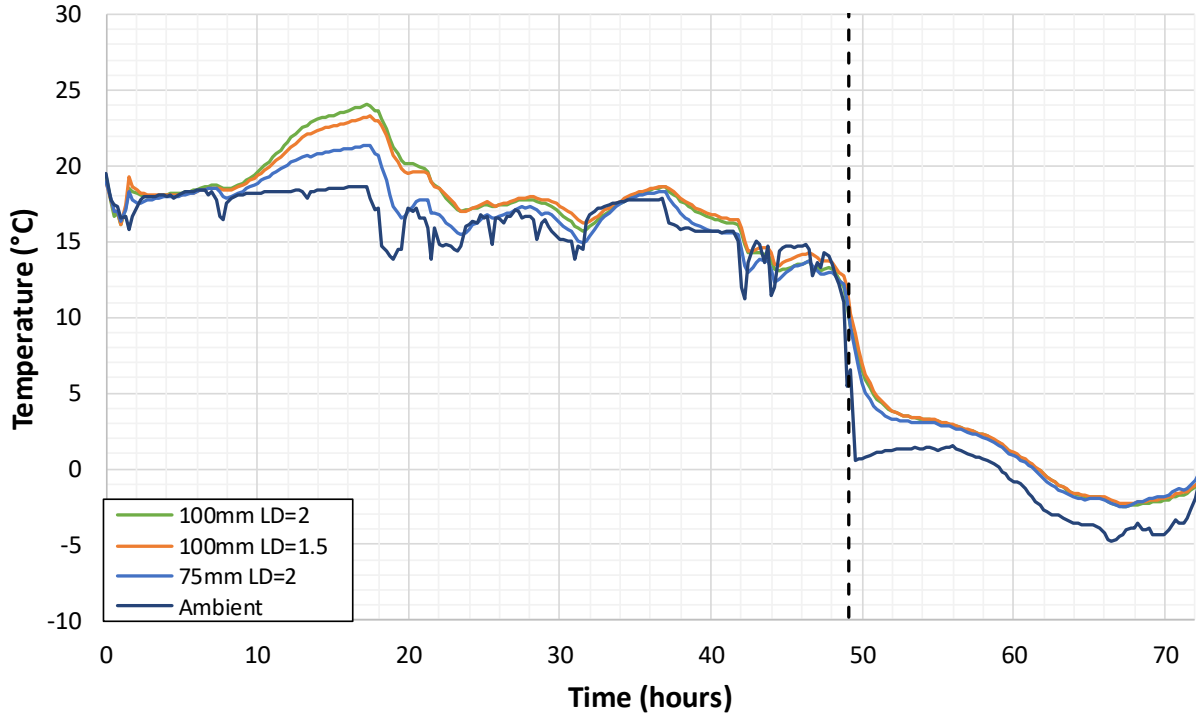

Figure B.25: Temperature Monitoring of Multiple CC Cylinders over 3 Days

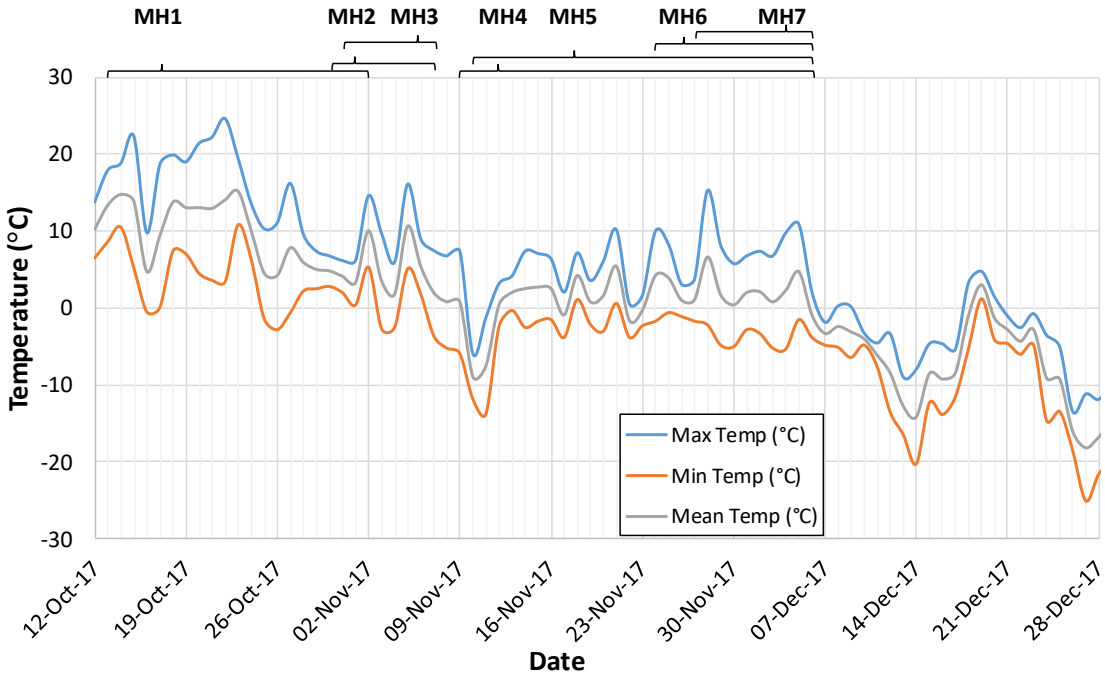

Figure B.26: Ambient Temperature of MH for the Duration Samples Were Outdoors (Obtained from Government of Canada [88]**)**

Appendix C - Variability of Factors

C.1 Length-to-Diameter Factor Variability Equations

This section includes the variability equations for the models of $F_{l/d}$, which are derived by the first order approximation method, as shown by the following:

$$V_{l/d} = \frac{\sqrt{Var\left[F_{l/d}\right]}}{E\left[F_{l/d}\right]} = \frac{\sqrt{\sum_{i=1}^{n} \frac{\partial F_{l/d}}{\partial \beta_i} Var[\beta_i]}}{F_{l/d}} \quad \text{(C.1.1)}$$

Model 1	$V_{l/d} = \frac{\sqrt{Var\left[\frac{2}{1.5 + d/l}\right]}}{E\left[\frac{2}{1.5 + d/l}\right]}$ $= \frac{\sqrt{\left(\frac{1}{1.5 + d/l}\right)^2 Var[2] + \left(-\frac{2}{(1.5 + d/l)^2}\right)^2 Var[1.5]}}{\frac{2}{1.5 + d/l}}$ $= \begin{matrix} 1.568\% \mid l/d = 2 \\ 1.508\% \mid l/d = 1.5 \end{matrix}$	(C.1.2)
Model 2	$V_{l/d} = \frac{\sqrt{Var\left[\frac{1}{1 + 0.8(1 - 0.5 * l/d)^2}\right]}}{E\left[\frac{1}{1 + 0.8(1 - 0.5 * l/d)^2}\right]}$ $= \frac{\sqrt{\left(\frac{-(1 - 0.5 * l/d)^2}{(1 + 0.8(1 - 0.5 * l/d)^2)^2}\right)^2 Var[0.8] + \left(\frac{2 * 0.8 * \mathrm{l/d} * (1 - 0.5 * l/d)}{(1 + 0.8(1 - 0.5 * l/d)^2)^2}\right)^2 Var[0.5]}}{\frac{1}{1 + 0.8(1 - 0.5 * l/d)^2}}$ $= \begin{matrix} 0\% \mid l/d = 2 \\ 0.256\% \mid l/d = 1.5 \end{matrix}$	(C.1.3)

Model 3	$V_{l/d} = \frac{\sqrt{Var\left[\frac{1}{1+0.8(d/l)(1-0.5*l/d)^2}\right]}}{E\left[\frac{1}{1+0.8(1-0.5*l/d)^2}\right]}$ $= \frac{\sqrt{\left(\frac{-l/d\,(1-0.5*l/d)^2}{(l/d+0.8(1-0.5*l/d)^2)^2}\right)^2 Var[0.8] + \left(\frac{2*0.8*(l/d)^2*((1-0.5*l/d))}{(l/d+0.8(1-0.5*l/d)^2)^2}\right)^2 Var[0.5]}}{\frac{1}{1+0.8(l/d)(1-0.5*l/d)^2}}$ $= \begin{matrix} 0\% \mid l/d = 2 \\ 0.208\% \mid l/d = 1.5 \end{matrix}$	(C.1.4)
Model 4	$V_{l/d} = \frac{\sqrt{Var\left[1*Z_{l/d=2} + 0.96*Z_{l/d=1.5}\right]}}{E\left[1*Z_{l/d=2} + 0.96*Z_{l/d=1.5}\right]}$ $= \frac{\sqrt{Z_{l/d=2}^2 Var[1] + Z_{l/d=1.5}^2 Var[0.96]}}{1*Z_{l/d=2} + 0.96*Z_{l/d=1.5}}$ $= \begin{matrix} 0.009\% \mid l/d = 2 \\ 0.036\% \mid l/d = 1.5 \end{matrix}$	(C.1.5)
Model 5	$V_{l/d} = \frac{\sqrt{Var[1-\{0.117-4.3*10^{-4}*f_{core}\}(2-l/d)^2]}}{E[1-\{0.117-4.3*10^{-4}*f_{core}\}(2-l/d)^2]}$ $= \frac{\sqrt{(-(2-l/d)^2)^2 Var[0.117] + (f_{core}(2-l/d)^2)^2 Var[4.3*10^{-4}] + \left(-\ln(2-l/d)\,(0.117-4.3*10^{-4}f_{core})\left(2-\frac{l}{d}\right)^2\right)^2 Var[2]}}{E[1-\{0.117-4.3*10^{-4}*f_{core}\}(2-l/d)^2]}$ $f_{core} = 55$ MPa $= \begin{matrix} 0\% \mid l/d = 2 \\ 0.559\% \mid l/d = 1.5 \end{matrix}$	(C.1.6)
Model 6	$V_{l/d} = \frac{\sqrt{Var[0.1385\ln(l/d) + 0.9069]}}{E[0.1385\ln(l/d) + 0.9069]}$ $= \frac{\sqrt{\ln(l/d)^2 * Var[0.1385] + Var[0.9069]}}{0.1385\ln(l/d) + 0.9069}$ $= \begin{matrix} 0.076\% \mid l/d = 2 \\ 0.063\% \mid l/d = 1.5 \end{matrix}$	(C.1.7)

Model 7	$V_{l/d} = \frac{\sqrt{Var\left[\bar{f}_{l/d=2} / \bar{f}_{l/d=1.5}\right]}}{E\left[\bar{f}_{l/d=2} / \bar{f}_{l/d=1.5}\right]}$ $= \frac{\sqrt{Var\left[\bar{f}_{l/d=2} / \bar{f}_{l/d=1.5}\right]}}{\bar{f}_{l/d=2} / \bar{f}_{l/d=1.5}}$ $= \begin{matrix} 0.012\% \mid l/d = 2 \\ 0.012\% \mid l/d = 1.5 \end{matrix}$	(C.1.8)
Model 8	$V_{l/d} = \frac{\sqrt{Var\left[1 - \beta_1\left(2 - {}^{l}/_{d}\right)^{\beta_2}\right]}}{E\left[1 - \beta_1\left(2 - {}^{l}/_{d}\right)^{\beta_2}\right]}$ $= \frac{\sqrt{\left(-\left(2 - \frac{l}{d}\right)^{\beta_2}\right)^2 Var[\beta_1] + ((-\beta_1 \ln(2 - l/d) * (2 - l/d)^{\beta_2})^2 Var[\beta_2]}}{1 - \beta_1\left(2 - {}^{l}/_{d}\right)^{\beta_2}}$ $\beta_1 = 626.91$ $\beta_2 = 17.349$ $= \begin{matrix} 0\% \mid l/d = 2 \\ 0.899\% \mid l/d = 1.5 \end{matrix}$	(C.1.9)
Model 9	$V_{l/d} = \frac{\sqrt{Var[1 + \beta_1(2 - l/d) + \beta_2(4 - (l/d)^2)]}}{E[1 + \beta_1(2 - l/d) + \beta_2(4 - (l/d)^2)]}$ $= \frac{\sqrt{(2 - l/d)^2 Var[\beta_1] + (4 - (l/d)^2)^2 Var[\beta_2]}}{1 + \beta_1(2 - l/d) + \beta_2(4 - (l/d)^2)}$ $\beta_1 = -0.2437$ $\beta_2 = 0.0660$ $= \begin{matrix} 0\% \mid l/d = 2 \\ 4.642\% \mid l/d = 1.5 \end{matrix}$	(C.1.10)

Model 10	$V_{l/d} = \frac{\sqrt{Var[1-\{\beta_1-\beta_2*f_{core}\}(2-l/d)^{\beta_3}]}}{E[1-\{\beta_1-\beta_2*f_{core}\}(2-l/d)^{\beta_3}]}$ $= \frac{\sqrt{(-(2-l/d)^{\beta_3})^2 Var[\beta_1] + (f_{core}(2-l/d)^{\beta_3})^2 Var[\beta_2] + \left(-\ln(2-l/d)\,(\beta_1-\beta_2 f_{core})\left(2-\frac{l}{d}\right)^{\beta_3}\right)^2 Var[\beta_3]}}{E[1-\{\beta_1-\beta_2*f_{core}\}(2-l/d)^{\beta_3}]}$ $f_{core} = 55$ MPa $\beta_1 = -0.4776$ $\beta_2 = -0.00835$ $\beta_3 = 0.2697$ $= \begin{matrix} 0\% \mid l/d = 2 \\ 0.594\% \mid l/d = 1.5 \end{matrix}$	(C.1.11)
Model 11	$V_{l/d} = \frac{\sqrt{Var[1-\{\beta_1-\beta_2*f_{core}\}(2-l/d)^2]}}{E[1-\{\beta_1-\beta_2*f_{core}\}(2-l/d)^2]}$ $= \frac{\sqrt{(-(2-l/d)^2)^2 Var[\beta_1] + (f_{core}(2-l/d)^2)^2 Var[\beta_2]}}{E[1-\{\beta_1-\beta_2*f_{core}\}(2-l/d)^2]}$ $f_{core} = 55$ MPa $\beta_1 = -1.5039$ $\beta_2 = -0.02632$ $= \begin{matrix} 0\% \mid l/d = 2 \\ 0.916\% \mid l/d = 1.5 \end{matrix}$	(C.1.12)
Model 12	$V_{l/d} = \frac{\sqrt{Var[\beta_1 \ln(l/d)+\beta_2]}}{E[\beta_1 \ln(l/d)+\beta_2]}$ $= \frac{\sqrt{\ln(l/d)^2 * Var[\beta_1] + Var[\beta_2]}}{\beta_1 \ln(l/d)+\beta_2}$ $\beta_1 = 0.02323$ $\beta_2 = 0.98401$ $= \begin{matrix} 0.129\% \mid l/d = 2 \\ 0.098\% \mid l/d = 1.5 \end{matrix}$	(C.1.13)

C.2 Damage Caused by Coring Factor Variability Equations

This section includes the variability equations for the models of F_{dam}, which are derived by the first order approximation method, as shown above in Equation (C.1.1).

Model 1	$$V_{l/d} = \frac{\sqrt{Var[1+\beta_{dam1}Z_{core}]}}{E[1+\beta_{dam1}Z_{core}]} = \frac{Z_{core}\sqrt{Var[\beta_{dam1}]}}{1+\beta_{dam1}Z_{core}} = 0.077\%$$	(C.2.1)
Model 2	$$V_{l/d} = \frac{\sqrt{Var\left[1+\left(\begin{matrix}\beta_{100@2}Z_{100@2}+\beta_{100@1.5}Z_{100@1.5}\\+\beta_{75@2}Z_{75@2}+\beta_{75@1.5}Z_{75@1.5}\end{matrix}\right)Z_{core}\right]}}{E\left[1+\left(\begin{matrix}\beta_{100@2}Z_{100@2}+\beta_{100@1.5}Z_{100@1.5}\\+\beta_{75@2}Z_{75@2}+\beta_{75@1.5}Z_{75@1.5}\end{matrix}\right)Z_{core}\right]} = \frac{Z_{Core}\sqrt{\begin{matrix}Z_{100@2}^2Var[\beta_{100@2}]+Z_{100@1.5}^2Var[\beta_{100@1.5}]+\\Z_{75@2}^2Var[\beta_{75@2}]+Z_{100@1.5}^2Var[\beta_{75@1.5}]\end{matrix}}}{1+\left(\begin{matrix}\beta_{100@2}Z_{100@2}+\beta_{100@1.5}Z_{100@1.5}\\+\beta_{75@2}Z_{75@2}+\beta_{75@1.5}Z_{75@1.5}\end{matrix}\right)Z_{core}} = \begin{matrix}0.096\% \mid 100\ mm\ Diameter, l/d=2\\0.165\% \mid 100\ mm\ Diameter, l/d=1.5\\0.101\% \mid 75\ mm\ Diameter, l/d=2\\0.076\% \mid 75\ mm\ Diameter, l/d=1.5\end{matrix}$$	(C.2.2)
Model 3	$$V_{l/d} = \frac{\sqrt{Var\left[1+\left(1-\frac{\beta_{dam2}}{D}\right)^{-1}Z_{core}\right]}}{E[1+\beta_{dam1}Z_{core}]} = \frac{Z_{core}\sqrt{\left(\frac{D}{(D-\beta_{dam2})^2}\right)^2Var[\beta_{dam2}]}}{1+\left(1-\frac{\beta_{dam2}}{D}\right)^{-1}Z_{core}} = \begin{matrix}0.010\% \mid 100\ mm\ Diameter\\0.014\% \mid 75\ mm\ Diameter\end{matrix}$$	(C.2.3)

Appendix D - Raw Data

Type	Label (* dictates Outlier)	Use	Avg Length (mm)	Avg Diameter (mm)	Day Cored	Day Tested	Compressive Strength (MPa)	Bulk Resistivity (kΩ·cm)	Mass (g)	X Location (mm)	Y Location (mm)
Core	MH1-D-T-14-28-1*	COMP	189.06	93.80	14	28	63.04	28.47	3293.4		
Core	MH1-D-T-14-28-2	COMP	190.34	93.87	14	28	57.81	28.18	3324.8		
Core	MH1-D-T-14-28-3	COMP	192.26	93.69	14	28	54.47	26.40	3345.8		
Core	MH1-D-T-14-28-4	COMP	191.86	93.73	14	28	56.73	26.98	3336.4		
Core	MH1-D-B-14-28-1	COMP	190.95	93.92	14	28	58.07	26.26	3296.6		
Core	MH1-D-B-14-28-2	COMP	189.29	93.61	14	28	55.56	25.98	3238.5		
Core	MH1-D-B-14-28-3	COMP	193.93	93.60	14	28	56.50	25.77	3315.3		
Core	MH1-D-B-14-28-4	COMP	192.62	93.76	14	28	56.02	27.85	3323.2		
Cylinder	MH1-D-28-1	COMP	197.69	102.57		28	59.94	24.49	3998.5		
Cylinder	MH1-D-28-2	COMP	198.62	102.41		28	60.47	23.55	4037.1		
Cylinder	MH1-D-28-3	COMP	197.30	102.30		28	58.28	23.83	3985.0		
Cylinder	MH1-D-28-4	COMP	197.90	102.56		28	61.86	29.23	4056.3		
Cylinder	MH1-D-28-5	COMP	198.70	102.61		28	60.35	29.07	4023.9		
Cylinder	MH1-D-28-6	COMP	196.78	102.31		28	62.50	27.24	3998.4		
Core	MH2-D-4-28-1	COMP	187.97	93.45	4	28	44.14	56.70	3223.9		
Core	MH2-D-4-28-2	COMP	185.08	93.39	4	28	33.33	59.52	3146.2		
Core	MH2-D-4-28-3	COMP	185.51	93.45	4	28	57.01	54.04	3203.5		
Cylinder	MH2-D-28-1	COMP	200.75	102.58		28	66.44	59.14	4047.2		
Cylinder	MH2-D-28-2	COMP	199.54	102.25		28	68.02	57.91	4020.4		
Cylinder	MH2-D-28-3	COMP	197.28	102.42		28	66.18	50.90	3963.0		
Core	MH3-D-3-28-1	COMP	187.08	93.47	3	28	54.19	42.86	3167.3		
Core	MH3-D-3-28-2	COMP	187.44	93.66	3	28	52.19	48.49	3204.9		
Core	MH3-D-3-28-3	COMP	187.65	93.53	3	28	45.81	43.71	3116.0		
Cylinder	MH3-D-28-1	COMP	200.38	102.87		28	70.09	54.38	4029.9		
Cylinder	MH3-D-28-2	COMP	198.86	102.56		28	67.30	53.76	4012.5		

Appendix D - Raw Data

Type	Label (* dictates Outlier)	Use	Avg Length (mm)	Avg Diameter (mm)	Day Cored	Day Tested	Compressive Strength (MPa)	Bulk Resistivity (kΩ·cm)	Mass (g)	X Location (mm)	Y Location (mm)
Cylinder	MH3-D-28-3	COMP	200.73	102.40		28	67.17	52.58	4038.3		
Core	MH4-D-21-28-1	COMP	189.87	93.64	21	28	38.84	9.68	3231.3		
Core	MH4-D-21-28-2	COMP	190.12	93.64	21	28	34.12	10.33	3215.2		
Core	MH4-D-21-28-3	COMP	190.26	93.70	21	28	42.48	9.93	3250.1		
Cylinder	MH4-D-28-1	COMP	195.98	102.18		28	46.03	13.02	3956.1		
Cylinder	MH4-D-28-2	COMP	198.14	102.44		28	44.50	13.10	4015.2		
Cylinder	MH4-D-28-3	COMP	197.19	102.19		28	45.37	12.68	3961.8		
Core	MH5-D-20-28-1	COMP	189.46	93.84	20	28	46.88	15.66	3252.8		
Core	MH5-D-20-28-2	COMP	189.13	93.76	20	28	50.77	14.22	3222.5		
Core	MH5-D-20-28-3	COMP	188.49	93.87	20	28	39.96	15.59	3244.7		
Cylinder	MH5-D-28-1	COMP	198.91	102.53		28	59.10	17.16	4087.2		
Cylinder	MH5-D-28-2	COMP	197.74	102.36		28	57.35	17.08	4033.4		
Cylinder	MH5-D-28-3	COMP	197.19	102.27		28	59.25	17.15	4005.5		
Core	MH6-D-6-28-1	COMP	187.64	93.67	6	28	53.93	34.30	3203.2		
Core	MH6-D-6-28-2	COMP	185.12	93.96	6	28	52.81	34.35	3145.8		
Core	MH6-D-6-28-3	COMP	186.50	94.02	6	28	56.76	33.21	3199.6		
Cylinder	MH6-D-28-1	COMP	198.76	102.10		28	72.72	35.36	4034.0		
Cylinder	MH6-D-28-2	COMP	200.81	102.49		28	71.57	33.81	4104.8		
Cylinder	MH6-D-28-3	COMP	201.09	102.51		28	71.41	34.89	4123.4		
Core	MH7-D-3-25-1	COMP	185.22	93.80	3	25	44.81	42.65	3133.3		
Core	MH7-D-3-25-2	COMP	187.04	93.79	3	25	47.58	39.29	3178.6		
Core	MH7-D-3-25-3	COMP	187.10	93.88	3	25	49.23	38.89	3196.5		
Cylinder	MH7-D-25-1	COMP	198.32	102.51		25	65.28	50.02	4063.0		
Cylinder	MH7-D-25-2	COMP	198.84	102.07		25	65.11	51.87	4037.0		
Cylinder	MH7-D-25-3	COMP	201.62	102.55		25	60.45	48.21	4123.2		
Cylinder	G2-D-1-1	COMP				1	45.01				
Cylinder	G2-D-1-2	COMP				1	46.47				

Type	Label (* dictates Outlier)	Use	Avg Length (mm)	Avg Diameter (mm)	Day Cored	Day Tested	Compressive Strength (MPa)	Bulk Resistivity (kΩ·cm)	Mass (g)	X Location (mm)	Y Location (mm)
Cylinder	G2-D-1-3	COMP				1	48.04				
Cylinder	G2-D-3-1	COMP	195.87	101.30		3	60.24				
Cylinder	G2-D-3-2	COMP	196.00	101.66		3	60.29	6.97			
Cylinder	G2-D-3-3	COMP	195.76	101.65		3	60.62	6.04			
Cylinder	G2-S-7-1	COMP	196.53	101.33		7	66.22	9.62			
Cylinder	G2-S-7-2	COMP	194.36	101.74		7	63.97	10.30			
Cylinder	G2-S-7-3	COMP	194.47	101.34		7	65.80	10.06			
Cylinder	G2-S-28-1	COMP	196.59	101.86		28	71.83	16.28	3734.1		
Cylinder	G2-S-28-2	COMP	196.30	101.66		28	75.25	16.19	3744.0		
Cylinder	G2-S-28-3	COMP	194.33	101.64		28	72.64	15.70	3717.4		
Cylinder	G2-S-56-1					56					
Cylinder	G2-S-56-2					56					
Cylinder	G2-S-56-3					56					
Core	G2-S-T-3-O-5	RCP	157.33	99.76	3	O				1000	1005
Core	G2-S-T-3-O-9	AVS	161.90	99.92	3	O				1596	995
Core	G2-D-T-3-3-1	COMP	158.21	75.18	3	3	44.65	5.85	1601.7	140	1110
Core	G2-D-T-3-3-6	COMP	157.73	75.16	3	3	46.19	6.16		1070	1165
Core	G2-D-T-3-3-10	COMP	157.74	75.16	3	3	39.13	6.37		1915	1150
Core	G2-S-T-3-28-12	COMP	156.24	75.21	3	28	64.87	15.24	1575.8	2250	1110
Core	G2-S-T-3-28-8	COMP	157.18	75.24	3	28	57.62	15.41	1588.6	1460	1025
Core	G2-S-T-3-28-3	COMP	156.72	75.18	3	28	51.36	14.54	1574.6	700	1050
Core	G2-D-M-3-3-5	COMP	156.25	75.23	3	3	57.08	7.35	1617.1	1410	725
Core	G2-D-M-3-3-8	COMP	156.72	75.10	3	3	54.07	7.02	1604.2	1590	550
Core	G2-D-M-3-3-9	COMP	157.29	75.12	3	3	52.29	7.21	1604.2	1720	720
Core	G2-S-M-3-28-6	COMP	157.55	75.19	3	28	76.79	14.92	1645.2	1400	545
Core	G2-S-M-3-28-7	COMP	157.07	75.23	3	28	64.58	15.06	1602.4	1605	720
Core	G2-S-M-3-28-10	COMP	156.50	75.10	3	28	69.52	15.20	1604.2	1705	555

Type	Label (* dictates Outlier)	Use	Avg Length (mm)	Avg Diameter (mm)	Day Cored	Day Tested	Compressive Strength (MPa)	Bulk Resistivity (kΩ·cm)	Mass (g)	X Location (mm)	Y Location (mm)
Core	G2-S-B-3-O-5	RCP	152.84	99.79	3	O				990	145
Core	G2-S-B-3-O-9	AVS	155.56	99.82	3	O				1600	140
Core	G2-D-B-3-3-1	COMP	152.64	75.18	3	3	54.70	5.80	1605.8	130	180
Core	G2-D-B-3-3-6	COMP	155.80	75.11	3	3	59.32	6.74	1632.4	1105	240
Core	G2-D-B-3-3-10	COMP	153.36	75.16	3	3	58.62	6.53	1597.0	1565	260
Core	G2-S-B-3-28-12	COMP	152.05	75.23	3	28	77.53	14.80	1589.4	2230	190
Core	G2-S-B-3-28-4	COMP	155.80	75.22	3	28	79.71	14.87	1641.7	800	125
Core	G2-S-B-3-28-8	COMP	157.21	75.23	3	28	76.28	15.00	1637.7	1410	140
Core	G2-D-T-28-28-2	COMP	150.00	75.08	28	28	66.70	11.47	1524.4	425	1150
Core	G2-D-T-28-28-7	COMP	149.67	75.07	28	28	51.23	12.17	1508.8	1300	1090
Core	G2-D-T-28-28-11	COMP	149.97	75.15	28	28	63.58	12.26	1529.4	1970	1015
Core	G2-D-M-28-28-2	COMP	147.15	75.13	28	28	72.17	12.72	1535.4	750	510
Core	G2-D-M-28-28-3*	COMP	152.22	75.15	28	28	59.16	12.72	1554.8	1040	765
Core	G2-D-M-28-28-4	COMP	146.84	75.14	28	28	72.45	12.56	1532.8	1065	515
Core	G2-D-B-28-28-2	COMP	148.77	75.14	28	28	73.39	11.47	1554.5	400	190
Core	G2-D-B-28-28-7	COMP	152.43	75.17	28	28	69.42	12.31	1599.5	1310	245
Core	G2-D-B-28-28-11	COMP	150.52	75.05	28	28	70.99	11.79	1584.7	1885	105
Cylinder	G1-D-3-1	COMP	197.63	101.30		3	50.60	3.21	3793.9		
Cylinder	G1-D-3-2	COMP	198.58	101.52		3	51.32	3.00	3790.0		
Cylinder	G1-D-3-3	COMP	197.47	101.45		3	49.89	2.88	3796.9		
Cylinder	G1-S-7-1	COMP	197.43	101.74		7	58.94	4.35	3807.3		
Cylinder	G1-S-7-2*	COMP	197.06	101.70		7	60.27	4.23	3750.4		
Cylinder	G1-S-7-3	COMP	196.60	101.75		7	58.95	4.73	3786.8		
Cylinder	G1-S-14-1	COMP	198.11	101.56		14	67.55	5.98	3802.8		
Cylinder	G1-S-14-2	COMP	197.31	101.13		14	69.28	6.00	3772.6		
Cylinder	G1-S-14-3	COMP	195.07	101.55		14	68.22	6.07	3762.5		
Cylinder	G1-S-21-1	COMP	196.23	101.32		21	72.99	7.06	3760.3		

Type	Label (* dictates Outlier)	Use	Avg Length (mm)	Avg Diameter (mm)	Day Cored	Day Tested	Compressive Strength (MPa)	Bulk Resistivity (kΩ·cm)	Mass (g)	X Location (mm)	Y Location (mm)
Cylinder	G1-S-21-2	COMP	193.01	101.41		21	67.28	7.27	3715.8		
Cylinder	G1-S-21-3	COMP	194.90	101.31		21	69.24	7.40	3755.7		
Cylinder	G1-S-28-O	RCP	195.52	101.42		28		7.82	3727.8		
Cylinder	G1-S-28-1	COMP	196.67	101.37		28	71.86	8.89	3785.7		
Cylinder	G1-S-28-2	COMP	196.23	101.52		28	71.73	8.67	3755.9		
Cylinder	G1-S-28-3*	COMP	193.04	101.58		28	77.74	8.54	3704.2		
Cylinder	G1-S-56-1	COMP	195.98	101.27		56	77.95	10.91	3785.5		
Cylinder	G1-S-56-2	COMP	197.43	101.46		56	80.09	10.91	3815.0		
Cylinder	G1-S-56-3	COMP	196.74	101.29		56	80.30	10.69	3794.1		
Core	G1-D-T100-1.5-3-3-1	COMP	150.33	100.73	3	3	61.04	5.24	2827.5	125	1445
Core	G1-D-T100-1.5-3-3-3		151.11	100.73	3	3			2832.7	445	1445
Core	G1-D-T100-1.5-3-3-5	COMP	151.00	100.75	3	3	59.79	5.40	2824.4	765	1450
Core	G1-D-T100-1.5-3-3-8	COMP	151.26	100.75	3	3	61.06	5.19	2839.4	1250	1460
Core	G1-D-T100-1.5-3-3-10		151.61	100.75	3	3			2868.2	1585	1465
Core	G1-S-T100-1.5-3-28-12	AVS	150.24	100.76	3	28			2804.8	295	1285
Core	G1-S-T100-1.5-3-28-14	COMP	151.22	100.70	3	28	77.74	8.74	2854.6	600	1280
Core	G1-S-T100-1.5-3-28-16	COMP	148.99	100.70	3	28	65.38	8.42	2780.7	930	1290
Core	G1-S-T100-1.5-3-28-17	RCP	149.49	100.68	3	28		7.63	2808.4	1100	1275
Core	G1-S-T100-1.5-3-28-19	COMP	151.53	100.77	3	28	69.34	8.71	2837.1	1410	1290
Core	G1-D-B100-1.5-3-3-1	COMP	149.55	100.54	3	3	56.82	5.51	2823.4	125	350
Core	G1-D-B100-1.5-3-3-3		151.19	100.52	3	3			2844.1	445	360
Core	G1-D-B100-1.5-3-3-5	COMP	152.33	100.58	3	3	57.00	6.05	2863.9	775	325
Core	G1-D-B100-1.5-3-3-8	COMP	155.27	100.63	3	3	55.26	5.51	2903.5	1255	330
Core	G1-S-B100-1.5-3-28-10	COMP	156.68	100.76	3	28	68.00	9.12	2952.3	1585	335
Core	G1-S-B100-1.5-3-28-12	AVS	150.55	100.66	3	28			2862.2	300	160
Core	G1-S-B100-1.5-3-28-14	COMP	152.49	100.54	3	28	71.65	9.49	2866.6	615	170
Core	G1-S-B100-1.5-3-28-16*		151.97	100.59	3	28	68.00	9.22	2868.4	940	160

Type	Label (* dictates Outlier)	Use	Avg Length (mm)	Avg Diameter (mm)	Day Cored	Day Tested	Compressive Strength (MPa)	Bulk Resistivity (kΩ·cm)	Mass (g)	X Location (mm)	Y Location (mm)
Core	G1-S-B100-1.5-3-28-17	RCP	152.21	100.63	3	28		8.69	2867.0	1110	175
Core	G1-S-B100-1.5-3-28-19	COMP	153.48	100.82	3	28	68.14		2894.1	1425	180
Core	G1-D-T75-2-3-3-11	COMP	155.10	75.74	3	3	61.01	5.39	1654.3	125	1270
Core	G1-D-T75-2-3-3-13		155.33	75.70	3	3			1628.8	455	1290
Core	G1-D-T75-2-3-3-15	COMP	149.33	75.94	3	3	56.71	5.56	1582.0	775	1280
Core	G1-D-T75-2-3-3-18	COMP	152.12	75.85	3	3	58.37	5.66	1617.6	1250	1285
Core	G1-D-T75-2-3-3-20		152.63	75.81	3	3			1630.9	1590	1280
Core	G1-S-T75-2-3-28-2		155.81	75.85	3	28			1647.2	285	1445
Core	G1-S-T75-2-3-28-4	COMP	152.18	75.89	3	28	67.64	8.89	1624.1	610	1445
Core	G1-S-T75-2-3-28-6	COMP	151.74	75.94	3	28	63.37	8.10	1600.7	935	1455
Core	G1-S-T75-2-3-28-7		150.36	75.90	3	28			1618.1	1095	1465
Core	G1-S-T75-2-3-28-9	COMP	152.07	75.80	3	28	69.77	8.57	1618.2	1425	1475
Core	G1-D-B75-2-3-3-11	COMP	154.14	75.84	3	3	56.87	5.27	1659.2	135	155
Core	G1-D-B75-2-3-3-13		154.00	75.90	3	3			1649.1	460	155
Core	G1-D-B75-2-3-3-15	COMP	150.75	75.85	3	3	54.79	5.81	1612.6	775	155
Core	G1-D-B75-2-3-3-18	COMP	152.00	75.88	3	3	53.03	5.52	1628.8	1270	170
Core	G1-D-B75-2-3-3-20		150.10	75.91	3	3			1613.6	1590	185
Core	G1-S-B75-2-3-28-2		153.04	75.83	3	28			1631.2	295	345
Core	G1-S-B75-2-3-28-4	COMP	150.54	75.89	3	28	67.14	9.05	1611.4	610	335
Core	G1-S-B75-2-3-28-6	COMP	150.99	75.94	3	28	67.05	8.94	1619.3	935	335
Core	G1-S-B75-2-3-28-7		150.62	75.87	3	28			1608.6	1100	345
Core	G1-S-B75-2-3-28-9	COMP	151.60	75.86	3	28	65.73	8.93	1622.8	1420	340
Core	G1-D-T100-1.5-7-7-1	COMP	149.74	100.67	7	7	70.41	6.81	2822.8	135	1455
Core	G1-D-T100-1.5-7-7-3		149.97	100.85	7	7			2813.6	460	1460
Core	G1-D-T100-1.5-7-7-5	COMP	151.59	100.71	7	7	69.02	7.51	2852.5	770	1465
Core	G1-D-T100-1.5-7-7-8	COMP	153.39	100.66	7	7	65.89	6.82	2859.1	1245	1465
Core	G1-D-T100-1.5-7-7-10		151.60	100.63	7	7			2853.3	1585	1460

Type	Label (* dictates Outlier)	Use	Avg Length (mm)	Avg Diameter (mm)	Day Cored	Day Tested	Compressive Strength (MPa)	Bulk Resistivity (kΩ·cm)	Mass (g)	X Location (mm)	Y Location (mm)
Core	G1-S-T100-1.5-7-28-12		149.66	100.66	7	28			2805.3	290	1285
Core	G1-S-T100-1.5-7-28-14	COMP	149.03	100.62	7	28	74.66	9.23	2811.5	610	1290
Core	G1-S-T100-1.5-7-28-16	COMP	150.23	100.69	7	28	63.72	8.97	2809.9	930	1285
Core	G1-S-T100-1.5-7-28-17	RCP	153.01	100.65	7	28		8.28	2862.6	1085	1295
Core	G1-S-T100-1.5-7-28-19	COMP	149.36	100.73	7	28	67.91	9.25	2798.0	1410	1300
Core	G1-D-B100-1.5-7-7-1	COMP	148.98	100.74	7	7	63.58	7.82	2836.8	135	330
Core	G1-D-B100-1.5-7-7-3		148.08	100.73	7	7			2803.2	455	330
Core	G1-D-B100-1.5-7-7-5	COMP	152.20	100.73	7	7	67.16	7.83	2879.2	765	340
Core	G1-D-B100-1.5-7-7-8	COMP	149.86	100.72	7	7	62.99	7.21	2825.3	1240	330
Core	G1-D-B100-1.5-7-7-10		150.12	100.63	7	7			2831.4	1575	335
Core	G1-S-B100-1.5-7-28-12		152.77	100.65	7	28			2898.5	310	155
Core	G1-S-B100-1.5-7-28-14	COMP	149.74	100.77	7	28	72.11	9.44	2840.0	615	160
Core	G1-S-B100-1.5-7-28-16	COMP	149.90	100.73	7	28	74.37	9.55	2854.0	925	155
Core	G1-S-B100-1.5-7-28-17	RCP	152.61	100.73	7	28		8.79	2879.6	1100	1650
Core	G1-S-B100-1.5-7-28-19	COMP	150.19	100.62	7	28	68.33	9.80	2839.5	1415	165
Core	G1-D-T75-2-7-7-11	COMP	150.35	75.87	7	7	62.63	7.08	1602.1	125	1295
Core	G1-D-T75-2-7-7-13		147.96	75.85	7	7			1571.2	455	1290
Core	G1-D-T75-2-7-7-15	COMP	147.42	75.79	7	7	65.06	7.33	1567.9	770	1290
Core	G1-D-T75-2-7-7-18	COMP	150.09	75.83	7	7	66.83	7.02	1593.1	1245	1295
Core	G1-D-T75-2-7-7-20		150.03	75.83	7	7			1598.7	1575	1305
Core	G1-S-T75-2-7-28-2		146.48	75.85	7	28			1547.3	295	1460
Core	G1-S-T75-2-7-28-4	COMP	150.57	75.86	7	28	75.06	8.71	1604.8	610	1455
Core	G1-S-T75-2-7-28-6	COMP	151.03	75.83	7	28	73.96	8.83	1621.3	940	1460
Core	G1-S-T75-2-7-28-7		147.13	75.85	7	28			1570.2	1080	1460
Core	G1-S-T75-2-7-28-9	COMP	147.24	75.89	7	28	69.58	9.03	1562.5	1410	1460
Core	G1-D-B75-2-7-7-11	COMP	153.39	75.74	7	7	65.01	7.20	1645.1	150	140
Core	G1-D-B75-2-7-7-13		150.50	75.80	7	7			1619.1	465	165

Type	Label (* dictates Outlier)	Use	Avg Length (mm)	Avg Diameter (mm)	Day Cored	Day Tested	Compressive Strength (MPa)	Bulk Resistivity (kΩ·cm)	Mass (g)	X Location (mm)	Y Location (mm)
Core	G1-D-B75-2-7-7-15	COMP	146.19	75.55	7	7	65.73	7.77	1560.3	765	160
Core	G1-D-B75-2-7-7-18	COMP	147.47	75.81	7	7	60.65	7.69	1582.9	1240	155
Core	G1-D-B75-2-7-7-20		147.90	75.78	7	7			1585.0	1570	150
Core	G1-S-B75-2-7-28-2		150.18	75.81	7	28			1611.9	300	320
Core	G1-S-B75-2-7-28-4	COMP	147.33	75.75	7	28	69.55	9.17	1583.5	620	335
Core	G1-S-B75-2-7-28-6	COMP	149.81	75.72	7	28	68.45	9.22	1603.3	930	340
Core	G1-S-B75-2-7-28-7		150.26	75.75	7	28			1612.1	1085	340
Core	G1-S-B75-2-7-28-9	COMP	150.35	75.74	7	28	69.08	9.43	1610.5	1405	330
Core	G1-D-T100-1.5-28-28-12		151.36	100.66	28	28			2831.6	300	1295
Core	G1-D-T100-1.5-28-28-14	COMP	151.75	100.85	28	28	73.82	10.83	2845.1	615	1290
Core	G1-D-T100-1.5-28-28-16	COMP	151.61	100.80	28	28	64.67	10.71	2847.9	945	1290
Core	G1-S-T100-1.5-28-56-17	COMP	151.15	100.82	28	56	70.43	10.20	2824.2	1105	1290
Core	G1-D-T100-1.5-28-28-19	COMP	151.10	100.71	28	28	66.78	10.40	2839.3	1420	1290
Core	G1-S-T100-1.5-28-56-1	COMP	150.86	100.72	28	56	75.83	10.82	2854.9	145	1460
Core	G1-S-T100-1.5-28-56-3		152.14	100.86	28	56			2867.5	460	1460
Core	G1-S-T100-1.5-28-56-5	COMP	151.40	100.68	28	56	74.12	10.94	2861.8	780	1465
Core	G1-S-T100-1.5-28-56-8		150.81	100.76	28	56			2843.5	1270	1455
Core	G1-S-T100-1.5-28-56-10		152.60	100.73	28	56			2870.5	1590	1455
Core	G1-D-B100-1.5-28-28-12		151.78	100.66	28	28			2867.8	280	140
Core	G1-D-B100-1.5-28-28-14	COMP	150.90	100.82	28	28	72.90	11.32	2841.4	615	140
Core	G1-D-B100-1.5-28-28-16	COMP	151.85	100.86	28	28	74.76	10.71	2859.4	935	150
Core	G1-S-B100-1.5-28-56-17	COMP	150.90	100.73	28	56	74.66	10.99	2851.4	1085	150
Core	G1-D-B100-1.5-28-28-19	COMP	151.21	100.68	28	28	70.90	10.72	2834.9	1415	145
Core	G1-S-B100-1.5-28-56-1	COMP	151.59	100.65	28	56	75.88	10.97	2872.4	130	320
Core	G1-S-B100-1.5-28-56-3		150.73	100.58	28	56			2832.2	455	330
Core	G1-S-B100-1.5-28-56-5	COMP	150.86	100.82	28	56	73.26	10.50	2838.5	775	320
Core	G1-S-B100-1.5-28-56-8				28	56				1250	300

Type	Label (* dictates Outlier)	Use	Avg Length (mm)	Avg Diameter (mm)	Day Cored	Day Tested	Compressive Strength (MPa)	Bulk Resistivity (kΩ·cm)	Mass (g)	X Location (mm)	Y Location (mm)
Core	G1-S-B100-1.5-28-56-10				28	56				1585	305
Core	G1-D-T75-2-28-28-2		149.97	75.81	28	28			1591.7	930	1455
Core	G1-D-T75-2-28-28-4	COMP	149.02	75.81	28	28	70.40	10.16	1580.3	615	1460
Core	G1-D-T75-2-28-28-6	COMP	151.95	75.82	28	28	71.53	10.49	1621.5	945	1460
Core	G1-S-T75-2-28-56-7	COMP	152.36	75.72	28	56	74.37	9.87	1618.1	1115	1450
Core	G1-D-T75-2-28-28-9	COMP	150.71	75.75	28	28	72.33	10.12	1600.3	1435	1455
Core	G1-S-T75-2-28-56-11	COMP	151.42	75.79	28	56	71.51	10.39	1611.1	140	1290
Core	G1-S-T75-2-28-56-13		152.29	75.73	28	56			1613.5	460	1295
Core	G1-S-T75-2-28-56-15	COMP	151.04	75.98	28	56	72.94	10.06	1606.7	775	1280
Core	G1-S-T75-2-28-56-18		151.59	75.71	28	56			1614.0	1260	1300
Core	G1-S-T75-2-28-56-20		148.33	75.66	28	56			1583.9	1585	1295
Core	G1-D-B75-2-28-28-2		151.85	75.67	28	28			1612.0	285	320
Core	G1-D-B75-2-28-28-4	COMP	151.37	76.12	28	28	71.07	10.47	1619.8	610	310
Core	G1-D-B75-2-28-28-6	COMP	150.74	75.82	28	28	70.62	10.99	1613.5	925	320
Core	G1-S-B75-2-28-56-7	COMP	153.55	75.91	28	56	63.07	10.42	1635.7	1085	310
Core	G1-D-B75-2-28-28-9	COMP	152.65	75.92	28	28	65.94	11.33	1629.6	1415	310
Core	G1-S-B75-2-28-56-11	COMP	150.77	75.96	28	56	71.46	10.61	1625.5	125	155
Core	G1-S-B75-2-28-56-13		150.37	75.85	28	56			1615.2	445	150
Core	G1-S-B75-2-28-56-15	COMP	152.19	75.96	28	56	73.52	10.20	1619.8	785	145
Core	G1-S-B75-2-28-56-18		152.41	75.82	28	56			1623.4	1250	140
Core	G1-S-B75-2-28-56-20				28	56				1575	115
Cylinder	B2-D-3-1	COMP	201.39	102.00		3	42.80	3.76	3887.4		
Cylinder	B2-D-3-2	COMP	200.91	102.67		3	41.11	3.74	3951.5		
Cylinder	B2-D-3-3	COMP	199.54	102.30		3	40.07	3.78	3890.6		
Cylinder	B2-D-3-4	OTHER	199.82	101.66		3					
Cylinder	B2-D-3-5	OTHER	198.94	102.45		3					
Cylinder	B2-S-7-1	COMP	200.33	102.98		7	48.43	6.44	3907.2		

Type	Label (* dictates Outlier)	Use	Avg Length (mm)	Avg Diameter (mm)	Day Cored	Day Tested	Compressive Strength (MPa)	Bulk Resistivity (kΩ·cm)	Mass (g)	X Location (mm)	Y Location (mm)
Cylinder	B2-S-7-2	COMP	197.91	101.82		7	51.78	7.08	3911.1		
Cylinder	B2-S-7-3	COMP	199.11	101.62		7	50.12	6.31	3832.2		
Cylinder	B2-S-7-4	RCP	197.29	101.86		7		27.92			
Cylinder	B2-S-7-5					7					
Cylinder	B2-S-28-1	COMP	200.70	102.44		28	68.52	26.21	3888.8		
Cylinder	B2-S-28-2	COMP	200.09	102.29		28	65.25	27.50	3930.2		
Cylinder	B2-S-28-3	COMP	198.78	102.47		28	69.65	26.83	3889.9		
Cylinder	B2-S-28-4					28					
Cylinder	B2-S-28-5					28					
Cylinder	B2-S-56-1	COMP	198.94	101.81		56	71.48	38.22	3900.8		
Cylinder	B2-S-56-2	COMP	200.61	101.96		56	69.26	38.01	3852.0		
Cylinder	B2-S-56-3	COMP	200.18	102.07		56	73.17	37.83	3882.7		
Cylinder	B2-S-56-4					56					
Cylinder	B2-S-56-5					56					
Cylinder	B2-M-7-1	COMP	200.12	102.63		7	50.41	6.75	3920.3		
Cylinder	B2-M-7-2	COMP	199.57	102.16		7	51.62	6.62	3934.9		
Cylinder	B2-M-7-3	COMP	198.86	102.06		7	51.42	6.48	3910.8		
Cylinder	B2-M-28-1	COMP	196.34	101.91		28	68.11	29.09	3801.9		
Cylinder	B2-M-28-2	COMP	199.41	102.96		28	67.54	30.34	3889.6		
Cylinder	B2-M-28-3	COMP	201.07	102.46		28	68.71	30.46	3945.3		
Cylinder	B2-M-56-1	COMP	199.85	102.54		56	68.64	40.50	3905.4		
Cylinder	B2-M-56-2	COMP	201.62	102.46		56	73.96	38.88	3979.7		
Cylinder	B2-M-56-3	COMP	199.40	102.09		56	72.41	40.23	3872.0		
Core	B2-D-V-3-3-L8	COMP	200.91	100.59	3	3	54.42	26.18	3732.6		
Core	B2-D-V-3-3-R7	COMP	201.88	100.69	3	3	45.96	30.58	3775.3		
Core	B2-D-V-3-3-L1	COMP	199.22	100.68	3	3	56.40	21.24	3727.2		
Core	B2-D-V-3-3-R1	RCP	200.38	100.52	3	3		43.95			

Type	Label (* dictates Outlier)	Use	Avg Length (mm)	Avg Diameter (mm)	Day Cored	Day Tested	Compressive Strength (MPa)	Bulk Resistivity (kΩ·cm)	Mass (g)	X Location (mm)	Y Location (mm)
Core	B2-D-V-3-3-L2	OTHER	199.96	100.65	3	3					
Core	B2-D-H-3-3-L2	COMP	199.51	100.71	3	3	55.41	37.12	3777.9		
Core	B2-D-H-3-3-L7	COMP	199.96	100.60	3	3	57.21	39.12	3781.7		
Core	B2-D-H-3-3-L5	COMP	198.04	100.61	3	3	55.63	43.38	3726.9		
Core	B2-D-H-3-3-L5	OTHER	197.98	100.76	3	3					
Core	B2-D-H-3-3-L3	RCP	198.77	100.24	3	3		51.04			
Core	B2-D-V-3-28-R6				3	28					
Core	B2-D-V-3-28-L7*	OTHER	202.37	100.76	3	28	43.45	43.90	3796.2		
Core	B2-D-V-3-28-R2		199.89	100.75	3	28	65.06	46.27	3741.8		
Core	B2-D-V-3-28-L5	OTHER			3	28					
Core	B2-D-V-3-28-R5		197.79	100.60	3	28	63.94	44.27	3677.0		
Core	B2-D-H-3-28-L1	OTHER			3	28					
Core	B2-D-H-3-28-L4	COMP	200.69	100.60	3	28	64.39	50.59	3795.9		
Core	B2-D-H-3-28-L8	COMP	198.66	100.70	3	28	63.79	56.92	3690.7		
Core	B2-D-H-3-28-L6	COMP	200.47	100.79	3	28	63.31	51.00	3776.8		
Core	B2-D-H-3-28-L6	OTHER			3	28					
Core	B2-S-V-3-28-L6	COMP	200.36	100.61	3	28	62.86	35.40	3776.3		
Core	B2-S-V-3-28-R8	COMP	201.72	100.69	3	28	58.02	37.20	3735.4		
Core	B2-S-V-3-28-R4	RCP	198.36	100.59	3	28		39.26			
Core	B2-S-V-3-28-R3				3	28					
Core	B2-S-V-3-28-L3	COMP	198.73	100.57	3	28	63.45	36.16	3725.9		
Core	B2-S-H-3-28-L3	COMP	199.29	100.82	3	28	61.94	38.75	3761.6		
Core	B2-S-H-3-28-L8	COMP	199.72	100.84	3	28	64.87	38.85	3769.2		
Core	B2-S-H-3-28-L7	RCP	201.79	100.39	3	28		41.89			
Core	B2-S-H-3-28-L2	COMP	199.37	100.72	3	28	62.79	39.33	3756.8		
Core	B2-S-H-3-28-L4				3	28					
Core	B2-D-V-7-7-L8	COMP	198.83	100.80	7	7	58.72	31.63	3718.2		

Type	Label (* dictates Outlier)	Use	Avg Length (mm)	Avg Diameter (mm)	Day Cored	Day Tested	Compressive Strength (MPa)	Bulk Resistivity (kΩ·cm)	Mass (g)	X Location (mm)	Y Location (mm)
Core	B2-D-V-7-7-L7	COMP	199.57	100.78	7	7	57.22	31.59	3773.9		
Core	B2-D-V-7-7-R5	COMP	198.40	100.87	7	7	56.11	32.67	3737.8		
Core	B2-D-V-7-7-L1				7	7					
Core	B2-D-V-7-7-R3	RCP	199.14	100.55	7	7		50.77			
Core	B2-D-H-7-7-L5	COMP	198.26	100.47	7	7	61.22	41.70	3697.7		
Core	B2-D-H-7-7-L7	COMP	198.89	100.46	7	7	59.70	37.72	3706.7		
Core	B2-D-H-7-7-L1	COMP	199.64	100.75	7	7	61.00	24.08	3822.2		
Core	B2-D-H-7-7-L3	OTHER			7	7					
Core	B2-D-H-7-7-L6	RCP	199.94	100.83	7	7		50.01			
Core	B2-D-V-7-28-R7	COMP	201.39	100.88	7	28	64.62	48.03	3769.4		
Core	B2-D-V-7-28-R6	OTHER			7	28					
Core	B2-D-V-7-28-R4	COMP	199.71	100.81	7	28	61.59	48.21	3750.1		
Core	B2-D-V-7-28-R2				7	28					
Core	B2-D-V-7-28-L2	COMP	199.96	100.56	7	28	62.47	44.92	3758.1		
Core	B2-S-V-7-28-R8	COMP	198.21	100.83	7	28	62.21	36.10	3697.5		
Core	B2-S-V-7-28-L6	COMP	195.69	100.81	7	28	61.83	38.95	3700.0		
Core	B2-S-V-7-28-L4				7	28					
Core	B2-S-V-7-28-L5	COMP	198.47	100.73	7	28	59.84	37.67	3764.2		
Core	B2-S-V-7-28-L3	RCP	199.01	100.59	7	28		37.13			
Core	B2-D-H-7-28-L8	OTHER			7	28					
Core	B2-D-H-7-28-L4	COMP	198.29	100.50	7	28	64.37	53.95	3705.8		
Core	B2-D-H-7-28-L2	COMP	199.13	100.46	7	28	64.64	48.51	3762.9		
Core	B2-D-H-7-28-L4	COMP	199.56	100.76	7	28	62.04	45.02	3765.6		
Core	B2-D-H-7-28-L5				7	28					
Core	B2-S-H-7-28-L6	RCP	200.86	100.51	7	28		40.36			
Core	B2-S-H-7-28-L3	COMP	202.53	100.46	7	28	61.87	40.65	3814.3		
Core	B2-S-H-7-28-L2	COMP	198.46	100.82	7	28	60.97	37.07	3769.5		

Type	Label (* dictates Outlier)	Use	Avg Length (mm)	Avg Diameter (mm)	Day Cored	Day Tested	Compressive Strength (MPa)	Bulk Resistivity (kΩ·cm)	Mass (g)	X Location (mm)	Y Location (mm)
Core	B2-S-H-7-28-L8	COMP	198.56	100.78	7	28	62.51	37.86	3741.4		
Core	B2-S-H-7-28-L7				7	28					
Core	B2-D-V-14-28-R8	COMP	198.60	100.72	14	28	63.71	45.37	3706.7		
Core	B2-D-V-14-28-R6	COMP	201.30	100.13	14	28	57.85	46.53	3709.3		
Core	B2-D-V-14-28-L5	RCP	202.07	100.46	14	28		42.22			
Core	B2-D-V-14-28-L1	COMP	199.29	100.76	14	28	64.31	38.21	3786.5		
Core	B2-D-V-14-28-R3	OTHER			14	28					
Core	B2-D-H-14-28-R8				14	28					
Core	B2-D-H-14-28-R5	COMP	199.75	100.80	14	28	61.30	49.36	3740.5		
Core	B2-D-H-14-28-R1	COMP	195.03	100.84	14	28	66.97	37.05	3747.1		
Core	B2-D-H-14-28-R4	COMP	200.64	98.95	14	28	62.40	48.96	3683.4		
Core	B2-D-H-14-28-R6	RCP	198.01	100.80	14	28		48.61			
Core	B2-S-V-14-28-L7	COMP	199.00	100.52	14	28	62.50	38.24	3771.2		
Core	B2-S-V-14-28-R5	COMP	198.58	100.70	14	28	61.02	37.96	3716.9		
Core	B2-S-V-14-28-L4	AVS			14	28					
Core	B2-S-V-14-28-R4	COMP	200.27	100.50	14	28	62.80	37.82	3749.2		
Core	B2-S-V-14-28-L2	RCP	200.57	100.87	14	28		37.21			
Core	B2-S-H-14-28-R7	COMP	200.46	100.76	14	28	61.72	42.65	3752.7		
Core	B2-S-H-14-28-R4	COMP	201.00	100.82	14	28	59.49	42.59	3771.2		
Core	B2-S-H-14-28-R1	RCP	198.93	100.83	14	28		40.34			
Core	B2-S-H-14-28-R8				14	28					
Core	B2-S-H-14-28-R5	COMP	199.34	100.78	14	28	59.69	43.74	3754.9		
Core	B2-D-V-28-28-R6	COMP	200.95	100.49	28	28	59.66	44.63	3735.2		
Core	B2-D-V-28-28-R5	COMP	201.51	100.48	28	28	56.45	41.86	3737.8		
Core	B2-D-V-28-28-R2	COMP	202.10	100.57	28	28	60.76	42.64	3785.9		
Core	B2-D-V-28-28-L1				28	28					
Core	B2-D-V-28-28-L4	OTHER			28	28					

Type	Label (* dictates Outlier)	Use	Avg Length (mm)	Avg Diameter (mm)	Day Cored	Day Tested	Compressive Strength (MPa)	Bulk Resistivity (kΩ·cm)	Mass (g)	X Location (mm)	Y Location (mm)
Core	B2-D-H-28-28-R7	COMP	201.19	100.79	28	28	64.76	47.34	3788.0		
Core	B2-D-H-28-28-R1	COMP	201.42	101.01	28	28	67.06	43.32	3800.6		
Core	B2-D-H-28-28-R1	COMP	199.14	100.85	28	28	62.57	47.54	3726.8		
Core	B2-D-H-28-28-R4				28	28					
Core	B2-D-H-28-28-R7				28	28					
Core	B2-D-V-28-56-R1	COMP	199.85	100.49	28	56	68.12	52.85	3740.0		
Core	B2-D-V-28-56-R3				28	56					
Core	B2-D-V-28-56-L5	COMP	199.37	100.50	28	56	65.09	49.33	3714.7		
Core	B2-D-V-28-56-L8	COMP	201.38	100.81	28	56	70.75	51.62	3757.4		
Core	B2-D-V-28-56-R7				28	56					
Core	B2-S-V-28-56-L2	COMP	199.45	100.94	28	56	68.55	38.31	3785.3		
Core	B2-S-V-28-56-L3				28	56					
Core	B2-S-V-28-56-R4	COMP	201.38	100.38	28	56	64.88	39.83	3772.6		
Core	B2-S-V-28-56-R8	COMP	201.06	100.76	28	56	60.40	41.85	3761.8		
Core	B2-S-V-28-56-L7				28	56					
Core	B2-D-H-28-56-R3	COMP	201.20	100.76	28	56	64.90	56.11	3778.3		
Core	B2-D-H-28-56-R5				28	56					
Core	B2-D-H-28-56-R8	COMP	202.55	100.69	28	56	63.07	61.25	3752.1		
Core	B2-D-H-28-56-R6	COMP	200.27	100.53	28	56	66.10	55.94	3738.8		
Core	B2-D-H-28-56-R4				28	56					
Core	B2-S-H-28-56-R2	COMP	200.52	100.80	28	56	65.95	40.67	3795.3		
Core	B2-S-H-28-56-R6				28	56					
Core	B2-S-H-28-56-R8	COMP	202.08	100.87	28	56	65.77	42.07	3811.1		
Core	B2-S-H-28-56-R5	COMP	199.46	100.43	28	56	62.78	41.42	3742.3		
Core	B2-S-H-28-56-R3	AVS			28	56					
Cylinder	B1-D-3-1	COMP	199.39	102.10		3	23.04	3.47			
Cylinder	B1-D-3-2	COMP	198.51	102.26		3	25.26	3.85			

Type	Label (* dictates Outlier)	Use	Avg Length (mm)	Avg Diameter (mm)	Day Cored	Day Tested	Compressive Strength (MPa)	Bulk Resistivity (kΩ·cm)	Mass (g)	X Location (mm)	Y Location (mm)
Cylinder	B1-D-3-3	COMP	201.78	102.08		3	24.88	3.45			
Cylinder	B1-D-3-4					3					
Cylinder	B1-D-3-5					3					
Cylinder	B1-S-7-1	COMP	201.95	102.81		7	28.11	4.44	3990.9		
Cylinder	B1-S-7-2	COMP	199.91	102.40		7	28.70	4.31	3927.6		
Cylinder	B1-S-7-3	COMP	198.90	102.65		7	30.30	4.57	3939.7		
Cylinder	B1-S-7-4					7					
Cylinder	B1-S-7-5					7					
Cylinder	B1-S-28-1	COMP	200.18	102.08		28	38.78	7.62	3922.5		
Cylinder	B1-S-28-2	COMP	201.94	102.84		28	42.41	8.41	4013.7		
Cylinder	B1-S-28-3	COMP	202.62	102.24		28	37.87	7.38	3937.4		
Cylinder	B1-S-28-4					28					
Cylinder	B1-S-28-5					28					
Cylinder	B1-S-56-1	COMP	201.77	101.61		56	44.84	8.67	3966.9		
Cylinder	B1-S-56-2	COMP	201.42	101.87		56	45.82	8.54	3906.8		
Cylinder	B1-S-56-3	COMP	198.15	102.02		56	46.92	8.54	3897.1		
Cylinder	B1-S-56-4					56					
Cylinder	B1-S-56-5					56					
Cylinder	B1-M-7-1	COMP	200.06	102.23		7	30.00	4.66	3931.1		
Cylinder	B1-M-7-2	COMP	202.62	101.95		7	27.25	4.57	3914.3		
Cylinder	B1-M-7-3	COMP	201.26	102.71		7	28.37	4.55	3930.8		
Cylinder	B1-M-28-1	COMP	197.93	101.58		28	39.90	7.06	3848.7		
Cylinder	B1-M-28-2	COMP	198.15	102.33		28	41.22	7.25	3912.9		
Cylinder	B1-M-28-3	COMP	197.07	102.37		28	40.60	7.15	3878.6		
Cylinder	B1-M-56-1	COMP	197.34	101.63		56	51.79	9.35	3874.4		
Cylinder	B1-M-56-2	COMP	198.58	101.48		56	44.91	9.36	3892.7		
Cylinder	B1-M-56-3	COMP	198.46	101.73		56	47.80	10.67	3913.4		

Type	Label (* dictates Outlier)	Use	Avg Length (mm)	Avg Diameter (mm)	Day Cored	Day Tested	Compressive Strength (MPa)	Bulk Resistivity (kΩ·cm)	Mass (g)	X Location (mm)	Y Location (mm)
Core	B1-D-V-3-3-1	COMP	202.69	100.70	3	3	25.69	3.93			
Core	B1-D-V-3-3-2	COMP	201.80	100.63	3	3	25.67	3.85			
Core	B1-D-V-3-3-3	COMP	205.21	100.57	3	3	19.15	4.10			
Core	B1-D-V-3-3-4	Density			3	3					
Core	B1-D-V-3-3-5	RCP			3	3					
Core	B1-D-H-3-3-1	COMP	203.27	100.65	3	3	29.81	4.26			
Core	B1-D-H-3-3-2	COMP	202.73	100.54	3	3	28.77	4.30			
Core	B1-D-H-3-3-3	COMP	204.51	100.32	3	3	25.21	4.08			
Core	B1-D-H-3-3-4	AVS			3	3					
Core	B1-D-H-3-3-5	RCP			3	3					
Core	B1-D-V-3-28-1	COMP	198.00	100.71	3	28	42.75	8.49	3755.9		
Core	B1-D-V-3-28-2	COMP	199.98	100.71	3	28	42.29	8.59	3777.4		
Core	B1-D-V-3-28-3	COMP	200.33	100.63	3	28	42.39	8.46	3800.3		
Core	B1-D-V-3-28-4				3	28					
Core	B1-D-V-3-28-5				3	28					
Core	B1-D-H-3-28-1	COMP	202.08	100.49	3	28	43.13	9.19	3810.1		
Core	B1-D-H-3-28-2*	COMP	203.49	100.67	3	28	39.57	8.96	3851.8		
Core	B1-D-H-3-28-3	COMP	201.35	100.56	3	28	44.89	8.56	3794.0		
Core	B1-D-H-3-28-4				3	28					
Core	B1-D-H-3-28-5				3	28					
Core	B1-S-V-3-28-1	COMP	199.61	100.74	3	28	41.66	7.42	3824.7		
Core	B1-S-V-3-28-2	COMP	201.59	100.62	3	28	41.66	7.35	3865.9		
Core	B1-S-V-3-28-3*	COMP	199.22	100.68	3	28	44.34	6.98	3807.3		
Core	B1-S-V-3-28-4				3	28					
Core	B1-S-V-3-28-5	RCP			3	28					
Core	B1-S-H-3-28-1	COMP	202.00	100.61	3	28	41.64	7.53	3836.6		
Core	B1-S-H-3-28-2	COMP	199.85	100.58	3	28	44.88	7.13	3812.2		

Type	Label (* dictates Outlier)	Use	Avg Length (mm)	Avg Diameter (mm)	Day Cored	Day Tested	Compressive Strength (MPa)	Bulk Resistivity (kΩ·cm)	Mass (g)	X Location (mm)	Y Location (mm)
Core	B1-S-H-3-28-3	COMP	199.77	100.52	3	28	42.17	7.24	3789.9		
Core	B1-S-H-3-28-4	AVS			3	28					
Core	B1-S-H-3-28-5	RCP			3	28					
Core	B1-D-V-7-7-1	COMP	201.93	100.75	7	7	32.98	5.27	3823.1		
Core	B1-D-V-7-7-2	COMP	204.18	100.76	7	7	31.92	5.17	3874.7		
Core	B1-D-V-7-7-3	COMP	200.77	100.80	7	7	31.65	5.14	3818.2		
Core	B1-D-V-7-7-4	AVS			7	7					
Core	B1-D-V-7-7-5	RCP			7	7					
Core	B1-D-H-7-7-1	COMP	199.20	100.67	7	7	33.61	5.89	3743.5		
Core	B1-D-H-7-7-2	COMP	201.06	100.54	7	7	34.57	5.71	3784.2		
Core	B1-D-H-7-7-3	COMP	202.78	100.77	7	7	34.07	5.95	3805.6		
Core	B1-D-H-7-7-4	Density			7	7					
Core	B1-D-H-7-7-5	RCP			7	7					
Core	B1-D-V-7-28-1	COMP	201.96	100.67	7	28	44.52	9.97	3831.7		
Core	B1-D-V-7-28-2	COMP	200.37	100.69	7	28	41.51	9.05	3785.8		
Core	B1-D-V-7-28-3	COMP	202.83	100.71	7	28	42.04	8.77	3843.3		
Core	B1-D-V-7-28-4				7	28					
Core	B1-D-V-7-28-5				7	28					
Core	B1-S-V-7-28-1	COMP	201.05	100.72	7	28	39.40	7.10	3854.1		
Core	B1-S-V-7-28-2	COMP	200.93	100.61	7	28	41.44	6.86	3825.9		
Core	B1-S-V-7-28-3	COMP	201.00	100.69	7	28	40.51	7.02	3842.1		
Core	B1-S-V-7-28-4	AVS			7	28					
Core	B1-S-V-7-28-5	RCP			7	28					
Core	B1-D-H-7-28-1	COMP	200.81	100.48	7	28	42.76	9.54	3774.2		
Core	B1-D-H-7-28-2	COMP	201.29	100.34	7	28	45.79	9.53	3757.8		
Core	B1-D-H-7-28-3				7	28					
Core	B1-D-H-7-28-4	COMP	200.97	100.54	7	28	44.72	9.02	3793.5		

Type	Label (* dictates Outlier)	Use	Avg Length (mm)	Avg Diameter (mm)	Day Cored	Day Tested	Compressive Strength (MPa)	Bulk Resistivity (kΩ·cm)	Mass (g)	X Location (mm)	Y Location (mm)
Core	B1-D-H-7-28-5	Density			7	28					
Core	B1-S-H-7-28-1	COMP	199.73	100.62	7	28	41.85	7.62	3736.1		
Core	B1-S-H-7-28-2	COMP	200.91	100.74	7	28	43.15	7.51	3790.7		
Core	B1-S-H-7-28-3	COMP	198.12	100.47	7	28	39.26	7.57	3736.1		
Core	B1-S-H-7-28-4				7	28					
Core	B1-S-H-7-28-5	RCP			7	28					
Core	B1-D-V-14-28-1	COMP	200.31	100.61	14	28	40.00	9.92	3741.0		
Core	B1-D-V-14-28-2	COMP	200.29	101.00	14	28	42.12	9.30	3757.5		
Core	B1-D-V-14-28-3	COMP	201.04	100.87	14	28	41.32	8.39	3789.7		
Core	B1-D-V-14-28-4	Density			14	28					
Core	B1-D-V-14-28-5	RCP			14	28					
Core	B1-D-H-14-28-1	COMP	199.26	100.70	14	28	46.34	9.11	3763.0		
Core	B1-D-H-14-28-2	COMP	200.74	100.80	14	28	45.59	9.24	3810.8		
Core	B1-D-H-14-28-3	COMP	200.18	100.89	14	28	44.03	9.13	3785.5		
Core	B1-D-H-14-28-4				14	28					
Core	B1-D-H-14-28-5	RCP			14	28					
Core	B1-S-V-14-28-1	COMP	201.11	100.63	14	28	39.37	7.82	3805.5		
Core	B1-S-V-14-28-2	COMP	200.27	100.55	14	28	41.14	7.62	3806.8		
Core	B1-S-V-14-28-3	COMP	200.52	100.47	14	28	39.20	7.77	3797.9		
Core	B1-S-V-14-28-4	AVS			14	28					
Core	B1-S-V-14-28-5	RCP			14	28					
Core	B1-S-H-14-28-1	COMP	200.83	100.72	14	28	40.28	7.48	3812.9		
Core	B1-S-H-14-28-2	COMP	199.98	100.52	14	28	41.43	7.30	3788.5		
Core	B1-S-H-14-28-3	COMP	200.59	100.68	14	28	41.80	7.55	3782.3		
Core	B1-S-H-14-28-4				14	28					
Core	B1-S-H-14-28-5	RCP			14	28					
Core	B1-D-V-28-28-R7	COMP	201.74	100.55	28	28	43.15	8.32	3801.4		

Type	Label (* dictates Outlier)	Use	Avg Length (mm)	Avg Diameter (mm)	Day Cored	Day Tested	Compressive Strength (MPa)	Bulk Resistivity (kΩ·cm)	Mass (g)	X Location (mm)	Y Location (mm)
Core	B1-D-V-28-28-R6*	COMP	200.52	100.60	28	28	34.19	8.47	3780.3		
Core	B1-D-V-28-28-L7	COMP	202.19	100.65	28	28	41.10	8.68	3807.7		
Core	B1-D-V-28-28-L6	Density			28	28					
Core	B1-D-V-28-28-				28	28					
Core	B1-D-H-28-28-L5	COMP	203.06	100.67	28	28	45.48	8.59	3867.9		
Core	B1-D-H-28-28-L7	COMP	203.38	100.68	28	28	43.66	8.48	3864.9		
Core	B1-D-H-28-28-L4	COMP	203.00	100.70	28	28	44.56	8.17	3841.3		
Core	B1-D-H-28-28-				28	28					
Core	B1-D-H-28-28-				28	28					
Core	B1-D-V-28-56-R3	COMP	201.33	100.70	28	56	44.12	11.38	3789.5		
Core	B1-D-V-28-56-L3	COMP	201.86	100.68	28	56	44.87	11.88	3784.6		
Core	B1-D-V-28-56-L2				28	56			3781.3		
Core	B1-D-V-28-56-L4	COMP	202.24	100.64	28	56	40.87	11.70	3779.1		
Core	B1-D-V-28-56-L5				28	56			3764.1		
Core	B1-S-V-28-56-R5	OTHER	202.49	100.57	28	56	35.61	9.46			
Core	B1-S-V-28-56-R1	COMP	200.48	100.64	28	56	42.19	9.34	3799.9		
Core	B1-S-V-28-56-R5	COMP	202.49	100.57	28	56	35.61	9.46	3801.8		
Core	B1-S-V-28-56-R2	COMP	201.59	100.56	28	56	41.94	9.37	3801.3		
Core	B1-S-V-28-56-				28	56					
Core	B1-D-H-28-56-L1	COMP	201.37	100.80	28	56	53.22	12.98	3806.1		
Core	B1-D-H-28-56-L1				28	56			3810.5		
Core	B1-D-H-28-56-L4				28	56			3806.2		
Core	B1-D-H-28-56-L2	COMP	200.34	100.80	28	56	51.26	12.48	3779.3		
Core	B1-D-H-28-56-L5	COMP	201.65	100.77	28	56	50.75	12.67	3798.1		
Core	B1-S-H-28-56-L2	OTHER			28	56					
Core	B1-S-H-28-56-L3	COMP	201.36	100.84	28	56	47.07	9.47	3828.0		
Core	B1-S-H-28-56-L8	COMP	199.88	100.80	28	56	51.14	9.25	3790.6		

Type	Label (* dictates Outlier)	Use	Avg Length (mm)	Avg Diameter (mm)	Day Cored	Day Tested	Compressive Strength (MPa)	Bulk Resistivity (kΩ·cm)	Mass (g)	X Location (mm)	Y Location (mm)
Core	B1-S-H-28-56-L6	COMP	201.02	100.76	28	56	50.04	9.44	3819.3		
Core	B1-S-H-28-56-L7	AVS			28	56					
Cylinder	G3-D-1-1	COMP	200.00	100.00		1	45.60				
Cylinder	G3-D-1-2	COMP	200.00	100.00		1	49.40				
Cylinder	G3-D-1-3	COMP	200.00	100.00		1	48.60				
Cylinder	G3-D-3-1	COMP	200.00	100.00		3	56.50				
Cylinder	G3-D-3-2	COMP	200.00	100.00		3	57.20				
Cylinder	G3-D-3-3	COMP	200.00	100.00		3	57.70				
Cylinder	G3-S-7-1	COMP	200.00	100.00		7	63.20				
Cylinder	G3-S-7-2	COMP	200.00	100.00		7	66.00				
Cylinder	G3-S-7-3	COMP	200.00	100.00		7	67.80				
Cylinder	G3-S-28-1	COMP	201.27	102.53		28	72.30		3950.0		
Cylinder	G3-S-28-2	COMP	200.85	102.16		28	85.06		3900.0		
Cylinder	G3-S-28-3	COMP	201.76	102.24		28	84.46		3900.0		
Cylinder	G3-S-52-1	COMP	196.03	102.24		52			3800.0		
Cylinder	G3-S-52-2	COMP	201.39	102.84		52			3950.0		
Cylinder	G3-S-52-3	COMP	199.77	102.09		52			3850.0		
Core	G3-D-TF-3-3-1	COMP	198.00	93.00	3	3	45.39				1900
Core	G3-D-TF-3-3-2	COMP	200.00	93.00	3	3	42.50				1900
Core	G3-D-TF-3-3-3	COMP	196.00	93.00	3	3	53.12				1900
Core	G3-D-M-3-3-1	COMP	140.00	93.00	3	3	49.96				1100
Core	G3-D-M-3-3-2	COMP	140.00	93.00	3	3	55.12				1100
Core	G3-D-M-3-3-3	COMP	140.00	93.00	3	3	52.80				1100
Core	G3-D-BF-3-3-1	COMP	195.00	93.00	3	3	25.52				135
Core	G3-D-BF-3-3-2	COMP	198.00	93.00	3	3	25.48				135
Core	G3-D-BF-3-3-3	COMP	196.00	93.00	3	3	35.60				135
Core	G3-M-TF-3-7-4	COMP	207.27	93.63	3	7	49.48		3250.0		1900

Appendix D - Raw Data

Type	Label (* dictates Outlier)	Use	Avg Length (mm)	Avg Diameter (mm)	Day Cored	Day Tested	Compressive Strength (MPa)	Bulk Resistivity (kΩ·cm)	Mass (g)	X Location (mm)	Y Location (mm)
Core	G3-M-TF-3-7-5	COMP	206.14	94.31	3	7	50.89		3250.0		1900
Core	G3-M-TF-3-7-6	COMP	206.45	93.57	3	7	56.96		3300.0		1900
Core	G3-M-BF-3-7-8	COMP	203.09	93.81	3	7	44.88		3350.0		135
Core	G3-M-BF-3-7-9	COMP	208.82	93.50	3	7	52.23		3400.0		135
Core	G3-M-BF-3-7-10	COMP	213.63	93.66	3	7	50.51		3450.0		135
Core	G3-M-TF-3-28-8	COMP	156.43	93.50	3	28	60.89		2450.0		1900
Core	G3-M-TF-3-28-9*	COMP	150.74	93.78	3	28	37.48		2350.0		1900
Core	G3-M-TF-3-28-11	COMP	187.01	93.86	3	28	46.77		2950.0		1900
Core	G3-M-TF-3-28-7	RCP			3	28					1900
Core	G3-M-TF-3-28-10	AVS			3	28					1900
Core	G3-M-M-3-28-4	COMP	145.72	94.16	3	28	70.57		2350.0		1100
Core	G3-M-M-3-28-5	COMP	143.05	93.73	3	28	63.15		2350.0		1100
Core	G3-M-M-3-28-6	COMP	144.38	93.66	3	28	59.15		2300.0		1100
Core	G3-M-BF-3-28-4	COMP	189.40	93.86	3	28	69.47		3000.0		135
Core	G3-M-BF-3-28-5	COMP	188.55	93.76	3	28	69.39		3050.0		135
Core	G3-M-BF-3-28-11*	COMP	189.03	93.74	3	28	65.75		3050.0		135
Core	G3-M-BF-3-28-7	RCP			3	28					135
Core	G3-M-BF-3-28-6	AVS			3	28					135
Core	G3-D-TF-28-28-1	COMP	170.00	94.10	28	28	70.53		2715.0		1900
Core	G3-D-TF-28-28-2	COMP	155.00	94.10	28	28	61.95		2450.0		1900
Core	G3-D-TF-28-28-3	COMP	156.00	94.10	28	28	68.20		2472.0		1900
Core	G3-D-T-28-28-1	COMP	144.00	94.10	28	28	82.62		2417.0		1600
Core	G3-D-T-28-28-2	COMP	144.00	94.10	28	28	81.03		2392.0		1600
Core	G3-D-T-28-28-3	COMP	144.00	94.10	28	28	83.21		2371.0		1600
Core	G3-D-T-28-28-4	COMP	142.00	94.10	28	28	85.57		2385.0		1600
Core	G3-D-T-28-28-5	COMP	143.00	94.10	28	28	78.84		2387.0		1600
Core	G3-D-T-28-28-6	COMP	147.00	94.10	28	28	85.27		2465.0		1600

Type	Label (* dictates Outlier)	Use	Avg Length (mm)	Avg Diameter (mm)	Day Cored	Day Tested	Compressive Strength (MPa)	Bulk Resistivity (kΩ·cm)	Mass (g)	X Location (mm)	Y Location (mm)
Core	G3-D-M-28-28-1	COMP	144.00	94.10	28	28	72.16		2372.0		1100
Core	G3-D-M-28-28-2	COMP	147.00	94.10	28	28	69.86		2453.0		1100
Core	G3-D-M-28-28-3	COMP	147.00	94.10	28	28	80.38		2453.0		1100
Core	G3-D-M-28-28-4	COMP	147.00	94.10	28	28	65.86		2454.0		1100
Core	G3-D-M-28-28-5	COMP	147.00	94.10	28	28	78.45		2450.0		1100
Core	G3-D-M-28-28-6	COMP	144.00	94.10	28	28	74.93		2421.0		1100
Core	G3-D-B-28-28-1	COMP	143.00	94.10	28	28	75.94		2383.0		600
Core	G3-D-B-28-28-2	COMP	144.00	94.10	28	28	66.25		2370.0		600
Core	G3-D-B-28-28-3	COMP	147.00	94.10	28	28	78.23		2453.0		600
Core	G3-D-B-28-28-4	COMP	144.00	94.10	28	28	80.99		2404.0		600
Core	G3-D-B-28-28-5	COMP	144.00	94.10	28	28	85.19		2456.0		600
Core	G3-D-B-28-28-6	COMP	144.00	94.10	28	28	80.60		2456.0		600
Core	G3-D-BF-28-28-1	COMP	186.00	94.10	28	28	70.67		3025.0		135
Core	G3-D-BF-28-28-2	COMP	199.00	94.10	28	28	70.94		3222.0		135
Core	G3-D-BF-28-28-3	COMP	194.00	94.10	28	28	76.29		3160.0		135
Cylinder	VC-D-3-1	COMP	190.67	101.78		3	46.29	4.95	3603.8		
Cylinder	VC-D-3-2	COMP	190.25	101.52		3	45.46	4.60	3552.7		
Cylinder	VC-D-3-3	COMP	190.32	101.60		3	45.72	4.87	3591.8		
Cylinder	VC-S-7-4	COMP	197.70	101.46		7	50.54	5.72	3737.4		
Cylinder	VC-S-7-8	COMP	197.96	101.59		7	50.70	5.69	3741.3		
Cylinder	VC-S-7-12	COMP	200.20	101.82		7	46.40	5.62	3803.8		
Cylinder	VC-S-14-9	COMP	198.90	101.50		14	56.31	6.49	3795.3		
Cylinder	VC-S-14-5	COMP	198.09	101.45		14	57.07	6.79	3785.6		
Cylinder	VC-S-14-13	COMP	198.46	101.41		14	55.49	6.60	3756.1		
Cylinder	VC-S-21-11	COMP	197.20	101.60		21	50.86	7.09	3746.1		
Cylinder	VC-S-21-14	COMP	197.99	101.48		21	62.33	7.46	3780.1		
Cylinder	VC-S-21-15	COMP	194.98	101.59		21	59.22	7.38	3742.0		

Type	Label (* dictates Outlier)	Use	Avg Length (mm)	Avg Diameter (mm)	Day Cored	Day Tested	Compressive Strength (MPa)	Bulk Resistivity (kΩ·cm)	Mass (g)	X Location (mm)	Y Location (mm)
Cylinder	VC-S-28-7	COMP	193.67	101.63		28	47.32	8.82	3723.0		
Cylinder	VC-S-28-10	COMP	198.82	101.56		28	60.67	8.21	3761.4		
Cylinder	VC-S-28-6	COMP	198.07	101.60		28	62.41	8.43	3801.2		
Cylinder	VC-S-O-16	RCP	198.55	101.44		O			3745.8		
Core	VC-D-3-3-1	COMP	184.90	93.77	3	3	41.42		2981.4	830	1355
Core	VC-D-3-3-3	COMP	184.54	93.78	3	3	40.81		2973.0	605	1000
Core	VC-D-3-3-5	COMP	183.98	93.74	3	3	41.90		2953.8	1090	1000
Core	VC-S-3-28-2	COMP	185.35	93.85	3	28	58.77	8.54	3003.3	840	1210
Core	VC-S-3-28-6	COMP	183.89	93.77	3	28	59.15	8.70	2976.2	825	865
Core	VC-S-3-28-7	COMP	184.83	93.81	3	28	60.00	8.55	2991.4	1095	860
Core	VC-S-3-O-4	RCP	186.59	93.79	3	O			3025.1	825	1010
Core	VC-D-7-7-1	COMP	188.74	93.79	7	7	41.44		3032.2	825	1385
Core	VC-D-7-7-3	COMP	189.89	93.85	7	7	39.54		3045.4	615	1040
Core	VC-D-7-7-5	COMP	189.45	93.82	7	7	42.59		3061.9	1100	1030
Core	VC-S-7-28-2	COMP	188.97	93.76	7	28	54.31	8.00	3029.2	830	1235
Core	VC-S-7-28-7	COMP	189.28	93.81	7	28	58.37	8.23	3060.8	840	885
Core	VC-S-7-28-8	COMP	189.70	93.83	7	28	57.14	7.91	3066.4	1100	880
Core	VC-S-7-O-6	AVS	190.15	93.81	7	O			3056.9	590	900
Core	VC-S-7-O-4	RCP	190.03	95.80	7	O			3045.0	820	1030
Core	VC-S-14-28-01*	COMP	186.09	94.17	14	28	56.81	7.18	3026.8	1090	1370
Core	VC-S-14-28-02	COMP	184.48	94.00	14	28	54.98	7.04	3015.5	1100	1230
Core	VC-S-14-28-03	COMP	183.08	94.06	14	28	53.02	7.41	2989.8	1310	865
Core	VC-S-14-O-04	RCP	182.17	94.07	14	O			2959.9	1365	1010
Core	VC-D-28-28-1	COMP	189.30	94.90	28	28	44.02	5.63	3082.8	1100	1385
Core	VC-D-28-28-2	COMP	189.97	94.94	28	28	44.31	5.82	3110.0	1105	1235
Core	VC-D-28-28-3	COMP	188.26	94.85	28	28	45.93	5.60	3098.9	1330	880
Core	VC-S-100-2-14-28-1	COMP	201.14	100.79	14	28	54.12	7.34	3730.2	745	1585

Type	Label (* dictates Outlier)	Use	Avg Length (mm)	Avg Diameter (mm)	Day Cored	Day Tested	Compressive Strength (MPa)	Bulk Resistivity (kΩ·cm)	Mass (g)	X Location (mm)	Y Location (mm)
Core	VC-S-75-2-14-28-2	COMP	150.86	76.01	14	28	48.06	7.31	1591.2	890	1570
Core	VC-S-100-1.5-14-28-3	COMP	150.73	100.87	14	28	51.99	7.53	2783.1	1090	1565
Core	VC-S-75-1.5-14-28-4	COMP	113.88	75.94	14	28	51.05	7.30	1208.4	1240	1565
Core	VC-S-100-2-14-28-5	COMP	199.56	100.81	14	28	51.82	7.35	3702.5	1380	1560
Core	VC-S-75-2-14-28-6	COMP	150.33	75.94	14	28	52.02	7.03	1587.5	1575	1580
Core	VC-S-100-1.5-14-28-7	COMP	150.42	100.78	14	28	55.12	7.40	2789.5	1725	1570
Core	VC-S-75-1.5-14-28-8	COMP	113.29	75.71	14	28	53.31	7.29	1203.0	1870	1565
Core	VC-S-100-2-14-28-9	COMP	198.54	100.71	14	28	55.82	7.07	3708.5	2065	1565
Core	VC-S-75-2-14-28-10*	COMP	152.39	75.78	14	28	42.11	7.45	1617.8	2215	1555
Core	VC-S-75-1.5-14-28-11	COMP	113.90	75.89	14	28	52.74	7.30	1206.5	730	1390
Core	VC-S-100-1.5-14-28-12	COMP	151.27	100.77	14	28	53.78	7.55	2819.8	880	1390
Core	VC-S-75-2-14-28-13	COMP	149.58	75.87	14	28	52.10	7.21	1578.1	1080	1380
Core	VC-S-100-2-14-28-14	COMP	199.84	100.73	14	28	53.99	7.28	3719.3	1235	1370
Core	VC-S-75-1.5-14-28-15	COMP	113.23	75.97	14	28	52.53	7.38	1196.6	1380	1375
Core	VC-S-100-1.5-14-28-16	COMP	151.26	100.83	14	28	51.12	7.56	2816.7	1575	1385
Core	VC-S-75-2-14-28-17	COMP	150.25	76.04	14	28	50.31	7.19	1583.3	1720	1380
Core	VC-S-100-2-14-28-18	COMP	200.20	100.77	14	28	55.58	7.57	3726.2	1865	1365
Core	VC-S-75-1.5-14-28-19	COMP	114.17	75.77	14	28	53.40	7.23	1209.3	2080	1370
Core	VC-S-100-1.5-14-28-20	COMP	151.37	100.82	14	28	55.50	7.73	2840.1	2225	1370
Core	VC-S-100-2-14-28-21	COMP	199.38	100.77	14	28	51.95	7.19	3697.7	720	1230
Core	VC-S-75-2-14-28-22	COMP	150.99	75.93	14	28	50.02	7.31	1595.7	875	1230
Core	VC-S-100-1.5-14-28-23	COMP	149.66	100.80	14	28	54.81	7.71	2798.1	1080	1220
Core	VC-S-75-1.5-14-28-24	COMP	113.49	75.91	14	28	51.94	7.23	1206.2	1230	1210
Core	VC-S-100-2-14-28-25	COMP	199.55	100.82	14	28	54.05	7.32	3714.1	1365	1220
Core	VC-S-75-2-14-28-26	COMP	151.34	75.94	14	28	51.42	7.68	1611.2	1565	1220
Core	VC-S-100-1.5-14-28-27	COMP	150.50	100.73	14	28	56.27	7.47	2806.3	1710	1215
Core	VC-S-75-1.5-14-28-28	COMP	112.54	75.81	14	28	55.25	7.36	1187.7	1865	1205

Type	Label (* dictates Outlier)	Use	Avg Length (mm)	Avg Diameter (mm)	Day Cored	Day Tested	Compressive Strength (MPa)	Bulk Resistivity (kΩ·cm)	Mass (g)	X Location (mm)	Y Location (mm)
Core	VC-S-100-2-14-28-29	COMP	199.12	100.75	14	28	53.48	7.48	3701.6	2075	1215
Core	VC-S-75-2-14-28-30	COMP	151.77	75.82	14	28	52.01	7.35	1600.3	2220	1205
Core	VC-S-75-1.5-14-28-31	COMP	115.23	75.95	14	28	51.08	7.43	1220.4	730	1025
Core	VC-S-100-1.5-14-28-32	COMP	152.06	100.76	14	28	54.75	7.49	2823.0	870	1015
Core	VC-S-75-2-14-28-33	COMP	151.84	76.02	14	28	50.40	7.55	1612.1	1065	1020
Core	VC-S-100-2-14-28-34	COMP	199.03	100.57	14	28	55.33	7.24	3717.7	1210	1010
Core	VC-S-75-1.5-14-28-35	COMP	112.06	75.99	14	28	53.59	7.49	1190.9	1370	1015
Core	VC-S-100-1.5-14-28-36	COMP	150.16	100.72	14	28	56.71	7.44	2809.8	1570	1015
Core	VC-S-75-2-14-28-37	COMP	150.64	75.81	14	28	51.29	7.40	1598.6	1715	1010
Core	VC-S-100-2-14-28-38	COMP	199.35	100.78	14	28	55.11	7.61	3734.0	1875	1005
Core	VC-S-75-1.5-14-28-39	COMP	112.57	75.76	14	28	54.33	7.63	1189.4	2090	1010
Core	VC-S-100-1.5-14-28-40	COMP	149.43	100.78	14	28	52.18	7.74	2800.2	2220	1015
Core	VC-S-100-2-14-28-41	COMP	201.33	100.71	14	28	53.93	7.21	3747.0	720	865
Core	VC-S-75-2-14-28-42	COMP	150.76	75.84	14	28	54.00	7.30	1596.3	875	870
Core	VC-S-100-1.5-14-28-43	COMP	150.10	100.66	14	28	56.20	7.37	2793.5	1070	870
Core	VC-S-75-1.5-14-28-44	COMP	113.11	75.84	14	28	46.85	7.78	1198.7	1210	860
Core	VC-S-100-2-14-28-45	COMP	199.10	100.86	14	28	55.33	7.36	3718.9	1370	865
Core	VC-S-75-2-14-28-46*	COMP	152.17	75.96	14	28	39.52	7.48	1625.4	1565	860
Core	VC-S-100-1.5-14-28-47	COMP	150.97	100.77	14	28	54.97	7.50	2820.1	1720	860
Core	VC-S-75-1.5-14-28-48	COMP	112.44	75.77	14	28	50.00	7.46	1192.1	1880	850
Core	VC-S-100-2-14-28-49	COMP	199.18	100.79	14	28	54.61	7.42	3719.5	2080	855
Core	VC-S-75-2-14-28-50	COMP	150.84	75.82	14	28	52.51	7.35	1595.3	2230	845
Core	VC-S-75-1.5-14-28-51	COMP	112.41	75.90	14	28	55.74	7.35	1201.7	715	680
Core	VC-S-100-1.5-14-28-52	COMP	150.00	100.88	14	28	56.11	7.90	2812.4	875	675
Core	VC-S-75-2-14-28-53	COMP	151.98	75.93	14	28	49.67	7.45	1609.4	1060	690
Core	VC-S-100-2-14-28-54	COMP	198.65	100.94	14	28	56.57	7.30	3706.6	1195	675
Core	VC-S-75-1.5-14-28-55	COMP	112.10	75.90	14	28	51.93	7.05	1189.6	1370	680

Type	Label (* dictates Outlier)	Use	Avg Length (mm)	Avg Diameter (mm)	Day Cored	Day Tested	Compressive Strength (MPa)	Bulk Resistivity (kΩ·cm)	Mass (g)	X Location (mm)	Y Location (mm)
Core	VC-S-100-1.5-14-28-56	COMP	150.85	100.70	14	28	54.40	7.58	2823.8	1565	685
Core	VC-S-75-2-14-28-57	COMP	149.61	75.86	14	28	53.24	7.45	1586.8	1725	680
Core	VC-S-100-2-14-28-58	COMP	200.19	100.69	14	28	55.76	7.36	3749.6	1875	665
Core	VC-S-75-1.5-14-28-59	COMP	114.27	75.81	14	28	55.88	7.35	1220.7	2080	665
Core	VC-S-100-1.5-14-28-60	COMP	149.68	100.87	14	28	56.01	7.71	2807.9	2230	660
Core	VC-S-100-1.5-14-28-61	COMP	151.32	100.88	14	28	52.14	7.26	2804.6	715	1550
Core	VC-S-75-1.5-14-28-62	COMP	112.76	75.84	14	28	56.43	7.33	1198.0	870	1555
Core	VC-S-100-2-14-28-63	COMP	199.04	100.97	14	28	56.13	7.50	3726.5	1055	1550
Core	VC-S-75-2-14-28-64	COMP	152.42	76.06	14	28	54.13	7.55	1619.8	1200	1560
Core	VC-S-100-1.5-14-28-65	COMP	151.95	100.81	14	28	57.87	7.63	2835.2	1360	1560
Core	VC-S-75-1.5-14-28-66	COMP	116.32	75.98	14	28	53.51	7.26	1230.2	1570	1555
Core	VC-S-100-2-14-28-67	COMP	200.61	100.69	14	28	55.66	7.36	3748.0	1745	1550
Core	VC-S-75-2-14-28-68	COMP	148.03	75.95	14	28	52.13	7.42	1569.4	1905	1560
Core	VC-S-100-1.5-14-28-69	COMP	150.56	100.82	14	28	56.92	7.44	2787.0	2130	1555
Core	VC-S-75-1.5-14-28-70	COMP	114.49	75.86	14	28	53.32	7.44	1213.3	2280	1550
Core	VC-S-75-2-14-28-71	COMP	148.85	76.01	14	28	55.85	7.00	1577.8	725	1380
Core	VC-S-100-2-14-28-72	COMP	200.58	100.90	14	28	55.06	7.31	3742.0	870	1380
Core	VC-S-75-1.5-14-28-73	COMP	112.10	75.98	14	28	51.28	7.17	1189.4	1050	1390
Core	VC-S-100-1.5-14-28-74	COMP	150.32	100.83	14	28	58.95	7.50	2812.3	1200	1375
Core	VC-S-75-2-14-28-75	COMP	152.61	75.88	14	28	56.05	7.47	1625.3	1360	1375
Core	VC-S-100-2-14-28-76	COMP	198.29	100.77	14	28	56.86	7.29	3701.1	1595	1370
Core	VC-S-75-1.5-14-28-77	COMP	114.66	75.89	14	28	47.68	7.35	1216.0	1730	1370
Core	VC-S-100-1.5-14-28-78	COMP	149.95	100.63	14	28	57.98	7.44	2793.4	1890	1370
Core	VC-S-75-2-14-28-79	COMP	152.53	75.93	14	28	50.96	7.25	1611.9	2130	1380
Core	VC-S-100-2-14-28-80	COMP	200.04	100.78	14	28	51.94	7.10	3715.6	2280	1380
Core	VC-S-100-1.5-14-28-81	COMP	149.59	100.64	14	28	58.47	7.37	2786.5	720	1205
Core	VC-S-75-1.5-14-28-82	COMP	112.37	76.01	14	28	56.67	6.97	1192.5	875	1210

Type	Label (* dictates Outlier)	Use	Avg Length (mm)	Avg Diameter (mm)	Day Cored	Day Tested	Compressive Strength (MPa)	Bulk Resistivity (kΩ·cm)	Mass (g)	X Location (mm)	Y Location (mm)
Core	VC-S-100-2-14-28-83	COMP	199.72	100.69	14	28	57.07	7.25	3715.1	1045	1210
Core	VC-S-75-2-14-28-84	COMP	149.82	75.95	14	28	54.01	7.49	1591.1	1190	1205
Core	VC-S-100-1.5-14-28-85	COMP	150.18	100.78	14	28	53.29	7.52	2793.5	1355	1210
Core	VC-S-75-1.5-14-28-86	COMP	113.70	75.88	14	28	42.82	7.41	1209.9	1600	1205
Core	VC-S-100-2-14-28-87	COMP	201.99	100.63	14	28	55.91	7.52	3762.9	1740	1190
Core	VC-S-75-2-14-28-88	COMP	150.88	75.82	14	28	53.98	7.44	1595.1	1915	1210
Core	VC-S-100-1.5-14-28-89	COMP	150.08	100.70	14	28	54.53	7.62	2796.0	2115	1200
Core	VC-S-75-1.5-14-28-90	COMP	112.33	75.78	14	28	53.06	7.60	1193.8	2265	1190
Core	VC-S-75-2-14-28-91	COMP	150.79	75.89	14	28	50.46	7.39	1601.7	725	1020
Core	VC-S-100-2-14-28-92	COMP	200.00	100.77	14	28	52.13	7.25	3747.4	870	1025
Core	VC-S-75-1.5-14-28-93	COMP	112.73	76.02	14	28	56.50	7.66	1205.2	1050	1025
Core	VC-S-100-1.5-14-28-94	COMP	149.81	100.83	14	28	56.18	7.68	2818.4	1205	1015
Core	VC-S-75-2-14-28-95	COMP	149.68	75.89	14	28	54.63	7.37	1593.6	1365	1015
Core	VC-S-100-2-14-28-96	COMP	199.57	100.73	14	28	56.12	7.46	3726.3	1605	1015
Core	VC-S-75-1.5-14-28-97	COMP	113.93	75.84	14	28	55.09	7.11	1209.4	1740	1015
Core	VC-S-100-1.5-14-28-98	COMP	148.87	100.69	14	28	57.04	7.77	2791.5	1925	1015
Core	VC-S-75-2-14-28-99	COMP	149.67	75.79	14	28	51.60	7.46	1584.1	2115	1015
Core	VC-S-100-2-14-28-100	COMP	200.04	100.76	14	28	54.85	7.46	3739.7	2265	1010
Core	VC-S-100-1.5-14-28-101	COMP	149.05	100.85	14	28	56.53	7.54	2802.7	730	865
Core	VC-S-75-1.5-14-28-102	COMP	112.79	76.00	14	28	53.91	7.24	1214.5	870	865
Core	VC-S-100-2-14-28-103	COMP	200.00	100.89	14	28	53.72	7.42	3766.4	1055	875
Core	VC-S-75-2-14-28-104	COMP	147.96	75.97	14	28	54.15	7.15	1581.8	1205	865
Core	VC-S-100-1.5-14-28-105	COMP	150.06	100.87	14	28	55.09	7.76	2804.7	1370	875
Core	VC-S-75-1.5-14-28-106	COMP	113.53	75.86	14	28	53.60	7.60	1214.3	1585	875
Core	VC-S-100-2-14-28-107	COMP	198.76	100.71	14	28	53.29	7.40	3721.5	1730	870
Core	VC-S-75-2-14-28-108	COMP	151.64	75.80	14	28	54.56	7.25	1603.1	1920	875
Core	VC-S-100-1.5-14-28-109	COMP	149.75	100.73	14	28	57.26	7.69	2806.1	2125	875

Type	Label (* dictates Outlier)	Use	Avg Length (mm)	Avg Diameter (mm)	Day Cored	Day Tested	Compressive Strength (MPa)	Bulk Resistivity (kΩ·cm)	Mass (g)	X Location (mm)	Y Location (mm)
Core	VC-S-75-1.5-14-28-110	COMP	112.14	75.92	14	28	53.42	7.30	1178.3	2260	855
Core	VC-S-75-2-14-28-111	COMP	150.46	76.00	14	28	53.01	7.37	1605.7	715	680
Core	VC-S-100-2-14-28-112	COMP	199.68	100.81	14	28	54.05	7.57	3741.7	860	670
Core	VC-S-75-1.5-14-28-113	COMP	114.08	76.05	14	28	49.68	7.15	1217.8	1045	670
Core	VC-S-100-1.5-14-28-114	COMP	151.60	100.71	14	28	57.41	7.79	2848.2	1210	675
Core	VC-S-75-2-14-28-115	COMP	149.48	75.66	14	28	53.75	7.67	1591.6	1370	680
Core	VC-S-100-2-14-28-116	COMP	200.10	100.70	14	28	56.53	7.55	3737.6	1605	670
Core	VC-S-75-1.5-14-28-117*	COMP	113.64	75.72	14	28	44.77	7.52	1200.7	1725	675
Core	VC-S-100-1.5-14-28-118	COMP	148.95	100.80	14	28	55.67	7.65	2779.9	1895	665
Core	VC-S-75-2-14-28-119	COMP	150.99	75.89	14	28	54.69	7.49	1603.2	2100	680
Core	VC-S-100-2-14-28-120	COMP	199.48	100.69	14	28	55.75	7.51	3728.7	2250	660
Cylinder	CC-D-3-1	COMP	193.12	101.36		3	37.32	3.15	3716.4		
Cylinder	CC-D-3-2	COMP	195.34	101.52		3	38.78	2.76	3615.6		
Cylinder	CC-D-3-3	COMP	194.68	101.62		3	38.98	3.09	3720.0		
Cylinder	CC-S-7-4	COMP	193.12	101.99		7	46.58	4.91	3722.2		
Cylinder	CC-S-7-5	COMP	196.80	101.94		7	48.49	4.62	3691.3		
Cylinder	CC-S-7-6	COMP	195.33	101.56		7	49.66	4.79	3757.8		
Cylinder	CC-S-14-7	COMP	196.47	101.43		14	57.61	7.11	3762.3		
Cylinder	CC-S-14-8	COMP	194.25	101.31		14	55.65	6.93	3666.0		
Cylinder	CC-S-14-9	COMP	194.87	101.67		14	59.09	7.00	3763.0		
Cylinder	CC-S-21-10	COMP	196.70	101.54		21	59.74	8.22	3684.6		
Cylinder	CC-S-21-11	COMP	191.48	102.09		21	61.61	8.63	3680.6		
Cylinder	CC-S-21-12	COMP	192.70	101.67		21	61.79	8.35	3673.5		
Cylinder	CC-S-28-13	COMP	196.59	101.41		28	63.12	9.29	3751.0		
Cylinder	CC-S-28-14	COMP	197.93	101.62		28	65.70	9.44	3817.1		
Cylinder	CC-S-28-15	COMP	195.33	101.71		28	61.69	9.27	3659.0		
Cylinder	CC-S-100-2-28-1	COMP	195.50	101.43		28	62.13	7.46	3602.7		

Type	Label (* dictates Outlier)	Use	Avg Length (mm)	Avg Diameter (mm)	Day Cored	Day Tested	Compressive Strength (MPa)	Bulk Resistivity (kΩ·cm)	Mass (g)	X Location (mm)	Y Location (mm)
Cylinder	CC-S-100-2-28-2	COMP	196.72	101.38		28	62.02	7.94	3737.6		
Cylinder	CC-S-100-2-28-3	COMP	196.76	101.91		28	61.94	7.73	3702.0		
Cylinder	CC-S-100-2-28-4	COMP	194.10	101.39		28	57.90	7.35	3605.4		
Cylinder	CC-S-100-2-28-5	COMP	195.06	101.64		28	61.13	7.49	3652.8		
Cylinder	CC-S-100-2-28-6	COMP	197.26	101.41		28	62.60	7.72	3736.2		
Cylinder	CC-S-100-2-28-7	COMP	196.48	101.46		28	58.97	7.43	3652.4		
Cylinder	CC-S-100-2-28-8	COMP	196.78	101.28		28	60.57	7.22	3669.2		
Cylinder	CC-S-100-2-28-9	COMP	199.45	101.77		28	59.34	7.65	3758.3		
Cylinder	CC-S-100-2-28-10	COMP	194.29	101.50		28	60.80	7.27	3621.1		
Cylinder	CC-S-100-2-28-11	COMP	191.86	101.78		28	60.47	7.55	3583.9		
Cylinder	CC-S-100-2-28-12	COMP	196.10	101.98		28	59.94	8.11	3796.7		
Cylinder	CC-S-100-2-28-13*	COMP	192.64	101.56		28	66.35	7.57	3675.7		
Cylinder	CC-S-100-2-28-14	COMP	194.25	101.68		28	62.45	7.49	3622.9		
Cylinder	CC-S-100-2-28-15	COMP	196.69	101.82		28	59.69	7.51	3650.7		
Cylinder	CC-S-100-2-28-16	COMP	197.18	101.62		28	61.62	7.24	3720.0		
Cylinder	CC-S-100-2-28-17	COMP	196.47	101.86		28	60.74	7.09	3654.9		
Cylinder	CC-S-100-2-28-18	COMP	196.84	101.46		28	61.45	7.28	3730.0		
Cylinder	CC-S-100-2-28-19	COMP	192.58	101.37		28	61.31	7.02	3612.9		
Cylinder	CC-S-100-2-28-20	COMP	195.06	101.65		28	61.55	7.47	3760.7		
Cylinder	CC-S-100-2-28-21	COMP	198.87	101.55		28	61.77	7.68	3749.2		
Cylinder	CC-S-100-2-28-22	COMP	197.37	101.54		28	63.05	7.47	3842.1		
Cylinder	CC-S-100-2-28-23	COMP	193.44	101.30		28	59.29	7.42	3605.2		
Cylinder	CC-S-100-2-28-24	COMP	198.72	101.94		28	59.48	7.65	3722.9		
Cylinder	CC-S-100-2-28-25	COMP	194.99	101.92		28	62.61	7.45	3769.7		
Cylinder	CC-S-100-2-28-26	COMP	196.19	101.37		28	58.90	7.34	3671.7		
Cylinder	CC-S-100-2-28-27	COMP	194.48	101.50		28	60.89	7.32	3601.9		
Cylinder	CC-S-100-2-28-28	COMP	194.41	101.67		28	60.22	7.35	3648.8		

Appendix D - Raw Data

Type	Label (* dictates Outlier)	Use	Avg Length (mm)	Avg Diameter (mm)	Day Cored	Day Tested	Compressive Strength (MPa)	Bulk Resistivity (kΩ·cm)	Mass (g)	X Location (mm)	Y Location (mm)
Cylinder	CC-S-100-2-28-29	COMP	194.52	101.46		28	60.52	7.33	3614.4		
Cylinder	CC-S-100-2-28-30	COMP	197.40	101.76		28	62.17	7.94	3810.7		
Cylinder	CC-S-100-2-28-31	COMP	196.20	101.46		28	61.51	7.68	3710.6		
Cylinder	CC-S-100-1.5-28-1	COMP	151.94	101.34		28	60.78	7.83	2916.7		
Cylinder	CC-S-100-1.5-28-2	COMP	151.67	101.78		28	56.43	7.64	2815.9		
Cylinder	CC-S-100-1.5-28-3	COMP	148.09	101.43		28	57.12	7.79	2769.6		
Cylinder	CC-S-100-1.5-28-4	COMP	148.86	101.50		28	63.63	7.69	2859.8		
Cylinder	CC-S-100-1.5-28-5	COMP	150.97	101.51		28	55.23	7.90	2834.3		
Cylinder	CC-S-100-1.5-28-6	COMP	150.26	101.66		28	62.42	7.83	2875.7		
Cylinder	CC-S-100-1.5-28-7	COMP	151.47	101.40		28	58.82	7.66	2825.6		
Cylinder	CC-S-100-1.5-28-8	COMP	151.09	101.27		28	57.96	7.99	2904.2		
Cylinder	CC-S-100-1.5-28-9	COMP	148.93	101.52		28	57.16	8.20	2834.2		
Cylinder	CC-S-100-1.5-28-10	COMP	152.62	101.27		28	61.06	8.44	2952.7		
Cylinder	CC-S-100-1.5-28-11	COMP	148.76	101.68		28	62.20	7.93	2817.5		
Cylinder	CC-S-100-1.5-28-12	COMP	149.73	101.47		28	54.81	7.60	2769.0		
Cylinder	CC-S-100-1.5-28-13	COMP	150.36	101.44		28	59.73	8.44	2871.7		
Cylinder	CC-S-100-1.5-28-14	COMP	150.50	101.33		28	63.30	8.24	2884.0		
Cylinder	CC-S-100-1.5-28-15	COMP	150.63	101.29		28	62.11	8.07	2852.4		
Cylinder	CC-S-100-1.5-28-16	COMP	152.75	101.49		28	57.89	7.81	2848.9		
Cylinder	CC-S-100-1.5-28-17	COMP	148.20	101.35		28	59.39	7.91	2776.0		
Cylinder	CC-S-100-1.5-28-18	COMP	147.97	101.76		28	60.82	8.70	2863.7		
Cylinder	CC-S-100-1.5-28-19	COMP	147.83	101.68		28	60.22	8.26	2807.9		
Cylinder	CC-S-100-1.5-28-20	COMP	149.12	101.65		28	58.06	7.86	2875.4		
Cylinder	CC-S-100-1.5-28-21*	COMP	151.62	101.70		28	48.70	7.56	2815.3		
Cylinder	CC-S-100-1.5-28-22	COMP	146.95	101.38		28	60.30	8.19	2831.8		
Cylinder	CC-S-100-1.5-28-23	COMP	148.61	101.60		28	56.83	7.91	2830.1		
Cylinder	CC-S-100-1.5-28-24	COMP	149.46	101.70		28	59.67	8.47	2871.9		

Type	Label (* dictates Outlier)	Use	Avg Length (mm)	Avg Diameter (mm)	Day Cored	Day Tested	Compressive Strength (MPa)	Bulk Resistivity (kΩ·cm)	Mass (g)	X Location (mm)	Y Location (mm)
Cylinder	CC-S-100-1.5-28-25	COMP	149.32	101.45		28	57.26	8.28	2836.4		
Cylinder	CC-S-100-1.5-28-26	COMP	151.05	101.78		28	57.15	8.03	2857.5		
Cylinder	CC-S-100-1.5-28-27	COMP	150.32	101.27		28	57.40	7.70	2794.7		
Cylinder	CC-S-100-1.5-28-28	COMP	152.01	101.47		28	59.17	8.18	2886.3		
Cylinder	CC-S-100-1.5-28-29	COMP	151.45	101.35		28	60.77	7.92	2908.8		
Cylinder	CC-S-100-1.5-28-30	COMP	149.93	101.38		28	54.48	7.58	2774.5		
Cylinder	CC-S-100-1.5-28-31	COMP	150.38	101.44		28	62.52	8.37	2906.6		
Cylinder	CC-S-75-2-28-1	COMP	145.11	76.08		28	59.23	7.37	1558.0		
Cylinder	CC-S-75-2-28-2	COMP	148.15	76.07		28	60.35	7.90	1603.9		
Cylinder	CC-S-75-2-28-3	COMP	149.39	76.14		28	61.39	7.86	1617.6		
Cylinder	CC-S-75-2-28-4	COMP	146.63	76.08		28	55.98	7.61	1565.6		
Cylinder	CC-S-75-2-28-5	COMP	150.87	76.15		28	59.24	7.85	1606.2		
Cylinder	CC-S-75-2-28-6	COMP	149.42	76.17		28	60.24	7.59	1612.4		
Cylinder	CC-S-75-2-28-7	COMP	148.64	76.07		28	61.28	7.74	1600.7		
Cylinder	CC-S-75-2-28-8	COMP	146.03	76.13		28	58.03	7.66	1586.4		
Cylinder	CC-S-75-2-28-9	COMP	147.17	76.15		28	60.64	8.02	1590.5		
Cylinder	CC-S-75-2-28-10	COMP	149.01	76.18		28	59.28	7.75	1616.4		
Cylinder	CC-S-75-2-28-11	COMP	145.81	76.14		28	58.68	8.04	1579.5		
Cylinder	CC-S-75-2-28-12	COMP	149.69	76.13		28	58.31	7.86	1599.9		
Cylinder	CC-S-75-2-28-13	COMP	145.72	76.11		28	59.04	7.82	1558.3		
Cylinder	CC-S-75-2-28-14	COMP	146.88	76.23		28	59.18	7.50	1573.7		
Cylinder	CC-S-75-2-28-15	COMP	147.98	76.15		28	58.03	7.64	1576.4		
Cylinder	CC-S-75-2-28-16	COMP	147.92	76.02		28	60.44	7.83	1594.5		
Cylinder	CC-S-75-2-28-17	COMP	150.72	76.26		28	57.41	7.54	1631.6		
Cylinder	CC-S-75-2-28-18	COMP	150.05	76.27		28	62.42	8.19	1623.6		
Cylinder	CC-S-75-2-28-19	COMP	150.58	76.18		28	58.62	7.90	1622.4		
Cylinder	CC-S-75-2-28-20	COMP	150.29	76.14		28	61.18	7.85	1579.6		

Type	Label (* dictates Outlier)	Use	Avg Length (mm)	Avg Diameter (mm)	Day Cored	Day Tested	Compressive Strength (MPa)	Bulk Resistivity (kΩ·cm)	Mass (g)	X Location (mm)	Y Location (mm)
Cylinder	CC-S-75-2-28-21	COMP	149.77	76.11		28	63.04	7.66	1618.8		
Cylinder	CC-S-75-2-28-22	COMP	150.47	76.14		28	59.27	8.10	1628.2		
Cylinder	CC-S-75-2-28-23	COMP	146.10	76.10		28	61.69	8.45	1588.3		
Cylinder	CC-S-75-2-28-24	COMP	149.08	76.10		28	59.89	7.96	1622.2		
Cylinder	CC-S-75-2-28-25	COMP	145.46	76.24		28	54.98	7.44	1560.3		
Cylinder	CC-S-75-2-28-26	COMP	149.37	76.10		28	62.73	7.59	1620.0		
Cylinder	CC-S-75-2-28-27	COMP	149.99	76.18		28	57.37	7.66	1606.8		
Cylinder	CC-S-75-2-28-28	COMP	150.73	76.13		28	58.63	7.78	1627.1		
Cylinder	CC-S-75-2-28-29	COMP	150.08	76.22		28	57.65	8.00	1631.7		
Cylinder	CC-S-75-2-28-30	COMP	150.68	76.15		28	59.10	7.67	1628.3		
Cylinder	CC-S-75-2-28-31	COMP	148.29	76.30		28	57.47	8.19	1607.9		
Cylinder	CC-S-75-2-28-32	COMP	150.19	76.14		28	60.25	7.72	1615.3		
Cylinder	CC-S-75-2-28-33	COMP	150.69	76.21		28	57.28	7.80	1606.2		
Cylinder	CC-S-75-2-28-34	COMP	146.70	76.15		28	59.62	7.83	1567.2		
Cylinder	CC-S-75-1.5-28-1	COMP	110.90	76.06		28	59.49	8.13	1177.8		
Cylinder	CC-S-75-1.5-28-2	COMP	115.81	76.02		28	60.28	7.91	1240.0		
Cylinder	CC-S-75-1.5-28-3	COMP	112.39	76.12		28	62.54	9.07	1214.9		
Cylinder	CC-S-75-1.5-28-4	COMP	114.58	75.94		28	53.40	8.69	1202.3		
Cylinder	CC-S-75-1.5-28-5	COMP	114.92	76.13		28	62.79	8.44	1254.2		
Cylinder	CC-S-75-1.5-28-6	COMP	114.36	76.05		28	58.30	8.70	1245.6		
Cylinder	CC-S-75-1.5-28-7*	COMP	110.72	76.11		28	50.18	7.93	1187.3		
Cylinder	CC-S-75-1.5-28-8	COMP	114.16	76.19		28	57.68	8.18	1214.6		
Cylinder	CC-S-75-1.5-28-9	COMP	113.35	76.21		28	63.30	8.41	1218.5		
Cylinder	CC-S-75-1.5-28-10	COMP	108.88	76.08		28	61.23	8.11	1166.0		
Cylinder	CC-S-75-1.5-28-11	COMP	114.49	76.03		28	60.08	8.27	1251.7		
Cylinder	CC-S-75-1.5-28-12	COMP	115.18	76.14		28	64.12	8.44	1237.0		
Cylinder	CC-S-75-1.5-28-13	COMP	115.53	76.05		28	60.24	8.56	1252.6		

Type	Label (* dictates Outlier)	Use	Avg Length (mm)	Avg Diameter (mm)	Day Cored	Day Tested	Compressive Strength (MPa)	Bulk Resistivity (kΩ·cm)	Mass (g)	X Location (mm)	Y Location (mm)
Cylinder	CC-S-75-1.5-28-14	COMP	110.10	76.07		28	63.71	7.64	1183.9		
Cylinder	CC-S-75-1.5-28-15	COMP	112.95	76.19		28	62.66	8.01	1195.8		
Cylinder	CC-S-75-1.5-28-16	COMP	114.79	76.01		28	57.08	8.36	1222.9		
Cylinder	CC-S-75-1.5-28-17	COMP	116.55	76.03		28	61.29	8.61	1241.6		
Cylinder	CC-S-75-1.5-28-18	COMP	115.30	76.04		28	60.38	7.74	1231.0		
Cylinder	CC-S-75-1.5-28-19	COMP	115.05	76.06		28	56.73	8.62	1249.3		
Cylinder	CC-S-75-1.5-28-20	COMP	112.90	76.05		28	64.13	8.63	1224.6		
Cylinder	CC-S-75-1.5-28-21	COMP	110.96	75.87		28	62.63	8.65	1206.9		
Cylinder	CC-S-75-1.5-28-22	COMP	112.36	76.44		28	56.46	8.01	1187.0		
Cylinder	CC-S-75-1.5-28-23	COMP	116.98	75.98		28	61.81	8.38	1250.7		
Cylinder	CC-S-75-1.5-28-24	COMP	112.99	76.04		28	60.33	8.38	1231.9		
Cylinder	CC-S-75-1.5-28-25	COMP	115.35	76.22		28	63.72	8.02	1215.5		
Cylinder	CC-S-75-1.5-28-26	COMP	109.95	76.08		28	63.06	7.78	1154.3		
Cylinder	CC-S-75-1.5-28-27	COMP	114.60	76.46		28	62.64	8.59	1250.6		
Cylinder	CC-S-75-1.5-28-28	COMP	114.67	76.10		28	58.62	8.89	1217.7		
Cylinder	CC-S-75-1.5-28-29	COMP	110.82	76.09		28	66.89	8.66	1194.5		
Cylinder	CC-S-75-1.5-28-30	COMP	112.25	76.09		28	63.95	8.09	1211.4		
Cylinder	CC-S-75-1.5-28-31	COMP	112.77	75.90		28	62.45	8.32	1234.7		
Cylinder	CC-S-75-1.5-28-32	COMP	115.72	75.90		28	59.90	8.17	1225.6		
Cylinder	CC-S-75-1.5-28-33	COMP	115.11	75.82		28	61.72	8.85	1250.4		
Cylinder	CC-S-75-1.5-28-34	COMP	115.51	76.02		28	55.15	8.28	1233.7		
Cylinder	CC-S-75-1.5-28-35	COMP	110.42	75.96		28	66.21	7.99	1188.8		